INAUGURAL – DISSERTATION

zur
Erlangung der Doktorwürde
der
Naturwissenschaftlich-Mathematischen Gesamtfakultät
der Ruprecht-Karls-Universität
Heidelberg

vorgelegt von
Andréia Feijão

Tag der mündlichen Prüfung:

DISSERTATION

Submitted to the
Combined Faculties for the Natural Sciences and for Mathematics
of the Ruperto-Carola University of Heidelberg, Germany
for the degree of
Doctor of Natural Sciences

Presented by
Andréia Feijão

Date of oral examination:

The role of phosphorylation in the *Schizosaccharomyces pombe* EB1 homolog mal3p

Referees: Dr. Marko Kaksonen

Prof. Dr. Oliver Gruss

To my mother…

Acknowledgments

In the end of my PhD I can only recall Vinnie Jones last sentence in Lock, Stock and Two Smoking Barrels – It has been intense...

EMBL was a central part in all this. Probably the best part. Thru EMBL I had the privilege to meet some of the most inspiring people crossing my life. It's to them, whom I am undoubtedly grateful, that the following lines are dedicated.

No words are ever going to be good enough to thank my supervisor Damian Brunner. For his unconditional support, both scientific and non-scientific, and his truly admirable character. Damian, thank you with all my heart.

I would like to extend my gratitude the members of my thesis advisory committee, Eric Karsenti and specially, Anne Ephrussi. I thank Anne for all the support, for being there exactly when I needed. This was of great help for me and will not be forgotten.

I'm also extremely grateful to Prof. Cláudio Sunkel, for his support on my project and for doing everything he could to make my life easier. I also thank the members of my PhD jury. I specially thank Marko for letting me use (and abuse!) his lab when I became labless in the very last stages of my PhD.

I would also like to acknowledge the E-STAR Marie Curie fellowship for funding, which allowed me to attend conferences and courses, improve my scientific knowledge and meet the right people at the right time.

To Helke Hillebrand, the dean of the graduate studies, I thank all the support, understanding and will to help. You took a lot of great stress from me.

A BIG thank you to all present and past members of the Brunner Lab (and surroundings). First and foremost I thank Manolo for his kindness, friendship and never-ending patience with me in the first years of my PhD. I owe you everything I know of working in a lab (and that's a hell of a lot, considering I know so much...). I also want to thank Imola Balogh-

Aprill for all the dedication while working on my project as it were her own. Thank you also to Mika, Manuel, Ferenc (and family), Linda, Lindsay, Jerome, Tatyana, Steve, Nadia, Aynur, Catarina and Paulo. Specially, I want to thank Aynur for the privilege of her constant visits, despite all the work, bringing every time laughter and fresh air. Lindsay, I thank you the big support I got from you, also recently, in correcting my PhD thesis. E claro, a ti, Catarina, obrigada por tudo.

I also thank Luís, for ringing my bell at 7 o'clock in the morning, insistently, and when I though I was going to see the that religious woman that occasionally wakes me up at weekends, I saw you telling me: Get dressed, let's go for a walk in Trier!

I also warmly thank Anna Christa, for patiently repairing me with her magic hands and meaningful advices.

E agora, claro, à gente da minha terra! Conheci algumas das gerações que passaram pelo EMBL. Em primeiro lugar, agradeço à minha querida Raposinha, por tantos, e tão bons tempos passados no início dos nossos doutoramentos. Pelas dancing machines, pelas semanas diabólicas (e a Maya nunca se engana!), pelos jantares à meia-noite, por tudo o que de tão intenso foi partilhado. Agradeço também ao meu chafariz pragmático com saudades de casa. Hélio, realmente nem sei bem que te diga… Essa tua estranha mistura de enorme delicadeza aliada à força equivalente de um tsunami, faz de ti um amigo insubstituível. Ragazza, como é que eu vou esquecer as conversas na Casa del Café, a girl talking e essa forma que tens de me fazer rir?

Agradeço, ainda, a todos os outros portugueses que passaram pelo EMBL, por tantos jantares e companheirismo. Obrigado ao Pedro, Jaqueline, Sónia, Hugo, Ana Zhu, Sofia Pinto, Sofia Costa, Sandra Caldeira, Alexandra Manaia, André... Um agradecimento especial à Jaqueline, Hugo e Sónia que me ajudaram na tradução, correcção e impressão da tese.

Agradeço também ao meu mais "velho" amigo, Nuno Amaral. O rapaz que acabou com melhor nota do que eu no exame de português B.... após responder, sucintamente, que "os Lusíadas tratam dos descobrimentos (ponto final)"... Já lá vão quantos? Dezasseis anos?

Aos três mosqueteiros, João, Munhá e Petronilho. Por me terem desafiado a ir a Paris à última hora, tendo eu, por esse motivo, ter de alegar motivos pessoais, inesperados e inadiáveis. Agradeço ainda a todos os morangos sem açúcar, mas com champanhe, no alto do monte, nesse dia de vento de 25 de Janeiro.

Paulo, talvez o silêncio consiga falar aquilo que não pode ser dito aqui…

À minha família, especialmente aos irmãos de meu pai, Isabel, Rosa, João e Maria pelo apoio incondicional e sincero que nos deram em momentos difíceis. Às minhas tias, Isabel e Rosa, queria agradecer do fundo do coração a dedicação que tiveram para com o pai. Tio João, há coisas que nunca se podem esquecer. Agradeço-lhe muito todo o espaço e a confiança que nos concedeu. Ainda uma nota especial de agradecimento aos meus primos, Nuno e Mário João. Ao Nuno pela calma que sempre me inspirou e ao Marinho, o mais próximo de irmão que tive.

Aos meus avós, Constância e Luís, porque por mais que caminhe, chegar a vossa casa é chegar à minha infância. E à minha bisavó Adelaide, por tanto que me lembrei de si.

As minhas últimas palavras são dedicadas, aos meus pais, António e Gabriela. Pai, que dizer… Onde abrimos o champanhe? A ti, mãe, não agradeço, porque já sei que não gostas. Mas acho que podemos ir dançar a noite toda, que sei que é coisa que te agrade mais…

Não há, para mim, ideia mais feliz do que pensar que sou feita em proporções que medem exactamente 50% de cada um dos dois, com todas as qualidades e (maus) feitios que me couberam por defeito. Porque a perfeição não será nunca perfeita. Por isso, quanto mais tempo passa, mais me espanto, e incrédula contemplo, a sorte, sorte, imensa sorte, de ter crescido ao vosso lado…

A todos, obrigada.

Heidelberg, 26th July, 2011

Summary

Microtubules are highly dynamic polymers that have widespread, essential functions in a number of fundamental processes, such as the establishment and maintenance of cell polarity, chromosome segregation during mitosis, and organelle positioning and transport. In order to perform all these functions, microtubule organization and dynamics have to be precisely regulated. Members of the end binding (EB) protein family have recently emerged as master regulators of growing microtubule plus-ends, but the molecular mechanisms controlling the multiple activities of these proteins in the various biological contexts and processes in which microtubules participate are poorly understood.

In this study we show that mal3p, the fission yeast end binding protein 1 (EB1) homologue, is phosphorylated on a cluster of five serine residues lying in the flexible linker region that connects the microtubule binding calponin homology domain with the conserved EB1 domain. From these sites, S144 and S145 are “dominant”, since the lack of phosphorylation at these sites impairs phosphorylation of S147, S148 and S151. Furthermore, we show that phosphorylation changes in a cell cycle-dependent manner. Mal3p is dephosphorylated at the transition from interphase to mitosis, when the intranuclear microtubule spindle needs to form while cytoplasmic microtubule nucleation ceases. Mal3p subsequently becomes phosphorylated again at the transition from metaphase to anaphase, when spindle microtubules become stabilized to allow for spindle elongation. This phosphorylation appears to be involved in the regulation of spindle elongation and proper microtubule organization in the spindle mid-zone.

Concomitant with the phosphorylation states, mal3p levels are highest at mitotic onset and decrease during mitosis, reaching a minimum at the time when cytokinesis occurs. Together with the finding that mal3p protein levels are much increased in the absence of phosphorylation, these results suggest that mal3p phosphorylation regulates overall mal3p protein levels in a cell cycle-dependent manner. Surprisingly, microtubules have higher catastrophe rates when mal3p protein levels increase, which contradicts the proposed microtubule growth-promoting activity of mal3p. Our findings thus reveal new insights into the pleiotropic functions of the EB1 protein family members and into the regulatory mechanisms that modulate these functions.

Zusammenfassung

Mikrotubuli sind hochdynamische Polymere, die wesentliche Funktionen in einer Reihe von grundlegenden zellulären Prozessen haben. Zum Beispiel sind das Generieren und Erhalten von Zellpolarität, die Chromosomensegregation während der Mitose oder die Positionierung und der Transport von Organellen ohne Mikrotubuli nicht möglich. Um all diese Aufgaben zu erfüllen, müssen Mikrotubuli Organisation und Dynamik genau geregelt werden. Angehörige der EB (end binding) Proteinfamilie sind vor kurzem als zentrale Regulatoren der wachsenden Mikrotubuli Plus-Enden bekannt geworden. Trotzdem sind die molekularen Mechanismen, welche die vielfältigen Aktivitäten dieser Proteine in den verschiedenen biologischen Zusammenhängen und Prozessen kontrollieren noch weitgehend unverstanden.

In dieser Studie zeigen wir, dass mal3p, das EB1 (end binding protein 1) Homologe der Spalthefe, an einem Cluster von fünf Serinen phosphoryliert wird. Das Cluster liegt in einer flexiblen Proteinregion, welche die mikrotubulibindende Calponinhomologie-domäne mit der konservierten EB1-Domäne verbindet. Von den Serinen sind S144 und S145 „dominant“, da die Absenz von Phosphorylierung an diesen Serinen, die Phosphorylierung der Serine S147, S148 und S151 verhindert. Darüber hinaus zeigen wir, daß sich die Phosphorylierung von mal3p während des Zellzyklus in einem bestimmten Muster ändert. Dabei ist mal3p am Übergang von der Interphase zur Mitose dephosphoryliert. Zu diesem Zeitpunkt bilden sich anstelle der zytoplasmatischen Interphasenmikrotubuli, intranukleäre Mikrotubuli welche die mitotische Spindel aufbauen. Mal3p wird anschließend, am Übergang von der Metaphase zu Anaphase, wieder phosphoryliert. Das geschieht wenn die Spindelmikrotubuli stabilisiert werden müssen damit die Spindel sich verlängern kann. Diese mal3p Phosphorylierung scheint sowohl an der Regulation der Anaphase als auch an der richtigen Mikrotubuli-Organisation im Mittelbereich der Spindel beteiligt zu sein.

Parallel zum Phosphorylierungsstand, ist die Menge an mal3p Protein zu Beginn der Mitose am höchsten und nimmt dann während der Mitose sukzessive ab wobei sie zum Zeitpunkt der Zytokinese ein Minimum erreicht. Zusammen mit der Feststellung, daß die mal3p Proteinmenge in mutanten Zellen, in denen mal3p nicht phosphoryliert werden kann, generell erhöht ist, legt dies nahe, daß die Phosphorylierung den mal3p Proteingehalt der Zelle reguliert. Überraschenderweise haben Mikrotubuli in Gegenwart von höheren Mengen von unphosphoryliertem mal3p eine erhöhte Katastrophenrate. Dies widerspricht der bisherigen Ansicht, wonach mal3p Protein für Mikrotubuli wachstumsfördernd ist. Unsere Ergebnisse geben

somit neue Einblicke in die pleiotropen Funktionen der EB1 Proteine und in die regulatorischen Mechanismen, die diese Funktionen kontrollieren.

Table of contents

List of Figures and Tables

Chapter 7

Abbreviations

ABP(s)	Actin binding protein(s)
ADP	Adenosine diphosphate
AMPK	5’ adenosine monophosphate-activated protein kinase
ATP	Adenosine triphosphate
Cdc2	Cyclin dependent kinase 2
CLASP	Cytoplasmic linker associated protein
CLIP	Cytoplasmic linker protein
CH	Calponin homology
CK1 (2)	Casein kinase 1 (2)
C-terminal	Carboxy terminal
DNA	Deoxyribonucleic acid
DMSO	Dimethylsulphoxide
EB1	End binding protein 1
EMM2	Edinburgh minimal medium 2
eMTOC	Equatorial microtubule organizing center
FL	Full length
GDP	Guanosine diphosphate
GFP	Green fluorescent protein
GSK3β	Glycogen synthase kinase 3 beta
GTP	Guanosine triphosphate
h	Hour
IF(s)	Intermediate filament(s)
IMA	Interphase microtubule array
IPG	Immobilized pH gradient
iMTOC	Interphase microtubule organizing center
kDa	Kilo dalton
M	Molar
mA	Miliampere
MAP	Microtubule associated protein
MBC	Methyl-2-benzimidazole
MS	Mass Sepctrometry

MT	Microtubule
MTOC	Microtubule organizing center
mTOR	Mammalian target of rampamycin
N.A.	Numerical aperture
NEB	Nuclear envelope breakdown
NETO	New end take off
N-terminal	Amino terminal
nm	Nanometer
nM	Nanomolar
μm	Micrometer
O.D.	Optical density
PAA	Post-anaphase array
PCR	Polymerase chain reaction
PIP	Phosphatidylinositol phosphate
PI3K	Phosphoinositide 3-kinase
PKA (B or C)	Protein kinase A (B or C)
Pnmt	Promoter no message in thiamine
RSK	Ribosomal S6 kinase
Rpm	Revolutions per minute
RT	Room temperature
RNA	Ribonucleic acid
SEM	Standart error of the mean
S. cerevisiae (budding yeast)	*Saccharomyces cerevisiae*
S. pombe (fission yeast)	*Schizosaccharomyces pombe*
SPB	Spindle pole body
YE5S	Yeast extract medium containing 5 supplements
t	Time
ts-mutants	Temperature sensitive mutants
+Tip	Microtubule plus end associated protein
WT	Wild type
μl	Microliter
μM	Micromolar
γ-TURC	Gamma tubulin ring complex

2D-gel	Two dimensional gel electrophoresis
’	Minutes
’’	Seconds
°C	Degree celsius

Chapter 1

Introduction

1. Introduction

1.2 The cell's cytoskeleton

The cell is a highly complex, dynamic and structured system with its components organized in a well-defined and cell-specific way. In order to organize themselves, assume the correct shape, be physically robust and perform motile processes such as growth, chromosome segregation or cell migration, cells depend on a remarkable cooperative system of filaments – the cytoskeleton.

The various functions of the cytoskeleton are performed only by three families of proteins that polymerize into the different types of cytoskeleton filaments found in eukaryotic cells – intermediate filaments, actin filaments and microtubules (Figure 1.1).

Cytoskeleton filaments are highly dynamic and able to respond rapidly to changing circumstances. Understanding the regulation of this dynamic behavior in space and time is thus a central question in cell biology.

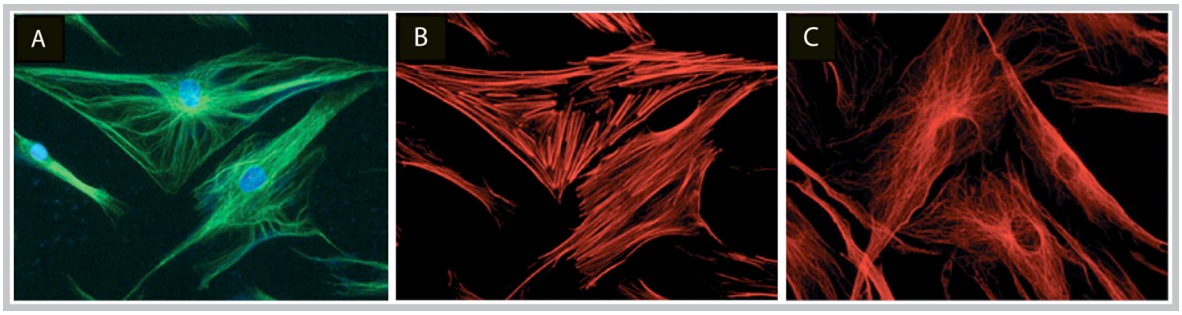

Figure 1.1: Cytoskeleton organization in fibroblasts. Fibroblast immunostaining of vimentin, actin and tubulin allow the observation of (A) Intermediate filaments (B) Filamentous actin, (C) Microtubules (Bomont and Koenig, 2003).

1.2.1 Intermediate filaments

Intermediate filaments (IFs) are named after their intermediate diameter (10-12nm), as compared to actin filaments (Section 1.2.2) and microtubules (Section 1.3). IF proteins are present in all vertebrates, and in budding yeast, one IF-like protein was described (McConnell and Yaffe, 1993). However, no IF protein was described in fission yeast.

The elementary building blocks of intermediate filaments are very elongated (~45nm) and thin (2-3nm) rod-like dimers. The individual polypeptides that constitute the dimers exhibit a tripartite molecular organization composed of a central α-helical domain, the "rod", flanked by non-α-helical "head" and "tail" domains located N and C-terminally, respectively (Strelkov *et al.*, 2003; Herrmann and Aebi, 2004).

The molecular mechanisms that rule IF assembly differ depending on the IF class (Herrmann and Aebi, 2004). Of these mechanisms, the *in vitro* assembly of desmin-like proteins (class III) is the best understood process. In this case, after dimer formation, tetramers rapidly associate laterally to form unit-length filaments (ULFs). These ULFs then longitudinally anneal to form short filaments that grow by end-to-end association to form loosely packed filaments. On further elongation, these filaments start to compact by reducing their diameter. This internal compaction propagates throughout the filament, leading to mature IFs (Chang and Goldman, 2004). However, in other IF classes the ULF stage can be completely absent or the dimer may show a high tendency for head-to-tail association instead of lateral association (Strelkov *et al.*, 2003). Importantly, unlike microtubules and actin filaments, IFs can self-assemble *in vitro* in the absence of ATP or GTP and do not have an intrinsic polarity, as individual dimers are oriented both in an "up" and in a "down" direction along the filament (Strelkov *et al.*, 2003).

The first mechanical properties of IFs to be studied were the viscoelastic properties of macroscopic IF networks. These studies showed that crosslinked IF networks are softer and can withstand larger deformations without breaking, when compared to other cytoskeletal gels. More recently, single filament measurements made by atomic force microscopy revealed that IFs are not only flexible filaments but they also have an unusual extensibility and a strong resistance to breakage.

All these properties taken together make IFs uniquely adapted for dealing with mechanical stress (Herrmann *et al.*, 2007; Wagner *et al.*, 2007; Herrmann *et al.*, 2009). Thus, one of the IFs main functions is to impart mechanical stability to animal cells and tissues. However, many other functions have also been attributed to IF networks. Because of their extensive distribution throughout the cell, they provide an enormous area that can act as a scaffold to which numerous types of regulatory and signaling molecules can bind. In fact, a direct role in signal transduction has been suggested. IFs might also be an important constituent of cellular mechanotransduction processes, they may mediate cytoskeleton crosstalk, and organize organelles in the cytoplasm (Herrmann *et al.*, 2007; Goldman *et al.*, 2008; Minin and Moldaver, 2008).

1.2.2 Actin filaments

Actin is a highly conserved and abundant protein present in eukaryotic cells. However, an ancestral actin gene has been also found in bacteria (van den Ent *et al.*, 2001). The integrity of the actin cytoskeleton is important for cells to maintain their shape and structure, and undergo polarized growth. Its filaments are highly dynamic and able to respond to external and internal stimuli. This allows actin filaments to rapidly reorganize and to play a crucial role in important dynamic processes such as cell motility and cell division. During cell motility, actin filaments treadmill to push out membrane protrusions and thus produce the forces required for movement. In mitosis, actin plays an important role in the separation of the two daughter cells when it forms the cytokinetic ring which is capable of exerting a contractile force by the concerted action of actin and the actin motor protein myosin. Actin is also required for endo- and exocytosis and RNA, organelle and vesicle trafficking (dos Remedios *et al.*, 2003; Pollard and Borisy, 2003; Robinson and Spudich, 2004). Finally, actin filaments are the major component in *lamellipodia* and *filopodia*, highly dynamic structures involved in cell-cell signaling, guidance toward chemoattractants, and adhesion to the extracellular matrix (Gupton and Gertler, 2007). Nevertheless, actin filaments are also able to form very stable structures, like those present in stereocilia in the inner ear. Despite its high abundance in the cell's cytosol, actin is also a nuclear protein, playing a role in gene transcription and long-range chromatin organization (Visa and Percipalle, 2010).

Actin exists in a dynamic equilibrium between monomeric G-actin and polymerized F-actin. Monomeric G-actin polymerizes into filaments above the critical concentration, defined as the concentration of free monomers in equilibrium with a population of actin filaments. Actin filaments can be described as a two-start right-handed helix that is intrinsically polar, because the asymmetric monomeric G-actin subunits add to the filaments in the same orientation with respect to the filament axis. This polarity was observable by electron microscopy when the filaments were decorated with myosin sub fragment 1 (S-1), displaying an arrowhead-like appearance (Pollard and Borisy, 2003). Thanks to the latter, the filament's extremities were named the "barbed" and the "pointed" ends. Actin polymerization can occur at both ends of the F-actin filament, although it occurs predominantly at the "barbed" end (dos Remedios *et al.*, 2003).

Actin is an ATPase that strongly binds ATP. Its hydrolysis was once thought to be closely linked to the polymerization process, since monomeric G-actin mostly contains exchangeable ATP, while F-actin contains mostly non-exchangeable ADP. However, several studies showed that ATP hydrolysis is instead closely linked to another property of actin filaments – *treadmilling*

(Wegner, 1976; Brenner and Korn, 1979; Pollard and Mooseker, 1981; Hill and Kirschner, 1982). This phenomenon, also present in microtubules, occurs when one end of the filament grows in length while the other end shrinks producing the effect of monomers "moving" along the filament. In the case of actin, this can be driven by the fact that ADP actin dissociates faster from the barbed end than ATP-actin subunits, but both ATP- and ADP-actin slowly dissociate from the pointed end (Pollard and Borisy, 2003).

In order to perform all its functions F-actin assumes a wide variety of structures with different properties. These structures are regulated essentially by a large number of actin-binding proteins (ABPs). These involve filament stabilizers/destabilizers and ABPs that promote branching, filament bundling and *de novo* actin nucleation. This last process is triggered by the Arp2/3 complex and the formin class of proteins (dos Remedios *et al.*, 2003; Zigmond, 2004). Regulation of ABPs is critical for cells to rapidly adapt and respond to new conditions. It is carried out mainly by post-translational modifications, ion binding, or interactions with co-factors that either change the conformation of ABPs or compete with them for actin (Revenu *et al.*, 2004).

1.3 The microtubule cytoskeleton

Microtubules can form stable or transient structures and are involved in a myriad of cellular functions. They are the main components of the mitotic spindle, a highly dynamic and regulated structure responsible for chromosome segregation. Microtubules are also responsible for the fast and directional transport of cellular organelles that can travel over long distances through the action of microtubule motors. Besides, members of well-known signaling pathways are transported along the microtubules, implicating the latter as important components in cell signaling transduction. Stable structures can be found in *cilia* and *flagella* that upon ATP hydrolysis allow specific cells – such as sperm cells, for example – to move. Finally, microtubules are essential for cell polarization. This is a well-studied mechanism in fission yeast, where microtubules are important for the deposition of polarity markers, like tea1p and tea4p, at cell tips (Mata and Nurse, 1997; Martin *et al.*, 2005). These associate in a complex that recruits for3p to promote actin assembly leading to polarized cell growth (Martin *et al.*, 2005).

Due to the general importance of microtubules, it is thus essential for the cell to tightly control their dynamics and nucleation in space and time – a regulation which will be discussed in some detail in the subsequent chapters.

1.3.1 α- and β-tubulin are the microtubule's building blocks

The microtubule's structural unit is the α-β-tubulin heterodimer, composed of the highly conserved globular proteins α- and β-tubulin. These proteins are ~55kDa and share 40% similarity with each other (Figure 1.2)(Wade, 2009).

α- and β-tubulin interact non-covalently to form a very stable α-β-tubulin heterodimer. This process depends on the cytosolic chaperonin CCT, which releases both monomers in a *quasi native* state in which they later interact with several cofactors (A, B, C and D) to form the native α-β-tubulin heterodimer. These cofactors have been shown to directly interact with microtubules, indicating that they may also be involved in regulating microtubule dynamics (Nogales, 2000).

The multiple expression of tubulin genes leads to several coexisting and slightly different α- and β-tubulins, commonly called isotypes. Other tubulins have also been identified and appear to have specialized functions (Dutcher and Trabuco, 1998; Chang and Stearns, 2000; Ruiz *et al.*, 2000; Dutcher, 2003). One of the most studied – γ-tubulin – was discovered in the fungus *Aspergillus nidulans* and has a crucial function in microtubule nucleation and stabilization (Oakley and Oakley, 1989; Wade, 2009).

Both α- and β-tubulin bind guanosine triphosphate (GTP). However, in the heterodimer only β-tubulin is able to hydrolyze and exchange the GTP because α-tubulin GTP is buried in the intra-dimer interface (Figure 1.2). Thus α-tubulin GTP seems mainly to have a structural role, whereas β-tubulin GTP is essential in microtubule polymerization since only β-tubulin in the GTP state is competent to polymerize into microtubules (Nogales, 2000; Amos and Schlieper, 2005)(Section 1.3.3).

Finally, α- and β-tubulin are subject to many different post-translational modifications that occur mainly at their C-terminal region. This region is probably exposed at the microtubule surface, as inferred by the docking of tubulin's structure into a 20-A microtubule reconstruction (Nogales, 2000). The biological significance of these modifications seems to be connected with either the stability and/or structure of microtubule assemblies or the regulation of microtubule associated proteins (McKean *et al.*, 2001; Hammond *et al.*, 2008).

1.3.2 Microtubules are intrinsically polar polymers

Microtubules are relatively rigid hollow tubes, about 25nm in diameter, formed by the lateral association of protofilaments that result from the head-to-tail assembly of α-β-tubulin heterodimer (Figure 1.2) (Desai and Mitchison, 1997). Due to the alternation of α- and β-tubulin, microtubules are intrinsically polar, with β-tubulin at the "plus" end and α-tubulin and the "minus" end (Nogales *et al.*, 1999). Both *in vitro and in vivo*, "plus" and "minus" ends have different properties, since growth occurs preferentially at the plus end.

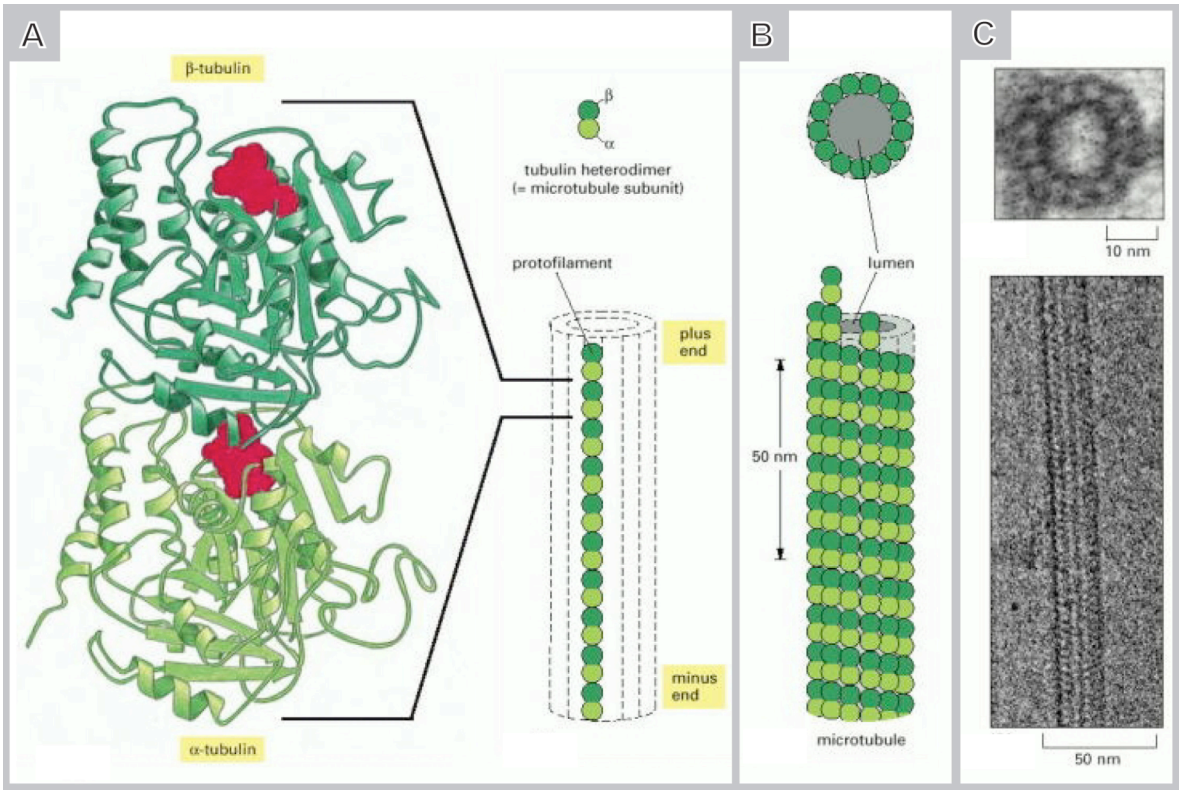

Figure 1.2: Microtubule structure. (A) Ribon diagram of α,β-tubulin heterodimer is shown. Each subunit has a GTP-bound nucleotide. Note that in α-tubulin GTP is buried inside the heterodimer and is therefore non-exchangeable. The head-to-tail packing of the α-β-tubulin heterodimer constitutes the protofilament, a polar filament with β-tubulin at the "plus" end and α-tubulin at its "minus" end. (B) Through the lateral interaction of protofilaments, a microtubule is formed. (C) Upper figure: electron micrograph of a cross-section of a 13 protofilament microtubule. Lower figure: electron micrograph of a microtubule short segment (adapted from Alberts B., *et al*, 2002).

In vivo, microtubules generally have 13 protofilaments (Tilney *et al.*, 1973; Savage *et al.*, 1989; Afzelius *et al.*, 1990). In these microtubules, adjacent protofilaments run parallel to the microtubule axis and are staggered by ~0.9 nm (Mandelkow *et al.*, 1986). This results in staggered tubulin subunits in neighboring protofilaments that follow a left handed three-start

helix, meaning that the helix spans three subunits of a protofilament before it completes one turn (Wade, 2007).

Lateral interactions between protofilaments can have two possible arrangements: A-lattices, which exhibit α-α and β-β contacts, and B-lattices, which have alternate α-β interactions (Amos and Klug, 1974). *In vivo*, B-lattices seem to predominate (Mcintosh *et al.*, 2009) and B-lattice 13 protofilament microtubules are not symmetrical, requiring a mismatch in order to allow tube formation (Mandelkow *et al.*, 1986; Kikkawa *et al.*, 1994). This mismatch is called the microtubule seam. It has an A-lattice configuration and is the weakest part of the microtubule according to the higher free energy of the A-lattice interaction (Sept *et al.*, 2003). The current model for microtubule growth is that at their growing plus-ends the microtubules form sheet structures that later close into a tube, joining at the microtubule seam, which can be stabilized by specific microtubule-associated proteins (Chretien *et al.*, 1995; Arnal *et al.*, 2000; Sandblad *et al.*, 2006) (Section 1.5.4.3.3).

1.3.3 The microtubule dynamic instability model

Microtubules are inherently dynamic, undergoing repeated transitions from growth to shrinkage by addition or loss of tubulin subunits (Figure 1.3A). This phenomenon is called dynamic instability and was first proposed by Mitchison and Kirchner (Mitchison and Kirschner, 1984).

Direct visualization of this property was possible after *in vitro* microtubule assembly. These microtubules showed periods of growth that were stochastically interrupted by periods of shrinkage (Horio and Hotani, 1986). This transition is called “catastrophe” while the transition from shrinkage to growth is called “rescue”. In contrast with *in vitro* assembled microtubules, *in vivo,* microtubules can also “pause”, a state in which they neither grow nor shrink. Therefore, microtubule dynamics is determined primarily by four parameters: i) growth speed, ii) shrinkage speed, iii) catastrophe frequency and iv) rescue frequency.

Growth at microtubule plus-end involves the interaction of the α-tubulin subunit of the incoming tubulin dimer with a pre-existent β-tubulin, thereby activating its GTPase activity and releasing phosphate (P_i) (Wade, 2009). This process changes the conformation of the protofilament from slightly bent to a more profoundly curved tubulin-GDP, weakening the protofilament’s lateral interactions. However, because tubulin-GDP is part of the microtubule wall it is forced to remain straight, leading to a mechanical strain that weakens microtubule

stability. Lattice microtubule stabilization is then possible, thanks to a GTP cap at the "plus" end that originates when the rate of new added dimer is faster than the rate of GTP hydrolysis (Nogales, 2000; Nogales and Wang, 2006). If these conditions are not met, the microtubule looses its GTP cap and becomes unstable, precipitating a catastrophic event. This is characterized by the transition from straight/slightly bent protofilament sheets seen at microtubule growing ends into fountain-like structures of ring protofilaments characteristic of depolymerizing microtubules (Akhmanova and Steinmetz, 2008). Interestingly, GTP hydrolysis from the exchangeable site at β-tubulin subunit is not required for microtubule polymerization *per se*, as microtubules polymerize in the presence of a non-hydrolyzable GTP analogue, GMPCPP. Rather, GTP hydrolysis seems to be involved in microtubule depolymerization, since microtubules assembled *in vitro* in the presence of GMPCPP are more stable and do not show dynamic instability (Wade, 2009).

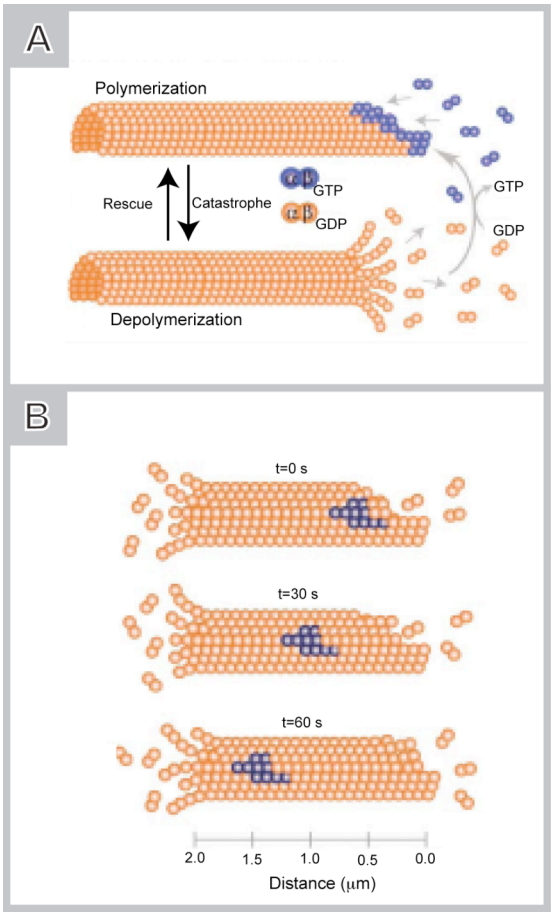

Figure 1.3: Microtubule dynamics. (A) Microtubule dynamic instability. Microtubules switch between stages of polymerization and depolymerization. GDP-bound tubulin is shown in orange and GTP-bound tubulin, which generates the GTP cap, is in purple. (B) Microtubule treadmiling. The group of dark blue tubulin represents a single "speckle" that can be tracked over time to determine the rate of flux. Adapted from (Kline-Smith and Walczak, 2004).

Like actin filaments, microtubules also exhibit treadmilling (Margolis and Wilson, 1998) (Figure 1.3B). This behavior was first established unequivocally in the mitotic spindle, being hypothesized as an important mechanism for production of tension or for passive chromosome segregation. The importance of microtubule treadmilling *in vivo* remains elusive, but it is thought that both treadmilling and dynamic instability coexist in cells as intrinsic dynamic microtubule properties (Margolis and Wilson, 1981; Rodionov and Borisy, 1997; Waterman-Storer and Salmon, 1997; Margolis and Wilson, 1998).

1.3.4 Microtubule organizing centers – MTOCs

Microtubules can spontaneously polymerize *in vitro* in the presence of high concentration of α,β-tubulin heterodimer, GTP and Mg^{2+} (Voter and Erickson, 1984). However, *in vivo*, tubulin concentration is not high enough for spontaneous nucleation, and so this process is assisted by specialized structures attached to microtubule minus-ends, called microtubule organizing centers (MTOCs). Importantly, MTOCs also control when and where microtubules nucleate and are therefore crucial for spatial control of microtubule organization over the cell cycle (Lüders and Stearns, 2007).

MTOCs vary greatly in shape, size and occurrence, both within a given cell and between species (Wiese and Zheng, 2006). Two structures were identified and visualized by electron microscopy as important MTOCs. These were the centrosome in animal cells and the spindle pole body (SPB) in yeast (Lüders and Stearns, 2007) (Section 1.6.2.2). In addition to centrosomes and SPBs, microtubules are also nucleated by transient cell cycle-regulated nucleation sites, such as fission yeast interphase and equatorial MTOCs (iMTOC and eMTOC, respectively) (Hagan and Petersen, 2000). Analogous to the eMTOC is the animal cell midbody, which also transiently nucleates microtubules (Wiese and Zheng, 2006).

The most intensively studied MTOC is the centrosome. This structure is composed of two centrioles that are surrounded by an electron-dense matrix, the pericentriolar material (PCM). The canonical centriole is a barrel-shaped cylinder composed of nine microtubule triplets whose function and importance is still not clear, since many fungi and higher plants lack centrioles in their MTOCs (Bettencourt-Dias and Glover, 2007; Lüders and Stearns, 2007). The capacity of centrosomes to anchor and nucleate the microtubule arrays resides in the PCM. One of the most important PCM proteins is γ-tubulin. This tubulin isotype is present in a large ring-shaped complex referred to as the γ-tubulin ring complex (γTuRC). This complex has two main

functions: 1) to stabilize the microtubules by capping the minus-ends, thereby preventing depolymerization (Wiese and Zheng, 2000) and 2) to serve as a template for microtubule nucleation (Keating and Borisy, 2000).

1.4 Cell cycle-dependent microtubule organization

1.4.1 Microtubule organization and dynamics in interphase

In most eukaryotic cells in interphase, microtubules form an extensive web of filaments that extend from the cell center to its periphery, exhibiting aster-like arrays. Thus, microtubule webs are denser around the nucleus than at the cell border. These microtubule arrays are usually very dynamic and composed of microtubule bundles held together by a variety of motor and bundling proteins (Section 1.5). Microtubules grow from the centrossome, generally located near the nucleus, until they find the cell border. Because catastrophe rate at the cell margin is higher than in the cell interior, microtubules tend to pause or undergo catastrophe once they touch the cellular membrane, but not while they are growing in the cytoplasm. However, rescue rate is also higher at the cell periphery and so microtubule depolymerization all the way to the centrossome is a relatively rare event (Komarova *et al.*, 2002). As a consequence, most of the microtubule plus-ends undergo repeated cycles of polimerization/depolymerization, generating persistently dynamic microtubule plus-tips at the cell margin.

This dynamic instability is tightly regulated by proteins associated with the microtubules, although some *in vitro* studies suggested that the pushing forces exerted by microtubules at cell border may also induce catastrophic events (Janson *et al.*, 2003)(Section 1.5).

In addition to aster-like arrays, microtubules are also present in asymmetric arrangements, like those seen in neuronal axons or flagellar axonemes. Microtubule arrays in these structures are much more stable and rely on their specialized and uniformly oriented microtubule assemblies (Baas *et al.*, 1988). These specialized neuronal arrays arise from the interplay between very unique subsets of tubulin only expressed in neurons, specific tubulin post-translational modifications and neuronal microtubule-associated proteins that play an important role in microtubule stabilization (Ramírez *et al.*, 1999).

1.4.2 Microtubule organization and dynamics in mitosis

At the transition from interphase to mitosis, a dramatic rearrangement of microtubule organization and dynamics occurs. The cytoplasmic array of microtubules disassembles and a completely different microtubule-based structure starts to assemble: the mitotic spindle.

1.4.2.1 The structure of the mitotic spindle

The heart of cellular division lies in the mitotic spindle. This fusiform structure is composed of an antiparallel microtubule array with their minus-ends focused at the poles and the plus-ends at the cell's equator. Its function is to correctly separate the sister chromatids into opposite sides of the cell. To accomplish this purpose a coordinated interaction between chromosome and microtubules is necessary. This interaction is mediated by the kinetochore, a specialized protein structure located at the chromosome. In animal cells, 20 to 30 bundled microtubules make end-on attachments that connect the kinetochore to the centrosome. These bundled microtubules are called the kinetochore fibers (K-fibers) (Walczak and Heald, 2008).

However microtubules at the K-fibers are only a subpopulation of all microtubules present in the mitotic spindle. The vast majority are the interpolar microtubules. These come from opposite ends of the mitotic spindle and interdigitate at the spindle equator, conferring stability to the spindle. Extending away from the centrosomes are the astral microtubules that have an important role in mitotic spindle positioning within the cells (Mastronarde *et al.*, 1993; Winey and O'Toole, 2001; Wittmann *et al.*, 2001).

1.4.2.2 Mitosis in higher eukaryotes

The initial steps for spindle assembly rely on centrosome duplication and motor-dependent separation of the two centrosomes to opposite ends of the prophase nucleus (Maiato *et al.*, 2004). The subsequent nuclear envelope breakdown (NEB) in prometaphase allows the centrosome-nucleated microtubules to enter the nuclear space and become attached to chromosome kinetochores. These became bi-oriented and move to the mitotic spindle's equator. This arrangement is known as the metaphase plate and corresponds to the proper chromosome alignment in the cell center, where chromosome oscillation occurs within a relatively short region of the cell. This alignment prior to chromosome segregation is important to ensure synchronous

chromosome separation during anaphase. Anaphase has been traditionally divided into anaphase A and B, despite the fact that in many organisms these two phases cannot be temporarily distinguished. In anaphase A the sister chromatids separate to opposing spindle poles whereas anaphase B consists of spindle elongation towards opposite sides of the cell, further separating the genetic material of the future daughter cells. Finally, during telophase, the genetic material from the two daughter cells decondenses and the two new nuclei form. A cleavage furrow forms between the two cells and contraction of the cleavage furrow divides the cytoplasm during cytokinesis.

Mitosis is a complex and highly controlled process that involves several proteins. However, understanding how these proteins function and are regulated; when, where and how they interact with each other, is still a major biological challenge. Many large-scale studies have been undertaken to address this question, but they are only a starting point for the major work that still remains to be done (Goshima *et al.*, 2005b; Neumann *et al.*, 2006; Walczak and Heald, 2008).

1.4.2.3 Microtubule's dynamic properties change during mitosis

Microtubule dynamics change dramatically in a cell cycle-dependent way. Live analysis of GFP-EB1 allowed the measurement of microtubule dynamics during mitosis. These studies revealed that before NEB in early prophase, microtubule growth rates are increased. Also, while microtubules in the vicinity of the nucleus are stable, those growing away from the nucleus become shorter. This fact suggests that microtubule transition frequencies are altered, promoting microtubule destabilization away from the nucleus (Piehl and Cassimeris, 2003). As a consequence, upon NEB, there is a dramatic decrease in microtubule polymer levels. Nevertheless, the higher nucleating capacity of the centrosome results in the highly dynamic microtubules seen in early mitosis. At this point, the mitotic spindle starts to form until it achieves the fusiform structure characteristic of a metaphase cell (Section 1.4.2.1). Metaphase microtubules are not static. Instead, they show treadmilling (Section 1.3.3), also known as microtubule poleward flux. This implies that microtubules are constantly being polymerized at their plus-ends and depolimerized at their minus-ends (Danuser and Waterman-Storer, 2003; Kline-Smith and Walczak, 2004). It is probable that K-fibers exhibit different dynamics from interpolar microtubules. Several studies have indicated that K-fibers might be significantly more stable than non-kinetochore microtubules. Nevertheless, kinetochore microtubule plus-ends are

highly dynamic. Chromosome oscilation in metaphase is thought to be due to constant polymerization/depolymerization at the microtubule-kinetochore interface (Maiato *et al.*, 2004).

In order to allow chromosome segregation, the metaphase steady-state has to be perturbed upon entry into anaphase. During this process, microtubule turnover decreases significantly. It is not yet well understood how chromosomes are segregated during anaphase A, and several models exist to explain this process (Maiato and Lince-Faria, 2010). One of the most widely accepted models is the "Pac Man model", where chromosome segregation in anaphase A is coupled to kinetochore plus-end depolymerization. However, a slow poleward flux of K-fibers still exists, indicating that depolymerization takes place at the minus-end. Upon entry into anaphase B, spindle depolymerization at microtubule minus-ends stops, and the bundled overlapping microtubules in the spindle mid-zone start to slide on each other. At the same time, tubulin polimerization occurs preferentially at the microtubule plus-ends, allowing spindle elongation (Kline-Smith and Walczak, 2004). In late anaphase the spindle disassembles and a major microtubule re-organization has to occur to promote the formation of the normal cytoplasmic microtubule array in the newly-formed cells.

1.5 Microtubule associated proteins - MAPs

Purified microtubules *in vitro* can reconstitute the dynamic properties of *in vivo* microtubules, like treadmilling or dynamic instability. However, within interphase cells, microtubules can be more dynamic than those assembled *in vitro* (Desai and Mitchison, 1997). Additionally, transition frequencies from growth to catastrophe can be very different. This suggested that cellular factors regulate microtubule dynamics *in vivo*. This function is performed by a specialized group of proteins that associate with microtubules, the microtubule associated proteins (MAPs). These can be divided into several groups: motors, bundlers, microtubule destabilizers and microtubule stabilizers.

1.5.1 Microtubule motors

Molecular motors use the energy from ATP hydrolysis to carry out mechanical work, generally in the form of movement along microtubules. They participate in a variety of functions in the cells, namely transport of cargoes, microtubule organization and microtubule plus-ends destabilization (Vale, 2003; Bartolini and Gundersen, 2006; Moores and Milligan, 2006;

Hirokawa *et al.*, 2009). There are two main classes of microtubule motors: kinesins and dyneins (Vale, 2003). Dyneins exist in the cytoplasm (cytoplasmic dynein), where together with dynactin, they mediate minus-end-directed transport; or within the integral structure of the axonemes (axonemal dynein) (Nicastro *et al.*, 2005; Pfister, 2005). Cytoplasmic dynein is a large multi-subunit complex (1.2MDa) composed of two identical dynein heavy chains (DHC) and several other associated chains, some of which govern its many associations with the different cargoes (Vale, 2003). Kinesin superfamily proteins (KIFs) are a large and heterogeneous group of motor proteins. The typical kinesin is a dimer consisting of two globular motor domains that also contain the binding sites for microtubules. The globular domains are generally followed by a flexible neck region, which is connected to a long α-helical stalk ending in a tail region involved in cargo binding. KIFs comprise several families that can be broadly grouped into three classes, depending on the localization of the motor domain. If the motor domain is localized N-terminally, kinesins are termed N-kinesins. M-kinesins have the motor domain in the middle and C-kinesins have the motor domain in the carboxy-terminal region. This is important, because in general, N-kinesins display plus-end-directed motility, C-kinesins tend to have minus-end-directed motility and M-kinesins depolimerize microtubules (for example, kinesin 13, Section 1.5.3).

1.5.2 Microtubule bundlers

The function of microtubule bundlers is to organize microtubule bundles by fixing microtubules to each other, in an unrestrained way. These proteins form electron-dense bridges between microtubules, keeping a regular spacing and orientation in relation to each other (Chan *et al.*, 1999; Roque *et al.*, 2010). The main group of proteins responsible for this function is the Map65/Ase1/PRC1 family. This family plays important roles in mitosis, by ensuring the stability of the spindle's mid-zone (Mollinari *et al.*, 2002; Schuyler *et al.*, 2003; Verbrugghe and White, 2004; Loïodice *et al.*, 2005) and in interphase, by promoting microtubule bundle organization (Loïodice *et al.*, 2005).

1.5.3 Microtubule destabilizers

Microtubule destabilizers are very important because they allow a rapid re-structuring of the microtubule network in response to external or internal clues. These proteins include the stathmin (also known as oncoprotein-18, Op18), the katanin and spastin families, as well as the

kinesin-13 family. Stathmin promotes microtubule destabilization either by sequestering microtubule dimers or by stimulating plus-end catastrophes (Howell *et al.*, 1999a; Howell *et al.*, 1999b). Additionally, the katanin and spastin family destabilize microtubules by severing, while kinesin-13 family members use the hydrolysis of ATP to bind protofilaments and peel them apart (Moores *et al.*, 2006; Moores and Milligan, 2006).

1.5.4 Microtubule stabilizers

Microtubule stabilizers comprise several protein families, such as the Dis1/XMAP215 family, the CLASP family, the EB family or the CLIP-170 family. Their main functions are microtubule stabilization, promotion of growth and microtubule-cortex interactions. Most of the stabilizing MAPs associate with more than one tubulin heterodimer, stabilizing the straight conformation of tubulin subunits and cross-linking and trapping the subunits into the lattice. The CLASP, EB1 and CLIP-170 families belong to a special subgroup of microtubule stabilizers, the +Tips, because they accumulate specifically at microtubule plus-ends (Sections 1.5.4.2 and 1.5.4.3).

1.5.4.1 +Tips accumulate specifically at microtubule plus-ends

Microtubule +Tips are a very diverse group of proteins whose main feature is the fact that they accumulate specifically at microtubule plus-tips. In general they form comet-like dashes that move through the cell together with the growing microtubule end. Most +Tips are involved in regulating microtubule dynamics, and their localization is ideally suited for this function. In this respect, some +Tips promote growth (e.g. XMAP215 and EB1) others catastrophes (e.g. kinesin-13, MCAK), rescues (e.g. CLIP-170) or stabilizing interactions between microtubules and the cell's cortex (e.g. CLASPs) (Akhmanova and Steinmetz, 2010). Besides, +Tips also have important functions in coordinating microtubule attachment to mitotic kinetochores (e.g. CLIP-170 and CLASPs) or contributing to the loading of cargo for minus-end directed-motors. Additionally, +Tips contribute to the organization of microtubule bundles (e.g klp2p, Section 1.6.2.2.2) or mitotic spindles, e.g. *Drosophila* kinesin-14, Ncd (Goshima *et al.*, 2005b). Finally +Tips also accumulate at centrosomes and/or MTOCs, although their role in these structures remains obscure.

How +Tips track the microtubule plus-ends is not well understood. Current hypotheses are that +Tips recognize the microtubule GTP cap or some specific protofilament arrangement, like the tubulin sheets present at microtubule plus-ends (Sandblad *et al.*, 2006). However, most +Tips do not track plus-ends in an autonomous manner. In fact, many +Tips are targeted to growing ends via their association with EB proteins, which autonomously track plus-tips, making EB proteins the core components of +Tip networks (Busch and Brunner, 2004; Bieling *et al.*, 2007; Bieling *et al.*, 2008). Plus-end directed kinesins are also involved in the accumulation of some +Tips at the tip of microtubules. Well-studied examples are the yeast CLIP-170 homologues, tip1p and BIK1, which require the kinesins tea2p and KIP2 to concentrate at plus-ends (Busch and Brunner, 2004; Carvalho *et al.*, 2004; Bieling *et al.*, 2007; Dixit *et al.*, 2009).

1.5.4.2 The CLIP-170 family of +Tips

Citoplasmic linker protein 170 (CLIP-170) was first discovered as a MAP with a molecular weight of 170kDa and it was later identified as the first +Tip (Rickard and Kreis, 1990; Perez *et al.*, 1999).

All proteins in the CLIP-170 family have a basic N-terminal head that comprises a Cap-Gly domain and a serine-rich region, followed by a long central coiled-coil region and an acidic C-terminal metal-binding domain ("zink knuckle") (Pierre *et al.*, 1992; Pierre *et al.*, 1994). The head, through the Cap-Gly domain, is responsible for CLIP-170 localization at microtubule plus-ends. This occurs via the interaction of this Cap-Gly domain with tubulin and EB1, by specifically recognizing EB protein family C-terminal EEY/F sequence motifs (Honnappa *et al.*, 2006). Nevertheless, the serine-rich regions are also necessary for CLIP-170 localization, and they play an essentially regulatory role (Gupta *et al.*, 2009; Lee *et al.*, 2010) (Section 1.7.1.1). The long central coiled-coil allows protein homodimerization, although it can also provide binding interfaces for some protein-protein interactions (Miller *et al.*, 2006). Finally, the acidic C-terminal region, besides being also involved in mediating protein interactions (e.g. $p150^{Glued}$ and LIS1), is additionally involved in the inhibitory head-to-tail CLIP-170 interaction with itself (Lansbergen *et al.*, 2004; Miller *et al.*, 2006). Yeasts have only one CAP-Gly and "zink knukle" domain, whereas higher eukaryotes have two, but the functional significance of these facts still awaits further elucidation (Brunner and Nurse, 2000).

1.5.4.2.1 CLIP-170 spatially controls microtubule dynamics in interphase

CLIP-170 was initially identified as a factor that linked endocytic vesicles to microtubules, suggesting that CLIP-170 belonged to a class of cytoplasmic linker proteins (CLIPs) that mediate interaction between organelles and microtubules (Pierre *et al.*, 1992).

However, CLIP-170's striking effects on microtubule dynamics were recognized several years later (Pierre *et al.*, 1994; Perez *et al.*, 1999; Brunner and Nurse, 2000; Komarova *et al.*, 2002; Arnal *et al.*, 2004). Early studies in HeLa cells showed that when over-expressed, CLIP-170 binds the microtubule lattice, promoting its bundling into think rings that surround the nucleus. Later studies confirmed the microtubule-stabilizing effect of CLIP-170. It was also shown that the effect of CLIP-170 is local, i.e., the stabilizing effect on the microtubule depends on where the microtubule is in the cell (Brunner and Nurse, 2000; Komarova *et al.*, 2002) (Section 1.6.2.3.1). In mammalian cells, over-expression of a CLIP-170 dominant negative mutant revealed highly reduced rescues at the cell periphery, implying that microtubule rescues specifically at the cell border are no longer taking place. This results in symmetrical distribution of microtubule plus-ends throughout the cell and a significant decrease in the average lifetime of a microtubule (Komarova *et al.*, 2002).

1.5.4.2.2 CLIP-170 may play a role in the kinetochore-microtubule interface

During mitosis, CLIP-170 colocalizes with tubulin at the centrosomes, along the mitotic spindle and at the astral microtubules and midbody (Li *et al.*, 2010). It accumulates at astral microtubule tips in anaphase and strongly at kinetochores in prometaphase. In contrast, CLIP-170 kinetochore accumulation during metaphase is weak. It was suggested that CLIP-170 binds to misaligned chromosomes, but not to properly aligned chromosomes (Dujardin *et al.*, 1998; Maiato *et al.*, 2004). Further studies showed that CLIP-170 is recruited to unattached kinetochores, but it is displaced upon kinetochore binding to the microtubules. Despite the fact that the severity of CLIP-170 RNAi defects varies from study to study, they suggest an important role for CLIP-170 in early mitosis (Wieland *et al.*, 2004; Tanenbaum *et al.*, 2006; Yang *et al.*, 2009). Reported effects of CLIP-170 RNAi range from problems with chromosome alignment to more severe defects, like multipolar spindles and lagging chromosomes that lead to mitotic blockage, and subsequent cell death (Wieland *et al.*, 2004; Tanenbaum *et al.*, 2006).

1.5.4.3 The EB protein family

End binding protein 1 (EB1) was first described as an adenomatous polyposis coli (APC) interacting protein (Su *et al.*, 1995). This association has been extensively studied, because the loss of the APC-EB1 binding site is associated with malignant colon tumors (Su *et al.*, 1995; Tirnauer and Bierer, 2000; Fodde *et al.*, 2001).

EB1 is highly conserved in eukaryotes, with homologues identified in all eukaryotes. Its domain architecture is widely conserved across all family members. Crystal structure of the highly conserved EB1 N-terminus (amino acids 1-130) showed that this region is globular and composed of six α-helices containing the so-called calponin homology (CH) domain (Hayashi and Ikura, 2003). EB family members have a single CH domain (amino acid 15-116 as calculated by SMART (http://smart.embl-heidelberg.de/). Tandem CH-domains are well known as the actin-binding domains of several F-actin binding proteins. However, pairs of CH domains, formed for example by the homodimerization of a CH-containing protein, confer binding to microtubules. This is what happens with EB1, which is a homodimer where the N-terminal globular domain plays an essential role in the ability to bind microtubules (Barth *et al.*, 2002; Bu and Su, 2003). The nature of this interaction is likely to have hydrophobic and electrostatic contributions, where the last are likely mediated by the net positive charge of the microtubule binding motifs and the acidic tubulin C-terminal tail (Hayashi and Ikura, 2003; Zanic *et al.*, 2009).

The globular N-terminal domain is connected via an unstructured and disordered linker of approximately 50 amino acids, to a more conserved region that contains the coiled-coil (residues 191-225) region, which in turn overlaps with the EB1 motif signature (residues 209-248). The linker region, which is also serine-rich, is important for EB1 binding, and may have important regulatory roles (Des Georges *et al.*, 2008)(Section 1.7.1.2). EB1 homodimerization occurs via its EB1-like domain (Rehberg and Gräf, 2002; Honnappa *et al.*, 2005). The EB1 signature is also the region where many EB1-interacting proteins, like APC or $p150^{Glued}$, bind (Su *et al.*, 1995; Honnappa *et al.*, 2005). The corresponding domain in fission yeast, mal3p, mediates binding with tip1p (Busch and Brunner, 2004; Busch *et al.*, 2004).

Finally, the flexible unstructured C-terminal tail (residues 249-263) is important for binding of EB1 to its specific partners. Additionally, it is also responsible for an auto-inhibitory state of EB1, since EB1 mutants lacking the C-terminal tail bind more efficiently to microtubules (Manna *et al.*, 2008).

1.5.4.3.1 The EB1 family binds with its interactor proteins via the EB1 domain and the C-terminal tail

EB1 interacts with several proteins and has recently emerged as a master regulator of dynamic +Tip interaction networks. This is mainly due to two reasons: 1) EB1 can autonomously track microtubule plus-tips and 2) Many +Tips are targeted to microtubule plus-ends via their association with EB1. It is thus interesting to know how EB1 can bind to so many different proteins and how this binding is regulated. It turns out that many EB1-binding proteins contain a short polypeptide motif, Ser-x-Ile-Pro (SxIP), which upon EB1 binding becomes deeply buried in the hydrophobic cleft of the EB1-like domain (Figure 1.4).

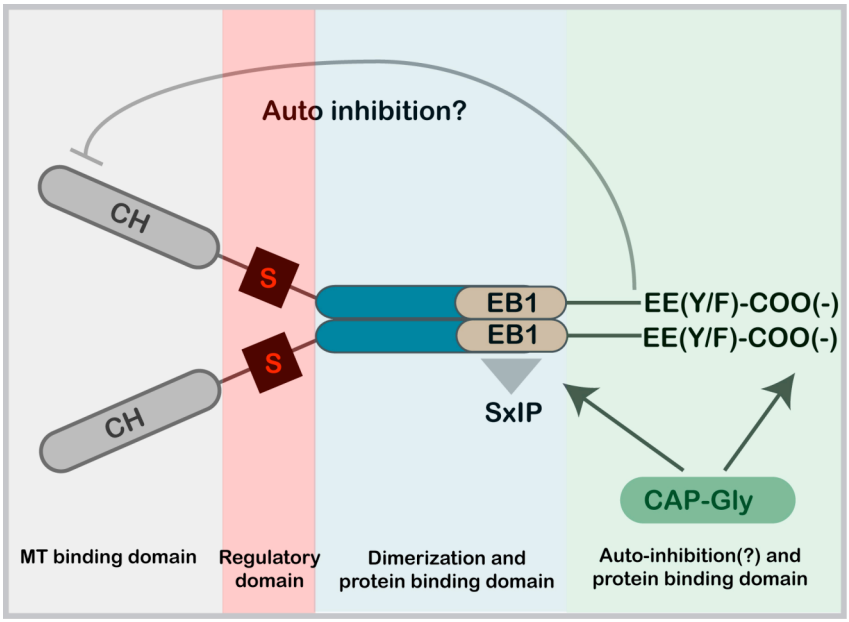

Figure 1.4: EB1 modular architecture. Members of the EB protein family are composed of several domains. Calponin homology domains (CH) are responsible for EB1 microtubule binding. These domains are linked, via an unstructured serine-rich linker, to the EB1 coiled-coil C-terminus that contains the EB1 domain responsible for protein homodimerization. The EB1 domain also serves as a platform for many EB1 binding partners. Many of these proteins contain the SxIP signature that interacts with EB1's hydrophobic cleft. An example of this is the CAP-Gly-containing proteins (e.g. CLIP-170 or p150-Glued), which bind EB1 though the SxIP motif. However, the C-terminal flexible acidic tail of EB1 also plays an important role in this interaction, since it interacts and becomes stabilized upon CAP-Gly binding. Finally it has been proposed that EB1 has a head-to-tail auto-inhibition mechanism that may be released after $p150^{Glued}$ dimer binding (Adapted from Tomasz Zimniak, PhD thesis, 2010).

This motif is present in several EB1-binding proteins, like APC, MACF, CLASP or CLIP-170, in the region through which these proteins are known to bind to EB1. Furthermore, the importance of the SxIP motif for EB1 binding has already been confirmed by mutagenesis and structural analysis for APC, MACF43 and CLASP2 (Honnappa *et al.*, 2005; Honnappa *et al.*, 2009). Importantly, these interactions seem to be controlled by phosphorylation in the vicinity of the SxIP motif.

However, residues on the flexible acidic tail also play an important role in EB1 binding to other proteins (Honnappa *et al.*, 2009). Although a crystallographic analysis was not possible for the acidic tail of EB1, structural studies of the complex formed between EB1's acidic tail and the CAP-Gly domain of p150Glued were possible. It was observed that the $p150^{Glued}$ CAP-Gly interacted and stabilized EB1's acidic tail. The last three amino acids of EB1, EEY-COO^-, played an important role in this interaction, being inserted deep at the highly conserved groove of CAP-Gly domain (Figure 1.4). Based on more extensive sequence alignment, the motif EEY/F-COO^- was deduced and shown to be a general motif-binding site for CAP-Gly domains to EB proteins (Honnappa *et al.*, 2006).

1.5.4.3.2 EB1 localizes on microtubules at all stages of the cell cycle

EB1 localizes on microtubules at all stages of the cell cycle. During mitosis, EB1 localizes on centrosomes, spindle microtubules, plus-ends of astral microtubules and midbody (Figure 1.5, Table 1.1). During interphase it localizes on the centrosome and weakly along the microtubule lattice, presumably due to its localization at the microtubule seam (Section 1.5.4.3.3). EB1 also strongly accumulates at the microtubule plus-tips, forming the comet-like shape characteristic of most +Tips (Mimori-Kiyosue *et al.*, 2000; Schuyler and Pellman, 2001). An interesting exception occurs in *Xenopus* egg interphase extract, where EB1 localizes all along the microtubule lattice, and only forms the comet-like shapes at microtubule plus-tips in mitotic extracts (Tirnauer *et al.*, 2002b). Plus-tip EB1 accumulation is seen only in growing microtubules, since EB1 disappears prior to microtubule catastrophe (Mimori-Kiyosue *et al.*, 2000). Thanks to this, EB1 proteins are currently widely used for *in vivo* detection of growing microtubules and microtubule plus-tips.

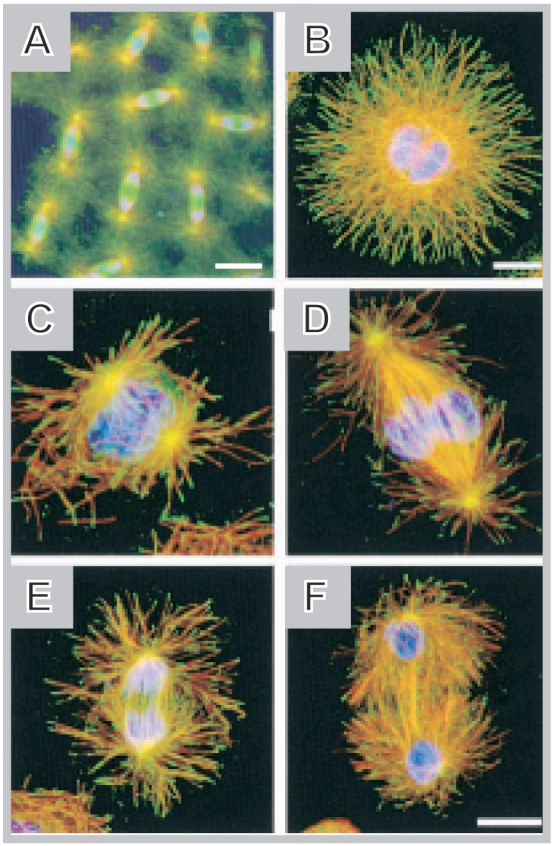

Figure 1.5: EB1 localization during the cell cycle. Immunofluorescent localization of DmEB1 (green), tubulin (red) and DNA (blue). (A) Drosophila synctitial blastoderm-stage embryos during anaphase. Scalebar= 10mm. (B-F) Drosophila S2 cells in interphase (B), prophase (C), metaphase (D), anaphase (E) and telophase (F). Scalebar= 5mm. Adapted from (Rogers *et al.*, 2002).

1.5.4.3.3 EB1 localizes at microtubule plus-tips and the microtubule seam

Proteins in the EB family autonomously track dynamic microtubules *in vivo* and *in vitro*, but how these proteins interact with microtubules and particularly how they recognize microtubule plus-ends is still not well understood. FRAP studies have shown that EB1 turnover at microtubules is very fast. However, the fraction of EB1 that binds the lattice had slower recovery times than the population bound at the tips and so it was soon hypothesized that EB family proteins bind to the microtubule lattice and microtubule tips by independent mechanisms (Tirnauer *et al.*, 2002a).

Structural studies using high resolution surface shadowing and electron microscopy have shown that the fission yeast EB1 homologue, malp3p, shows a preference for localizing at the A-lattice configuration seen along the microtubule seam (Sandblad *et al.*, 2006)(Section 1.3.2). Additionally, both EB1 and mal3p promote sheet closure into tubes over the open sheet conformation, an intermediate that forms during microtubule polymerization *in vitro* (Sandblad *et al.*, 2006; Vitre *et al.*, 2008). These data strongly suggest that mal3p stabilizes microtubules by

reinforcing the lateral interaction between adjacent protofilaments at the microtubule closure junction, though a zippering activity.

It is currently unknown which features of the growing microtubule plus-ends EB family proteins are recognizing. Nonetheless, the recognition of the GTP cap may be a plausible hypothesis. In fact, EB1 seems to preferentially bind GTP tublin, since microtubules polimerized using GMPCPP-tubulin, a slowly hydrolysable analogue of GTP-tubulin, caused EB1 to bind throughout the microtubule lattice (Zanic *et al.*, 2009).

1.5.4.3.4 The EB protein family regulates microtubule dynamics

It was soon realized that EB protein family have a stabilizing effect on microtubules. However, the precise parameter(s) this class of proteins is affecting remains rather controversial. In all organisms studied so far, EB1 proteins are important to suppress microtubule pausing time (Tirnauer *et al.*, 1999; Tirnauer *et al.*, 2002b; Rogers *et al.*, 2008; Komarova *et al.*, 2009). Furthermore, in *S. cerevisiae* and *Drosophila,* EB family members are important to promote microtubule dynamicity by increasing both catastrophe and rescue frequency (Tirnauer *et al.*, 1999; Rogers *et al.*, 2008). However, in contradiction with these results, in interphase *Xenopus* egg extracts and in mammalian cells, EB1 decreases catastrophe frequency. Thus, in these systems, EB1 acts as an anti-catastrophe factor (Tirnauer *et al.*, 2002b; Komarova *et al.*, 2009).

In vitro, EB1 proteins can promote the polymerization of pure tubulin. It is therefore possible to evaluate the dynamic properties of microtubules assembled in the presence or absence of EB family proteins (Sandblad *et al.*, 2006; Vitre *et al.*, 2008). In these studies, the reported effects are also far from being consistent. In some studies EB1 stimulated both rescues and catastrophes, while in others it had little effect on microtubule dynamics. Similarly, in some studies EB1 suppressed catastrophes whereas in others it had little or no effect on catastrophic events (Bieling *et al.*, 2007; Manna *et al.*, 2008; Vitre *et al.*, 2008; Dixit *et al.*, 2009; Katsuki *et al.*, 2009; Komarova *et al.*, 2009). These differences may be explained by different assay conditions.

It was also puzzling at first how in yeasts, the loss of EB family proteins resulted in shorter cytoplasmic microtubules, whereas in higher eukaryotes, like *Drosophila*, mammalian or *Xenopus* egg extracts this effect was not observed (Tirnauer *et al.*, 1999; Tirnauer *et al.*, 2002b; Rogers *et al.*, 2008; Komarova *et al.*, 2009). These observations can be explained by the fact that higher eukaryotes have three members of the EB protein familiy: EB1, EB2 and EB3. These proteins have partially redundant functions, as depletion of EB1 together with EB3 in mammalian

cells had dramatic effects on microtubules that were not observed for EB1 depletion alone. Interestingly, depletion of all members compromised cell viability (Komarova *et al.*, 2009).

EB family proteins may also contribute to microtubule bundling, since their over-expression induced microtubule bundling in both *Xenopus* egg extracts and mammalian cells (Bu and Su, 2001; Tirnauer *et al.*, 2002b). Furthermore, EB family proteins may be functional components of the centrosome (Louie *et al.*, 2004; Yan *et al.*, 2006). EB1 localizes at the centrosome, with higher accumulation in mitosis, showing a preference for the mother centriole (Louie *et al.*, 2004). It has been implicated in microtubule anchoring to the centrosome and is important for non-delayed microtubule nucleation from this structure during microtubule re-growth assays (Askham *et al.*, 2002; Louie *et al.*, 2004; Yan *et al.*, 2006). Despite the fact that, *in vitro*, high concentrations of EB1 seem to stimulate spontaneous microtubule nucleation, experiments in *Xenopus* egg extracts didn't find nucleation ability for EB1 (Popov *et al.*, 2002; Vitre *et al.*, 2008). Also, EB1 imunodepletion from mitotic *Xenopus* egg extracts caused microtubules nucleated from centrosomes to be much shorter (Tirnauer *et al.*, 2002b). Taken together, these facts suggest that the function of EB1 at the centrosomes resides more probably in the stabilization of nascent microtubules rather than in promoting microtubule nucleation.

1.5.4.3.5 Depletion of EB1 results in mitotic defects

EB1 localization and its important functions, both in regulating microtubule dynamics and as a scaffold for the proper localization of many proteins at the microtubules, suggest that EB1 should play a role in mitosis. Several studies have confirmed this idea, as it is summarized in Table 1.1. Generally, EB family proteins localize at the tips of growing astral and spindle microtubules, along the spindle, and at the centrosomes. They have also been localized at the kinetochores.

Depletion of EB1 usually results in mitotic defects in most studied organisms, the most common being a reduction of spindle size, chromosome segregation defects and cell cycle arrest. A reduced length of the spindle is likely to occur via the microtubule-stabilizing properties of EB1, since knockdowns of microtubule depolimerases caused spindle expansion (Goshima *et al.*, 2005a). On the other hand, mis-segregation defects are likely to occur because EB1 targets kinetochores in late-prometaphase in one study and in the metaphase to anaphase transition in another study (Tirnauer *et al.*, 2002a; Srayko *et al.*, 2005). EB1 localization at the kinetochore-microtubule interface seems important for proper kinetochore-microtubule attachment, since upon

EB1 RNAi the tension generated between sister kinetochores in metaphase cells drops considerably (Green *et al.*, 2005). These reported defects in chromosome segregation are likely to activate the spindle checkpoint leading to the prometaphase/metaphase arrest seen in some organisms in the absence of EB1 (Table 1.1). Intriguingly, in mammalian cells a cell cycle arrest is not observed despite the fact that EB1 RNAi-treated cells show misaligned chromosomes. Treatment of these cells with nocodazole activates the spindle checkpoint, showing that checkpoint is functional in EB1 RNAi-treated cells (Green *et al.*, 2005). These findings are similar to previous work on APC, which showed that APC mutations can modulate but not eliminate spindle checkpoint function. This results in chromosome instability but this process is not yet understood (Tighe *et al.*, 2004).

Finally, and again consistent with its stabilizing role on microtubules, depletion of EB1 also results in abnormal astral microtubules. Because astral microtubules are important for proper spindle positioning, the phenotypes observed for spindle mis-positioning in the absence of EB1 are expected (Tolić-Nørrelykke *et al.*, 2004; Kozlowski *et al.*, 2007). The random spindle orientation relative to the mother-bud axis seen in *S. cerevisiae* BIM1 mutants is also well-documented. In this case BIM1 is necessary for the proper localization of KAR9 at microtubule plus-tips, and the BIM1-KAR9-MYO2 complex is responsible for ensuring nucleus migration towards the bud neck, an important mechanism for the proper alignment of the mitotic spindle in this place (Paoletti and Bornens, 2003).

Despite all these studies on the functions of EB family proteins in mitosis, the molecular mechanisms underlying the observed mitotic defects are still not known. Furthermore, these studies are very crude for two main reasons. 1) Mitotic phenotypes in higher eukaryotes are probably more severe than those reported, since most studies used EB1 RNAi only, without also knocking down EB2 and EB3. Consistent with this is the fact that simultaneous RNAi of EB1, EB2 and EB3 in mammalian cells is lethal (Komarova *et al.*, 2009). 2) EB1 is recently emerging as an important scaffold for proper localization of many proteins at the microtubules. It is thus possible that depletions of EB1 may also cause other proteins to mis-localize, and so the effects seen on these studies are most likely not all a direct consequence of EB1 absence *per se*.

Table 1.1: Comparison of EB1 induced effects during mitosis in several model organisms.

	Mamalian	*Drosophila*	*Xenopus*	*Dictyostelium*	Sea urchin	*S. pombe*	*S. cerevisiae*
References	(Berrueta *et al.*, 1998)[1] (Morrison *et al.*, 1998)[2] (Bu and Su, 2001)[3] (Fodde *et al.*, 2001)[4] (Tirnauer *et al.*, 2002a)[5] (Green *et al.*, 2005)[6] (Piehl *et al.*, 2004)[7] (Ban *et al.*, 2009)[8]	(Lu *et al.*, 2001)[1] (Rogers *et al.*, 2002)[2] (Goshima *et al.*, 2005b)[3] (Buster *et al.*, 2007)[4]	(Mimori-Kiyosue *et al.*, 2000)[1] (Tirnauer *et al.*, 2002b)[2] (Kronja *et al.*, 2009)[3]	(Rehberg and Gräf, 2002)[1]	(Strickland *et al.*, 2005)[1]	(Asakawa *et al.*, 2005)[1] (Beinhauer *et al.*, 1997)[2]	(Schwartz *et al.*, 1997)[1] (Tirnauer *et al.*, 1999)[2]
Technique	Imunostaining with anti-EB1 in cultured mammalian cells[1, 2] Imunostaining with anti-EBF3 in cultured mammalian cells[3] Imunostaining with anti-EB1 antibody in embryonic steam cells[4] Microinjection of labelelled EB1 in cultured mammalian cells[5] EB1 RNAi in cultured mammalian cells[6] EB1-GFP in LLCPK cells[7] Imunostaining GFP-EB3 in mammalian cells[8]	DmEB1 RNAi on *Drosophila* embryos[1] Imunostaining with anti-EB1 in S2 *Drosophila* cells[2a] or in *Drosophila* synctitial embryos[2b] DmEB1 RNAi S2 *Drosophila* cells[2c,3,4] Microinjection of anti-DmEB1 antibodies in Drosophila synctitial embryos[2d]	EB1 depletion from *Xenopus* mitotic extracts[3] Labeled EB1 added to interphase or mitotic *Xenopus* extracts[2] Xenopus A6 epithelial cells[1]	Imunostaining with anti-EB1 antibody[1a] DdEB1 null mutant[1b]	Microinjection of GFP-EB1 into fertilized eggs[1a] Microinjection of anti-anti-EB1 antibodies[1b]	mal3p-GFP[1a, 2a] *mal3Δ*[1b, 2b] mal3p over-expression[2c]	GFP-BIM1[1a,2a] Bim1Δ[1b,2b] BIM1 over-expression[1c, 2c]
Mitotic EB Localization	Prometaphase – Centrossome, MT plus tips[1,2,3,8]	Prometaphase – Centrossome, MT plus tips[2a]		Prometaphase: Centrossome[1a]	Spindle microtubules, centrossomes[1a]	Spindle microtubules and Spindle plus tips[1a] Spindle MTs, more	Spindle microtubules[1a] PreAnaphase: Spindle microtubules[2a]

	Metaphase/Anaphase: Centrossomes, spindle microtubules[1,2,3,5], midzone acumulation[,8] Telophase: Centrossomes, spindle MTs, accumulation at the midbody[1,2,3,8] Cytokinesis: weaker association with centrossomes and spindle microtubules[2,3,7,8]	Metaphase/Anaphase: Centrossomes, spindle microtubules[2a,2b] Telophase: Centrossomes, interpolar microtbule bundles and midbody[2a,2b]	Metaphase: Centrossomes, spindle microtubules[1] MT plus-ends in mitotic extracts[2]	Metaphase/Anaphase: Spindle microtubules[1a] Telophase: Spindle microtubules, kinetochore region[1a]		intense in early mitosis[2b] Localized to ring in the cell equator in post-anaphase[2a] Plus tips of MTs from post-anaphase array	PosAnaphase: Spindle microtubules, spindle midzone acumulation[2a]
	Plus-ends of astral MTs[2,3,5,8]	Plus-ends of astral MTs[2a, 2b]	Plus-ends of astral MTs[1]	Plus-ends of astral MTs[1a]	Plus-ends of astral MTs[1a]	Plus-ends of astral MTs[1a]	Plus-ends of astral MTs[2a]
Spindle Length	*NS*	Metaphase: 33% shorter[2d] Anaphase: 44% shorter[2d] ~30%[2c]shorter[,2c,2d,3]	40% Shorter[3]	*NS*	*NS*	*NS*	Short[1b]
Spindle MTs	Modest reduction of spindle midzone MTs[6]	Fewer MT in spindle[2c,2d]	Lower MT density at spindle equator[3]	*NS*	*NS*	*NS*	*NS*
Chromossome Segregation Defects	Loss of tension between sister kinetochores, lagging and misaligned chromossomes[6]	Lagging chromosomes[2d] Proper chromossome segregation failure[2d]	*NS*	Aneuploidy[1b]	*NS*	Yes[1b, 2b, 2c]	
Cell Cycle Arrest	No[6]	Metaphase arrest[2c] Telophase arrest[2c]	Metaphase arrest (depends on SAC)[3]	Prometaphase arrest[1b]	No	Metaphase arrest[1b] Mitotic arrest[2c]	Mitotic arrest[1c]
Absence of Astral MTs	Yes[6]	Yes[2c]	*NS*	*NS*	Required for astral MT elongation[1b]	*NS*	
Spindle Mispositioning	Yes[6]	Yes[1,2c]	*NS*	*NS*	*NS*	*NS*	Yes, random orientation relative to mother bud

							axis[1b,2b]
Poleward Flux	*NS*	25% slower[4]	70% slower[3]	*NS*	*NS*	*NA*	
Spindle Dynamics	*NS*	**Spindle elongation dynamics[2d]** P-$M_{Control}$:~0.03μm/s P-M:~0.015μm/s $A_{Control}$:~0.07μm/s A:~0.01μm/s	*NS*	**Time spend in each phase of mitosis[1b]** P-$M_{Control}$: 8min vs P-M: 2min A:unaffected	*NS*	**Time spend in each phase of mitosis[1b]** P-$M_{Control}$: 11.6min P-M: 18.4min $A_{Control}$: 15.6min A: 21.3min **Spindle elongation dynamics[1b]** $A_{Control}$:0.65μm/min A:0.46μm/min	**Spindle elongation dynamics[2b]** P-$M_{Control}$:~0.59μm/min P-M:~0.41μm/min $A_{Control}$:~0.22μm/min A:~0.18μm/min
Other Abnormalities		Monopolar spindles[2d] Unfocused "Barrel shape" spindles[2c] Spindle compactation[2c] Spindle detachment from centrosomes[2c,3] Failure to form normal intertoplar MT bundles[2d] Absence of midbody[2d]	30% more tripolar and multipolar spindles[3]	Deformed spindles[1b]		Septum and PAA mispositioning[2b] Broken or fraying spindles[2c] Cytokinetic deffects[2c] Elongated cells – cell cycle entry defect?[2c]	Karyogamy defects[1b] Lethality[1c] Undivided nuclei[1b,c] Impared nuclear migration[1b1c] Nuclear position defect relative to the bud neck[2b] Spindle abnormalities[1b,c,2b]

Legend: NS – not studied; P-M – Prophase-Metaphase; A - Anaphase

1.6 Schizosaccharomyces pombe

1.6.1 Schizosaccharomyces pombe cell cycle

S. pombe is a cylindrically shaped cell with a diameter of 3-4 μm and a length of 7-15 μm depending on cell cycle stage. Fission yeast spends most of its cell cycle in G2, growing until in reaches a critical size upon which mitosis is triggered (Figure 1.6A). In fact, cell size can be correlated with the stage at which the cell is in the cycle. Therefore, a popular way to synchronize cells is to select cells with the same size within a given population. Until now it was relatively unclear how the cell senses its size and triggers mitosis, but two recent papers, published by the Nurse and Chang laboratory, implicated the kinase pom1p as an important player in coupling cell size with cell cycle (Martin and Berthelot-Grosjean, 2009; Moseley *et al.*, 2009). In *S. pombe*, mitosis is closed, meaning that unlike in higher eukaryotes, there is no NEB. This requires that, as the SPB duplicates in early mitosis, it gets inserted into the nuclear envelope, allowing the subsequent formation of the mitotic spindle (Ding *et al.*, 1997). In anaphase, the duplicates of the three fission yeast chromosomes are separated to opposite sides of the cell and the septum starts to form. This leads to two newly formed cells during cytokinesis. Interestingly, DNA duplication coincides with septum formation and so the two daughter-cells emerge already in G2 with a duplicated genome. These newly-formed cells are very small, and grow monopolarly only from the old end, which existed already before mitosis. When the cells reach a certain size they start growing bipolarly, a phenomenon called new end take off (NETO). The new site of growth is opposite to the old end, allowing the cells to grow in a polarized way. Microtubules play an important role in the proper positioning of both growth sites (La Carbona, *et al*., 2006).

1.6.2 The fission yeast cytoskeleton

1.6.2.1 The fission yeast actin cytoskeleton

In fission yeast, actin, mainly in the F-actin form, is organized into actin cables and actin patches. The localization of these structures varies with the cell cycle, appearing mainly in places where active membrane extension and cell growth takes place, namely, at cell tips and at the cell division site (Figure 1.6A) (La Carbona *et al*., 2006, Chang and Martin, 2009).

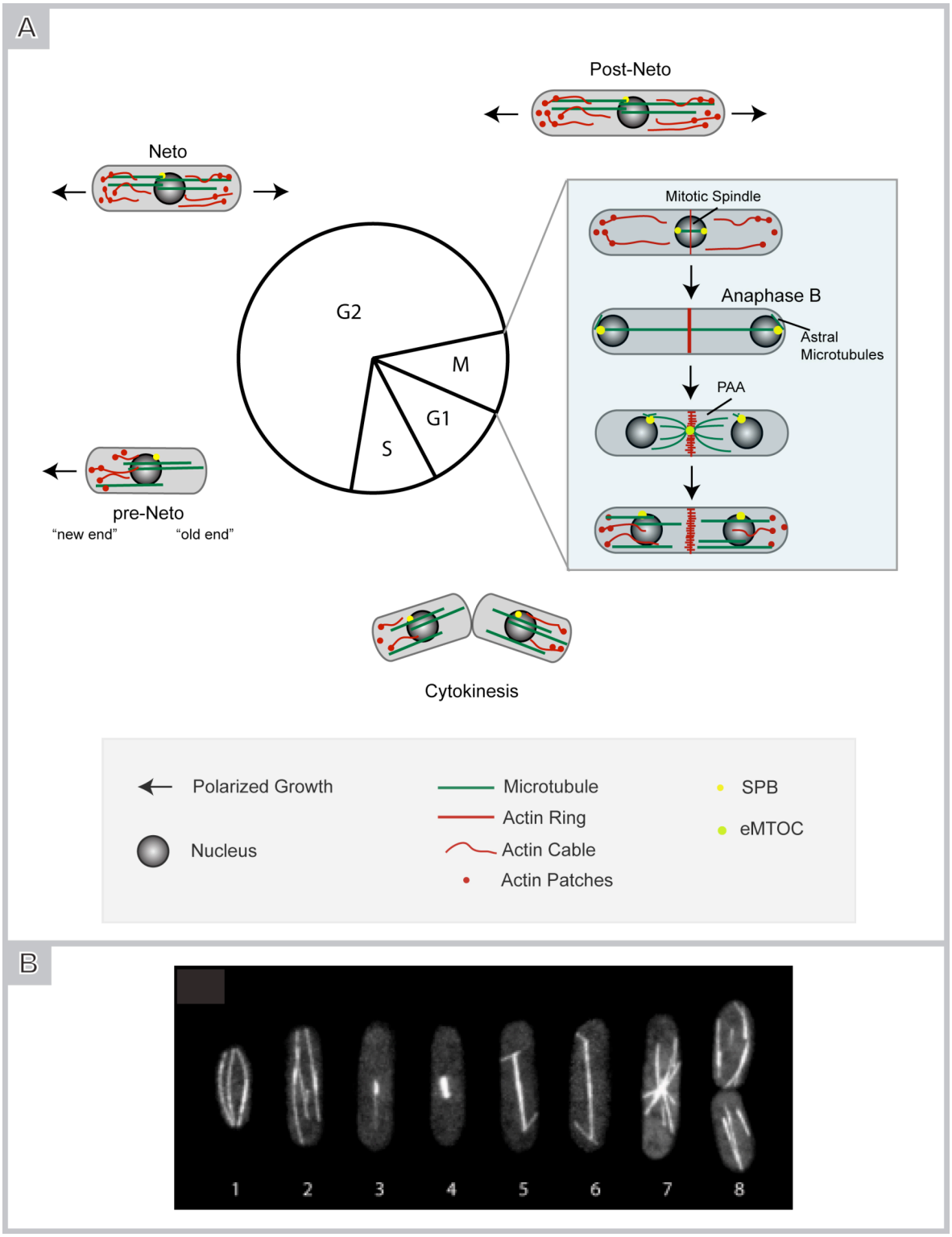

Figure 1.6: Cytoskeletal organization during the cell cycle. (A) Interphase *S. pombe* cells have three to five microtubule bundles that overlap with their minus-ends in the middle of the cell, whereas their plus-ends are located at the poles. Once the cell reaches a certain critical size, mitotic division starts with SPB duplication in late G2. In prophase the SPBs start to nucleate

microtubules which interdigitate to form a short mitotic spindle. There are three types of intra-nuclear microtubules: those which extend from one SPB to the other, those which interdigitate in the spindle mid-zone and those which terminate in an "amorphous material", chromatin (Sagolla *et al.*, 2003). The spindle then elongates to span the nucleus in prometaphase. At the same time, cytoplasmic astral microtubules extend tangentially from the SPB to the cytoplasm, helping spindle positioning. In metaphase the chromosomes align between the two poles. The sister chromatids migrate to the opposite poles in anaphase A and the two poles pull the two genomes to opposite ends of the cell in anaphase B. Once the nuclei reach the cell poles, microtubules extend from the cell equator. These microtubules form the post-anaphase array, which is nucleated from the eMTOC (Section 1.6.2.2.1.3). When the spindle breaks down, several microtubules start to nucleate from the outer part of the SPB, placing the nuclei at the cell's center and establishing the normal interphasic microtubule array. The newly-born cells emerge already in G2, since G1 and S phase are very short and partially overlap with later mitotic stages. After cytokinesis, the new cells grow monopolarly, later switching to bipolar growth by undergoing NETO (new end take off). Throughout the whole cell cycle, both actin patches and acting cables follow zones of active growth. Thus, such structures are present mainly at the cell tips. During mitosis actin forms the actinmyosin ring, which drives cytokinesis and the separation of the two daughter-cells. Adapted from (La Carbona *et al.*, 2006). **(B)** Microtubule cytoskeleton throughout the cell cycle is visualized in *S. pombe* expressing an integrated allele of GFP-α-tubulin (Adapted from Helio Roque, PhD thesis, 2009). 1. Pre-NETO, 2. Post-NETO, 3. Mitosis start, 4. Metaphase, 5. Early anaphase, 6. Late anaphase, 7. Post-anaphase Array, 8. Cytokinesis.

Actin cables, which are bundles of short, parallel actin filaments, are required for cell polarity. However, they are probably not involved in generating the force for growth. Rather, they may serve several functions in targeting membrane traffic to cell tips or in the endocytic recycling of membrane components (Chang and Martin, 2009). In fact, it seems likely that actin patches, nucleated by the Arp2/3 complex, may serve as sites of endocytosis, whereas actin cables, nucleated by the localized formin for3p, may serve as highways for the delivery of secretory components necessary for cellular growth (Bretscher, 2005). Myosin V (fission yeast myo52p), an ABP that moves along actin cables, has been shown to transport cargoes, such as vesicles, to the growing cell tips (Motegi *et al.*, 2001). Despite the fact that actin filaments are required for bipolar growth, they are not essential for this process. *For3Δ* cells do not contain detectable actin cables but are viable and, despite morphological defects, such cells are not round and are thus still able to grow in a polarized manner (Feierbach and Chang, 2001). It is therefore possible that other mechanisms and/or pathways, independent of actin and so far unknown, are involved in polarized secretion and cell growth. These may involve other molecules such as the exocyst complex or sterol-rich membrane domains and define an emerging area of research.

1.6.2.2 Microtubule organization and dynamics in fission yeast

1.6.2.2.1 Microtubule organizing centers

S. pombe nucleation sites are diverse and relatively well-characterized. Nucleation happens at multiple, decentralized MTOCs that are cell cycle-regulated. There are four classes of MTOCs: the spindle pole body (SPB), the tip associated MTOC that forms during conjugation (TAM), the equatorial MTOC (eMTOC) and multiple interphase MTOCs (iMTOCs).

1.6.2.2.1.1 The spindle pole body

The SPB is present throughout the entire *S. pombe* life cycle (Hagan and Petersen, 2000). During interphase the SPB lies in the cytoplasm close to the nuclear envelope and near the cytoplasmic membrane (Ding *et al.*, 1997). The SPB is composed of two components separated by the nuclear membrane. The cytoplasmic part is a highly organized structure, whereas the nuclear component is a less-defined amorphous mass which does not nucleate microtubules. The two parts seem to be connected by thin filaments that run though the nuclear membrane (Ding *et al.*, 1997). At the start of mitosis, the SPB duplicates and is embedded into the nuclear envelope. Once inside the nucleus, it starts nucleating microtubules that generate the mitotic spindle, later nucleating cytoplasmic astral microtubules (Ding *et al.*, 1997; Hagan and Petersen, 2000) (Section 1.6.2.2.3).

1.6.2.2.1.2 The Tip-associated MTOC that forms during conjugation (TAM)

When nutrient concentration in the medium is low, *S. pombe* cells undergo mating with partners of opposite mating type by pairwise fusion in a process called conjugation. This process involves the formation of a projection tip from both cells, which, upon contact, leads to the degradation of the cell walls separating the two cytoplasms. This allows the nuclei to migrate towards one another (Hagan and Petersen, 2000). An MTOC has been identified at the projection tips upon cell-to-cell contact before cell fusion (Petersen *et al.*, 1998). However, this tip-associated MTOC, referred to as TAM, remains poorly characterized and its function is still not well understood.

1.6.2.2.1.3 The equatorial MTOC (eMTOC)

A particularly interesting feature of mitosis in fission yeast is the formation of a transient MTOC at the actinmyosin contractile ring site (Figure 1.6A and B,7). This equatorial MTOC is able to nucleate microtubules that will later constitute the cytoplasmic microtubule array of the newly formed daughter-cells. The eMTOC assembles in a microtubule-independent manner in mid-anaphase as a partial γ-tubulin ring (Heitz *et al.*, 2001). As mitosis progresses, the γ-tubulin ring accompanies the actinmyosin ring constriction and forms a dot at the septum that disassembles at the end of cell division (Heitz *et al.*, 2001). Little structural evidence for eMTOC exists and its function is not yet fully understood. However eMTOC seems to play an important role in maintaining the position of the contractile ring (Pardo and Nurse, 2003).

1.6.2.2.1.4 The interphase MTOCs (iMTOCs)

When microtubules are depolimerized, two to four stable perinuclear tubulin stubs remain. Upon microtubule regrowth, growth occurs from these structures to rapidly form the normal interphase microtubule array (Tran *et al.*, 2001). One of these stubs is the SPB and the others are called iMTOCs. The generation of an interphase microtubule array may be explained by a model in which eMTOC disassembly leads to the formation of several iMTOCs. A key player in this process is rsp1p, which plays an important role on eMTOC disassembly, allowing the translocation of microtubule nucleating material to the iMTOC at the nucleus' periphery (Zimmerman *et al.*, 2004).

Re-growth experiments after microtubule depolymerization show that microtubule nucleation from iMTOCs is dependent on mto1p and that this protein is required for γ-TuRC recruitment at iMTOCs but not at the SPB (Sawin *et al.*, 2004). Further studies of mto2p, a protein that binds and has similar phenotypes to mto1p, provide evidence that γ-TuRCs bound to pre-existing microtubules are active microtubule nucleators (Janson *et al.*, 2005; Samejima *et al.*, 2005). These observations reinforce the idea that in *S. pombe* iMTOCs are dispersed and dynamic structures that can be formed and rearranged during interphase. Furthermore, nucleation along microtubules and the coordinated action of motors and bundling proteins facilitates the generation and maintenance of the bipolar microtubule bundles present in fission yeast (Section 1.6.2.2.2).

1.6.2.2.2 Dynamics of interphase microtubule arrays

Interphase cells are characterized by 3 to 6 interphase microtubule arrays (IMAs) that extend from the cell center to the cell tips (Hagan, 1998; Drummond and Cross, 2000). IMAs are bundles composed of 2-9 microtubules that overlap in an anti-parallel manner near the nucleus, where the microtubules' minus-ends are localized (Höög *et al.*, 2007). The plus-ends are localized mainly at the cell tips, and undergo repeated cycles of polimerization/depolymerization (Figure 1.7A). Microtubule shrinkage is much faster than growth, at rates of 8.5±2.2 μm/min and 3±0.6 μm/min, respectively (Busch and Brunner, 2004).

Depolymerization occurs shortly after microtubules touch the cell tip, and so microtubule bending around the cell is very rare in wild type strains. Compressive forces exerted on microtubules when they touch the cellular membrane trigger microtubule catastrophe at cell ends. This effect is amplified by the action of the depolymerizing kinesins klp5p and klp6p (Foethke *et al.*, 2009; Tischer *et al.*, 2009). The depolymerizing microtubule is later rescued, usually in a region around the cell center (Drummond and Cross, 2000; Busch and Brunner, 2004; Bratman and Chang, 2007).

IMA generation is thought to occur by targeted nucleation at preexisting microtubules by mto1p and mto2p (Section 1.6.2.2.1.4) and subsequent microtubule bundling. This is a self-organized system, where *de novo* microtubule arrays, with apparently normal dynamics, are formed after microtubule depolymerization in enucleated cells. This process is independent of nuclear MTOCs, but dependent on mto1p-ase1p-klp2p proteins (Carazo-Salas and Nurse, 2006; Daga *et al.*, 2006). Ase1p is known to bundle microtubules in an anti-parallel orientation and localizes in the overlap regions in *S. pombe* (Loïodice *et al.*, 2005; Janson *et al.*, 2007). However, other proteins besides ase1p are involved in microtubule bundling. For example, the XMAP215 homolog dis1p, the transforming acidic coiled-coil (TACC) protein mia1p/alp7p and the minus-end-directed kinesin klp2p. Klp2p is also responsible for the sliding of the newborn microtubule towards the minus-end of the pre-existing microtubule. This allows the confining of microtubule minus-end overlaps to regions at the cell center (Janson *et al.*, 2007; Thadani *et al.*, 2009; Roque *et al.*, 2010). Finally, in order to maintain a stable IMA, microtubules must be locally regulated. This task is performed by a CLASP-type protein, peg1p/cls1p, which promotes rescue when depolymerizing microtubules reach the central overlap regions (Bratman and Chang, 2007).

1.6.2.2.3 Microtubule organization and dynamics change dramatically during mitosis

In the G2 to M transition, a dramatic change in organization and microtubule dynamics occurs (Figure 1.6 and Figure 1.7). Cytoplasmic microtubules disappear as the spindle forms in early mitosis and the SPB duplicates, in prophase (Section 1.6.2.2.1.1). Microtubule dynamics during the transition from interphase to mitosis support a model where the interphase microtubule network disappears because no new microtubules are nucleated, rather than due to an increase in the depolymerization frequency (Sagolla *et al.*, 2003). Mitosis in *S. pombe* starts with phase 1, a phase of rapid spindle elongation where the spindle elongates at an average of 1μm/min until it achieves a size ~1.5μm. In phase 2, which extends from metaphase to anaphase A, elongation speed drops to an average of 0.09μm/min until the spindle reaches ~3μm (Mallavarapu *et al.*, 1999)(Table 1.2 and Figure 1.7B**)**.

Table 1.2: Spindle elongation dynamics in *S. pombe*

Reference	Marker	**Phase 1** (Prophase/ prometaphase)	**Phase 2** (Metaphase/ Anaphase A)	**Phase 3** (Anaphase B)
(Mallavarapu *et al.*, 1999)	GFP-tubulin	~1μm/min	~0.09μm/min	~0.8μm/min
(Nabeshima *et al.*, 1998)	sad1p-GFP (36°C)	~1.3μm/min	~0.2 μm/min	~1.4 μm/min
(Asakawa *et al.*, 2005)	mal3p-GFP	NS	NS	~0.65μm/min

NS-Not studied

Direct spindle observation using GFP-labeled tubulin allowed the observation that during metaphase the spindle is characterized by an intense fluorescence. This can be explained by the high number of microtubules at the SPB. In fact, electron microscopy shows that as many as 20 microtubules can be found per SPB. Of these, two to four are attached to each of the three kinetochores, while the others interdigitate in the spindle mid-zone or extend from one SPB to the other (Ding *et al.*, 1993; Sagolla *et al.*, 2003). During metaphase, plus-ends seem to be very dynamic, since the centromeres oscilate along the spindle. Additionally, the rapid recovery from photobleaching shows that microtubule turnover is very high at this stage (Mallavarapu *et al.*, 1999).

A dramatic change in microtubule dynamics happens in the transition from anaphase A to anaphase B. This is called phase 3 and is characterized by a rapid spindle elongation from 2-3μm to 10-12μm at an average speed of 0.8μm/min (Mallavarapu *et al.*, 1999). At the onset of anaphase B, the spindle suddenly elongates through anti-parallel microtubule sliding, and its fluorescence decreases due to the decrease in overall microtubule number and overlap. Microtubule sliding in anaphase B is dependent on kinesin-6 member klp9p, a plus-end-directed kinesin. Upon anaphase B, klp9 becomes dephosphorylated, inducing its binding to the mid-zone bundler ase1p and initiating spindle elongation (Fu *et al.*, 2009; Khmelinskii *et al.*, 2009). New tubulin subunits are added to microtubule plus-ends, allowing the spindle to grow, because depolymerization at minus-ends is nonexistent (Sagolla *et al.*, 2003). This is supported by FRAP experiments which showed no recovery of fluorescence in anaphase spindles, showing that upon anaphase B onset microtubule turnover rate diminishes abruptly, and spindle elongation speed is dependent on the rate of tubulin subunits added to microtubule plus-ends (Mallavarapu *et al.*, 1999; Sagolla *et al.*, 2003). During anaphase, microtubule plus-ends experience cycles of catastrophe and rescue events, although these are very different from the ones seen in interphase (Figure 1.7B). In this case, catastrophes are not as pronounced, because rescues are frequent at the spindle mid-zone. This rescue mechanism is dependent on the *S. pombe* CLASP, cls1p, which is present at the spindle mid-zone (Bratman and Chang, 2007). Furthermore, both growth but especially shrinkage speeds of individual microtubules at the spindle decrease when compared to interphase, suggesting that spindle microtubules are less dynamic than interphase microtubules (Sagolla *et al.*, 2003). Interestingly, the change in dynamics at the onset of anaphase B is also accompanied by a structural change in the spindle mid-zone. In fact, in metaphase the mid-zone microtubules interact through loose hexagonal packing, whereas in anaphase this region becomes extremely organized, assuming a square-packed arrangement of microtubules (Ding *et al.*, 1993).

In telophase, the spindle collapses due to depolymerization of individual microtubules from their plus-ends towards the SPB (Sagolla *et al.*, 2003). The post-anaphase array is formed by microtubule nucleation at the eMTOC and will later originate the interphase microtubules of the two newly-formed cells.

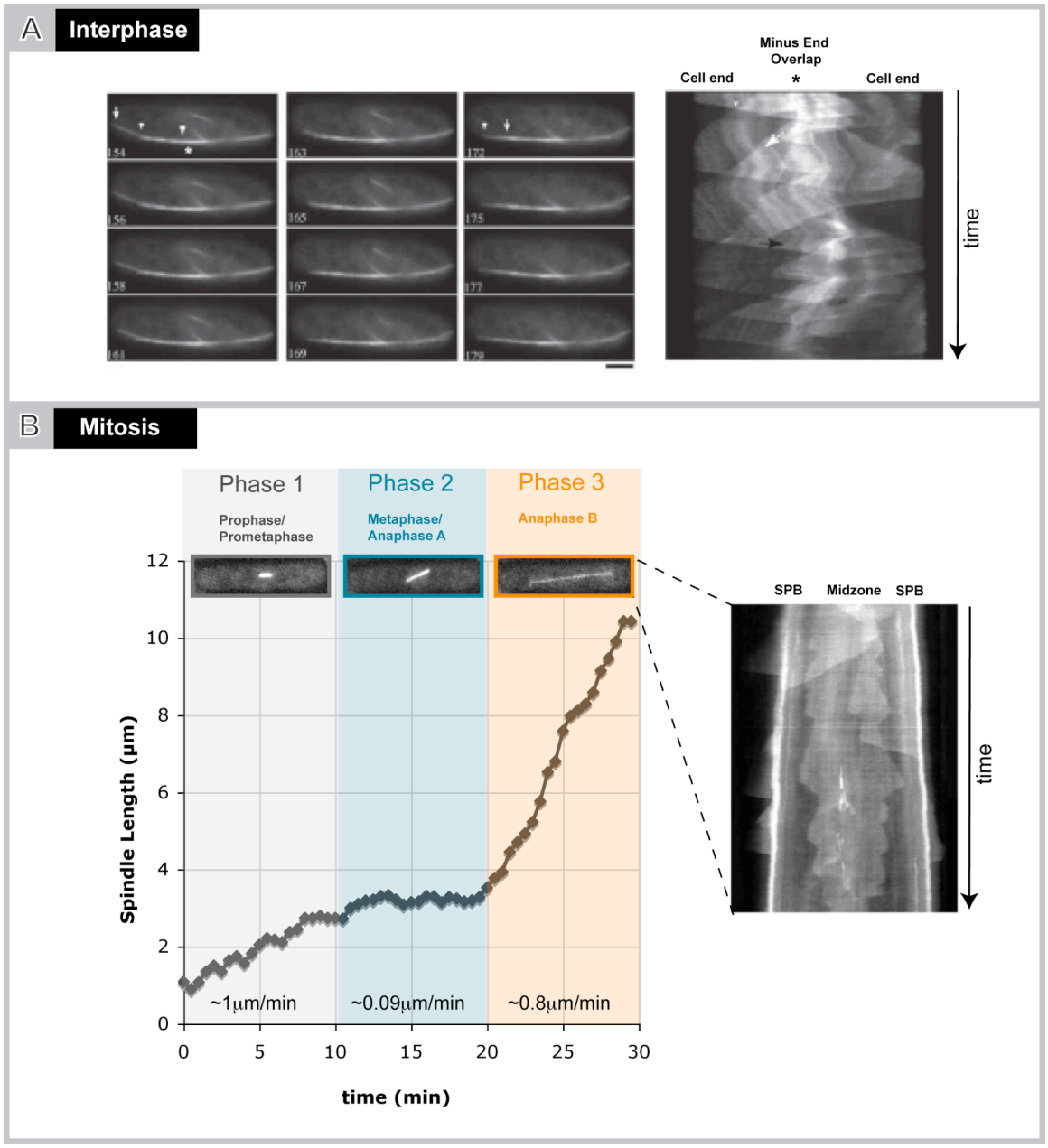

Figure 1.7: Interphase and mitotic microtubule dynamics. (A) Interphase microtubule dynamics. Left panel: Sequential images of a time-lapse movie of a cell expressing GFP-α-tubulin. Arrows and arrow-heads mark the plus-ends of individual microtubules, highlighting the presence of several microtubules in a bundle. Scalebar=2µm. Right panel: The same time-lapse movie represented as a kymograph. Lines descending from the minus-end overlap zone towards the cell end reflect polymerization (white arrow), whereas ascending lines reflect depolymerization (black arrow). (B) Mitotic spindle dynamics. Adapted from (Sagolla *et al.*, 2003). Left panel: Graphical representation of spindle growth over time in a typical mitotic cell. *S. pombe* spindle dynamics can be divided into three elongation phases: phase 1, of rapid elongation, which corresponds to prophase/prometaphase; phase 2, where growth is very limited and which corresponds to metaphase/anaphase A, and phase 3, of rapid spindle elongation, which corresponds to anaphase B. Right panel: Anaphase B spindle kymograph. Mitotic microtubule

dynamics is very different from an interphase microtubule bundle. The triangular patterns reflect the growth and shrinkage of individual microtubules. Note that rescues are very frequent in this case, with depolymerization rarely seen until the mid-zone. This is very different from the situation in (A), right panel. Adapted from (Sagolla *et al.*, 2003).

1.6.2.3 +Tips regulate microtubule dynamics in fission yeast

1.6.2.3.1 Tip1p spatially controls microtubule dynamics

Further insights into the functions of the CLIP-170 family come from studies in its fission yeast homologue, tip1p. Tip1p was initially isolated in a screen for morphogenesis mutants (Brunner and Nurse, 2000). Contrary to wild type cells, which display a straight cylindrical shape, most of *tip1Δ* cells display bent and T-shaped morphologies. This can be explained by the fact that in these cells microtubules are very short and rarely reach the cell's tips, preventing these cells from properly positioning the growth machinery at the cell poles. This is also why the *tip1Δ* phenotype is more pronounced in cells recovering from starvation. In this case cells need to go from a nearly round shape, characteristic of starved cells, to a cylindrical shape, and so need to re-position their growth machinery from scratch.

Like CLIP-170, tip1p is a +Tip protein that forms comet-like structures at microtubule tips. However, tip1p also accumulates at the cell poles, similarly to other well-know polarity markers (e.g. tea2p, tea1p) (Mata and Nurse, 1997; Browning *et al.*, 2000).

One of the most important functions of tip1p in cells is to spatially control microtubule dynamics. It has been shown that in *tip1Δ* cells, microtubules depolymerize as soon as they touch any part of the cell cortex. By contrast, in wild type cells, microtubule catastrophe only occurs when microtubules touch the cell cortex specifically at the cell tips, but not in the cell center. Tip1p is then essential for protecting microtubules from undergoing catastrophe at the cell center, but not at the cell poles, serving as a guiding mechanism that orients microtubules towards the cell ends. An important regulator of tip1p at the cells poles is one of the two fission yeast class V myosins, myo52p, which also localizes at the cell tips (Martín-García and Mulvihill, 2009). It has been shown that myo52p promotes the release of tip1p from microtubules specifically at the cell poles and that tip1p is later targeted to proteolisis via ubiquination.

1.6.2.3.2 Tip1p-deleted cells have problems with chromosome segregation

The role of tip1p during mitosis remains obscure. Tip1p is not localized at the mitotic spindle, being present only at tips of astral microtubules. However *tip1Δ* cells show a SAC-dependent delay in metaphase. Interestingly, and similarly to what happens with CLIP-170, *tip1Δ* cells show problems with chromosome alignment in the metaphase plate, exhibiting a high percentage of lagging chromosomes (40%) when compared to the 2.15% that normally occur in wild type cells (Goldstone *et al.*, 2010).

1.6.2.3.3 Mal3p has a positive effect on microtubule stabilization

Fission yeast is a good model organism for the study of EB family proteins, since EB1 can substitute for mal3p function in fission yeast, suggesting that the function of EB1 is evolutionarily conserved (Beinhauer *et al.*, 1997). Mal3p was identified for the first time in a screen designed to uncover genes required for chromosome segregation. In this screen, mutagenic mal3p cells showed a 380-fold increase in the loss of a marked non-essential mini-chromosome (Beinhauer *et al.*, 1997). Also, *mal3Δ* cells showed increased sensitivity to microtubule depolimerizing drugs, misplaced septum, displaced nucleus, and altered cell morphology, displaying frequently bent and T-shaped cells. These phenotypes can be interpreted as a consequence of an impaired cytoplasmic microtubule array in *mal3Δ* cells. Like EB1, malp3p localizes along the microtubule lattice with strong accumulation at the growing plus-tips, from where it disappears preceding catastrophes (Beinhauer *et al.*, 1997; Busch and Brunner, 2004). Growing dynamic microtubules are important for proper mal3p localization, since the latter's binding is severely reduced in mutants containing a temperature-sensitive tubulin allele (*atb2-983*) that compromises microtubule dynamics (Asakawa *et al.*, 2006). Moreover, *mal3Δ* cells show abnormally short microtubules with a 2-fold increase in both catastrophe frequency and average pausing time, whereas rescue frequency, growth and shrinkage rates remain the same (Busch and Brunner, 2004). These *in vivo* results indicate that mal3p promotes microtubule growth, and are consistent with results obtained in *Xenopus* egg extracts and mammalian cells (Section 1.5.4.3.4). Despite this fact, mal3p over-expression that results in stronger lattice accumulation does not increase microtubule length (Karl Emanuel Busch, PhD thesis, 2004). *In vitro* results are contradictory. Bieling and co-workers found that mal3p had no effect on the kinetics of microtubule growth or shrinkage, but it increased frequencies of catastrophes and rescues (Bieling *et al.*, 2007). On the other hand, Katsuki *et al*, found that mal3p had no effects

on catastrophic events, but reduced shrinkage rates and increased rescue frequency (Katsuki *et al.*, 2009).

Recent *in vivo* and *in vitro* studies showed that mal3p is responsible for the microtubule loading of tip1p and the kinesin-like motor, tea2p (Busch *et al.*, 2004; Bieling *et al.*, 2007). In solution, the three proteins form a stable ternary complex that is necessary for tea2p and tip1p loading at the microtubule. This leads to the subsequent mal3p dissociation and tea2p-mediated transport of tip1p along the microtubule walls towards the plus-tips.

1.6.2.3.4 Mal3Δ cells show abnormal mitosis

In mitosis, and similarly to what happens with its homologue EB1, mal3p localizes to the tips of astral microtubules and along the spindle in a dotted pattern. The dots move from the vicinity of the SPB towards the middle of the spindle, where they disappear. However, mal3p does not seem to localize at the SPB (Bu and Su, 2001; Piehl *et al.*, 2004; Asakawa *et al.*, 2005).

Despite the fact that mal3p has been identified as a protein with potential role in chromosome mis-segregation, almost nothing is known about its putative function during mitosis. Deletion, but especially mal3p over-expression, leads to mitotic defects (Table 1.1). Also, it is known that double mutants between mal3p and checkpoint proteins, namely bub1p, bub3p, mad3p and mph1p (but not mad1p and mad2p) show compromised growth defects which are temperature sensitive (Asakawa *et al.*, 2005). This is in agreement with *S. cerevisiae* data that shows synthetic lethality between *BIM1* and *BUB3* (Schwartz *et al.*, 1997). At the same time, mal3p double mutants with *BUB1*, *BUB3*, *MAD3* and *MPH1* show 40-80% chromosome mis-segregation at 36^{o}C. This suggests that mitotic errors caused by the absence of mal3p may be corrected by a spindle checkpoint.

1.7 Regulation of microtubule-associated proteins

Most complex biological processes involve regulation of activity, localization and binding partners for the proteins involved. A classical example is the cell cycle. Cell division is precisely regulated by post-translational modifications (PTMs), mainly reversible phosphorylation and ubiquitination. Ubiquitination usually occurs in later mitotic stages, triggering the exit from mitosis and leading to degradation of mitotic proteins once they are no

longer necessary. Similarly, most MAPs are regulated by post-translational modifications (PTMs), enabling a precise temporal and spatial control of microtubule dynamics.

Many different PTMs can occur in cells, e.g. SUMOylation, glycosilation, palmitoylation, and mirystoylation among dozens of other modifications. However, protein phosphorylation and ubiquitination are probably among the most abundant PTMs in cells.

1.7.1 Phosphoregulation of +Tips

Because +Tips have been shown to be some of the most important cytoskeleton regulators in the cell, they make ideal targets for PTMs that aim to modulate cytoskeletal dynamics. There are some examples in the literature of regulation of +Tips by phosphorylation, although generally, very little is known about this subject.

Phosphorylation is likely to play an important role in controlling the binding of +Tips to microtubules. Since microtubules are negatively charged, phosphorylation of +Tips will likely reduce their affinity towards microtubules. Indeed this is the case for APC and CLASPs where glycogen synthase kinase-3β (GSK3β) -mediated phosphorylation inhibits microtubule binding (Akhmanova and Steinmetz, 2008).

1.7.1.1 Phosphoregulation of the CLIP-170 protein family

It has been known for nearly 20 years that CLIP-170 is a phosphoprotein. Nevertheless, it was only very recently that the phosphorylation sites and the respective regulating kinases began to be unraveled. In fact, CLIP-170 was revealed to be a highly multiphosphorylated protein, probably with complex regulation, where multiple kinases can phosphorylate and/or compete for its dozens of different phosphorylation sites. This raises the possibility that multiple phophorylation combinations may exist, enabling very precise biological regulation.

1.7.1.1.1 CLIP-170 phosphorylation regulates its affinity to microtubules

Earlier models for CLIP-170 phosphoregulation proposed that a significant part of phosphorylated CLIP-170 was microtubule-bound and phosphorylation at multiple sites was necessary to release it from microtubules (Rickard and Kreis, 1990, 1991). Later, mTOR and

AMPK kinase were shown to phosphorylate some of the CLIP-170 sites (Choi *et al.*, 2000; Choi *et al.*, 2002; Nakano *et al.*, 2010). mTOR inhibition by rapamycin, inhibited CLIP-170 binding to microtubules, suggesting that phosphorylation by mTOR promotes binding between CLIP-170 and microtubules. In order to reconciliate these results with previous data, a model was proposed where mTOR was required to phosphorylate CLIP-170 for proper microtubule loading, whereas phosphorylation at non-mTOR sites would be inhibitory (Choi *et al.*, 2000; Choi *et al.*, 2002). AMP-activated protein kinase (AMPK) was shown to phosphorylate CLIP-170 in S311 and to promote its dissociation from microtubule tips (Nakano *et al.*, 2010). In fact, the non-phosphorylatable CLIP-170^{S311A} mutant accumulated at the microtubule plus-tips with much longer comet-tails than the wild type. Furthermore, this had an impact on microtubule dynamics, since these microtubules showed slower growth speeds and higher stability. CLIP-170 phosphorylation by AMPK is also important during cell polarization and subsequent cell migration. Blocking S311 phosphorylation resulted in impaired polarization and free cell migration (Nakano *et al.*, 2010).

Other studies have confirmed S311 phosphorylation and phenotype (Lee *et al.*, 2010). Additionally, other serines were found with similar phenotypes. Among them was S309, which together with S311, showed the strongest phenotype. Phosphorylation ablation at these sites led to a marked decrease of the CLIP-170 head-to-tail affinity, promoting an "open" conformation with increased affinity for microtubule binding (Lansbergen *et al.*, 2004). In this study other serines were found to be phosphorylated, but their biological significance remains unclear.

1.7.1.1.2 CLIP-170 phosphorylation plays an important role in mitosis progression and in kinetochore-microtubule attachments

It was recently shown that CLIP-170 is a substrate for cdc2p kinase. Cdc2 kinase phosphorylates CLIP-170 in the T287. This modification is important for normal G2/M transition, since CLIP-170^{T287A} mutants arrest in G2 and fail to separate the centrosomes in late G2 (Yang *et al.*, 2009). Another important mitotic kinase, polo-like kinase 1 (Plk1), was found to phosphorylate CLIP-170 at the S195. Phosphorylation in S195 is cell cycle-regulated, peaking in late G2/early mitosis, although the biological significance of this phosphorylation is not clear. Nevertheless, it enhances CLIP-170 binding to casein kinase 2 (CK2). CK2 was also found to phosphorylate CLIP-170 at S1318. This phosphorylation is necessary for CLIP-170 kinetochore localization via the dynein/dynactin complex. Furthermore, the presence of defects in kinetochore fibre formation in cells expressing CLIP-170^{S195A} and CLIP-170^{S1318A} mutants suggest that

phosphorylation is important for timely formation of kinetochore-microtubule attachments (Li *et al.*, 2010).

1.7.1.2 Phosphoregulation of the EB protein family

Like the CLIP-170 family, the EB protein family performs important functions both in interphase and in mitosis. In accordance with this, recent studies have shown that EB family proteins are post-translationally modified by phosphorylation and ubiquitination, although the biological consequences are not yet fully understood.

1.7.1.2.1 Phosphorylation of S. cerevisiae EB1 homologue BIM1 promotes its dissociation from microtubules and affects spindle elongation dynamics

BIM1-mapped phosphorylation sites cluster in the non-conserved serine-rich flexible region that connects the microtubule-binding calponin homology domain with its coiled-coil region. Six phosphorylation sites were identified: S139, S148, S149, S165, S166 and S176 (Zimniak *et al.*, 2009). These sites were all phosphorylated by IPL1, the budding yeast Aurora B homologue, in the presence of SLI15, an IPL1 activator. Phosphorylation at this serine cluster promotes a more compact BIM1 conformation, which may be responsible the lower microtubule affinity observed in phosphorylated or phosphomimetic BIM1 (Zimniak *et al.*, 2009).

Additionally, BIM1 phosphorylation varies in a cell cycle dependent way, peaking in a small window during anaphase (Figure 1.8). BIM1-6A has a faster spindle elongation and reached a higher maximum spindle length when compared to the wild type strain. In *S. cerevisiae*, BIM1 prominently localizes at the spindle mid-zone in anaphase, but this localization progressively decreases as the spindle grows and later disassembles. By contrast, BIM1-6A mutants showed marked accumulation of BIM1 at the spindle mid-zone even at later stages of anaphase, with BIM1 remaining at the ends of microtubules upon spindle breakage (Figure 1.8). This suggests BIM1 phosphorylation is important for proper spindle disassembly, despite the fact that these cells are all able to progress into telophase and do so with even faster kinetics than wild type (Zimniak *et al.*, 2009).

It is important to note, however, that in mammalian cells EB1 was also found to interact with Aurora B at spindle mid-zone and mid-body. However, contrary to BIM1, EB1 is not a substrate for Aurora B (Sun *et al.*, 2008; Ban *et al.*, 2009). Instead, the interaction between

Aurora B and EB1 enhances the activity of Aurora B by protecting it from dephosphorylation by protein phosphatase 2A (PP2A) (Sun *et al.*, 2008). The influence of BIM1 on IPL1 activity was also found in *S. cerevisiae* (Tomasz Zimniak, PhD thesis, 2010). IPL1 was found to associate with BIM1 via two redundant SxIP motifs and to be targeted to microtubules via BIM1 *in vitro*. Genetic evidence points towards a positive role of BIM1 in IPL1 activity, since BIM1 expression is essential for *ipl1-2* and *sli15-3* mutant viability at the permissive temperature (Tomasz Zimniak, PhD thesis, 2010).

1.7.1.2.2 EB3 is ubiquitinated and phosphorylation regulates protein levels during mitosis

In mammalian cells, EB3 localizes to the microtubules, centrosomes and spindle microtubules. Similarly to BIM1, EB3 is phosphorylated by the Aurora family. This phosphorylation occurs in S176, located in EB3's linker region (Ban *et al.*, 2009). Aurora RNAi experiments have suggested that Aurora A is responsible for EB3 centrosome phosphorylation in mitosis, whereas Aurora B is responsible for its phosphorylation at the mid-body. Moreover, EB3 phosphorylation changes in a cell cycle-dependent way. Phosphorylated S176 peaks in prometaphase and remains constant until cells start to undergo cytokinesis and mitotic exit (Figure 1.8). S176 phosphorylation seems to protect EB3 from degradation. In fact, EB3 is ubiquitinated and was shown to interact with SIAH-1 ligase. Moreover, EB3 levels change in a cell cycle-dependent way increasing in late S/G2 phase, peaking in mitosis and decreasing in the subsequent G1 phase (Figure 1.8). EB1 was also found to be ubiquitinated via the ubiquitin proteassome system (UPS) (Peth *et al.*, 2007). In this case, its association with the COP9 signalossome regulatory subunit, CSN5, stabilizes EB1. Furthermore, EB1 degradation is accelerated by inhibition of CSN-associated kinases, indicating that the protein is most likely protected from UPS degradation via CSN-mediated phosphorylation. The biological significance of EB1 and EB3 protein levels regulation awaits further investigation, but this process seem to be conserved, since it also occurs in BIM1p (Figure 1.8) (Tirnauer *et al.*, 1999). However, in this case, BIM1p levels seem to be regulated at the mRNA level, even though protein levels oscillate much less during the cell cyle than mRNA levels.

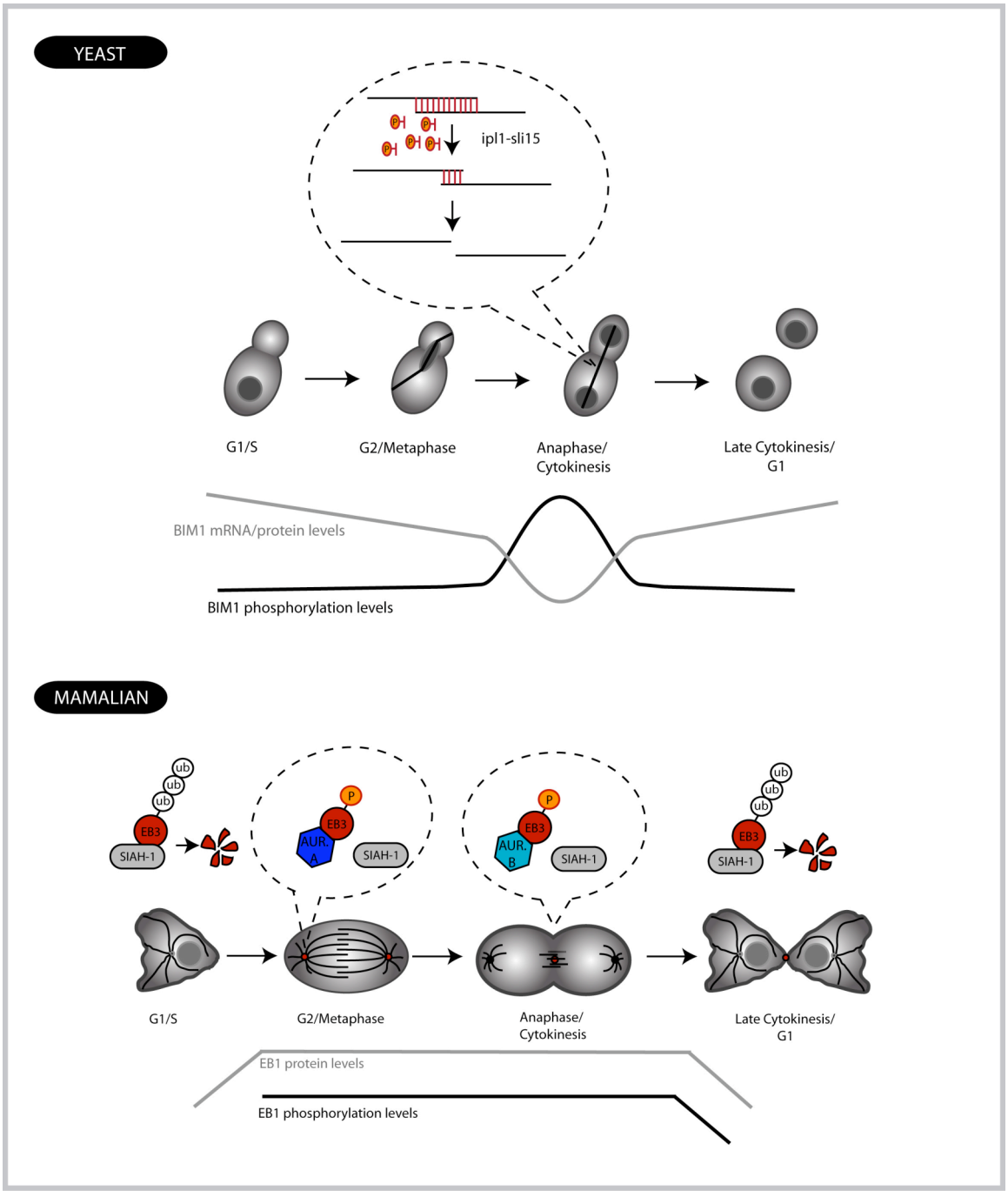
YEAST
ipl1-sli15
G1/S
G2/Metaphase
Anaphase/
Cytokinesis
Late Cytokinesis/
G1
BIM1 mRNA/protein levels
BIM1 phosphorylation levels
MAMALIAN
ub
EB3
SIAH-1
P
AUR.
A
AUR.
B
G1/S
G2/Metaphase
Anaphase/
Cytokinesis
Late Cytokinesis/
G1
EB1 protein levels
EB1 phosphorylation levels

Figure 1.8: Models for the EB protein family phosphoregulation. In yeast, Bim1p was proposed to have a role in spindle disassembly. In wild type cells, the complex IPL1p-SLI15p phosphorylates BIM1p during anaphase B and facilitates its removal from the mid-zone, allowing spindle disassembly. Adapted from (Zimniak *et al.*, 2009). In an earlier study, Tirnauer and co-workers had found BIM1p mRNA and protein levels to be down-regulated during mitosis, although the effect was much more pronounced at the mRNA levels (Tirnauer *et al.*, 1999). In mammalian cells EB3 phosphorylation seems to also play a role in mitosis. During G1/S, EB3 is targeted for degradation via SIAH-1. However, upon mitosis initiation, EB3 is phosphorylated by Aurora A specifically at the centrosomes, being protected from degradation. During anaphase/cytokinesis, Aurora A levels decrease but Aurora B now phosphorylates EB3, specifically at the midbody. In late citokinesis, Aurora B levels decrease, and so EB3 is no longer protected from degradation by phosphorylation, resulting in protein level decrease. Adapted from (Ban *et al.*, 2009).

1.8 Motivation of the present study

During a cell's lifetime, dramatic microtubule changes occur. For example, in the transition from interphase to mitosis the dynamic cytoplasmic array of microtubules must rearrange itself into the complex mitotic spindle. Also during mitosis, in the transition from metaphase to anaphase, microtubules are stabilized to allow spindle elongation. All these processes involve the precise spatio-temporal regulation of a myriad of microtubule-binding proteins.

+Tips are a class of proteins that bind the plus-ends of microtubules and are central in regulating microtubule dynamics (Akhmanova and Hoogenraad, 2005). Specifically, EB1 and CLIP-170 families have been shown to have a positive, stabilizing, effect on microtubules (Pierre *et al.*, 1994; Perez *et al.*, 1999; Brunner and Nurse, 2000; Komarova *et al.*, 2002; Tirnauer *et al.*, 2002b; Arnal *et al.*, 2004; Komarova *et al.*, 2009). However, nothing was known about the molecular mechanisms by which these proteins are regulated.

The aim of this thesis was to gain a better understanding on how both the EB1 and CLIP-170 families are regulated. To this end, we used fission yeast as a model organism, since it is a simple eukaryote with tractable and established genetics. Fission yeast is also a popular model organism for the study of microtubule dynamics, due to the simplicity of its microtubule cytoskeleton, which consists of only 3 to 6 microtubule bundles (Höög *et al.*, 2007) that can be easily imaged and modeled (Foethke *et al.*, 2009).

The fission yeast homologues of the mammalian EB1 and CLIP-170 are mal3p and tip1p, respectively. Mal3p is necessary for tip1p loading onto microtubules, and both proteins are necessary for proper microtubule dynamics in fission yeast (Busch and Brunner, 2004). Mal3p has been shown to be phosphorylated (Busch and Brunner, 2004). Furthermore, the presence of multiple tip1p isoforms had been detected, suggesting the presence of post-translational modifications (Niccoli and Nurse, 2002). In the beginning of this project we were able to confirm that at least some tip1p modifications were due to phosphorylation. This reversible post-translational modification is involved in nearly all signal transduction pathways in the cell, and responsible for the regulation of activity in most proteins. Thus, we decided to elucidate the role of tip1p and mal3p phosphorylation. One of the first questions we addressed was which kinases were responsible for this post-transational modification. With this aim, we screened all *S. pombe* non-essential kinases together with over-expression and/or down-regulation screening of selected kinases. Additionally, temperature-sensitive mutants for essential kinases available in the lab were also tested. We then focused our attention mainly on mal3p and asked what the mal3p

phosphorylation sites were. Finally, through a set of very different experiments, we tried to establish which processes mal3p phosphorylation was involved in.

In parallel with these experiments, we also tried to gain a better understanding of how the molecular domains of mal3p contribute to and analyzed them concerning morphological phenotype, mal3p localization, microtubule dynamics and tip1p localization.

Chapter 2

Results I

2. Results I – Towards the identification of mal3p and tip1p kinases

2.1 Mal3p and tip1p are phosphoproteins

At the beginning this project very little was known about how the activity of +TIPs is regulated. An earlier study had suggested that fission yeast mal3p is a phosphoprotein but nothing was known about putative phosphorylation states of other EB family protein members (Busch and Brunner, 2004). Similarly, phosphorylation of mammalian CLIP-170 was known to occur but the role and function of this modification remained elusive (Rickard and Kreis, 1990, 1991). The phosphorylation state of tip1p, the fission yeast homologue of CLIP-170, had not been analyzed but multiple protein bands were detected on western blots showing that also tip1p is post-translationally modified possibly by phosphorylation (Niccoli and Nurse, 2002).

To study phosphorylation of mal3p and tip1p we first investigated the phosphorylation state of the two proteins in exponentially growing cells. For this we made whole protein extracts and analyzed them with gel electrophoresis and western blotting using polyclonal α-mal3p and α-tip1p antibodies. The initial analysis was done using Anderson gels, which allowed for better band separation than classical protein gels (Section 6.7.5). With the availability of the phosphate binding "Phostag" reagent, we later switched to gels containing 75μM Phostag. Phostag is a dinuclear metal complex that binds phosphorylated protein residues. This changes the mobility of phosphorylated proteins and strongly improves the separation of phosphorylated and unphosphorylated protein isoforms in gel electrophoresis. For both mal3p and tip1p, we detected multiple protein bands that were best separated in the Phostag gels, indicating that at least some of these isoforms are modified by phosphorylation (Figure 2.1A and B). Particularly, tip1p displayed a very complex band pattern suggesting that multiple phosphorylation events occur.

Extract treatment with λ-phosphatase abolished the majority of slow running (upper) bands for both mal3p and tip1p. This was not the case in control experiments where of λ-phosphatase was inhibited with phosphatase inhibitors (NaV and NaF) (Figure 2.2A). This confirmed that the upper bands seen for mal3p and tip1p correspond to different isoforms of phosphorylated mal3p and tip1p proteins. Interestingly, the lowest tip1p band shifted down in λ-phosphatase treated extracts, suggesting that most of the protein is in a phosphorylated form (Figure 2.2A).

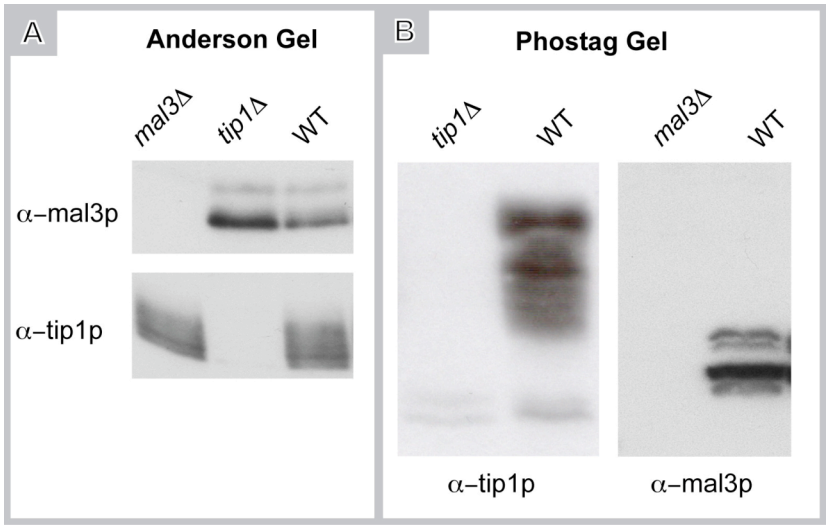

Figure 2.1: Mal3p and tip1p show multiple bands on western blots.
(A) Western blot of an Anderson gel. Total extracts of wild type cells and of *mal3*Δ or *tip1*Δ control cells were loaded. Multiple bands are seen for both mal3p and tip1p. (B) Western blot of a Phostag gel. Cell extracts were prepared as in (A). Additional protein isoforms are detectable for tip1p and mal3p as compared to the western blots of Anderson gels.

We could never completely dephosphorylate tip1p and a smearing of bands was always seen even after increasing λ-phosphatase concentrations and/or prolonging incubation times. Tip1p phosphorylation therefore may be very stable and partially "resistant" to λ-phosphatase treatment. Alternatively, other post-translational modifications may exist. From these first experiments we can conclude that mal3p and tip1p are phosphorylated on multiple sites and that tip1p is mostly present in a phosphorylated form in exponentially growing cells. This had been already suggested for its mammalian homologue CLIP-170 (Yang *et al.*, 2009) (Choi *et al.*, 2002).

To perform a more detailed analysis of mal3p phosphorylation, we labeled wild type cells with radioactive [^{32}P] ortophosphate and prepared a denatured protein lysate. Standard acrylamide gradient gel electrophoresis revealed a clear phosphoprotein band of the expected molecular size (~35KDa). This band was present in immunoprecipitates when using the α-mal3p antibody but not when using pre-immune serum. This confirmed that mal3p is phosphorylated *in vivo* (Figure 2.2B). The reason why only one band was detected is due to the fact that the multiple mal3p isoforms cannot be resolved with the standard acrylamide gradient gel used in this experiment.

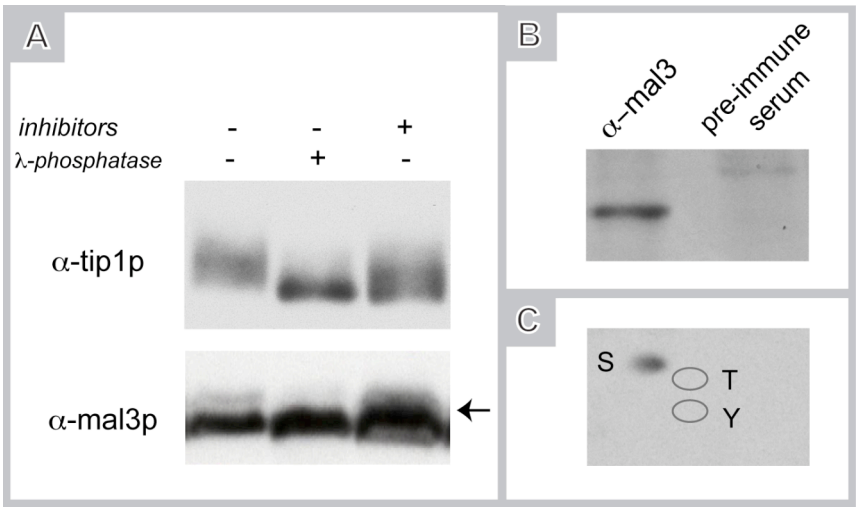

Figure 2.2: Mal3p and tip1p are phosphorylated
(A) Equal amounts of total protein were separated with a 12% Acrylamide gel and analyzed by western blot with α-tip1p or α-mal3p antibody (upper and lower panel, respectively). Extracts were prepared without phosphatase inhibitors and were subsequently treated with λ-phosphatase with or without addition of phosphatase inhibitors, as indicated. (B) Mal3p was immunoprecipitated with α-mal3p antibody from cells growing in the presence of $^{32}P_i$. As a control, immunoprecipitation was done with pre-immune serum instead of α-mal3p antibody. The immunoprecipitates were loaded on a 6%-20% gradient SDS-polyacrylamide gel that was transferred to a membrane and exposed to detect the radioactive signal. (C) The radioactive band corresponding to phosphorylated mal3p shown in (B) was excised, separated in two dimensions on a TLC plate and exposed. Indicated are the positions of serine (S), threonine (T) and thyrosin (Y) on the TLC plate.

To determine which type of amino acid is phosphorylated in mal3p, we performed phosphoamino acid analysis of the immunoprecipitated [^{32}P] labeled mal3p. The protein was subjected to acid hydrolysis at high temperatures to break the protein into its constitutive amino acids. These were subsequently separated using two-dimensional thin layer chromatography (TLC). The first dimension run was done at a pH of 1.9 and the second dimension at a pH of 3.5. These conditions allow a good separation of serine, threonine, and tyrosine, the three most common phosphorylatable residues, on the TLC plate. Radioactive amino acids were detected via autoradiography and the image was overlayed with amino acid standards to reveal which of the three amino acids were phosphorylated. We only observed phosphorylation of serine while no signal was detectable on threonine or tyrosine (Figure 2.2C). Mal3p thus appears to be selectively phosphorylated on serine residues.

2.2 Screen to identify kinases phosporylating mal3p and tip1p

Previous studies suggested that mammalian CLIP-170 is a target of mTOR kinase (Choi *et al.*, 2000; Choi *et al.*, 2002). In addition, these earlier works suggested that more than one protein kinase was involved in CLIP-170 phosphoregulation. Nothing was known about the kinase(s) responsible for phosphorylation of the fission yeast homologue tip1p. On the other hand, the kinases(s) phosphorylating EB family protein members, like mal3p, were also unknown. In this way, we attempted to identify such kinases by performing a screen where we systematically tested all *S. pombe* non-essential kinases. For this, we used a strain collection in which all genes encoding non-essential kinases had been deleted (kind gift from Mohan Balasabrumanian, (Bimbo *et al.*, 2005)). Only kinases assigned by Pfam (http://pfam.sanger.ac.uk) to contain a kinase catalytic domain were included in the strain collection. In the gene DB database (http://old.genedb.org/) a total of 181 proteins were assigned to the kinase category whereas only 108 were assigned by Pfam as containing a kinase catalytic domain. This happens because most kinases involved in carbohydrate or inositol/phosphatidylinositol phosphorylation are not assigned as containing a kinase catalytic domain. In this group are placed kinases that move the phosphate group exclusively onto proteins (http://pfam.sanger.ac.uk/family?acc=PF00069).

In this way we were able to test 90 non-essential kinases (Annex I). This amounts to 84% of the total *S. pombe* catalytic-domain containing kinases (Table 2.1). Six other kinases not assigned to have a kinase domain were also tested (mak1, ckb1p, rad3p, SPBC29A3.09c, SPCC1919.02c, gift from Mohan Balasabrumanian, and Fab1, Annex I) accomplishing a total of 96 tested kinases. For testing, we prepared total protein extracts from unsynchronized exponential growing cells of each kinase deletion strain. Protein extracts were resolved on a 12% acrylamide gel and analyzed by western blot using polyclonal antibodies against mal3p and tip1p. If a kinase were responsible for mal3p or tip1p phosphorylation, one would expect to see disappearance of one or several upper phosphorylation bands on a western blot. Unfortunately, we could not observe any change of the phosphorylation pattern of mal3p or tip1p under the conditions used in this screen. This could have various causes, but one of the most important may be kinase redundancy (Section 5.1.1). A search in the geneDB database (http://old.genedb.org/) revealed that 45% of the tested kinases have at least one putative paralogue in the *S. pombe* genome (Table 2.1 and Annex I).

Table 2.1: Summary of kinase-screen characteristics		
	n	**% total**
Number of kinases in *S. pombe* containg the catalytic kinase domain	108	
Number of non-essential kinases containing the catalytic kinase domain	90	84%
Number non-essential kinases with catalytic kinase domain that have putative paralogues in *S. pombe* genome	49	45%
Total number of tested kinases (including 6 kinases without the kinase catalytic domain)	**96**	

In addition to the problem of kinase redundancy, another drawback of this type of screen is the fact that it only allows testing of non-essential kinases. To overcome these problems, we decided to perform over-expression/down-regulation screens (Table 2.2). Kinases for both over-expression or down-regulation were chosen based on published data indicating increased likelihood for their targeting of mal3p or tip1p. In particular, we chose kinases suspected to interact with either mal3p or tip1p, (e.g. tor1p and ark1p, (Choi *et al.*, 2000; Choi *et al.*, 2002; Zimniak *et al.*, 2009), http://thebiogrid.org/, Annex III) or kinases that had been proposed to regulate cell polarity (e.g. kin1p, PKC family members and the Gsk3β or PI3k homologues). Selected kinases were placed under the control of the thiamine repressible Pnmt (no message in thiamine) promoters. There are three versions of the Pnmt promoters in fission yeast: the full strength promoter (Pnmt1) and two attenuated versions, with medium (Pnmt41), and week activity (Pnmt81). For our screen, we used mainly the full strength and the weakest promoters (Bahler *et al.*, 1998). The Pnmt1 promoter allows for strong gene over-expression when cells grow in the absence of thiamine while in the presence of thiamine, promoter leakiness still allows for sufficient gene expression to avoid lethality. In most cases, although dependent on the protein being expressed, fully repressed Pnmt1 promoter is over-expressing the gene. For example, in the case of mal3p, it was estimated that fully repressed Pnmt1 promoter generates 10x higher protein levels when compared to the endogenous levels (Karl Emanuel Busch, PhD thesis, 2004). In contrast, the Pnmt81 promoter generally needs to be fully activated to achieve sufficient gene expression, while presence of the thiamine results in strong down-regulation.

Table 2.2: Essential kinases tested in screen.

	Kinase	Process involved	Western blot result of screen (mal3p/tip1p)
Ts-strains	*sid2-250*	Cell cycle - Cytokinesis	NC / -
	shk1-34	Cell cycle – Cytokinesis, Actin cytoskeleton organization, MT organization, Cell polarity	NC / -
	plo1-25, Plo1-24	Cell cycle - Cytokinesis	- / -
	cdc2-33	Cell cycle - Mitotic onset	NC / -
	cka1-19	Cell polarity	- / -
	orb6-25	Cell cycle – Cytokinesis, Actin cytoskeleton organization, Cell polarity	- / NC[a]
Down-regulations	*Pnmt41-pck1 pck2Δ*	Actin cytoskeleton organization, Cell polarity	NC[b] / -
	Pnmt41-pck2 pck1Δ	Actin cytoskeleton organization, Cell polarity	- / -
	P81nmt1-pik3	Phosphoinositide-mediated signaling	- / -
	pRep82-ark1	Cell cycle - Kinetochore-microtubule attachments	- / NC[a]
	P81nmt1-cki2 cki1Δ	Cell cycle – Cytokinesis, Morphogenesis, Endocytosis	- / NT
	P81nmt1-cki1 cki2Δ	Cell cycle – Cytokinesis, Morphogenesis, Endocytosis	- / NT
Over-expressions	*P3nmt1-cki2*	Cell cycle – Cytokinesis, Morphogenesis, Endocytosis	NC[b] / NT
	P3nmt1-tor2	Synthesis of 1-phosphatidyl-1D-myo-inositol 3-phosphate, Growth control.	- / -
	P3nmt1-pik3	Phosphoinositide-mediated signaling	- / -
	P3nmt1-gsk3β	Cell cycle - Control of chromosome segregation and in regulating entry into meiosis	- / -
	P3nmt1-kin1	Cell cycle – Cytokinesis, actin cytoskeleton organization, MT organization, Cell polarity	- / -

NC: Result is non-conclusive, NT: The kinase was not tested, (a): Tip1p seems to be slightly hyperphosphorylated, (b): Mal3p levels seem to decrease substantially with kinase over-expression.

Gene over-expression with Pnmt1 allows to overcome kinase redundancy since it doesn't rely on deleting the kinase but uppon increasing its concentration. For the relevant kinases this should result in increased phosphorylation of the target protein. Such phosphorylation changes can then be easily detected as an intensity increase of the "upper" phosphorylation bands on a western blot.

On the other side, the testing of essential kinases was done either by down-regulation of kinase expression or by the use of temperature sensitive mutants (ts-mutants). Kinase ts-mutants bear a mutation in the gene coding for the kinase so that at the permissive temperature of 25°C the kinase is active, but at higher temperatures, generally 36°C, this activity is abolished. In both experiments several time points are taken while the kinase is being either down-regulated or inactivated by raising the temperature. A reduction of the upper phosphorylation band(s) of the target protein is expected, since the levels of the responsible kinase are gradually diminishing or the kinase is loosing its activity. In these experiments total protein extracts from exponential growing cells were collected for each time point and analysed on a western blot using polyclonal mal3p and tip1p antibodies. The results of these screens are summarized in Table 2.2.

None of the tested over-expressed kinases caused an upper-shift of tip1p phosphorylation bands. Similarly, the down-regulation screen did not show a down-shift in tip1p phosphobands. However, a change in the tip1p phosphorylation pattern was observed for both orb6p and ark1p. In these cases, tip1p seems to become hyper-phosphorylated when orb6 activity is ablated by temperature or when *ark1* is down-regulated (Figure 2.3A and Figure 2.5A). This was not expected since if orb6p or ark1p would be the kinases directly regulating tip1p, we would expect a tip1p dephosphorylation upon orb6p or ark1 down-regulation. These results are thus likely indirect effects, probably due to interconnection of signaling cascades, for example, orb6p or ark1p could be acting by inhibiting a kinase upstream tip1p (Section 5.1.3).

In the case of mal3p, we realized that at the restrictive temperatures for the ts-mutants, the bands depicting phosphorylated mal3p in a 12% acrylamide gel disappeared at the restrictive temperature of 36°C even in wild type control cells. The effect is evident, for example, in the *sid2-250* experiment shown in Figure 2.3D.

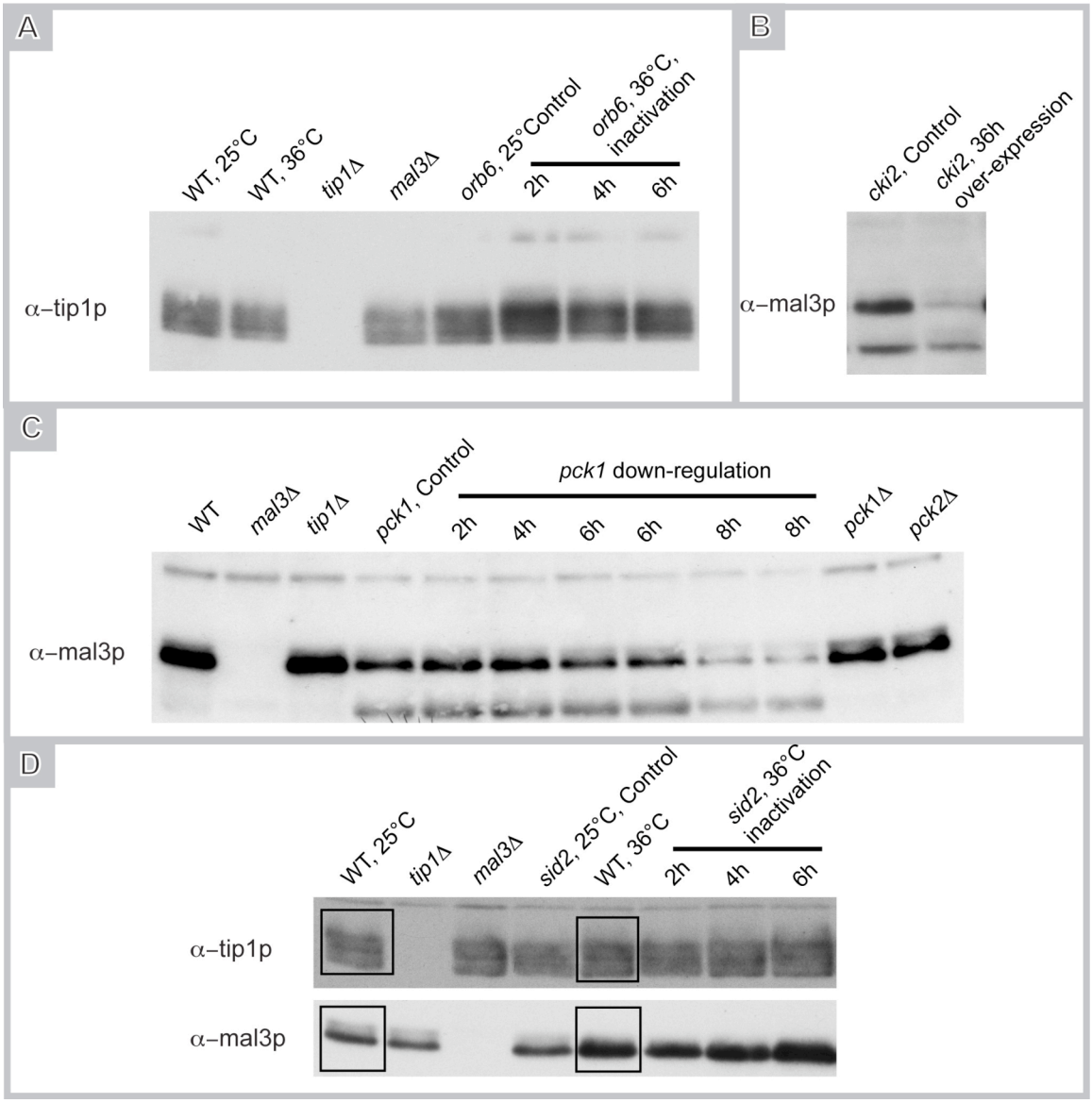

Figure 2.3: Screening results on selected western blots
(A) *Orb6-25* cells were grown at the permissive temperature (25°C) or at the restrictive temperature (36°C) for 2, 4 and 6 hours. Wild type cells grown at 25°C and 36°C for 2h, together with *tip1Δ* and *mal3Δ* cells grown at 25°C, were used as controls (C). Equal amounts of total protein were separated with an Anderson gel and analyzed by western blot with α-tip1p antibody. (B) *Cki2* was over-expressed under the Pnmt1 promoter in EMM2 without thiamine for 36h at 30°C. Control cells were grown in EMM2 with 30μM thiamine for 36h at 30°C. Equal amounts of total protein were separated with 12% acrylamide gel and analyzed by western blot with α-mal3p antibody. (C) Cells containing *pck2Δ* and *pkc1* under the moderate-strength Pnmt41 promoter, were grown at 25°C, in the absence (*pkc1*, control) or presence of 30μM thiamine, for 2, 4, 6, and 8 hours. Wild type, *mal3Δ*, *tip1Δ*, *pkc1Δ* and *pkc2Δ* strains, were used as aditional controls. Equal amounts of total protein were separated with an Anderson gel and analyzed by western blot with α-mal3p antibody. The lower mal3p band is probably due to protein degradation and was occasionally seen in other strains. (D) *Sid2-250* cells were grown at the permissive temperature (25°C) or at the restrictive temperature (36°C) for 2, 4 and 6 hours. Wild type cells grown at 25°C and 36°C for 2h, together with *tip1Δ* and *mal3Δ* strains grown at 25°C, were used as controls.

Equal amounts of total protein were separated with a 12% acrylamide gel and analyzed by western blot with α-tip1p antibody (upper panel) and a α-mal3p antibody (lower panel). Note that when cells were grown at 36°C is no longer possible to distinguish phosphorylated vs non-phosphorylated forms of mal3p (lanes highlighted by black boxes).

Sid2-250 cells were grown to exponential phase at the permissive temperature of 25°C. Thereafter, they were shifted to 36°C for 2h, 4h, and 6h respectively, to inactivate the sid2p kinase. Total protein extracts from the different time points were loaded onto a 12% acrylamide gel to evaluate mal3p and tip1p phosphorylation status (Figure 2.3D). As controls, protein extracts from wild type cells grown at 36°C and *sid2-250* grown at 25°C were prepared simultaneously. At first sight, the mal3p phosphorylation band seems to disappear when *sid2-250* is inactivated at 36°C (Figure 2.3D, compare sid2, 25°C, Control with 2h, 4h, and 6h lanes). However, the same was observed when the wild type strain was grown at 36°C, suggesting that the disappearance of the mal3p phosphorylation band was not an effect of sid2p kinase inactivation (Figure 2.3D, compare lanes WT, 25°C with WT, 36°C, highlighted by black boxes). This was further confirmed in an independent experiment, where the wild type strain was grown at different temperatures and protein extracts were resolved on an acrylamide gel and analyzed by western blot (Figure 2.4A). Also in this case was possible to observe that at higher temperatures was more difficult to observe the mal3p upper-band. Unfortunately, this effect rendered most experiments with ts-mutants inconclusive when analyzing mal3p (Table 2.2).

During the experiments with the ts-mutants we also noticed that total mal3p levels were higher when cells were grown at 36°C (Figure 2.3D, compare WT, 25°C with WT, 36°C lanes and Figure 2.4A). To further quantify the increase of mal3p levels with temperature, we analyzed total protein extracts of wild type cells grown at 25°C and 36°C on an acrylamide gel (Figure 2.4B). Quantification of the relative protein content in the bands using LI-COR odissay software (Section 6.7.8) suggested that that the total mal3p levels increased approximately 4-fold when cells were grown at 36°C as compared to 25°C. For tip1p we did not observe any effects on protein levels in connection with temperature changes (Figure 2.3D).

At this stage it was not clear if the difficulty to visualize mal3p phosphorylation band at high temperatures was due to mal3p dephosphorylation upon temperature shift or simply due to the higher protein levels.

With the availability of Phostag, we could discriminate between these two possibilities. For this, we loaded the same protein extracts we had quantified previously onto a Phostag gel (Figure 2.4C). Under these conditions we could detect both mal3p bands also in extracts grown at 36°C. This allowed us to quantify mal3p using imagej (http://rsbweb.nih.gov/ij/) in the

phosphorylated and unphosphorylated isoforms. We observed that the ratio of phosphorylated : unphosphorylated mal3p remained constant irrespective of the temperature indicating that temperature increases the levels of both isoforms (Figure 2.4C). From these results we conclude that mal3p is not dephosphorylated at high temperatures, since the phosphorylated : unphosphorylated ratio is constant. Instead, overall protein levels increase, and so the distinction between phosphorylated and unphosphorylated bands in conventional, non-Phostag gels is impaired, even when lower amounts of protein are loaded.

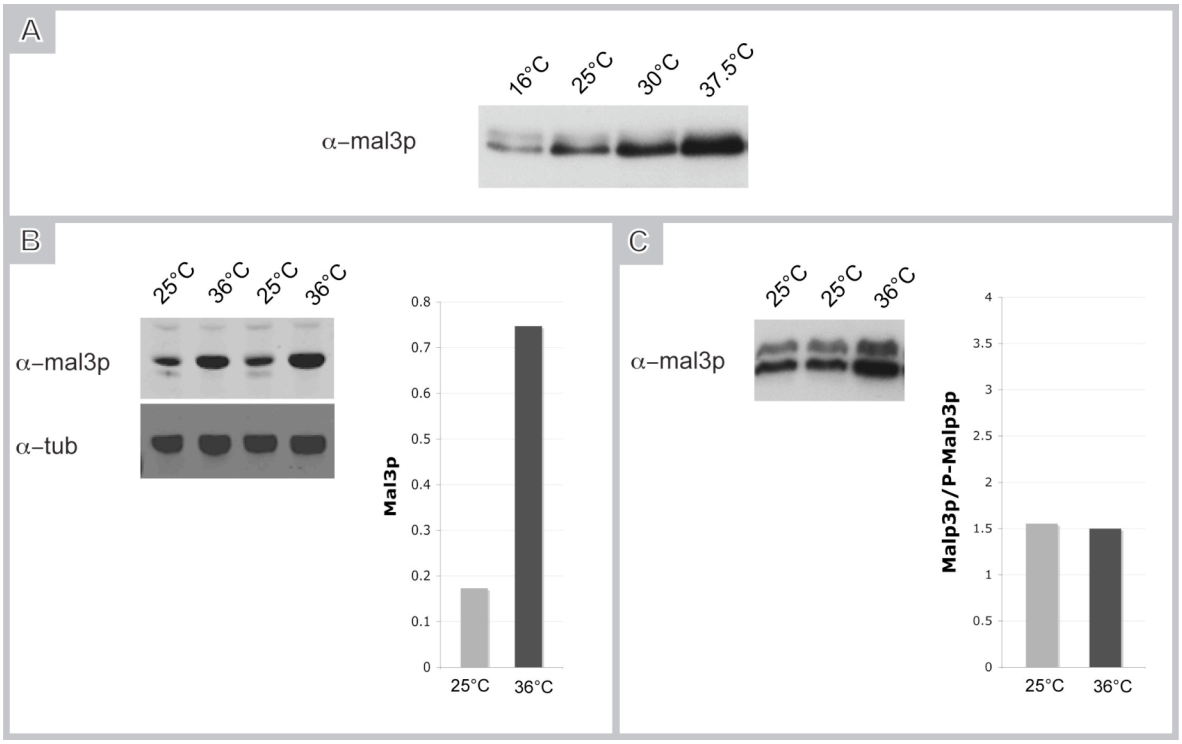

Figure 2.4: Mal3p protein levels increase with increasing temperature.
(A) Wild type cells were grown in YE5S at the specified temperatures, and harvested in exponential phase. Equal amounts of total protein were separated with a 12% Acrylamide gel and analyzed by western blot with α-mal3p antibody. (B) Wild type cells were grown in YE5S at the specified temperatures, and harvested in exponential phase. Equal amounts of total protein were separated with a 10% Acrylamide pre-cast gel and analyzed by western blot with α-mal3p antibody. Malp3p levels were quantified and tubulin was used as a loading control. (C) The same extracts used in (B) were run on a 75μM phos tag gel. The ratio of unphosphorylated *vs* phosphorylated mal3p is shown.

The reason why mal3p levels increase at higher temperatures is unknown. It is possible that mal3p expression increases by increased gene transcription or mRNA translation. Alternatively, the protein is more stable at higher temperatures. It is known that protein levels of

other EB1-family members are regulated either by protein degradation or by regulation of protein expression (Tirnauer *et al.*, 1999; Ban *et al.*, 2009). However, such regulation, to date, has not been implicated in the cellular response to temperature stress.

The kinases tested by over-expression and/or down-regulation did not affect mal3p phosphorylation state (Table 2.2). Interestingly, when overexpressing the casein kinase I homologue (cki2p), a pronounced decrease in mal3p levels was observed (Figure 2.3B). The same was seen when we down-regulated protein kinase C *S. pombe* homologue, *pck1*, in a *pck2Δ* background (Figure 2.3C). Although preliminary, these results raise the possibility that cki2p and/or members of the PkC protein family play a role in the regulation of mal3p levels (Section 5.1.2).

The aurora kinase IPL1-SLI15 complex was recently reported to phosphorylate BIM1p, the *S. cerevisiae* mal3p homologue (Zimniak *et al.*, 2009). In this study, the BIM1 phosphorylation band was abolished in the *ipl2-1* mutant at the restrictive temperature, suggesting that IPL1 targets BIM1 *in vivo*. To evaluate if the *S. pombe* IPL1 homologue, ark1p, was similarly responsible for mal3p phosphorylation we used a conditional ark1p shut-off strain (kind gift of Ian Hagan, (Petersen and Hagan, 2003)). In this strain *ark1Δ* cells were kept alive by Pnmt81 promoter-controlled expression of *ark1*. The gene was engineered to produce ark1p that in addition was fused to a Pk epitope tag. In the absence of thiamine the promoter was on and colonies could form. As previously published, addition of thiamine suppressed promoter activity, which led to the disappearance of ark1p on western blots within 8 hours (Figure 2.5A, (Petersen and Hagan, 2003)). However, the mal3p phosphorylation band was still visible in these cells, indicating that mal3p is not a direct target of ark1p (Figure 2.5A). We cannot exclude that residual ark1p is still present and sufficient to phosphorylate mal3p. Also, mal3p phosphorylation may be sustained for a certain period of time after ark1p disappearance. Unfortunately, we could not test this unambiguously as ~10h after *ark1* down-regulation cells started to die due to the lack of ark1p (Figure 2.5B, arrow). Nevertheless, after 14h, 18h and even 32h of *ark1* down-regulation, the mal3p phosphorylation band remained visible in the remaining cells (Figure 2.5A). In these cells a general down-shift of mal3p was detected. However, the late appearance of the down-shift suggests that it is due to secondary effects of processes being triggered in the dying cells.

In summary these results suggest that ark1p is unlikely to account for the major phosphorylation occurring on mal3p and that other kinases may be involved (Section 5.1.2).

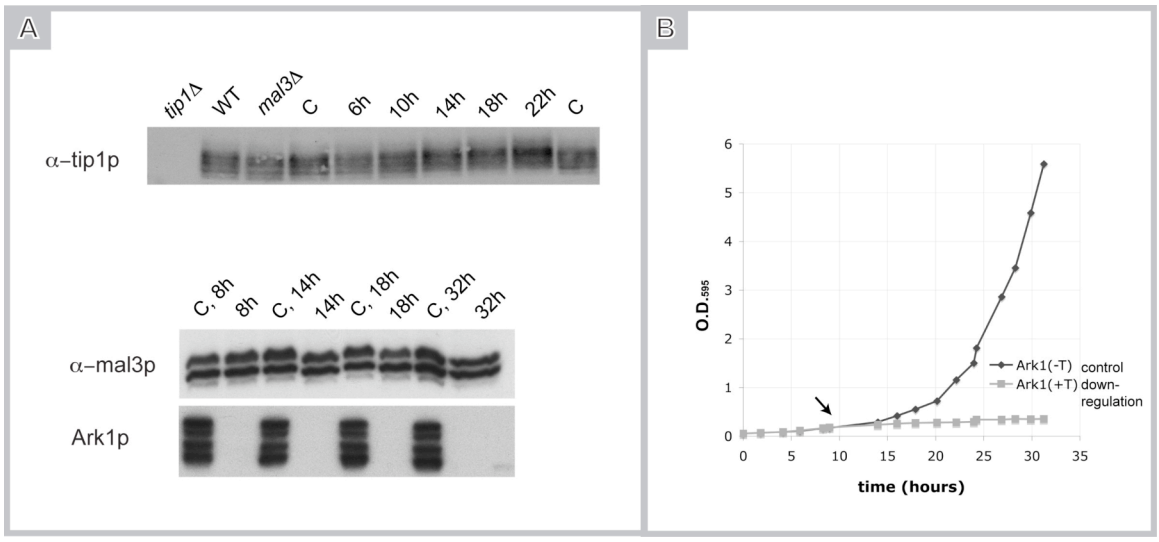

Figure 2.5: *S. pombe* Aurora kinase - ark1p - is not responsible for the bulk of mal3p phosphorylation in unsynchronized cells.
(A) Ark1p was down-regulated under low strength Pnmt82 promoter control. Upper panel: Cells were grown in the absence (Control, C) and presence of 30μM thiamine and extracts harvested after 6, 10, 14, 18 and 22 hours of down-regulation. Equal amounts of total protein were separated with an Anderson gel and analyzed by western blot with α-tip1p antibody. Lower panels: Cells were grown in the absence (Control, C) and presence of 4μM thiamine and extracts were harvested after 8, 14, 18, 32 hours. Equal amounts of protein were loaded on a 75μM Phostag gel and blotted with α-mal3p antibody. The same extracts were run on a 10% acrylamide gel and blotted with α-Pk antibody to detect ark1p fused to a triple "Pk" epitope. Note that after 8h down-regulation no ark1p is detectable by western blot but the phosphorylated mal3p band is still visible. (B) $O.D._{595}$ was measured every 2h, in cells growing in the absence (control) and presence of 4μM thiamine (down-regulation). Note that after 10h ark1p down-regulation cells start dying (arrow).

Chapter 3

Results II

3. Results II – Understanding mal3p phosphorylation

3.1 S4 is essential for mal3p function but it is not a phosphorylation site

While trying to identify the kinases responsible for tip1p and mal3p phosphorylation, we were simultaneously interested in identifying its phosphorylation sites. Knowing the phosphorylation sites would give us important clues to uncover the functions of both tip1p and mal3p phosporylation.

The structure of the EB1 amino-terminal calponin homology domain, which is essential for microtubule binding, suggested that within this domain S16 and T33 were potential phosphorylation sites (Figure 3.1A) (Hayashi and Ikura, 2003). Both S16 and T33 are exposed to the solvent and thus accessible to kinases that can target their phosphorylation. On the other hand, S16 was conserved and present in all species studied so far, with the exception of *Arabidopsis Thaliana* (Figure 3.1B, arrow). Aditionaly, this site lies within the recognition sequence of CK1 and CK2 kinases establishing S16 as the most promising putative regulatory site. Given this evidence, we focused our attention in the mal3p phosphorylation site identification. Knowing that mal3p is exclusively phosphorylated on serines, we only investigated the possibility of the EB1 S16 site being phosphorylated in fission yeast mal3p. Sequence alignments showed clearly that S4 of mal3p is the serine corresponding to S16 of EB1 (Figure 3.1B, arrow). Bioinformatic analysis using NetPhos suggested that S4 is likely to be phosphorylated (Annex II). Similar to its mammalian analog, S4 displayed a consensus site for casein kinase II phosphorylation (http://www.cbs.dtu.dk/services/NetPhosK/). Taken together, this strongly suggests that S4 in mal3p is phosphorylated. To further test this possibility we created mutant strains where S4 was replaced by alanine, which cannot be phosphorylated (S4A). S4 lies at mal3p N-terminal end, so we could easily introduce this mutation by homologous recombination using long (~100 bp) primers (Bahler *et al.*, 1998)(Section 6.3.1). The primers were designed such that the gene specific 80bp contained the S4 to A mutation, whereas 20bp were specific to a plasmid used to amplify the transformation cassette. This cassette contained a selection marker (kanamycin) and the Pnmt81 promoter that was positioned in the same reading frame as mal3p (Figure 3.1C).

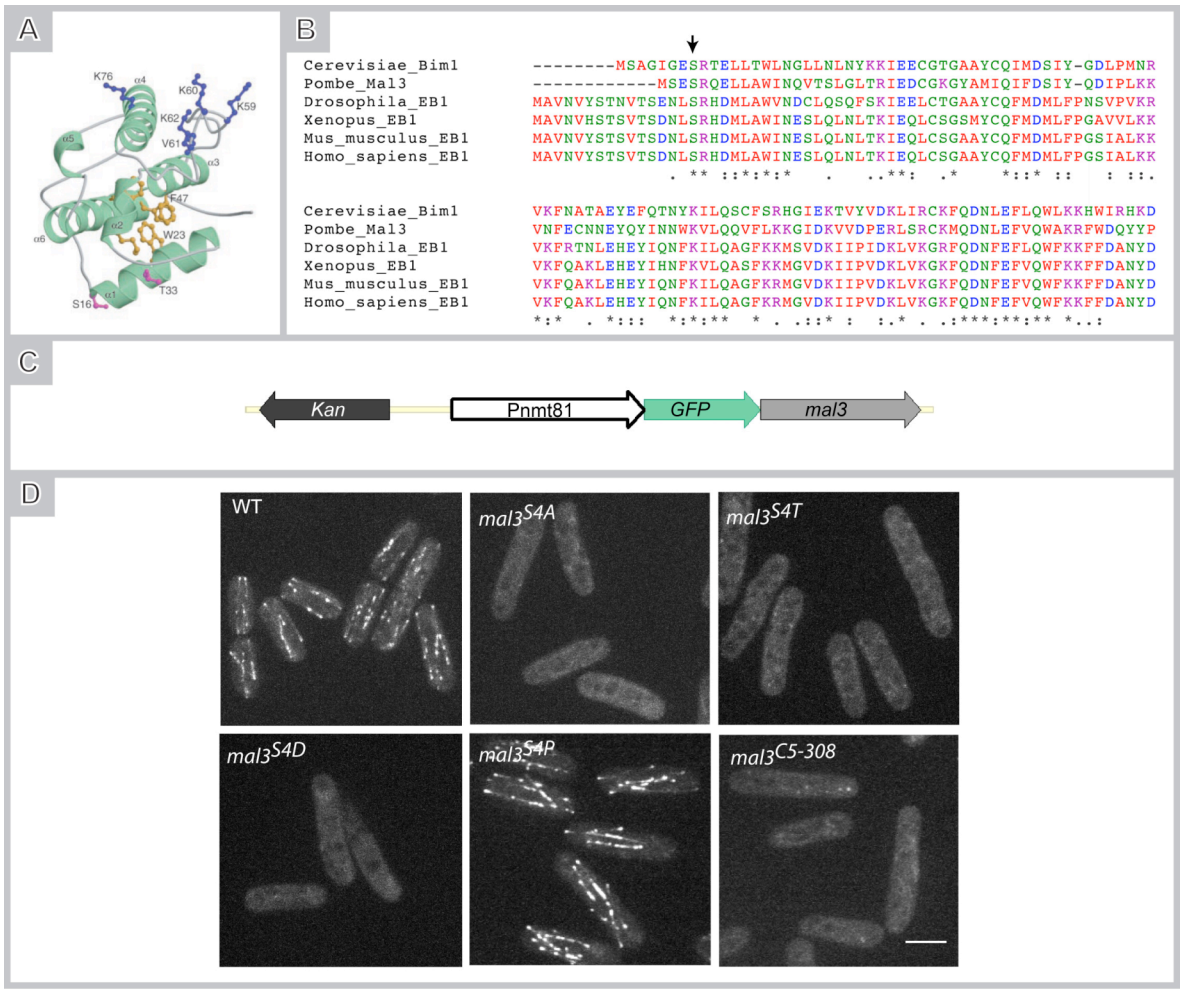

Figure 3.1: S4 is essential for proper mal3p localization on the microtubules.
(A) The crystal structure of the EB1 calponin homology domain (Hayashi and Ikura, 2003). (B) MUSCLE (http://www.ebi.ac.uk/Tools/msa/muscle/) sequence alignment of the calponin homology domain, for members of the EB protein family. Note that S4 is extremely conserved across species. (C) Schematic representation of the genetic background of strains depicted in (D). All point mutations and truncations were introduced by homologous recombination. (D) GFP-mal3p maximum projections of z-stacks images acquired for the control strain (wild type, WT) and strains containing the different point mutations. The last panel shows a truncated form of GFP-mal3p, lacking the first 4 amino acids. WT, *mal3*^{S4A}, *mal3*^{S4T} and *mal3*^{S4D} images were taken by Imola Balogh-Aprill. Scalebar = 5µm.

When de-repressed, this promoter displays mal3p expression levels similar to the endogenous promoter (Karl Emanuel Busch, PhD thesis, 2004). In order to visualize mal3p^{S4A} localization, we also constructed a strain where GFP was placed N-terminally to mal3p (GFP-mal3p)(Figure 3.1C). Using these strains, we observed that the localization of mal3p^{S4A} and wild type mal3p differed fundamentally. Localization to the microtubule lattice and accumulation at growing microtubule plus-ends was completely abolished, indicating that mal3p^{S4A} is not able to bind to microtubules. Occasionally some bright dots of unknown origin were seen in the cytoplasm

(Figure 3.1D). Consistent with these results we could occasionally observe abnormal morphologies in mal3p^{S4A} mutants. These included the presence of bent cells, similar to what is observed for *mal3Δ* cells. To investigate if a lack of phosphorylation of S4 was responsible for these effects, we constructed a mutant mimicking constitutive phoshorylation. Using the same method as described above, we replaced S4 by aspartic acid (mal3p^{S4D}). This residue can mimic phosphorylation as it provides a negative charge similar to the phosphate group. Surprisingly, mal3p^{S4D} showed a similar phenotype to mal3p^{S4A} and was not able to localize to the microtubules (Figure 3.1D). Since it is known that aspartic acid cannot always mimic phosphorylation we sought to explore S4 phosphorylation using another approach. We reasoned that substitution of S4 to threonine should give us a wild type phenotype, since kinases phosphorylating serines in general are also able to phosphorylate threonines. However, mal3p^{S4T} was also not able to rescue the mutant phenotype (Figure 3.1D). Moreover, removal of the first four amino acids of mal3p displayed the same phenotype as mal3p^{S4A}, mal3p^{S4D} and mal3p^{S4T} mutants (Figure 3.1D). These results suggest mal3p N-terminal residues 1-4 are crucial for mal3p microtubule binding, without clarifying whether S4 is the critical amino acid. To test if substitution of any of the first N-terminal amino acids would result in the same phenotype, we replaced S2 with proline (mal3p^{S2P}), an amino acid that due to its cyclic and rigid side chain may considerably change protein structure. This substitution however did not affect mal3p localization (Figure 3.1D), suggesting that mal3p localization on the microtubules may be specifically dependent on the S4 residue.

Since mal3p^{S4A} was not able to bind microtubules, we expected microtubule organization to be altered in these mutants. To explore microtubule organization in mutant strains, we transformed cells with a plasmid expressing GFP-tubulin under the control of the thiamine repressible Pnmt81 promoter. Non-repressed cells were imaged and the results are shown in Figure 3.2.

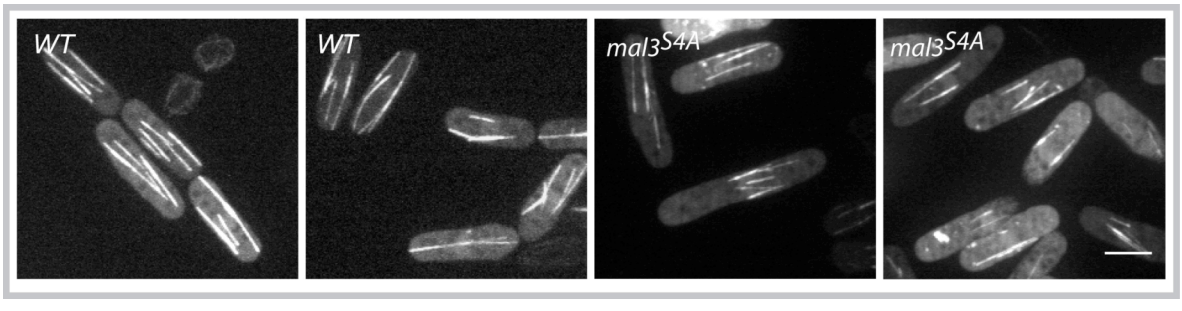

Figure 3.2: Mal3p^{S4A} mutants have short microtubules mimicking *mal3*Δ cells
Indicated strains transformed with a plasmid expressing GFP-tubulin from the Pnmt81 promoter, were grown in EMM2 for microtubule imaging. Scalebar = 5μm.

As expected, microtubules are very short and unstable in mal3p^{S4A} cells, thus phenocopying *mal3Δ* microtubule defects. Measurements on microtubule dynamics would nevertheless be required to further confirm our observations.

To evaluate the mal3p^{S4A} phosporylation state, whole protein extracts from unsynchronized mal3p^{S4A} and wild type control cells were prepared. Extracts were loaded on 12% acrylamide gels and subsequently analyzed by western blot using polyclonal α-mal3p antibodies. An upper phosphorylation band was still visible in mal3p^{S4A} mutants (Figure 3.3A). This result cannot rule out phosphorylation of S4 for several reasons. First, the mal3p phosphorylation band is difficult to properly resolve on a standard 12% acrylamide gel. In fact the mal3p upper phosphorylation band seen in Figure 3.3A is composed of several phosphobands that cannot be separated (for example Figure 2.1B, where using Phostag gels, mal3p upper band can now be separated into two). Secondly, some phosphorylation sites do not produce significant protein shifts with standard gel electrophoresis techniques. Moreover, also low abundance and/or labile phosphorylations are very difficult to detect. For this reason, we decided to perform a series of additional experiments to further analyze the putative phosphorylation of S4.

First, we analyzed wild type and mal3p^{S4A} mutant protein extracts from unsynchronized cells using Phostag gels (Figure 3.3C). Surprisingly, we observed that mal3p^{S4A} seemed hyperphosphorylated, since all bands seem shifted up and an extra band appears between the lower and the upper bands (Figure 3.3C). This result can be explained, for example, if the S4A mutation exposes some previously buried phosphorylation sites, causing extra phosphorylations to occur. This is unexpected, since S4 is located at the very N-terminus, and it is difficult to imagine how this would affect overall mal3p structure. However, it has recently been suggested that mal3p undergoes a conformational change after release of a head to tail auto-inhibitory mechanism (Hayashi *et al.*, 2005). It is possible that this mechanism is affected in the mal3p^{S4A} mutant. Alternatively, it is possible that the two pools of mal3p, the one bound to the microtubules and the one free in the cytoplasm, interact with different sets of proteins of leading to different post-translational modifications. In this way, and since mal3p^{S4A} is fully cytoplasmatic, we are now only able to see the cytoplasmatic-related post-translational modifications.

In a second approach to test for S4 phosphorylation we performed two-dimensional gel electrophoresis (2D-gels), followed by immuno-detection with polyclonal mal3p antibody (Figure 3.3E and F). 2D-gels separate complex protein mixtures by combining isoelectric focusing in a first separation direction with acrylamide gel electrophoresis in a second, perpendicular direction. In the first dimension proteins are placed in contact with an pH gradient (IPG) strip containing a

selected pH gradient immobilized in a pre-cast polyacrylamide gel. When a current is applied, proteins will migrate according to their isoelectric point (*pI*) and stop when their *pI* equals the strip pH, since at this point their net charge is zero. In the second dimension, proteins are separated according to their size by gel electrophoresis (Section 6.7.7). This method works particularly well for separation of phosphorylated protein isoforms since phosphorylation changes the *pI* of proteins when replacing the neutral hydroxyl groups on serine, threonine or thyrosine residues with negatively charged phosphate group(s). Addition of a phosphate group by phosphorylation usually leads to an acidic shift (towards lower pHs) of the protein *pI*. Thus, a "train of spots" seen in the first dimension of a 2D-gel electrophoresis is usually characteristic of phosphoproteins. As mal3p shows at least two phosphobands in western blots prepared from Phostag gels (Figure 2.1B), we were expecting at least three dots on a 2D-gel. The most basic spot corresponding to the least or even unphosphorylated mal3p and the two more acidic spots to the phosphorylated isoforms. Nevertheless, if S4 were phosphorylated we would expect to see a mal3p spot disappear in mal3p^{S4A} from acidic pHs and to merge with the non-phosphorylated isoform at more basic pH, thereby increasing its intensity.

To test if S4 is a phosphorylation site with 2D gels, we prepared whole protein extracts from unsynchronized S4A mutant and wild type strains (Section 6.7.1). The first thing we noticed when analyzing the resulting western blots of the 2D-gels, was that mal3p has multiple isoforms that could not be fully resolved with 1D gel electrophoresis (Figure 3.3E and F). At least five dots corresponding to five different isoforms, were detected when a narrow range IPG strip pH4-7 was used. Three of them were more prominent, suggesting high abundance of the respective protein isoform, while the remaining two were present in lower amounts. Two independent wild type runs are presented to show reproducibility (Figure 3.3E). Comparison between wild type mal3p and mal3p^{S4A} showed wild type number of dots for the mutant protein. However, their relative amounts differed considerably (Figure 3.3E). We observed a substantial signal increase of the third and fourth protein isoforms revealing a shift to more acidic pHs (Figure 3.3E). These results are consistent with the Phostag gel observations showing intensity changes towards slower moving bands (Figure 3.3C). When the same samples were ran on a micro range IPG pH4.7-5.9, acidic isoforms in both wild type and mutant proteins were not well resolved since the acidic *pH* in this strip is higher (Figure 3.3F). Again, we observed an increased signal, in particular of the fourth dot with the mal3p^{S4A} mutant (Figure 3.3F). Our 2D-gel experiments show that the relative amounts of mal3p isoforms change towards higher levels of acidic isoforms in the in mal3p^{S4A} mutants, suggesting protein phosphorylation.

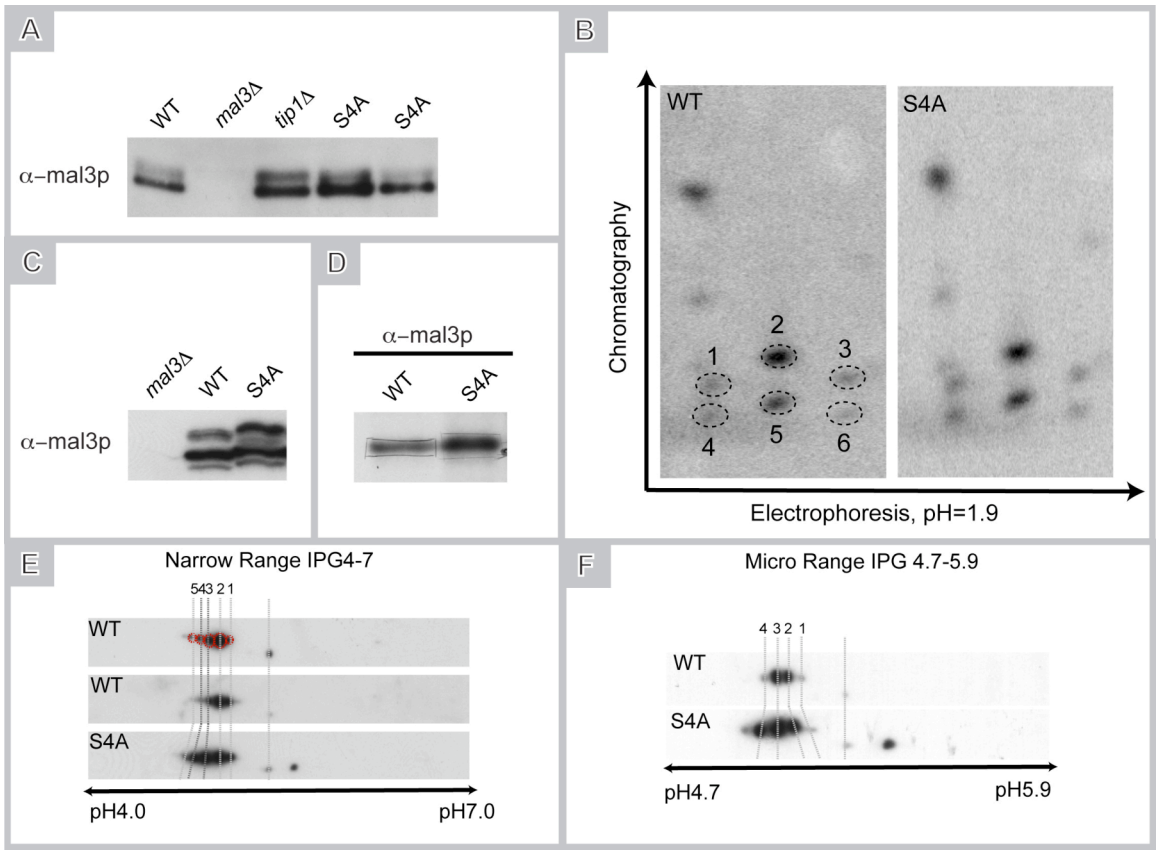

Figure 3.3: Evidence that S4A is not phosphorylated.
(A) Equal amounts of total protein were separated with a 12% Acrylamide gel and analyzed by western blot with α-mal3p antibody. (B) Two dimensional tryptic phosphopeptide maps of WT mal3p and mal3p^{S4A}. [32P]-Labeled mal3p shown in (D) was excised from the membrane and digested with trypsin. The tryptic phosphopeptides were separated in two dimentions as indicated. (C) Total cells extracts from the indicated strains were run on a 75μM Phostag gel. (D) Mal3p from WT and S4A strains was immunoprecipitated from total cell extracts prepared from cells growing in the presence of $^{32}P_i$. The immunoprecipitates were loaded on a 6%-20% gradient SDS-polyacrylamide gel and transferred to a membrane that was exposed to detect the radioactive signal. (E) Two-dimensional gel electrophoresis from total cell extracts of the indicated strains. The samples were run on a pH 4-7 first dimension isoelectric focusing strip and subsequently run on a 12% acrylamide gel. Map3p was detected using α-mal3p antibody. (F) Same conditions as in (E) with the exception that samples were run on a pH 4.7-5.9 first dimension isoelectric focusing micro range strip.

Besides the five upper dots seen in wild type strain in Figure 3.9E, we were also able to see one more lower molecular weight spot (Figure 3.9E, unnumbered dot). Although unclear, we interpreted this spot as resulting from protein degradation, as for the lower bands seen in Figure 2.3C. This lower band was stronger in protein extracts from specific strains (like in the *pck1* down-regulation, Figure 2.3C) but was also visible in the wild type strain (Figure 2.1B). Also, we noticed that this lower band seemed to be stronger if wild type cells were growing in thiamine.

We don't think this band is an unphosphorylated form since it was still present, in some of our experiments, after prolonged phosphatase treatment. However, it is also true, that an overall mal3p down-shift occurred when many of mal3p phosphorylation sites were abolished (below, Figure 3.5F), raising the possibility that phosphatase treatment may not be able to produce complete dephosphorylation. In any case, in the mutants two lower molecular weight dots were seen, instead of one. This "newly appeared" form in the mutants was not always reproducible and so, we think, it could result from the existence of different degradation products in the mutant strains.

In a final approach to detect S4 phosphorylation, we performed a phosphoamino acid analysis of both mal3p^{S4A} and wild type cells. For this, mal3p labeled *in vivo* with [^{32}P] ortophosphate was immunoprecipited and run on a 6-20% acrylamide gradient gel. After gel transfer to a PVDF membrane followed by film exposure, we detected the presence of a single radioactive band in both wild type and S4A strains (Figure 3.3D). Excision of the radioactive mal3p bands followed by tryptic digestion yielded several radioactively labeled phosphopeptides. These were separated by electrophoresis on thin-layer cellulose (TLC) plates in the first dimension followed by thin-layer chromatography in an organic buffer in the second dimension. In this way, peptides are separated according to their mass and charge in the first dimension and according to their hydrophobicity in the second. Using this method, a phosphorylation site can be confirmed by comparing maps derived from wild type and mutant strains, in which the putative phosphorylation site has been replaced by a non-phosphorylatable amino acid such as alanine. A missing spot on the mutant map is a strong indication for phosphorylation of the mutated residue. Our analysis revealed a complex pattern of peptide dots for wild type mal3p and mal3p^{S4A}, which is characteristic of multiphosphorylated proteins and confirmed the existence of multiple phosphorylation sites on mal3p. Unfortunately, we could not detect any difference when comparing mal3p^{S4A} and wild type phosphoamino acid maps (Figure 3.3B).

In conclusion, these experiments show that mal3p is phosprylated on multiple sites and that phosphorylation sites seem to be identical in wild type mal3p and mal3p^{S4A}. We do not find evidence for S4 phosphorylation. However, the mutant displays different protein isoform ratios. This could be explained if a change in mal3p conformation occurs when S4 is compromised and/or by the occurring of different post-translational modifications due to interaction with other binding partners on the cytoplasm.

3.2 Mal3p is phosphorylated in the linker region

The analysis of the wild type mal3p phosphopeptide map (Figure 3.3B) gave us some clues about the characteristics of the peptide containing most of the mal3p phosphorylation. Most of peptides present in the phosphopeptide maps (PPM) shown in Figure 3.3B do not migrate very far in the second dimension, suggesting they are not very hydrophobic. Furthermore, in the PPM map we find six symmetrical spots, which probably represent the same peptide (Figure 3.3B; spots numbered 1-6, Kathy Gould, personal communication). These are most likely generated as a result of variability in their phosphorylation pattern and/or due to multiple trypsin digestion sites at the ends of the peptide. Analysis of all peptides that can be generated by *in silico* tryptic digestion of mal3p, revealed only two peptides that fulfill these criteria (peptide 1 and peptide 2; Figure 3.5A). These peptides are both situated in the mal3p linker region connecting the calponin homology domain with the C-terminal coiled coil region (Figure 3.4A).

Figure 3.4: Mal3p linker region is flexible and non-conserved. (A) Structural representation of the EB1 protein. The conserved microtubule-binding and EB1 domains are shown as surface views. Represented as lines are the flexible peptide segments of EB1 dimer, composed of the linker region and the C-terminal tail. Highlighted in color are the sites where well-studied EB1 interactors were found to bind. For example, both APC and the dynactin/p150^{Glued} are known to bind in the region highlighted in green and blue. However, for efficient binding the dynactin/p150^{Glued} also needs to bind EB1 C-terminal segment (in red). Adapted from (Honnappa *et al.*, 2005). (B) Sequence alignments of the linker sequence (using "MUSCLE" http://www.ebi.ac.uk/Tools/msa/muscle/) for members of the EB protein family. Highlighted in grey is the serine rich region. The box contains a short stretch where the presence of multiple serines is conserved across species.

This linker region is very unstructured, which is why it was never possible to obtain its crystal structure (Hayashi and Ikura, 2003; Honnappa *et al.*, 2005). Furthermore, this region is also exposed to solvents making it a good candidate for harbouring phosphorylation sites. The amino acid sequence of the mal3p linker region is not conserved across species (Figure 3.4B), but it contains multiple serine residues that can be phosphorylated. Analysis of the mal3p sequence using NetPhosK (http://www.cbs.dtu.dk/services/NetPhosK/, Annex II), a program used to identify putative phosphorylation sites, indeed predicted all serines in the linker, and in peptide 1 and 2 in particular, to be phosphorylated. Importantly, NetPhosK predicted the serines to be phosphorylated by several kinases (Figure 3.5A). Of special relevance is S144, which is predicted to be phosphorylated by four different kinases. To verify which, if any, of these serines were modified by phosphorylation we mutated all serines on both peptide 1 and 2 to non-phosphorylatable alanine either individually or in various combinations using site-directed mutagenesis of *mal3* (Figure 3.5B). Mutated *mal3* was amplified from the plasmid and transformed by homologous recombination into *mal3*Δ cells such that all resulting strains expressed mal3p under the control of the native promoter (Section 6.4). We then prepared whole protein extracts from unsynchronized wild type, *mal3Δ,* and the mutated mal3p cells. These extracts were run on Anderson and Phostag gels and probed with polyclonal α-mal3p antibody (Figure 3.5C, D, F and G).

Concerning peptide 1 both Anderson and Phostag western blots show upper mal3p phosphorylated band to be present even after mutating the peptide 1 serines, namely, S130, S131, S138 (Figure 3.5B, C and D). Note that in Phostag gels depicted in Figure 3.5D, we used protein extracts obtained in t=120' and t=0' time points as controls for phosphorylated and unphosphorylated mal3p, respectively. These extracts were derived from the *cdc25-22* experiments described latter in this thesis (Figure 3.7B). During these experiments different mal3p phosphorylation states were observed. t=120' depicts extracts from cells collected 120 minutes after release from the synchronizing block at the G2/M transition. These contain normally phosphorylated mal3p. t=0' depicts extracts from cells synchronized by genetic blockage at the G2/M transition, which lack the upper mal3p phosphorylated band.

Despite upper phosphorylation bands being clearly visible in Figure 3.5D, a slight upper shift, similar but less pronounced to the one seen in mal3p^{S4A}, was observed for mal3p^{S130,131,138A} mutant (Figure 3.5D). These results indicate some unclear protein modifications may be occurring when all peptide 1 serines are replaced to alanine, leading to a seemingly hyperphosphorylated protein.

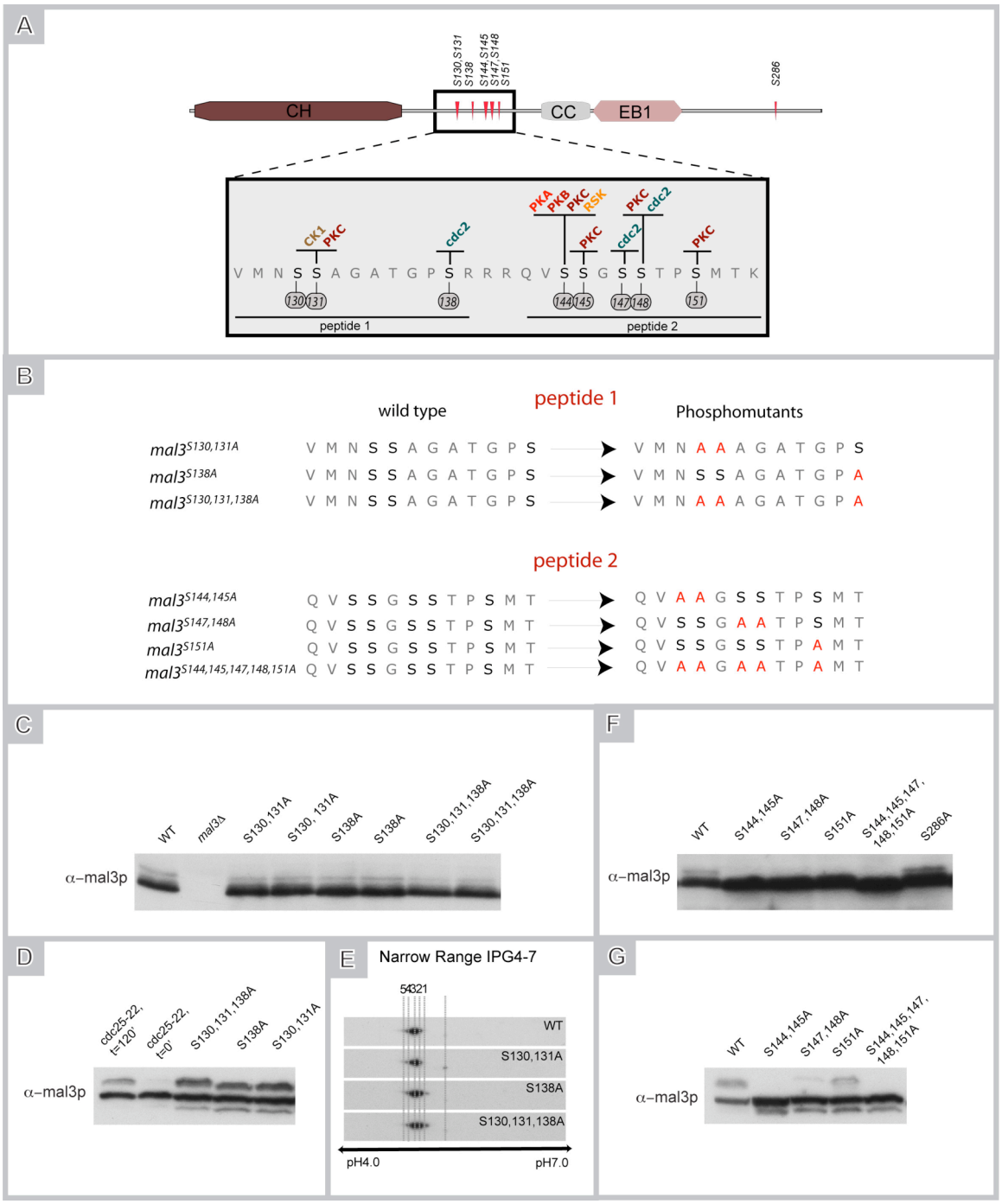

Figure 3.5: Mal3p is phosphorylated in the linker region. (A) Schematic representation of the mal3p linker region, the tested phosphorylation sites and the kinases predicted by NetphosK to phosphorylate the respective sites. (B) Schematic representation of the mutated serines. (C) Total cell extracts from wild type, *mal3Δ*, and the different phosphomutants in peptide 1 were loaded in equal amounts onto Anderson gels. Western blot analysis with α-mal3p antibody reveals multiple mal3p bands for all strains. (D) 75μM Phostag gel of the mutants shown in (C). *Cdc25-22* t=0' and *Cdc25-22* t=120' were used as controls for unphosphorylated and phosphorylated mal3p, respectively (see text for more details). (E) 2D-gel electrophoresis from total cell extracts of the indicated strains. Samples were run in the first dimension on a pH 4-7

isoelectric focusing strip and subsequently separated further on a 12% Acrylamide gel. Western blot analysis was done using α-mal3p antibody. (F) Same conditions as in (C) using peptide 2 mutants. Note the overall protein shift down if all serines are mutated. (G) 75μM Phostag gel of indicated peptide 2 mutants.

To try to clarify these observations, we performed 2D-gel electrophoresis to compare peptide 1 mutants with wild type mal3p. We could observe a spot appearing at higher *pH* values if the S138A mutation was present, which one would expect if less phosphorylated isoforms are generated (Figure 3.5E, dot 1). This indicates that S138 may be a phosphorylated site but represents a minor fraction of the mal3p protein pool that is not responsible for the bulk of mal3p phosphorylation.

In reality, most phosphorylation was found to occur in peptide 2, containing the linker S144, S145, S147, S148 and S151. Strains in which these serines had been mutated to alanines were viable and showed wild type growth curves (Figure 3.6).

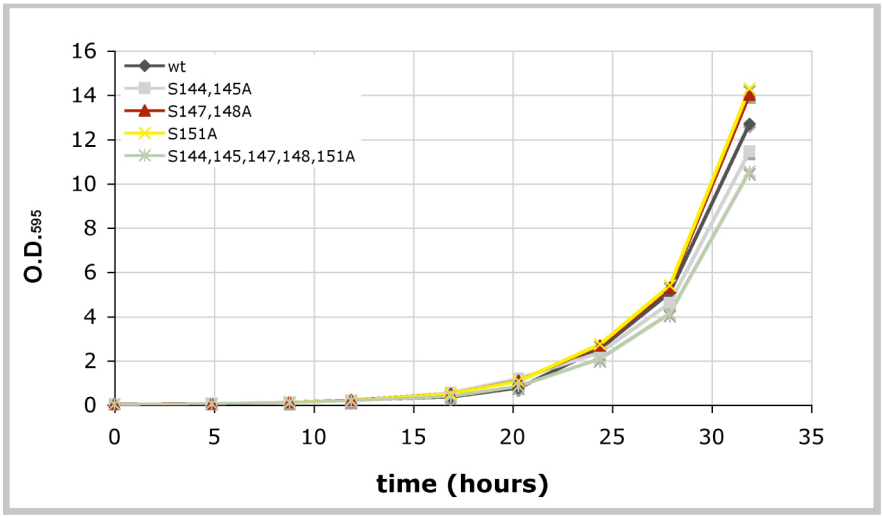

Figure 3.6: Growth curves of phosphomutants. Liquid cultures of the indicated strains were grown in EMM2 with all supplements at 30°C. The $O.D._{595}$ was measured roughly every 3 hours and cell diluted when necessary. Phosphomutants and wild type cells produce similar growth curves.

When running whole protein extracts of peptide 2 mutant cells on an Anderson gel we noticed the absence of the upper phosphorylation band in all the mutants (Figure 3.5F). Moreover, $mal3p^{S144,145,147,148,151A}$, that contains all peptide 2 serines mutated to alanines, showed an overall downshift of mal3p on an Anderson gel (Figure 3.5F). This observation indicates that wild type mal3p is predominantly in a phosphorylated state and that this state depends on the presence of

one or more serines in peptide 2. Notably, this effect was not produced with λ-phosphatase treatment suggesting that the enzyme does not produce complete dephosphorylation or that additional modifications occur which depend on these serines. The same extracts were then analyzed on a Phostag gel and we could confirm that the mal3p^{S144,145A} and the mal3p^{S144,145,147,148,151A} mutants completely lacked the upper band. In contrast, the mal3p^{S147,148A} and mal3p^{S151A} mutants still produced an upper band, which however was of much lower intensity (Figure 3.5G). This means that dephosphorylation of both S144 and S145 results in inability to phosphorylate S147, S148 and S151, indicating that phosphorylation at S144 or S145 (or both) is "dominating" and has a more prominent regulatory role. In this respect, it is interesting to note that S144 seems to be a phosphorylation "hot spot" with predicted consensus sites for many different kinases (Figure 3.5A).

Overall, these results are consistent with previously published data, showing that the mal3p homologs BIM1 from budding yeast and EB3 from human, are phosphorylated in the linker region (Ban *et al.*, 2009; Zimniak *et al.*, 2009). Although the amino acid residues of this region are not conserved across species, they are usually highly enriched in serines/threonines (Figure 3.4B, box).

NetPhosK predicted additional phosphorylation sites located in the C-terminal flexible tail of mal3p (Annex II). The mal3p tail is also a phosphorylation "hot-spot" since it is an unstructured region, exposed to the solvent. Further, regulation at this region could have important biological consequences, as this region is important for mal3p binding to partner proteins. Also, it has been suggested to be involved in a putative auto-inhibitory role (Manna *et al.*, 2008). From all serines predicted to be phosphorylated in the mal3p C–terminus, S286 was chosen because it shows the higher NetPhosK score (Annex II). Cells expressing mal3p^{S286A} still showed an upper phosphorylation band in Anderson gels western blots (Figure 3.5F). Once again, this is not sufficient to exclude that S286 is a phosphorylation site, as its phosphorylation may not produce a visible band shift or exist in low abundance. Phosphopeptide analysis would be required to explore the presence of additional lower abundance phosphorylation sites.

In conclusion, these experiments established that the serines within peptide 2 harbor most, if not all, mal3p phosphorylation sites. For this reason we decided to focus our subsequent analysis on these sites. Nevertheless, it would still be important to check for additional mal3p phosphorylation. In the future, phosphopeptide mapping of wild type and mal3p^{S144,145,147,148,151A} mutants would be useful in order to uncover additional phosphorylation sites.

3.3 Mal3p phosphorylation is cell cycle dependent

Members of the EB protein family are implicated in cell division in most studied organisms (Table 1.1, Section 1.5.4.3.5). Recently, BIM1 phosphorylation was shown to vary in a cell cycle dependent manner (Zimniak *et al.*, 2009). The protein is phosphorylated during anaphase and dephosphorylated at mitotic exit. Similarly, mammalian EB3 was found to be phosphorylated during mitosis (Ban *et al.*, 2009). However, in this case, phosphorylation appeared early in mitosis, during prometaphase, lasting until mitotic exit. We sought to investigate if also mal3p phosphorylation levels varied throughout the cell cycle. To obtain synchronous cultures of cells we used a temperature sensitive *cdc25-22* mutant strain expressing GFP-tagged tubulin (GFP-tubulin). Cdc25p is a phosphatase that triggers entry into mitosis by dephosphorylating the cyclin dependent kinase cdc2p (Nurse, 1990). When *cdc25-22* cells are grown at the restrictive temperature of 36°C, the cells cannot enter mitosis and remain blocked at the G2/M transition. In this way most cells are synchronized after 4 hours at the restrictive temperature. Such synchronized cells were used and released from the block by shifting the temperature to the permissive temperature of 25°C. Cell samples were then collected at multiple consecutive time points. A subset of the cells in each sample were imaged to detect the GFP-tubulin signal that enabled microtubule visualization and thus, monitor cell cycle progression (Figure 3.7A). The remaining cells were used to produce cell extracts in order to follow the mal3p phosphorylation state with acrylamide gel electrophoresis and western blotting (Figure 3.7B). Mal3p was mainly present in a single band in samples from cells at the time of release from the *cdc25-22* block. An additional phosphorylation band appeared 60 minutes after release (t=60'). This time point corresponds to the transition from metaphase to anaphase as judged from the GFP-tubulin images (Figure 3.7A and B). The band is maintained during mitotic exit and interphase but disappears when cells approach the subsequent mitosis (t=195') (Figure 3.7A and B). This experiment shows that mal3p phosphorylation is regulated in a cell cycle dependent manner, similar to its homologues BIM1 and EB3. Like BIM1, mal3p is dephosphorylated when mitosis starts and phosphorylated at the metaphase to anaphase transition. However, in contrast to BIM1, mal3p does not appear to be dephosphorylated at mitotic exit but rather late in G2 shortly before entry into the following mitosis.

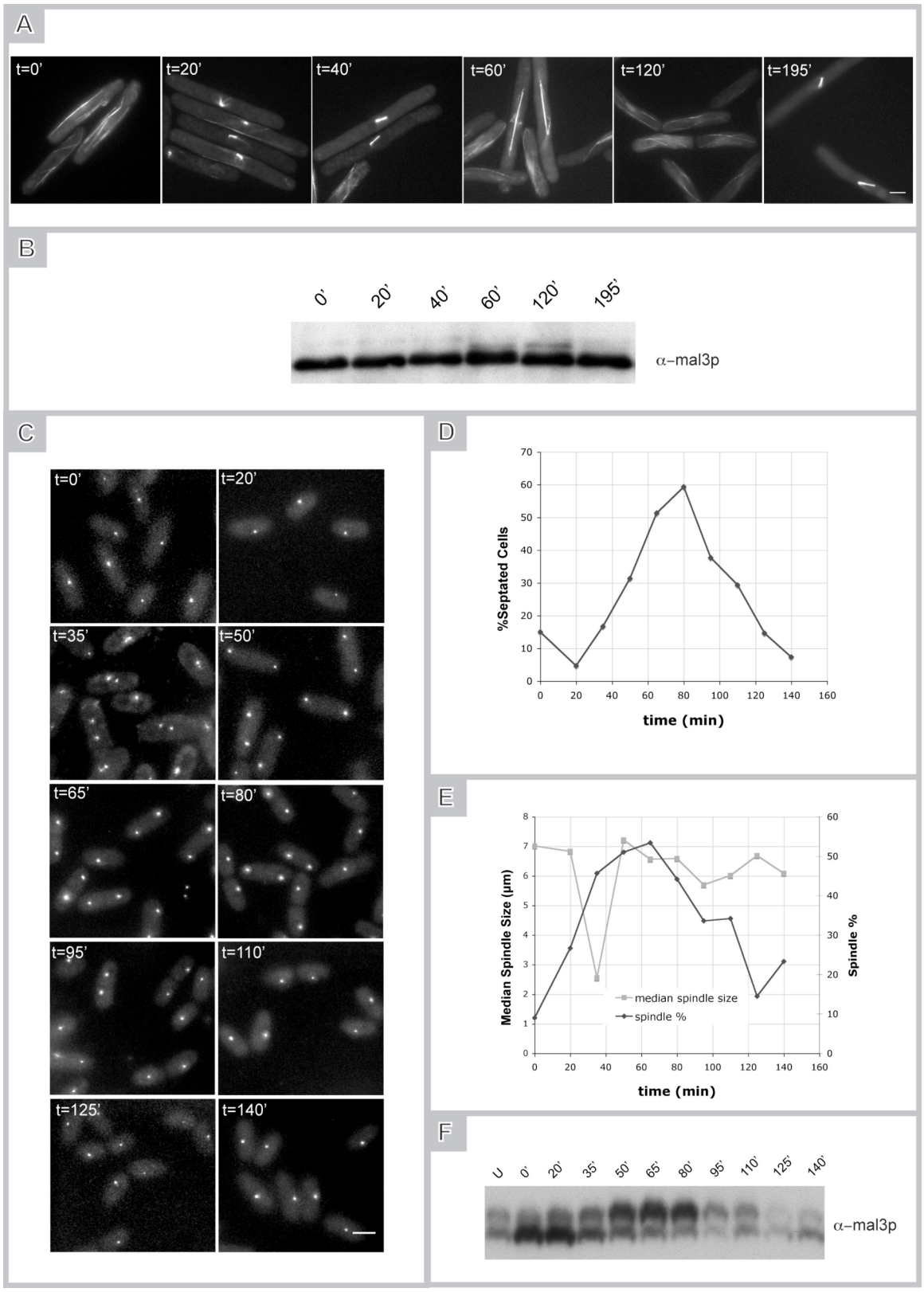
A
t=0'
t=20'
t=40'
t=60'
t=120'
t=195'
B
0'
20'
40'
60'
120'
195'
α–mal3p
C
t=0'
t=20'
t=35'
t=50'
t=65'
t=80'
t=95'
t=110'
t=125'
t=140'
D
%Septated Cells
time (min)
E
Median Spindle Size (µm)
Spindle %
median spindle size
spindle %
time (min)
F
U
0'
20'
35'
50'
65'
80'
95'
110'
125'
140'
α–mal3p

Figure 3.7: Mal3p phosphorylation is cell cycle dependent. (A and B) *cdc25-22* cells expressing GFP-tubulin were blocked in G2 for 4h at 36°C and synchronously released into mitosis by cooling the culture to 25°C. Samples were taken at the indicated time points. A) GFP-tubulin image in subsets of cells from each time point. B) Equal amounts of total protein for each time point were separated with a 12% Acrylamide gel and analyzed by western blot with α-mal3p antibody. (C, D, E and F) Cut12-GFP cells were synchronized in G2 using lactose concentration gradients and samples were collected at the indicated time points. (C) Cell cycle progression was monitored by direct observation of the SPB marker cut12p-GFP. Representative images are shown for each time point. Scalebar = 5μm. (D) Synchronization was controlled by labeling cell walls and septa with calcofluor and counting septated cells in a subset of cells of each time point. (E) From the images in (C) the median spindle size and the % of cells containing a spindle (i.e. a duplicated SPB) were calculated and plotted for each time point. (F) Mal3p phosphorylation levels in total cell extracts were analyzed by Phostag gel electrophoresis and western blotting. "U" depicts unsynchronized cells.

As shown above, mal3p levels change with increasing temperature (Figure 2.4). This makes it difficult to visualize mal3p phosphorylation band in 12% acrylamide gels. For this reason we could not exclude that our *cdc25-22* temperature shift experiments create apparent changes in mal3p phosphorylation that are due to temperature shifts rather than to cell cycle regulation. Therefore, we decided to confirm the cell cycle regulation of mal3p phosphorylation by synchronizing cells in a temperature-independent way. With this purpose, we sorted unsynchronized cells based on their size by centrifugation through a lactose gradient. In *S. pombe* the cell cycle stage is tightly linked to cell size, with longer cells undergoing mitosis and the shortest cells just starting a new cell cycle (Fantes, 1977). The latter cells are less dense than the other cells and following centrifugation can be recovered from the lactose gradient as the top layer. In this way, small G2 cells expressing the SPB marker cut12p tagged with GFP (cut12p-GFP), were recovered from lactose gradients, and further cultured to follow them through the subsequent synchronized mitosis. We chose cells expressing cut12-GFP that allow us to follow mitosis progression though the observation of SPB separation and thus, spindle elongation. Cell recovery time from lactose gradients was monitored to be exactly 30 minutes, and only then was time recording started. In this way at t=0', cells have already been growing for 30 minutes, and so, will quickly enter in mitosis. Cells were collected at the indicated time points for ~2.5 hours, which is when most cells had exited mitosis (Figure 3.7C). For each time point, subsets of cells were used for protein extraction, fluorescence cell imaging and calcofluor staining. Calcofluor labels the cell wall and the site of septation and was used to monitor the number of septated cells and calculate the septation index, which is a good measure of population synchrony. Based on the septation index we estimated that ~60% of our cells were synchronously going through mitosis (Figure 3.7D). The respective protein extracts were loaded on a Phostag gel and analyzed by western blotting to follow mal3p phosphorylation throughout the cell cycle. In these experiments

we observed an upper mal3p band in all samples. However, this band strongly increased in intensity relative to the lower band starting at approximately t=35' and increasing strongly until t=50' (Figure 3.7F). The cut12-GFP fluorescence showed a sudden increase in the median mitotic spindle length occurring in between these time points suggesting that this phase corresponds to the metaphase to anaphase transition (Figure 3.7C and E). These results confirm the *cdc22-25* experiments and show that mal3p is phosphorylated at the metaphase to anaphase transition and dephosphorylated at the onset of mitosis.

3.4 Mal3p protein levels decrease during mitosis

While performing the experiments described in the previous section, we realized that throughout the cell cycle, the overall levels of mal3p varied (Figure 3.7F). Cell cycle-dependent changes in protein levels have been described for BIM1 protein and mRNA. BIM1 levels peaked during G1/S and dropped during mitosis (Tirnauer *et al.*, 1999). Similarly, EB3 levels were shown to increase in late S/G2, and then decrease during the subsequent mitosis (Ban *et al.*, 2009). To better quantify mal3p protein levels, we separated the proteins from the cell extracts of the lactose gradient synchronization experiments on a 10% NuPage precast gel (Figure 3.8A and B). Quantification was performed using tubulin as a reference since the general assumption is that tubulin levels stay constant throughout the cell cycle. Mal3p levels were then plotted as a function of the time of mitotic progression and normalized to 1 for t=0', so that all different experiments could be compared. By averaging the results of three independent experiments, we found that mal3p levels peaked in early mitosis and decreased towards the end of mitosis. Mal3p levels reached a minimum around t=95', when most cells had completed cytokinesis (Figure 3.8B). These results agree well with previously published data, and suggest that regulation of EB protein family levels is an evolutionary conserved mechanism.

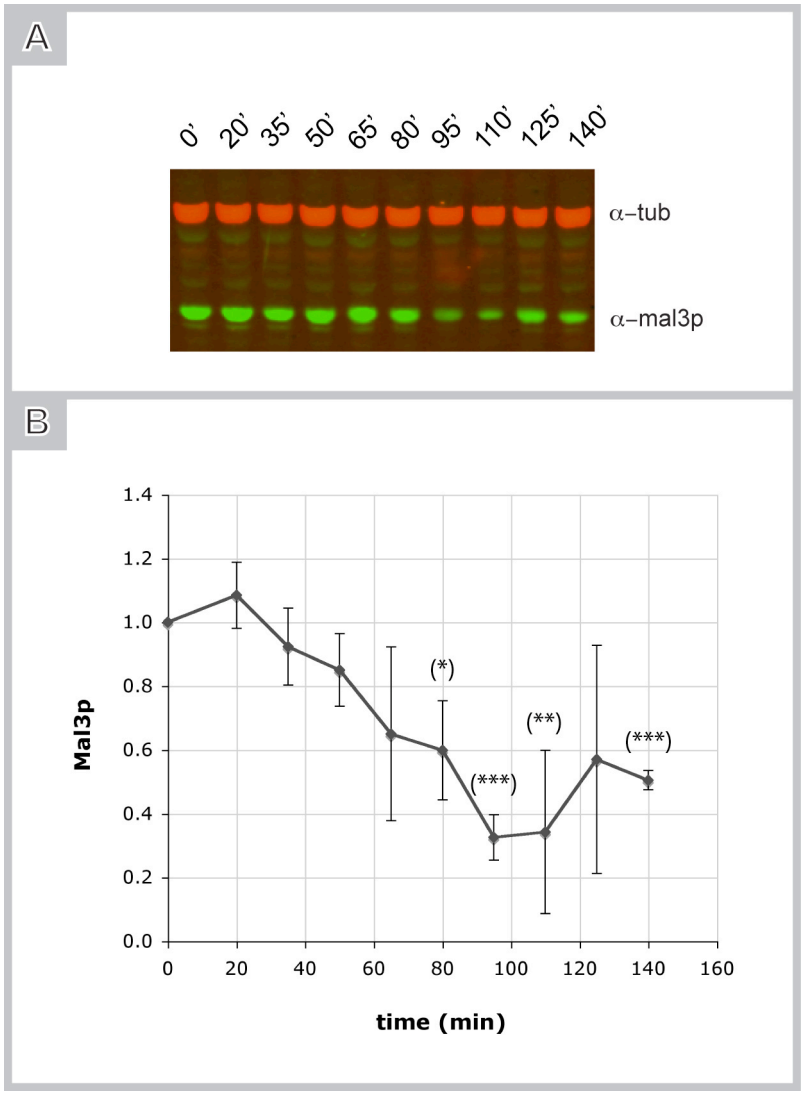

Figure 3.8: Mal3p levels decrease during mitosis. (A) Wild type *S. pombe* cells were synchronized in early G2 using lactose gradients. Samples were collected at the indicated time points and analyzed by western blot. Tubulin antibody was used as a loading control. (B) Mal3p levels were quantified by averaging three western blots as shown in (A) normalized by tubulin using LI-COR odissay software (Section 6.7.8). Mal3p levels were normalized to 1 for t=0' in all quantified experiments. The error bars represent the standard deviation from the mean. Significance is indicated as the difference between the maximal mal3p levels at t=20' and the time points marked with asterisks where *p<0.05, **p<0.01 and ***p<0.001.

3.5 Mitotic phosphorylation occurs in the mal3p linker region

Our data shows that the phosphorylated, upper mal3p band is regulated in a cell cycle dependent manner (Figure 3.7B and F). Additionally, we had observed that this band disappears, when S144, S145, S147, S148 and S151 are mutated to alanine, in unsynchronized cells (Figure 3.5F and G). Thus, it is likely that these sites are being regulated during mitosis. This does not exclude the existence of additional mitosis-specific phosphorylation sites, which would be underrepresented and therefore not detectable in an unsynchronized population of cells.

To investigate if the mal3p linker region accommodates all mitotic phosphorylation sites, we synchronized the phosphomutant strains using lactose gradients. The synchronized cells were cultured and followed through the subsequent mitosis. Protein extracts from cell samples collected at several time points during mitosis were prepared. Mitosis progression and synchronization was evaluated using calcofluor staining and septation index determination as described previously for the wild type strain (Section 3.3). From septation index curves we estimated a ~35% cell synchrony for the mal3p^{S144,145A} and mal3p^{S147,148A} mutants, whereas the mal3p^{S151A} mutant showed a slightly higher ~45% synchronization (Figure 3.9A, B and C). This synchrony is lower than that previously obtained for wild type cells (~60%, Figure 3.7D). However, the cell synchrony obtained in two other independent lactose gradient experiments using the wild type strain was lower (~42% and ~44%), indicating the variability of this experiment.

Analysis of the protein extracts with Phostag gels confirmed that the mal3p^{S144,145A} mutation completely abolished the phosphorylated upper mal3p band we had seen appearing at the metaphase to anaphase transition in wild type cells (Figure 3.9A). This suggests that phosphorylation of the serines in the mal3p linker region is essential for mitosis-specific mal3p phosphorylation. It also confirms the “dominant” nature of S144 and S145 amongst the tested serines since both, the mal3p^{S147,148A} and the mal3p^{S151A} mutants still produced a faint phosphorylation band that appeared at the expected time t=50’ (Figure 3.9B and C).

At this stage these experiments are still preliminary. However, it is interesting to note that the phosphorylation pattern of the mal3p^{S147,148A} and mal3p^{S151A} mutants seem to differ. This raises the possibility that the serines of the mal3p linker region are differentially phosphorylated. The mal3p^{S147,148A} mutant, shows a more sustained phosphorylation band that appears a t=50’ and persists until t=125’. In contrast, the mal3p^{S151A} mutant shows two discrete phosphorylation peaks appearing at time points t=50’ and t=80’. However, these experiments have only been performed once to date and will therefore need to be repeated in order to confirm the results.

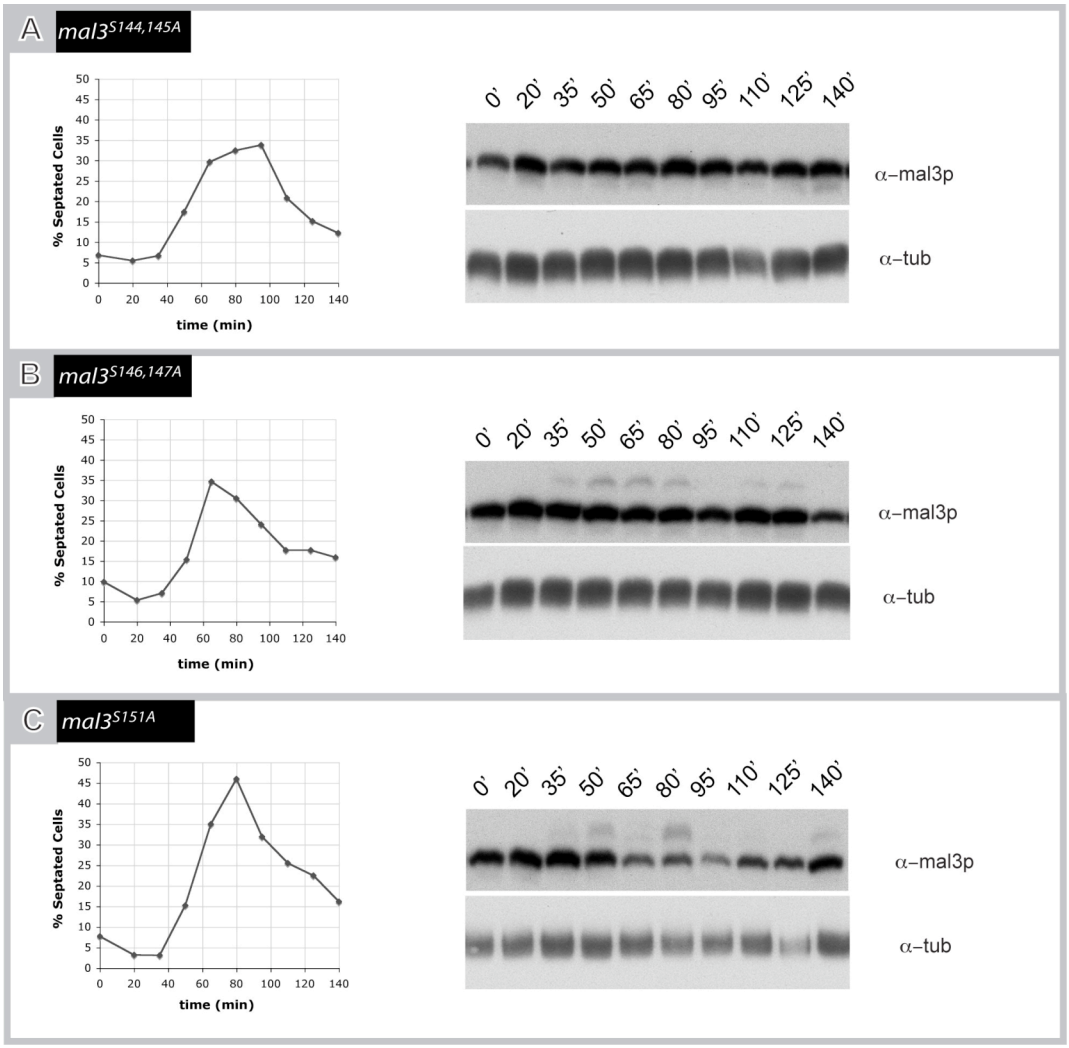

Figure 3.9: The mal3p linker region contains the mitosis-specific phosphorylation sites. (A, B and C) The indicated phosphomutants were synchronized in G2 using lactose gradients and samples were harvested at the indicated time points. Cells were stained with calcofluor to calculate the percentage of septated cells for each sample (left panel). Additionally, total cell extracts were prepared for western blot and loaded on a 75μM Phostag gel (right panel).

3.6 Phosphorylation may influence mal3p levels during mitosis

Phosphorylation of the EB3 linker region was proposed to influence protein degradation (Ban *et al.*, 2009). In this case, phosphorylation seemed to protect EB3 from ubiquitination, thus increasing protein stability. To explore the possible relationship between phosphorylation and mal3p protein levels we quantified mal3p protein levels during mitosis in the phosphomutant strains. If phosphorylation regulates ubiquitination and protein stability, we would expect mal3p levels to be constant during mitosis in the phosphomutant. Protein extracts derived from mutant cells that had been synchronized with lactose gradients were loaded onto 10% NuPage gels. Mal3p protein levels were quantified by western blot using α-mal3p and α-tubulin antibodies (Figure 3.10A).

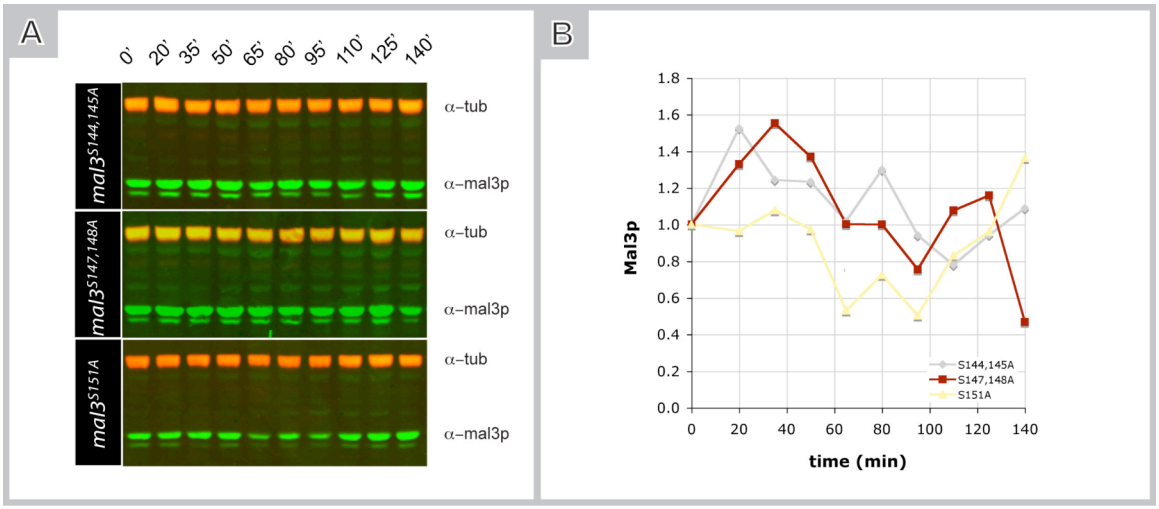

Figure 3.10: Mitotic protein levels of mal3p phosphomutants. (A) *S. pombe* cells with different serine to alanine point mutations were synchronized in early G2 using lactose gradients. Samples were collected at the indicated time points and analyzed by western blot. Tubulin antibody was used as a reference. These are n=1 datasets. (B) Mal3p levels were quantified from the western blots in (A). Mal3p levels were normalized to 1 for t=0' in all experiments.

As previously, tubulin antibodies were used as a loading control. In Figure 3.10B, the ratio of mal3p/tubulin levels were plotted as a function of time of mitotic progression and normalized to 1 for t=0'. In this way, the experiments derived from the different mutants could be compared. The analysis showed that even in the apparent absence of mal3p phosphorylation in mal3p^{S144,145A}, the cell cycle stage-dependent drop of mal3p protein levels persisted in the phosphomutants (Figure

3.10B). This suggests that linker phosphorylation is not responsible for the cell cycle dependent oscillation of protein levels. However, we found that the global mal3p protein levels were higher in the phosphomutants as compared to the wild type (compare Figure 3.8B with Figure 3.10B and Figure 3.11). In addition, *mal3*^{S151A} mutant cells, which show significant phosphorylation, display mal3p levels similar to wild type cells (Figure 3.11). This fits well with the possibility that phosphorylation regulates global mal3p levels by mediating protein degradation. Intriguingly, these results are opposite to what was found for EB3, where phosphorylation of the linker region was proposed to protect EB3 from degradation (Ban *et al.*, 2009). These experiments also need to be repeated to confirm our observations and to draw solid conclusions.

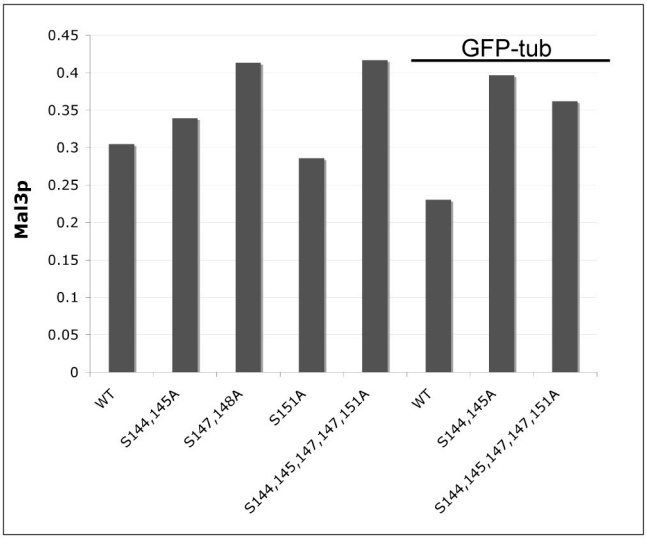

Figure 3.11: Total mal3p levels are higher on phosphomutants. Total *S. pombe* protein extracts from wild type and phosphomutants were recovered and quantified by western blot using α-mal3 antibody and LI-COR odissay software (Section 6.7.8). Tubulin antibody was used as a loading control. In the last three columns all strains express GFP-tubulin under the control of the fully repressed Pnmt1 promoter. The are n=1 datasets.

3.7 Mal3p phosphorylation decreases resistance to microtubule depolymerizing drugs

Mal3p is known to be a major regulator of microtubule dynamics and so we were interested in knowing if phosphomutants showed microtubule defects (Busch and Brunner, 2004). Many simple tests can be performed to evaluate microtubule stability. The most commonly used tests employ microtubule-destabilizing drugs like thiabendazole (TBZ) or methyl benzimidazol-2-yl-carbamate (MBC). Usually, strains with microtubule defects have increased TBZ/MBC sensitivity. Also strains with deficient mitosis due to microtubule or spindle checkpoint defects tend to show increased drug sensitivity.

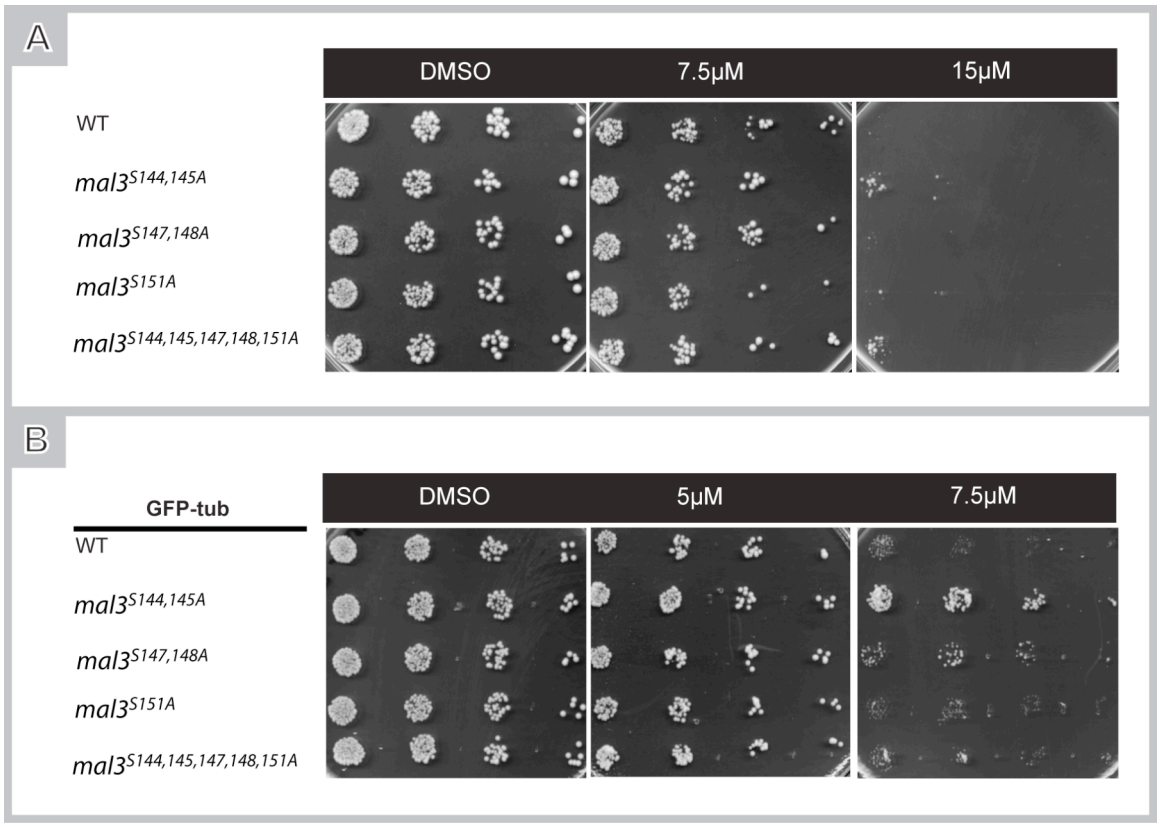

Figure 3.12: Non-phosphorylated mal3p is resistant to microtubule depolymerizing drugs. (A) Serially diluted cells were spotted on YE5S plates containing MBC to the concentrations of 5μM, 7.5μM and 15μM or DMSO as a control. Plates were incubated at 30°C for 3 days. (B) The same as in (A) but strains in addition express GFP-tubulin under the control of the fully repressed Pnmt1 promoter.

As a first approach to check microtubule integrity in phosphomutant cells, we tested the effects of microtubule depolymerizing drugs on cell viability. With this aim, we "spotted" serial dilutions of wild type and phosphomutant cells in plates with various MBC concentrations (Section 6.6). Surprisingly, strains with ablated mal3p phosphorylation showed increased viability at higher MBC concentrations, while strains that retained some mal3p phosphorylation (mal3p^{S147,148A} and mal3p^{S151A}) remained sensitive to MBC similarly to the wild type (Figure 3.12A and B). This effect was even more pronounced in mal3p^{S144,145A} expressing GFP-tubulin, although in the this case mal3p^{S144,145,147,148,151A} didn't show the same degree of resistance (Figure 3.12B). These experiments show that the lack of phosphorylation at S144 and S145 increases cell viability when cells are grown in the presence of microtubule depolymerizing drugs. This effect is increased in pre-sensitized backgrounds, such as for cells over-expressing GFP-tubulin that show an intrinsic increase in MBC sensitivity.

Another commonly used test in *S. pombe* to infer microtubule defects is growth re-initiation after glucose starvation. Cells with microtubule defects tend to produce many cells with bent or branched shapes rather than the usual straight cylinders. This happens because starved cells arrest growth and loose polarity, which needs to be re-established when conditions become favorable for growth (i.e, in new media containing glucose). Properly functioning microtubules ensure that the new growth sites are correctly positioned at the cell tips. However, if microtubules are short or unstable, growth sites tend to be mis-positioned resulting in bent or T-shaped cells (Sawin and Nurse, 1998; Brunner and Nurse, 2000). To test the presence of unstable microtubules in the mutants we performed recovery from glucose starvation experiments. As expected *mal3Δ* cells show many bent, kinked and branched cells whereas wild type cells remained cylindrical. With the exception of the weakest mutant mal3^{S151A}, we frequently detected bent and kinked cells in the phosphomutants (Figure 3.13, asterisks). This suggests that microtubule dynamics is affected in phosphomutants.

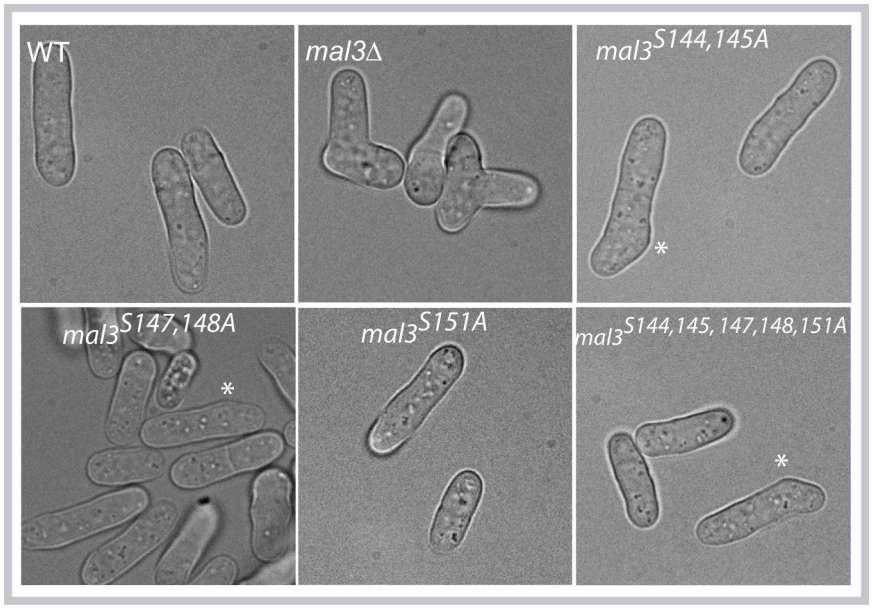

Figure 3.13: Phosphomutants show morphological defects when exiting starvation. Cells of the indicated strains were inoculated in YE5S with half glucose to an O.D.$_{595}$ of 0.05. These cells were grown for 48h at 30^{o}C, after which they were diluted 1:5 in fresh YE5S to recover for 2-4 hours at 30^{o}C. Representative images are shown. In all mutants except S151A, kinked cells are frequently seen (asterisks).

Up to this point, we had consistently found the most pronounced defects amongst all phosphomutants with mal3p^{S144,145A} or mal3p^{S144,145,147,148,151A} mutants. We therefore focused on these two strains in the following experiments.

3.8 Mal3p phosphorylation decreases microtubule shrinkage speed

Despite the results of the experiments described in the previous section, definitive evidence for microtubule impairment in the phosphomutants is only provided by direct microtubule observation and quantification of microtubule dynamics. In order to be able to visualize microtubules in living cells, we expressed GFP-tagged α2-tubulin in all phosphomutants (Figure 3.14A). While looking at the microtubules in the mutant strains, no apparent microtubule defects were detected by qualitative, visual inspection. We then decided to quantify microtubule dynamics. Time-lapse imaging of GFP-tubulin expressing mal3p^{S144,145,147,147,151A} and mal3p^{S144,145A} mutant cells allowed us to reconstruct kymographs depicting interphase microtubule dynamics. From the slopes produced by growing and shrinking microtubule tips in the kymographs we could easily determine growth and shrinkage rates of individual microtubules. While microtubule growth rates in the mutants were similar to the wild type, the microtubule shrinkage speeds increased by ~30% and ~5% in the mal3p^{S144,145,147,147,151A} and mal3p^{S144,145A} mutant cells respectively (Figure 3.14C). Since in fission yeast the interphase microtubules form bundles, increased shrinkage rates could result in a reduction of the total number of microtubules per bundle. To test for this, we measured tubulin fluorescence intensity in the mutants and wild type strains. A 37% and 19% reduction in fluorescence intensity of bundles was indeed detected in malp3^{S144,145,147,147,151A} and mal3p^{S144,S145A} cells respectively. This suggests that mal3p phosphorylation decreases microtubule shrinkage speeds, thereby promoting the presence of more microtubules per bundle. This could have impact on overall bundle stability and performance. When comparing average microtubule bundle number and bundle length of phosphomutant and wild type cells we did not find evidence for more and/or shorter microtubule bundles, which often accompanies compromised microtubule phenotypes (Figure 3.14D). However we observed a difference in the distribution when analyzing histograms. There we found a tendency towards increased numbers of microtubule bundles/cell with shorter sizes, particularly for the mal3p^{S144,145,147,147,151A} strain (Figure 3.14E and F). For example, the number of cells with 3, 4 and 5 microtubule bundles was higher in the mutants as compared to the wild type (Figure 3.14E, shadowed). Also, the frequency of microtubules found between 12 and 16μm was nearly double in mal3p^{S144,145,147,147,151A} compared to wild type cells (Figure 3.14F, shadowed). These typically present most of microtubules with sizes within 16 to 20μm. Together these results agree well with the presence of slightly unstable microtubules in the mutant strains, possibly explaining the shape abnormalities seen during exit from glucose starvation (Figure 3.13).

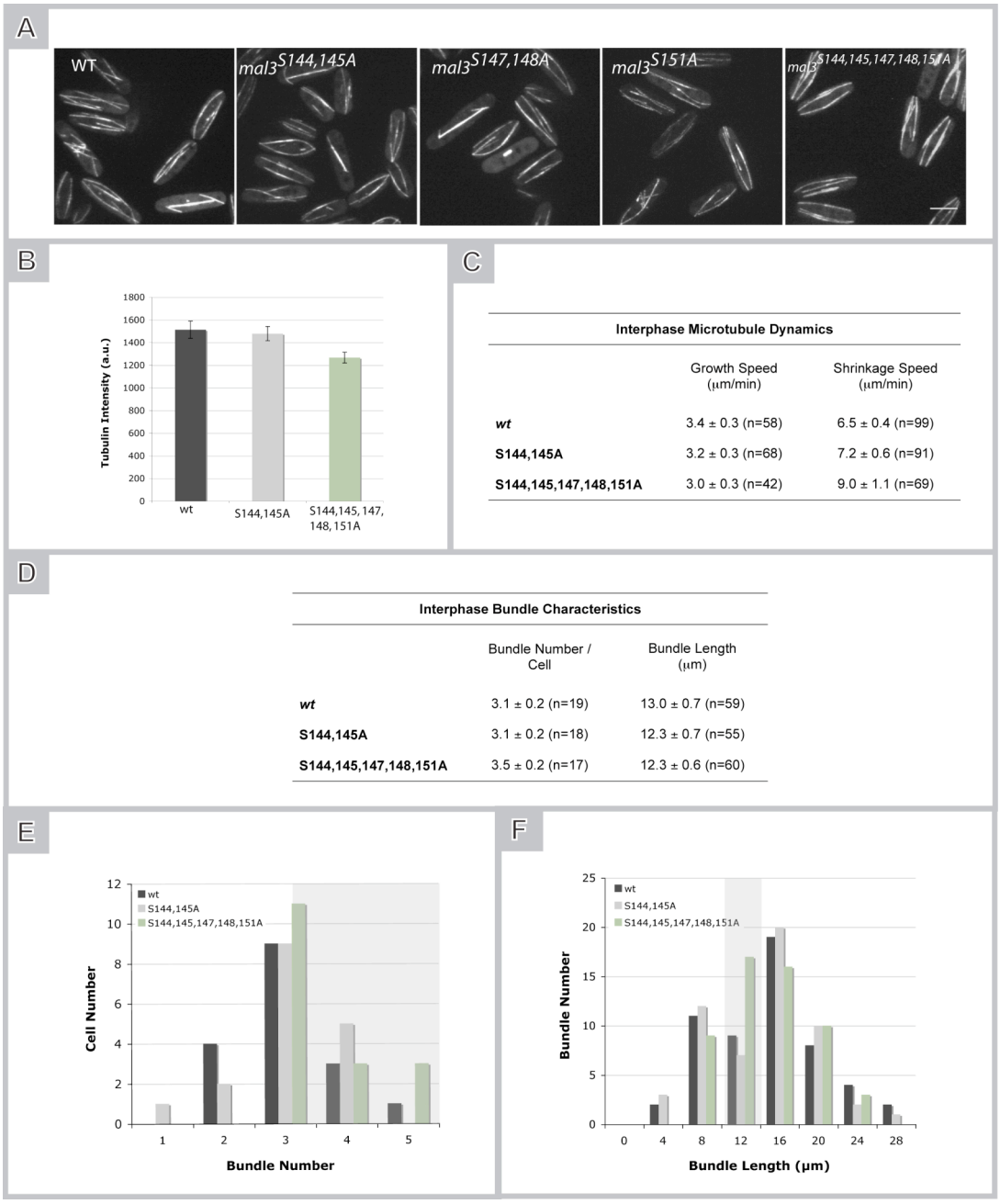

Figure 3.14: Eliminating mal3p phosphorylation mildly destabilizes microtubules. (A) Maximum projections of image stacks of GFP-tubulin expressing cells under the control of the fully repressed Pnmt1 promoter. Cells were grown in EMM supplemented with uracil and 30μM thiamine at 25^{o}C. Scalebar = 5μm. (B) Microtubule tubulin intensity was measured for the indicated strains from the maximum projections. The average tubulin intensity was plotted after background subtraction (mean ± SEM). (C) Average microtubule growth and shrinkage speeds were calculated from kymographs for the indicated strains (mean ± SEM). (D) The number of microtubule bundles per cell and bundle length was measured for the indicated strains (mean ± SEM). Mitotic cells and cells displaying post-anaphase arrays were excluded from the analysis. (E-F) Histograms showing the data distribution. Note that strain mal3p^{S144,145,147,148,151A} shows a trend for higher number of microtubules per cell but with decreased bundle length (regions shadowed in grey).

3.9 Mal3p phosphorylation affects spindle mid-zone organization

To investigate mal3p dynamics and localization in the phosphomutants we tagged mutated mal3p with GFP. N-terminal tagging is usually preferred, since a previously described C-terminal tagged mal3p caused altered cell morphology and microtubule appearance (Beinhauer *et al.*, 1997; Browning *et al.*, 2003). Several attempts to N-terminally tag mal3p with GFP failed, so we decided to nevertheless tag the protein at its C-terminus but to introduce a long linker between the protein and GFP. Such a linker was shown to preserve the function of C-terminally tagged mal3p (Emanuel Bush and D. Brunner, unpublished).

Both wild type and phosphomutants show mal3p accumulation at microtubule tips and also faintly along the microtubule lattice in interphase cells (Figure 3.15A). Additionally, during mitosis no differences in localization were observed between the wild type and phosphomutant proteins (Figure 3.15B). As previously described, wild type malp3 was formed a punctate pattern along the spindle, traveling from both SPBs towards the spindle center (Asakawa *et al.*, 2005). There, mal3p dots tended to disappear. The same behavior was found in the mal3p^{S144,145,147,147,151A} and mal3p^{S144,S145A} mutant. Wild type and mutant mal3p were also present at the growing tips of astral microtubules and enriched at the SPBs, and in more prominent dots, which flank the spindle mid-zone (Figure 3.15B, red, white and yellow asterisks, respectively).

To further study mal3p localization dynamics in mitosis, we produced kymographs of the spindles from consecutive frames of time-lapse movies. Such kymograph analyses enabled the visualization of individual microtubule tracks within the spindles, giving a clear picture of cell cycle dependent changes in mal3p localization dynamics (Asakawa *et al.*, 2005). As mal3p phosphorylation appears at the metaphase to anaphase transition, we particularly focused on mal3p behavior during this transition. Thus, image acquisition started when cells were in mid- to late metaphase and lasted until late anaphase.

In wild type metaphase spindles, mal3p dots travel all the way from the two opposite SPBs towards the center of the spindle until they eventually disappear as a consequence of microtubule catastrophe. This movement, creates a characteristic crisscross pattern (Figure 3.15, class A, metaphase). At the onset of anaphase B, mal3p dot movements become restricted to the regions flanking the mid-zone as a consequence of frequent rescue events in this region. At this stage, complete microtubule shrinkage towards the SPB is rare. Spindle microtubules thus undergo repeated cycles of growth and shrinkage in regions next to the spindle mid-zone, thereby creating inverted slopes flanking a basically mal3p-free mid-zone (Figure 3.15C, class A, anaphase) (Sagolla *et al.*, 2003).

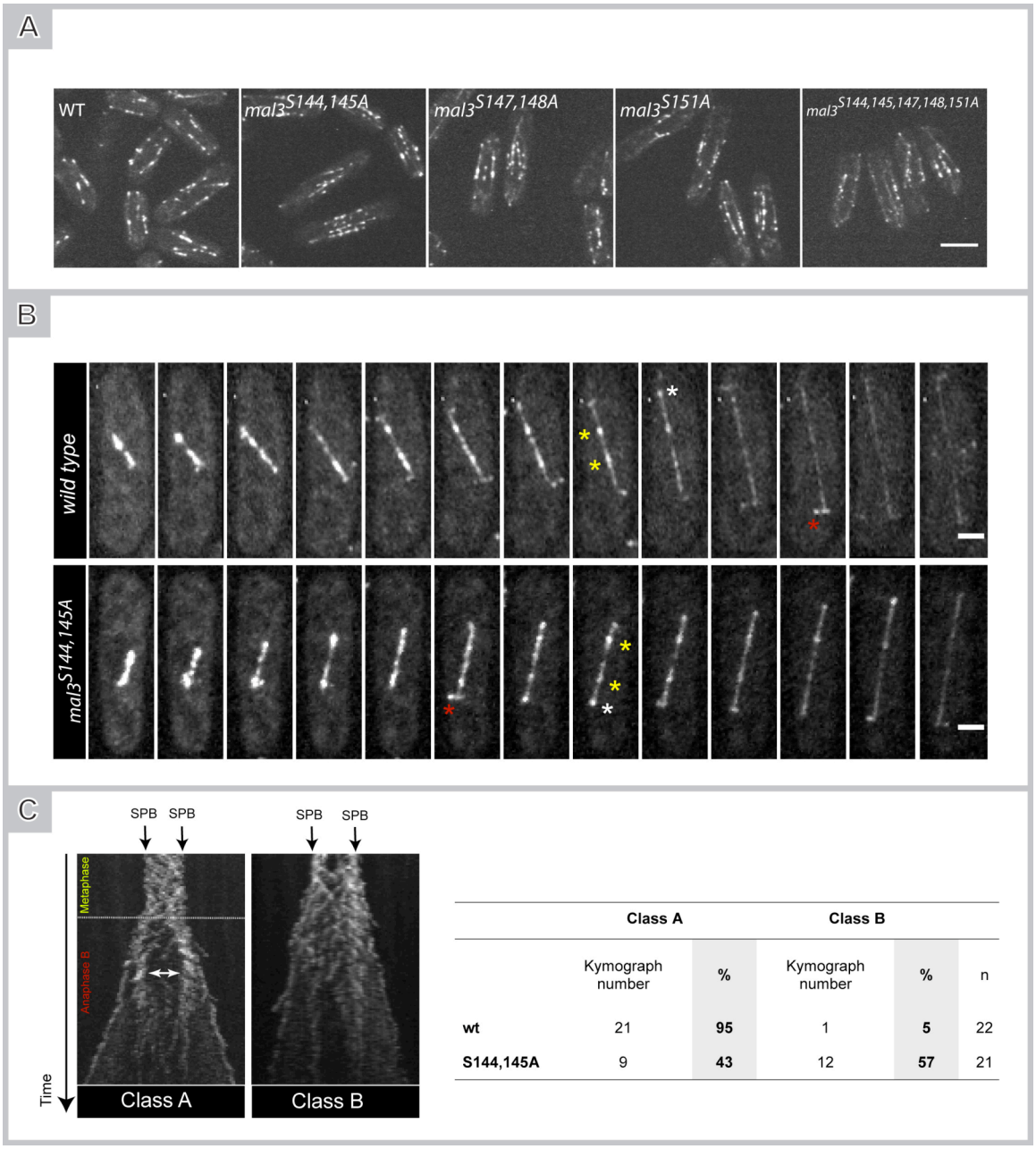

	Class A		Class B		
	Kymograph number	%	Kymograph number	%	n
wt	21	**95**	1	**5**	22
S144,145A	9	**43**	12	**57**	21

Figure 3.15: Mal3p phosphorylation affects mid-zone organization. (A) Maximum projections of mal3-GFP cells are shown for wild type strains and the different phosphomutants. Scalebar = 5µm. (B) Movie sequences of maximum projections of *mal3-GFP* expressing cells during metaphase and anaphase. Frames were taken every 50''. Mal3p accumulates on the spindle pole bodies (white asterisks), on growing tips of the cytoplasmatic astral microtubules (red asterisks) and on regions flanking the spindle mid-zone (yellow asterisks). Scalebar = 2µm. (C) Kymographs of *mal3-GFP* cells can be classified in two main classes: class A, where the spindle mid-zone is well defined and class B, where the mid-zone is less structured. The table on the right shows the quantification of class A and B kymographs obtained from imaging of both wild type strain and the S144,145A phosphomutant.

Within a cell population some variability to these patterns exists, but in our analysis we could group the kymographs into two major categories that we named class A and B. In class A kymographs a clear change occurred when comparing mal3p behavior before and after the onset of anaphase B where the spindle mid-zone became distinct due to the lack of mal3p dots. This did not happen in class B kymographs where the spindle mid-zone remained covered with dynamic mal3p dots during anaphase B (Figure 3.15C, class B). Our analysis showed that class A kymographs were by far the most common in wild type cells. From a total of 22 analyzed spindles, 95% produced class A kymographs with a clear, mal3p free mid-zone (Figure 3.15C, table). This is in striking contrast with the situation in mal3p^{S144,145A} mutants. In this case, 57% of obtained kymographs show a class B phenotype whereas only 43% were class A (Figure 3.15C, table). These results suggest that lack of mal3p linker phosphorylation partially impairs microtubule rescues at spindle mid-zones. This could be explained by the increased microtubule instability observed in the phosphomutants. Alternativelly, this result could also be produced if more microtubules are nucleated/stabilized in anaphase B (Section 5.7).

3.10 Mal3p phosphorylation affects spindle dynamics

We have shown that mal3p phosphorylation and global mal3p protein levels are regulated in a cell cycle dependent manner (Figure 3.7F and Figure 3.8). Furthermore mal3p phosphorylation affects spindle mid-zone organization (Figure 3.15). Thus, we decided to evaluate if lack of mal3p phosphorylation has an impact in spindle dynamics. Cells expressing GFP-tubulin under the control of the fully repressed Pnmt1 promoter were imaged through mitosis to follow spindle elongation speeds. In *S. pombe*, mitosis can be divided into three different phases. Phase 1, a phase of rapid spindle elongation that corresponds to prophase; Phase 2, a phase of constant spindle length that corresponds to metaphase and anaphase A; finally, Phase 3, which corresponds to the rapid spindle elongation in anaphase B. Spindles were imaged such that all three mitotic elongation phases could be observed. In these experiments, spindle length was followed through mitosis and plotted against time. For easy comparison, all plots were aligned, such that t=0' represents the onset of anaphase B. An overview of the acquired mitotic curves can be seen in Figure 3.16. Surprisingly, spindles from mutants that cannot be phosphorylated, i.e, *mal3*^{S144,145A} and *mal3*^{S144,145,147,148,151A} showed faster spindle elongation in mitosis.

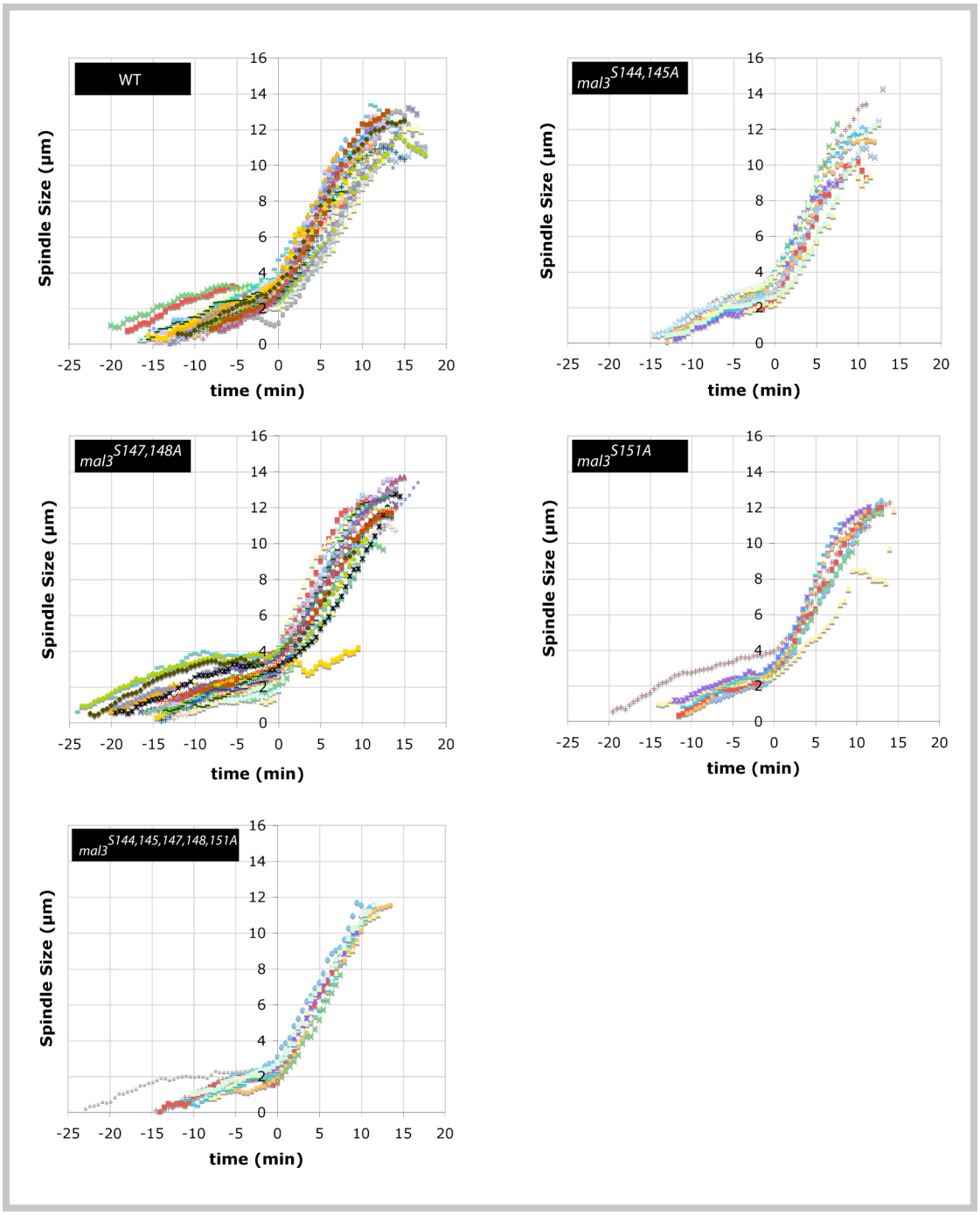

Figure 3.16: Mal3p phosphomutant spindle dynamics. Mitotic cells expressing GFP-tubulin under control of the fully repressed Pnmt1 promoter were imaged at 25°C. Spindle size was quantified over time and plotted to produce curves of spindle dynamics. t=0' is the time where cells start undergoing Anaphase B (fast elongation).

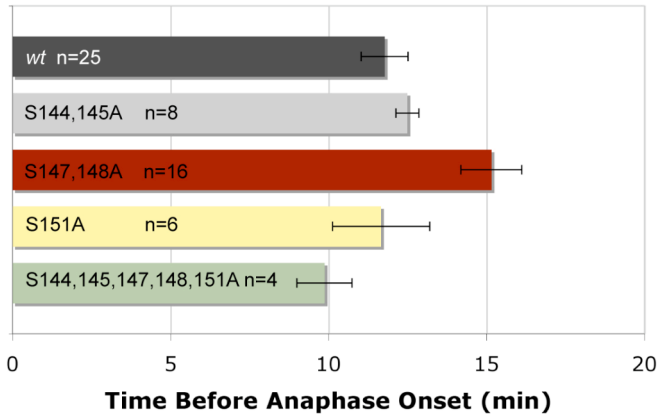

Figure 3.17: Mal3p^{S147,148A} shows a metaphase delay. Phase 1 and 2 duration was calculated for the indicated strains and averaged. Error bars represent SEM.

At ~10 minutes after anaphase B onset, these phosphomutants were already disassembling their spindles and obviously completing mitosis, whereas wild type cells did so at ~15 minutes. Consistently, spindle dynamics in *mal3*^{S151A} cells, which still contain most of the phosphorylation sites, resembled the wild type.

In addition to accelerated anaphase B, we noticed a clear metaphase delay when analyzing the first acquired spindles of *mal3*^{S147,148A} cells. To further investigate this observation, 36 spindles in total were analyzed for this mutant. Once again, a clear mitotic delay was observed, while anaphase B appeared to proceed with normal speed. These results were further confirmed by quantification of the time *mal3*^{S147,148A} mutants required before starting anaphase B, i.e, the time spent in phase 1 and phase 2. We observed that in *mal3*^{S147,148A} cells, phase 1 and phase 2 took ~15 minutes as compared to ~12 minutes in wild type cells (Figure 3.17). Conversely, *mal3*^{S144,145,147,148,151A} cells appeared to have a shorter phase 1 and 2, although for this mutant the number of observed mitosis was very low, and results have to be taken with care. These observations raise the intriguing possibility that different phosphorylation patterns within the mal3p linker region may have different effects on spindle dynamics.

From the slopes of the acquired mitotic curves we were able to calculate the average spindle growth speeds for phases 1 , 2, and 3. The speeds in this study were in agreement with published data, with the exception of phase 1 speeds, where we found slower values (Nabeshima *et al.*, 1998; Mallavarapu *et al.*, 1999)(Table 3.1 and Table 1.2). Discrepancies may be explained by the use of different experimental conditions and/or use of different strains. Nevertheless, the obtained phase 1 speeds were similar between wild type and the mutant strains, indicating that the early stages of mitotic elongation are not greatly affected by mal3p phosphorylation (Table 3.1). Phase 2 speeds were expectedly very slow for all mutants and wild type, consistent with the fact

that the metaphase spindle generally maintains its size. However, *mal3*^{S147,148A} cells displayed an even 4-fold slower phase 2 as compared to all other strains (Table 3.1). This can be explained by the presence of a metaphase arrest in this mutant. Metaphase arrests caused by the absence of EB1 proteins have been described in most studied organisms (Beinhauer *et al.*, 1997; Schwartz *et al.*, 1997; Rehberg and Gräf, 2002; Rogers *et al.*, 2002; Asakawa *et al.*, 2005; Kronja *et al.*, 2009).

Table 3.1: Spindle dynamics in the phosphomutants. Average spindle elongation speeds for phase 1, 2 and 3 were calculated for wild type and the different mutant strains (mean ± SEM). Note that phase 2 is sometimes indistinguishable from phase 1. Thus, phase 2 speeds were calculated only for spindles that showed a clear phase 2. In general, a clear distinction between phase 1 and 2 was more difficult to see for the phosphomutants than in the wild type.

	Spindle Dynamics		
	Phase1 (μm/min)	Phase2 (μm/min)	Phase3 (μm/min)
wt	0.22 ± 0.01 (n=28)	0.08 ± 0.02 (n=17)	0.79 ± 0.02 (n=27)
S144,145A	0.24 ± 0.01 (n=10)	0.10 ± 0.03 (n=5)	0.95 ± 0.03 (n=14)
S147,148A	0.17 ± 0.01 (n=26)	0.02 ± 0.02 (n=7)	0.81 ± 0.02 (n=34)
S151A	0.23 ± 0.03 (n=8)	0.10 ± 0.01 (n=7)	0.84 ± 0.04 (n=8)
S144,145,147,148,151A	0.20 ± 0.01 (n=7)	0.07 ± 0.02 (n=5)	0.85 ± 0.02 (n=8)

Our results raise the intriguing possibility that S147 and S148 play an important role specifically during metaphase. It is also interesting to note that these two serines are contained within cdc2p kinase consensus sites, whereas all other studied serines are not. An active cdc2p-cyclinB complex is the main trigger of entry into mitosis and a key regulator of mitosis progression. It thereby controls the activity and distribution of multiple proteins involved in spindle formation and chromosome segregation (Verde *et al.*, 1990; Nigg, 1995; Nigg *et al.*, 1996; Ohi and Gould, 1999).

Finally, the obtained phase 3 speeds were generally higher in the mutants than in wild type strain (Table 3.1). This effect is particularly clear in mal3p^{S144,145A} mutant that showed an ~20% increase in phase 3 elongation speed. These results suggest a role for mal3p

phosphorylation in controlling spindle elongation where phosphoablation increases anaphase B elongation speed. The same effect has already been reported for BIM1, where linker region dephosphorylation promotes higher spindle elongation speeds (Zimniak *et al.*, 2009).

We should stress however, that all these results are preliminary and should be further confirmed using alternative yeast strains. For example, the use of strains expressing the SPB marker cut12p-GFP would allow monitoring of spindle elongation and exclude possible artifacts generated by tagging tubulin with GFP.

3.11 Mal3p phosphorylation affects the post-anaphase array

Our results showed that mal3p phosphomutants affect spindle mid-zone organization (Section 3.9). Further, BIM1 linker phosphorylation is suggested to play a role in spindle breakage during the last steps of mitosis (Zimniak *et al.*, 2009). In *S. cerevisiae*, BIM1 localizes in the spindle mid-zone and the non-phosphorylatable BIM1-6A mutant shows a stronger mid-zone localization. Even after spindle breakage, strong accumulation of BIM1 at spindle ends is detected. This suggested that spindle mid-zone was maintained intact even when spindle was already breaking. Despite the fact that mal3p localization to the spindle differs significantly from its *S. cerevisiae* homologue, we decided to test wether the spindle mid-zone was affected in mal3p phosphomutants. For this purpose, we constructed a $mal3^{S144,145A}$ mutant strain expressing ase1p-GFP. Ase1p accumulates in the spindle mid-zone where it cross-links antiparallel microtubules, being a very good marker for spindle mid-zone lenght (Loïodice *et al.*, 2005). In wild type cells, ase1p-GFP kymographs showed that mid-zone length remained essentially constant during mitosis (Figure 3.18A). Therefore, we measured mid-zone lengths on selected spindles with a length of ~6μm in both wild type and $mal3^{S144,145A}$ mutants. In both cases the average mid-zone length was ~2.5μm (Figure 3.18A). Although mid-zone length is unaltered in $mal3^{S144,145A}$ mutants, we could observe differences in ase1p-GFP localization after spindle breakage, in the post-anaphase array. This is a transient microtubule structure, nucleated at the eMTOC and specific to *S. pombe* cells (Section 1.6.2.2.1.3, Section 1.6.1, Figure 1.6B,7). In wild type cells the ase1p-GFP signal was present at the SPBs and at the disappearing spindle mid-zones during spindle disassembly. Subsequently, the signal at the SPBs was progressively lost but a signal was retained at the centrally located eMTOC during cytokinesis (Figure 3.18B and C, class A). This signal persisted for a while and then disappeared, most likely coinciding with the completion of cytokinesis and the loss of the post-anaphase array (Section 1.6.1, Figure 1.6).

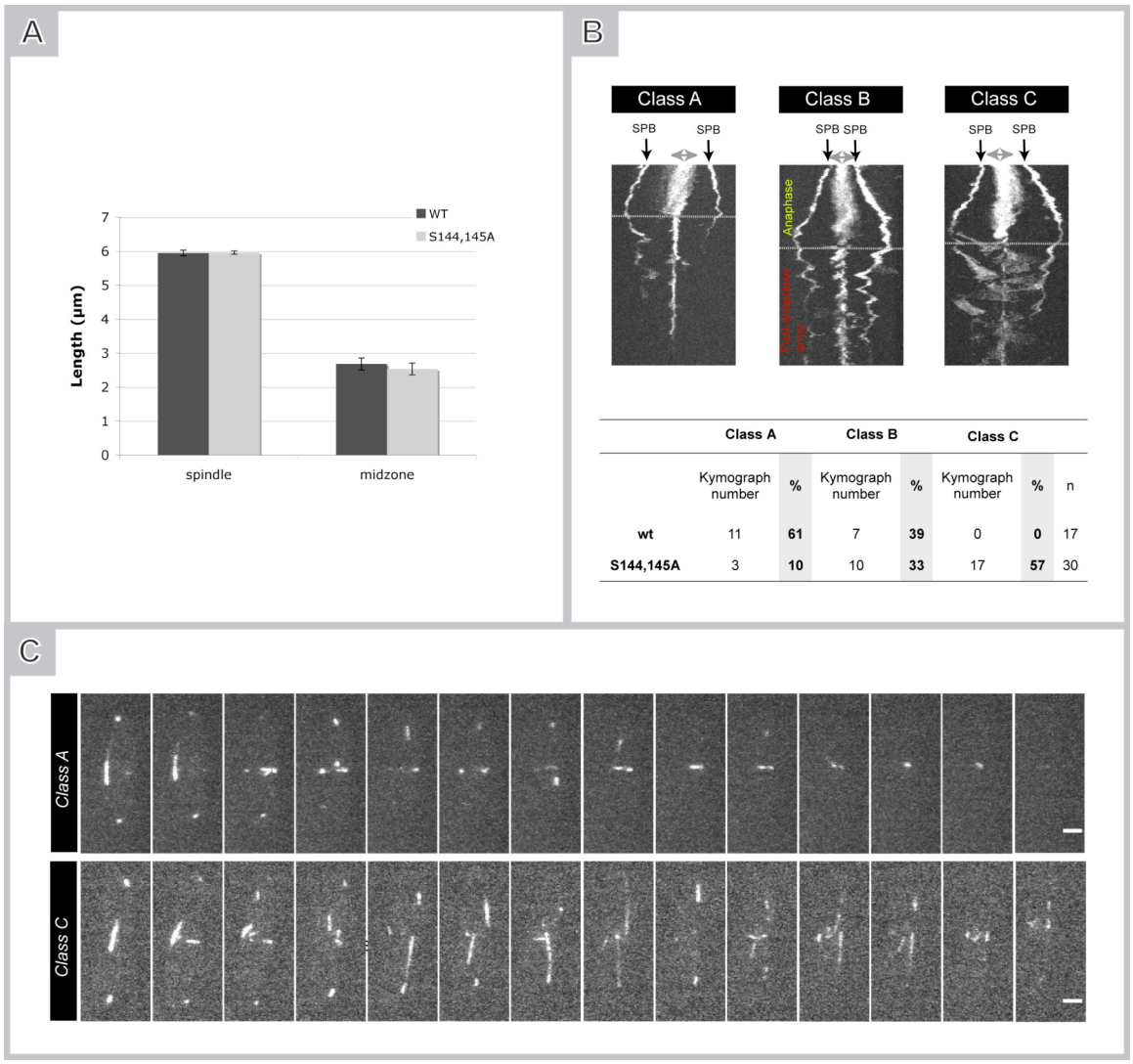

	Class A		Class B		Class C		
	Kymograph number	%	Kymograph number	%	Kymograph number	%	n
wt	11	**61**	7	**39**	0	**0**	17
S144,145A	3	**10**	10	**33**	17	**57**	30

Figure 3.18: Post-anaphase array microtubules are more bundled in *mal3*^{S144,145A} mutants. Ase1p, a protein that localizes on the antiparallel microtubule overlaps, was GFP tagged in wild type and mal3p^{S144,145A} phosphomutant. Time lapse images were taken every 30'' at RT. (A) The mid-zone size was measured for spindles ~6μm size, for both wild type and mal3p^{S144,145A} strains. No difference was found between the different strains. (B) Upper panel: Kymographs from wild type and mal3p^{S144,145A} strains were analyzed and divided into three different classes. In class A kymographs ase1p-GFP localizes only to the eMTOC after spindle disassembly. In class B, ase1p-GFP localizes at the eMTOC and mildly in some of the nucleated microtubules. Finally in class C kymographs ase1p-GFP localizes faintly at eMTOC, but strongly accumulates at the post-anaphase array microtubules. Lower panel: For each strain the different kymographs acquired were assigned to these different classes and their percentage caculated. n is the number of analyzed kymographs per strain. (C) Movie sequences of maximum projections from *ase1-GFP* expressing cells during late anaphase/cytokinesis where post-anaphase array can be seen. Frames were taken every 50''. Scalebar = 2μm.

In *mal3*^{S144,145A} mutant cells the ase1p-GFP signal at the eMTOC was much less defined. In addition, ase1p-GFP seemed to label large regions of the newly nucleated eMTOC microtubules suggesting a significant increase in antiparallel microtubule bundling (Figure 3.18B and C, class C). An intermediate phenotype (class B) was found with similar frequency in wild type and *mal3*^{S144,145A} mutants (Figure 3.18B class B). In these cases, more of the microtubules nucleating at the eMTOC were slightly labeled with ase1p-GFP, indicating extended regions of antiparallel microtubule overlap.

The fact that mal3p phosphorylation obviously decreases microtubule overlaps is very interesting but will need further investigation for example with simultaneous imaging of tagged ase1p and tubulin or by *in vitro* studies with purified proteins.

Chapter 4

Results III

4. Results III – Mal3p Molecular Dissection

4.1 Mal3p truncations

The EB protein family is responsible for the proper localization of many +Tips, facilitating their loading onto microtubules (Bieling *et al.*, 2007). In addition, they are able to directly bind and stabilize microtubules (Busch and Brunner, 2004; Sandblad *et al.*, 2006). Thus, EB protein family seems to have separable functions. To dissect these functions, it would be important to know which molecular domains of this family are involved in each of these functions and to separate them. With this aim, we constructed different mal3p constructs, each lacking a specific protein domain (Figure 4.1A, Section 1.5.4.3). The specific protein domains were deleted in the wild type *mal3* coding sequence by introducing a *ura4+* disruption cassette by homologous recombination (Bahler *et al.*, 1998) (Section 6.3.1).

These experiments were done in collaboration with Linda Sandblad who expressed and purified the same protein constructs from bacteria to use them for cryo-electron microscopy analysis of microtubules that were co-polymerized and decorated with the different truncated protein forms (Linda Sandblad, PhD thesis, 2007). Conserved regions of mal3p were determined by aligning the protein sequence of the different mal3p homologues using "MUSCLE" (http://www.ebi.ac.uk/Tools/msa/muscle/, Annex IV) and by using "SMART", a program designed to identify protein domain architecture (http://smart.embl-heidelberg.de/help/smart_about.shtml). All this information was used for the design of truncation constructs. Eventually we used similar domain boundaries as used in previous studies for mapping the interaction between mal3p and tip1p (Busch and Brunner, 2004) (Section 1.5.4.3, Figure 4.1A). Mal3p^{N123} was designed to contain the first 123 amino acids of mal3p, including the calponin homology domain, implicated in microtubule binding. Mal3p^{N166} covers the first 166 amino acids of mal3p, adding the flexible linker region of mal3p (Barth *et al.*, 2002; Bu and Su, 2003). This region contains the regulatory phosphorylation sites described above, and has been implicated in controlling mal3p microtubule binding (Des Georges *et al.*, 2008). Mal3p^{N203} contains not only the calponin homology domain and linker region, but also the part of the coiled coil region that does not contain the EB1 signature, and has a yet unknown function. Finally, mal3p^{N252} contains the full coiled coil region, thus containing the EB1 motif, but lacks the C-terminal flexible tail. Of all mutants, only mal3p^{N252} should be able to form dimers and to bind to

the known mal3p binding proteins, since the EB1 domain is believed to mediate these processes (Rehberg and Gräf, 2002), (Honnappa *et al.*, 2005). It should also be noted that the flexible C-terminal mal3p tail may be used for mal3p auto-inhibition, and so this mutant may be in a permanent inhibited state (Manna *et al.*, 2008).

As a first readout to test the degree of microtubule impairment in the truncations we performed starvation recovery experiments (Section 3.7). Not surprisingly, a very high percentage of T-shaped cells, suggesting abnormal microtubule function, were found in mal3p^{N123} expressing cells. This effect was progressively attenuated with longer mal3p forms, suggesting that shorter mal3p truncations have more severely impaired microtubules (Figure 4.1B). This was confirmed when observing microtubules in the mal3p truncation strains expressing GFP-α2-tubulin under the control of the fully repressed Pnmt1 promoter. In all cells expressing monomeric mal3p truncations, the microtubules were short, similar to those in *mal3Δ* cells (Figure 4.1E). Only in mal3p^{N252} expressing cells microtubules were more like the wild type although preliminary observations suggest that they were still somewhat shorter and less stable. Quantification of microtubule dynamics and bundle size would be necessary to further validate these conclusions. This would be interesting since the flexible C-terminal tail, which is missing in mal3p^{N252}, was proposed to be part of an auto-inhibitory mechanism making mal3p^{N252} a putative constitutively active protein form (Manna *et al.*, 2008).

The severe microtubule phenotypes found in cells expressing the mal3p truncations suggested that these protein forms are not properly localizing. To study how the different truncations affected mal3p localization, fully unrepressed cells expressing GFP-mal3p at nearly endogenous levels were imaged (Figure 4.1C). Localization to microtubules was significantly impaired for all truncated protein forms except for mal3p^{N252}. This agrees well with the fact that mal3p^{N252} is a dimer whereas all the other truncationss are monomers, as shown by previous gel filtration experiments (Linda Sandblad, PhD thesis, 2007). Thus, EB protein family dimerization seems essential for strong microtubule binding affinity. This was first shown by studies where leucine zipper mediated artificial dimerization of the EB1 calponin homology domain enabled perfect microtubule plus-end tracking (Slep and Vale, 2007, Komarova *et al.*, 2009). Our data further confirm that EB1 domain mediated mal3p dimerization greatly enhances microtubule binding affinity *in vivo*. These results also clarify why microtubules are strongly disturbed in cells expressing monomeric mal3p truncations.

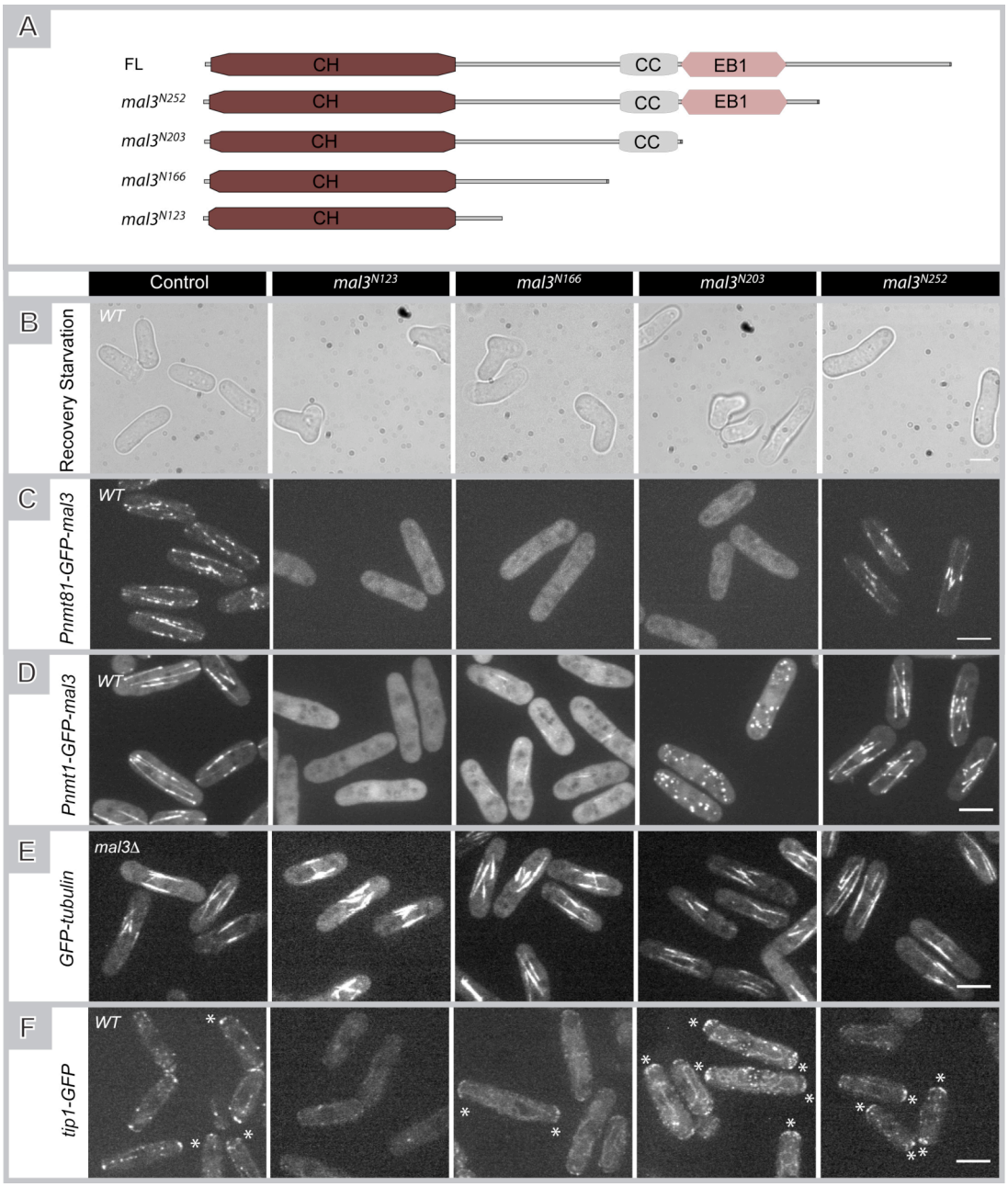

Figure 4.1: Mal3p N-terminal truncations. (A) Schematic representation of all mal3p N-terminal truncations used in this study. CH represents the calponin homology domain that is followed by the linker region in grey. CC represents the coiled coil region that does not contain the EB1 motif. EB1 corresponds to the coiled coil region that contains EB1 signature. These truncations are identical to the truncations used *in vitro* in other studies (Linda Sandblad, PhD thesis, 2007). (B-F) Representative pictures of cells expressing the different truncations in the specified experiments are shown. Scalebar = 5μm. B) Cells were starved in YE medium containing half the normal amount of glucose for 48h at 30°C. They were then diluted 1:5 in fresh YE medium and let recover for 3h. C) The localization of mal3p truncations expressed under the control of the derepressed Pnmt81 promoter is shown, D) The localization of mal3p truncations expressed under the control of the repressed Pnmt1 promoter (that causes ~10x mal3p overpression) is shown. E) Microtubules were visualized with GFP-tagged tubulin. F) Tip1p localization was followed in cells expressing GFP-tagged tip1p together with the respective mal3p truncations.

To investigate whether the inability of monomeric mal3p truncations to bind microtubules was due to reduced microtubule binding affinity or to a complete lack of microtubule binding ability, we overexpressed all truncations tagged with GFP under the control of the fully repressed Pnmt1 promoter, which results in ~10x over-expression as compared to the endogenous mal3p protein levels (Busch and Brunner, 2004). While under these conditions mal3p^{N123} was still unable to bind microtubules, we could now observe microtubule binding of the mal3p^{N166} truncation. Due to the weak signal and the relatively high fluorescent background, it was not possible to detect if mal3p^{N166} accumulated at the growing plus-ends of the short microtubules present in these cells or if it was evenly labeling the entire microtubule lattices. These results suggest a role for the linker region in mal3p microtubule binding since the only difference between mal3p^{N123} and mal3p^{N166} is the presence of the linker region in the latter (Figure 4.1D). The results also show that monomeric mal3p forms in principle can bind microtubules but only with very low affinity, while high affinity binding requires protein dimerization (Figure 4.1D).

Surprisingly, we couldn't detect any binding of mal3p^{N203} to the microtubules (Figure 4.1D). Instead, the protein accumulated in very bright and highly dynamic dots, that showed what appeared to be fusion (Figure 4.2, yellow asterisks) and division activities (Figure 4.2, white asterisks). These dots were found to be more concentrated at the cell periphery. Although the nature of the mal3p^{N203} dots is unknown, their localization and dynamics are strikingly similar to actin patches (Pelham and Chang, 2001). An intriguing possibility is that the single calponin homology domain of mal3p^{N203} binds actin instead of microtubules as is the case for the respective domain in IQGAP (Mateer *et al.*, 2004). This should be investigated in future studies by co-localization experiments with actin patch markers.

As expected, over-expressed mal3p^{N252} showed near wild type microtubule localization and similar to full-length mal3p, but the microtubule lattice binding was more pronounced in the over-expression as compared to endogenous levels (Figure 4.1C and D).

Besides being responsible for protein homodimerization, the coiled coil region containing the EB1 motif, is also an interaction platform for many EB1 binding proteins. Biochemical *in vitro* experiments in *S. pombe*, showed that this region was sufficient for direct interaction of tip1p with mal3p (Busch and Brunner, 2004). To verify tip1p localization in the cells expressing mal3p truncations, we co-expressed tip1p-GFP in all the truncation mutants. Mal3p^{N123} expressing cells did not show tip1p accumulation at the microtubule tips or at cell ends (Figure 4.1F).

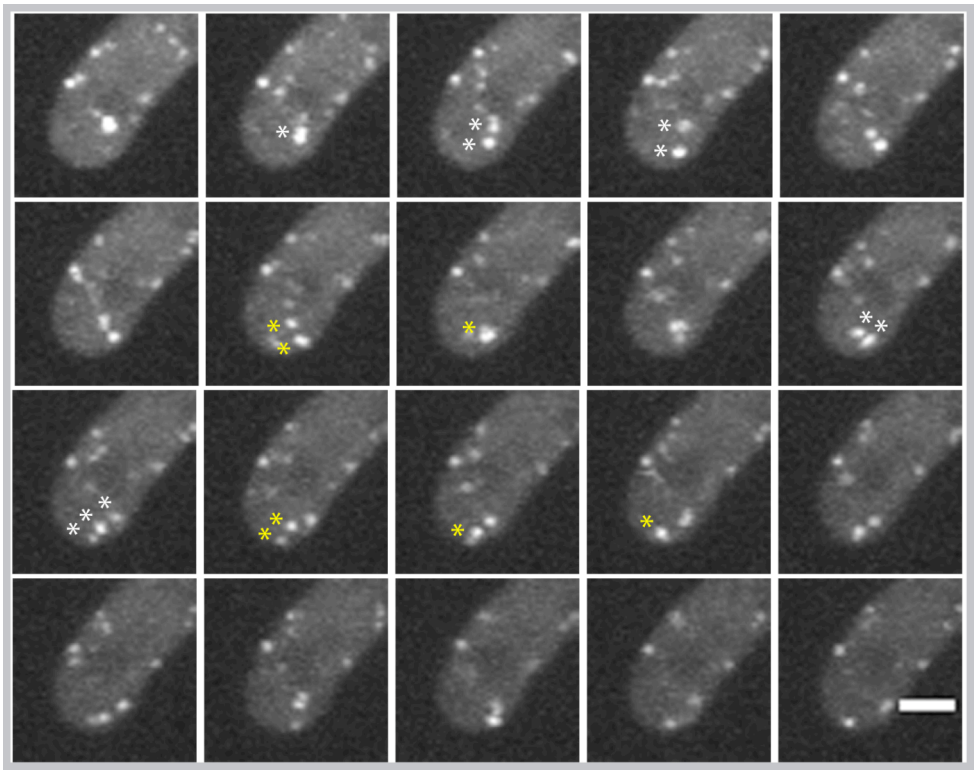

Figure 4.2: Mal3p^{N203} dynamics. Movie sequence of maximum projection of a cell tip expressing mal3p^{N203} truncation under the fully repressed Pnmt1 promoter. Frames were taken every 5". White asterisks highlight dot division events whereas yellow asterisks highlight dot fusion. Scalebar = 2μm.

This was expected, since mal3p^{N123} does not contain the coiled coil region where tip1p binds. However, mal3p^{N166} also lacks this region and yet we frequently observed tip1p at the cell ends (Figure 4.1F, asterisks). Furthermore, near wild type tip1p accumulation at cell ends was seen in mal3p^{N203} expressing cells. This was unexpected, since this mutant only contains a part of the coiled coil region that was shown not to bind tip1p (Busch and Brunner, 2004). These results suggest that mal3p promotes tip1p cell end localization by a yet unclear mechanism, or that these mutants, are able to bind mal3p (Section 5.10.3). Further imaging needs to be done to clarify if tip1p is present at the tips of short microtubules in mal3p^{N166}. This would be interesting because it could clarify if monomeric mal3p is able to load tip1p into microtubules (Bieling *et al.*, 2007).

Wild type tip1p localization was seen in mal3p^{N252} expressing cells. Mal3p^{N252} contains the tip1p binding region (Busch and Brunner, 2004) and is able to bind microtubules. In this way, mal3p^{N252} probably acts similarly to wild type mal3p, in loading tip1p onto the microtubules and promoting tip1p accumulation at cell ends (Bieling *et al.*, 2007).

Since the coiled coil region was shown to be sufficient for interaction of tip1p with mal3p (Busch and Brunner, 2004), we constructed a mal3p mutant which was truncated both N- and C-terminally such that only the coiled coil region remained (mal3p$^{163-252}$) (Figure 4.3A). Mal3p$^{163-252}$ cells expressing tip1p-GFP showed that tip1p could localize to cell ends in the presence of this mal3p protein form although less efficiently than in the wild type (Figure 4.3C). Unfortunately, it was not possible to see if tip1p is able to bind growing microtubule plus-ends in mal3p$^{163-252}$ expressing cells, due to the high cytoplasmatic background fluorescence in these mutants. Tip1p over-expression in mal3p$^{163-252}$ expressing cells may help to clarify this point.

Surprisingly, mal3p$^{163-252}$ expressed under the control of the fully repressed Pnmt1 promoter, showed a strong nuclear localization (Figure 4.3B). Mal3p$^{163-252}$ also accumulated on the SPBs, eMTOC and weakly along the spindle and spindle midzone (Figure 4.3B, asterisks blue, white, red and yellow, respectively). Mal3p$^{163-252}$ localization at the MTOCs was further confirmed by co-localization with the SPB marker sad1p, although co-localization was sometimes only partial (Figure 4.3E).

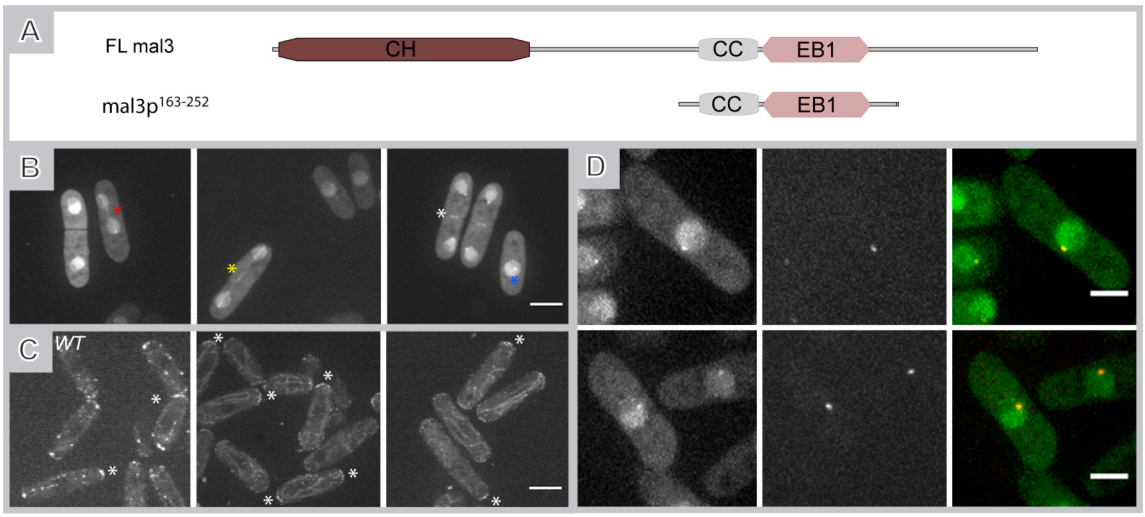

Figure 4.3: Mal3p coiled coil region localizes to MTOCs and is sufficient for tip1p cell end localization. (A) Schematic representation of the coiled coil mal3p region when compared to the full length protein. (B) Representative pictures of cells expressing mal3p$^{163-252}$ tagged with GFP under the fully repressed Pnmt1 promoter. Scalebar = 5μm. (C) Representative images of cells expressing tip1-GFP in mal3p$^{163-252}$ strain. Mal3p Pnmt1 promoter was kept fully repressed. Scalebar=5μm. (D) Representative cells expressing simultaneously GFP-mal3p$^{163-252}$ (left) and sad1 ds-red (middle). Mal3p$^{163-252}$ is shown in green and sad1 in red in the merged images (right). Scalebar = 3μm.

These results suggest mal3p is actively recruited to MTOCs and that mal3p presence in these structures is not merely due to its localization in the nascent microtubule plus-ends. Further studies need to be conducted in to evaluate if full-length protein is also recruited to MTOCs, how is it recruited, and what is its function there.

4.2 Mal3p^{N252} causes abnormal spindle disassembly and PAAs

While following the localization of the mal3p truncations, we noticed a marked difference in late mitotic localization of mal3p^{N252} as compared to the wild type. During spindle disassembly in wild type cells, mal3p is distributed along the spindle, the astral microtubules and the tips of post-anaphase array microtubules (Figure 4.4A). However, mal3p^{N252} accumulates strongly and uniformly only on the peripheral parts of the spindle, being almost completely absent from the spindle centre (Figure 4.4B and C). Furthermore, instead of a normal disassembly, the spindle carrying mal3p^{N252} seemed to be pushed towards the cell membrane before breaking apart. Frequently, the two fragments of the broken spindle remained associated with the SPBs in the newly formed cells, which soon thereafter established a normal interphasic microtubule array. This seems to be mainly done by microtubule nucleation at the SPBs, since microtubules emerging from the eMTOC were largely absent (Figure 4.4E and F). The same happened when mal3p^{N252} was overexpressed under the control of the fully repressed Pnmt1 promoter (Figure 4.4C and F). These data suggest an unexpected role for the flexible mal3p C-terminal tail in spindle disassembly and eMTOC microtubule nucleation and/or stabilization. However, during this experiments we were not directly looking at microtubules, and so it is still possible that microtubules are still emerging from the eMTOC in mal3p^{N252} cells, but that the truncated mal3p is not able to associate with its growing microtubule plus-ends. To clarify this point we looked directly at microtubules, in cells expressing mal3p^{N252} and GFP-α2-tubulin expressed under the fully repressed Pnmt1 promoter. As expected, we could observe that in late anaphase/cytokinesis, no microtubules were seen emerging from the eMTOC in mal3p^{N252} expressing cells when compared to the wild type control strain (Figure 4.5A). The same was observed for all other mal3p truncations and for *mal3Δ* cells. The only clearly visible structure was a tubulin ring in the center of the cell. The tubulin ring subsequently constricted and was visible only as a dot. At this stage very short and unstable microtubules emerged from the eMTOC in *mal3Δ* cells, while somewhat longer, but still short and unstable microtubules grew in mal3p^{N252} cells (Figure 4.5B).

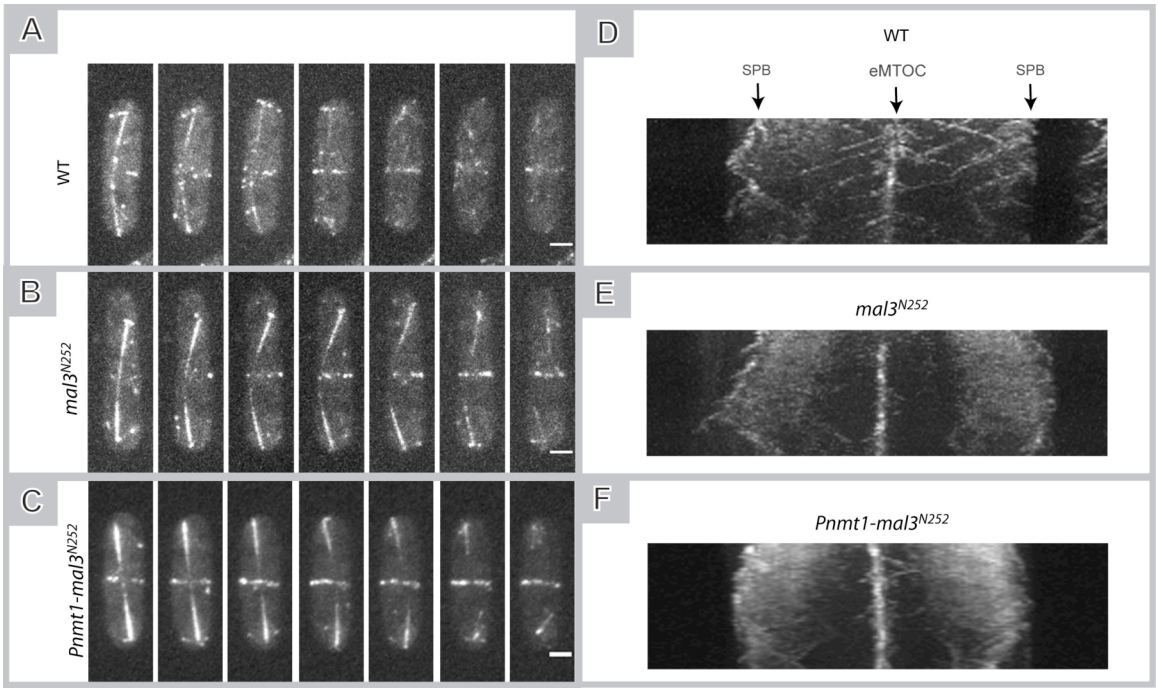

Figure 4.4: Mal3p^{N252} localization during late anaphase differs from the wild type. (A-C) Movie sequences of maximum projections of cells expressing full length and truncated GFP-mal3p protein forms during late anaphase/cytokinesis. Post-anaphase arrays can be seen forming. Protein expression was under the control of the fully derepressed Pnmt81 promoter except for Pnmt1-GFP-mal3^{N252} that is under the control of the fully repressed Pnmt1 promoter. Frames were taken every 50''. (A) In wild type cells mal3p forms a punctated pattern all along the spindle. Localization of mal3^{N252} is considerably different and the protein accumulates in peripheral spindle regions (B and C). Scalebar = 2μm. (D-F) Kymographs of the cells shown in (A-C). Note that microtubule growth from the eMTOC is very inefficient in the mal3^{N252} expressing cells (E and F).

This indicates that the eMTOC is still able to nucleate microtubules in *mal3Δ* and mal3p^{N252} expressing cells, but that these are not stabilized. Probably this effect is more pronounced in early post-anaphase arrays, since early equatorial microtubules are unstable as compared to microtubules in late post-anaphase arrays. However, more studies should be performed to understand the role of mal3p, and more specifically, its C-terminal tail, on post-anaphase array microtubule stabilization.

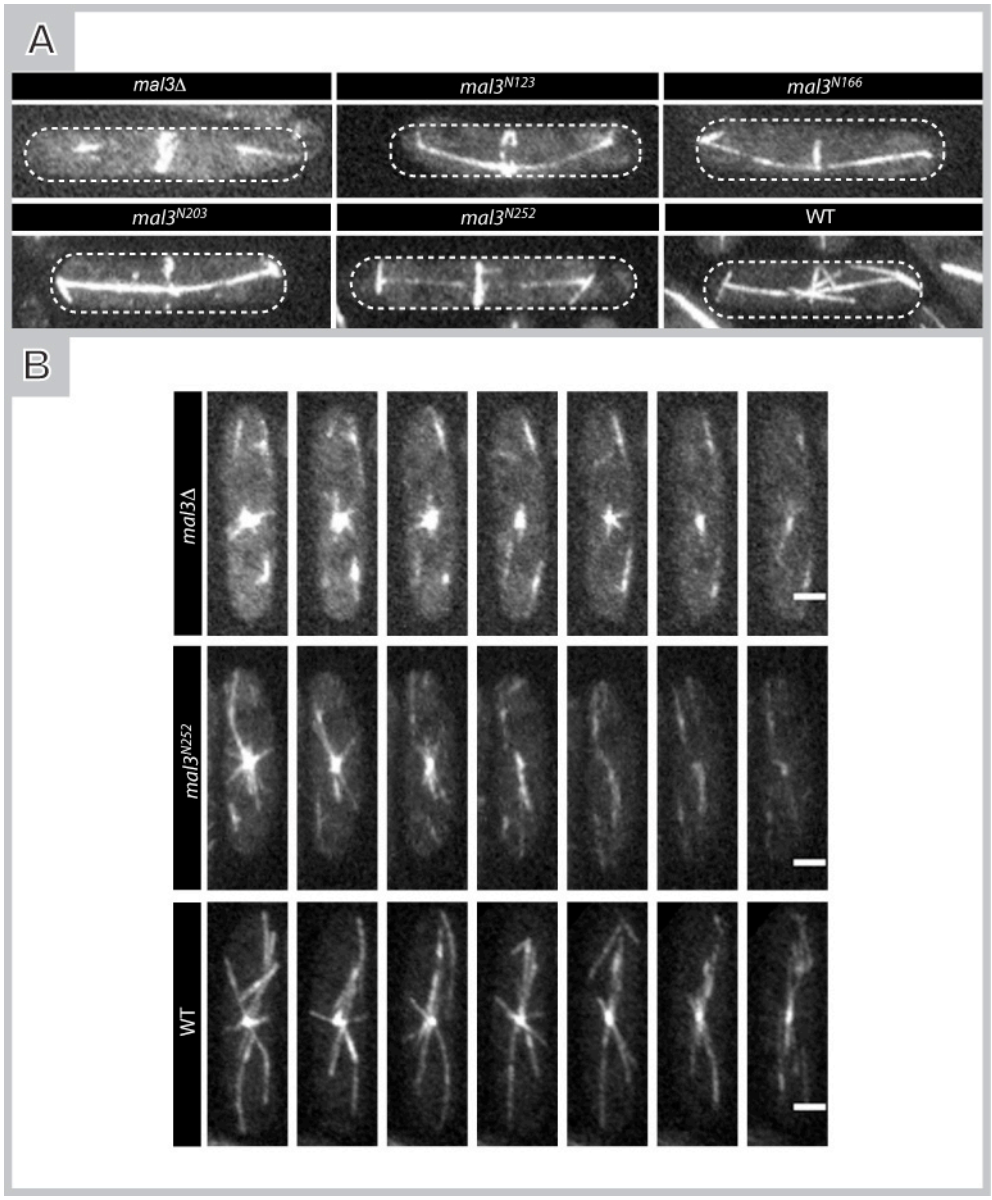

Figure 4.5: The mal3p C-terminus is essential for microtubule stabilization at the eMTOC. from Microtubules were visualized by expressing GFP-tubulin. Tubulin expression was under the control of the fully repressed Pnmt1 promoter. (A) Pictures of maximum projections of cells expressing full length (WT), *mal3Δ,* and truncated mal3p protein versions during late anaphase/cytokinesis when post-anaphase arrays form. (B) Movie sequences of maximum projections of cells expressing full length (WT), *mal3Δ,* and mal3p^{N252} during late post anaphase array stages. Scalebar = 2μm.

Chapter 5

Conclusions

5. Conclusions

5.1 Wich kinase(s) are phosphorylating mal3p and tip1p?

A search on BioGrid (http://thebiogrid.org/) for proteins interacting with tip1p and BIK1 or mal3p and BIM1, the CLIP-170 and EB1 homologues from fission yeast and budding yeast respectively, revealed several protein kinases possibly interacting with both protein family members (Annex III). Most of these interactions were suggested from high throughput genetic studies and are therefore likely to be indirect. Interestingly however, most of these kinases either regulate the cell cycle at several different stages or are involved in inositol or phosphatidylinositol phosphate (PIP) biosynthesis. While interaction with cell cycle kinases of tip1p and mal3p or their homologues in human and budding yeast had been proposed and is not surprising (Dujardin *et al.*, 1998; Tirnauer *et al.*, 2002a; Asakawa *et al.*, 2005; Green *et al.*, 2005; Srayko *et al.*, 2005; Tanenbaum *et al.*, 2006; Ban *et al.*, 2009; Yang *et al.*, 2009; Zimniak *et al.*, 2009; Goldstone *et al.*, 2010; Li *et al.*, 2010), the interaction with lipid phosphorylating kinases that participate in PIP byosynthesis is unexpected and unexplored. These interactions suggest novel mal3p and tip1p functions. Intriguingly, calponin homology domains, like the one found in mal3p, are also known to interact with phospholipids (Bogatcheva and Gusev, 1995; Fujii *et al.*, 1995).

5.1.1 Finding the kinases targeting tip1p and mal3p

To identify the kinase(s) responsible for mal3p and tip1p phosphorylation we screened a kinase deletion strain collection, in which all non-essential protein kinases were deleted (Bimbo *et al.*, 2005). Unfortunately, we weren't able to identify any kinase deletion strain that was lacking any of the mal3p or tip1p phosphorylation bands observed on western blots (Annex I). This may be due to the fact that the screen used has several limitations. First, it only allows testing non-essential kinases. To overcome this problem, we tested several essential kinases using temperature sensitive strains or by gene down-regulation under the weakest thiamine promoter, Pnmt81. However, we were not able to identify any essential kinase that would produce a phosphorylation band down-shift in either tip1p or mal3p (Table 2.2). Also, both proteins are phosphorylated on multiple sites most likely simultaneously and involving multiple kinases. This makes it difficult to detect changes in the absence of only one kinase. Analysis is especially difficult when using one-dimensional acrylamide gels with their limited resolution for protein

separation. Since we now know some, if not all, mal3p phosphorylation sites, an interesting follow-up experiment would be to repeat the screen using phospho-specific antibodies.

Finally, kinase redundancy may be a problem, meaning that one kinase compensates for the absence of the other. Redundancy is frequently associated with paralogues that are more likely to share an identical biochemical function (Prince and Pickett, 2002). However, promiscuity exists as well between non-homologous kinases (Costanzo *et al.*). Searching on the *S. pombe* Gene DB database (http://old.genedb.org) revealed that 45% of the kinases tested in this study do have a putative paralogue, suggesting that high degree of redundancy may indeed exist (Table 2.1). We tried to overcome this problem by over-expessing seletected kinases that were chosen based on their known involvement in processes where mal3p and tip1p are also involved. Unfortunately any of the tested kinases gave us an increase or an upper-shift in mal3p or tip1p phosphorylation bands when the kinases were over-expressed (Table 2.2). This does not rule out the possibility that the tested kinases are phosphorylating mal3p or tip1p, since some kinases require the presence of co-factors or adaptors that would simultaneously need to be over-expressed.

5.1.2 Kinases and mal3p

While we could not detect obvious changes in the phosphorylation pattern of mal3p by over-expressing or down-regulating kinases, we could observe significant changes in mal3p protein levels when pkc1p was down-regulated in cells deleted for pck2p (Figure 2.3C). The same happened when cki2p was over-expressed (Figure 2.3B). Initially, we did not pay much attention to these effects attributing mal3p disappearance to the fact that cells were very sick after prolonged pck1p down-regulation or cki2p over-expression. However, down-regulation of other kinases also resulted in very sick cells without affecting mal3p levels (e.g. ark1p dowregulation, Figure 2.5A). In light of recent findings and our results, showing that mal3p levels change in a cell cycle and phosphorylation dependent manner (Figure 3.7F and Figure 3.8), the effect now appears to be much more relevant and specific (Ban *et al.*, 2009). Interestingly, both pkc1p and pck2p localize to the cell division site and cell tip where also mal3p accumulates. In addition, PKCs and cki2p are involved in the regulation of cell shape, and so, may function in similar pathways.

Our results also show that mal3p phosphorylation correlates with protein level decrease, which is opposite to what was found in mammalian cells (Figure 3.7) (Ban *et al.*, 2009). Nevertheless, phosphorylation appears to globally regulate mal3p proteins levels, most likely by

promoting mal3p degradation. We would therefore expect over-expression of a critical kinase to cause mal3p degradation, which is exactly what happens when cki2p kinase is over-expressed. Yet, this alone does not prove that cki2p phosphorylates mal3p directly. The effect could still be indirect and additional experimental approaches would be necessary to rule out this possibility. On the other hand, pkc1p, is predicted to phosphorylate the serines in the mal3p linker region based on consensus sequence. Since the linker phosphorylation results in protein destabilization, pkc1p down-regulation should stabilize mal3p protein, if the protein would directly phosphorylate mal3p. However, it is the opposite that we observe. The action of pck1p is therefore most probably indirect.

The use of temperature sensitive kinase mutants to identify kinases phosphorylating mal3p, produced non-conclusive results, as mal3p levels increased considerably at higher temperatures (Figure 2.4). This made it virtually impossible to separate the different mal3p bands on western blots, which we initially produced with gel electrophoresis on 12% acrylamide gels (Table 2.2 and Figure 2.3D). With the availability of Phostag gels the respective protein extracts could now be revisited and separated on Phostag gels, which may improve our analysis and clarify the results.

Unlike studies in budding yeast and mammalian cells we could not find evidence that aurora kinase phosphorylates mal3p (Figure 2.5) (Ban *et al.*, 2009; Zimniak *et al.*, 2009). Zimniak and co-workers were able to show in budding yeast that in an unsynchronized cell culture, the ablation of aurora kinase function resulted in loss of the upper BIM1 phosphorylated band. This result confirmed that BIM1 was phosphorylated *in vivo* by aurora kinase. We also tested if *S. pombe* aurora kinase, ark1p, was phosphorylating mal3p. Due to the increase of mal3p protein levels at high temperatures and the resulting problems in protein analysis we did not use a temperature sensitive aurora kinase mutant. Instead, we performed a similar experiment where the weakest thiamine promoter, Pnmt81, was fully repressed to shut-down ark1p. Using these conditions, we were not able to reproduce the *S. cerevisiae* results, although an down-shift of mal3p protein bands was observable on western blots (Figure 2.5). However, this down-shift appeared only 14h after ark1p down-regulation when most cells were already dying. Thus, this effect is most likely secondary, resulting from altered cell metabolism and not from an overall mal3p dephosphorylation. This raises the possibility that in *S. pombe* ark1p does not phosphorylate mal3p. Alternatively, the sites phosphorylated by ark1p could also become phosphorylated by another kinase. In this case, the upper mal3p phosphorylation band would still be detectable in our unsynchronized cell population even if ark1p is not active. Using an unsynchronized cell population may also be a problem as it could mask ark1p phosphorylation.

We assume that ark1p should only be responsible for mal3p phosphorylation during mitosis, but not during interphase. Since only 10% of the cells were somewhere in mitosis in our experiments, the absence of a mitotic phosphorylation may not be noticed. To test this hypothesis it would be necessary to down-regulate ark1p in a synchronized cell population and check for mal3p phosphorylation state changes specifically during mitosis.

In conclusion, our results suggest either that mal3p is not phosphorylated by Aurora kinase in *S. pombe*, or, that the respective phosphorylation is not easily detactable, or, more likely, that there is more than one kinase phosphorylating ark1p phosphorylation sites in the mal3p linker region.

5.1.3 Kinases and tip1p

Two kinases were noticed to have slight effects on the tip1p phosphorylation pattern. When the conditional mutant *orb6-25* was inactivated by temperature or when ark1p was down-regulated, tip1p become hyper-phosphorylated, suggesting both proteins indirectly interfere with tip1p phosphorylation levels. Kinase activities are extensively inter-connected, and so deletion of one kinase will likely affect one or several other kinase or phosphatase activities (Bodenmiller *et al.*; Breitkreutz *et al.*). It is thus possible, that function ablation of either ark1p or orb6p kinases indirectly, activates the kinase(s) responsible for tip1p phosphorylation or inactivates a phosphatase, contributing in this way to tip1p hyper-phosphorylation.

We couldn't find any evidence for tip1p phosphorylation by tor2p over-expression *in vivo*, despite the fact that mTOR is able to bind and phosphorylate CLIP-170 *in vitro* (Choi *et al.*, 2000; Choi *et al.*, 2002). This could be explained by the high number of residues being phosphorylated in tip1p so that additional phosphorylation events will not significantly alter the overall phosphorylation pattern on a western blot. This is likely to also explain also why we couldn't find evidence for tip1p phosphorylation by ssp2p, the fission yeast homologue of mammalian AMPK, or by cdc2p. Both kinases were recently shown to phosphorylate CLIP-170 *in vivo* (Yang *et al.*, 2009; Nakano *et al.*, 2010). In these studies phospho-specific antibodies or metabolic labeling with [^{32}P] ortophosphate followed by phosphopeptide analysis were used, which allows to specifically look at the phosphorylation sites of interest eliminating the "background noise" caused by the other phosphorylation sites. In fact, nine phosphorylation sites in tip1p were previously identified by mass spectrometry in a large-scale study and it is likely that others can still be found (Wilson-Grady *et al.*, 2008; Yang *et al.*, 2009).

5.2 What is the importance of S4?

Another way to understand the role of mal3p phosphorylation is to identify and mutate its phosphorylation sites. S4 is a predicted phosphorylation site that is highly conserved and is considered a good candidate for phosphorylation when analyzing the crystal structure of the EB1 calponin homology domain (Figure 3.1A and B) (Hayashi and Ikura, 2003). Consistently, mal3p in cells with this site mutated to non-phosphorylatable alanine could not bind to the microtubules (Figure 3.1D). This dramatic effect seemed to be specifically associated with the S4 residue, since mutation of S2 to proline didn't cause these defects. Unfortunately, several attempts did not provide evidence that S4 is indeed phosphorylated (Figure 3.3). It is possible that S4 phosphorylation is too labile for analysis by western blot. Alternatively, only a very small pool of the overall mal3p protein is phosphorylated in this specific site and detection is thus difficult. However, mutating S4 to phosphorylatable threonine caused similar phenotypes as S4A mutation. This raises the possibility that other modifications may be occurring on S4.

Another possibility is that S4 has a structural role. Hayashi and co-workers had proposed that the EB1 C-terminal tail is part of an auto-inhibitory process that involves EB1 head to tail association (Hayashi *et al.*, 2005). This is possible due to the existence of the large mal3p flexible linker region that would enable such a conformation. Binding of interacting proteins such as $p150^{Glued}$ would then disassociate the EB1 C-terminal tail and release EB1 from its auto-inhibitory state. Because S4 sits at the very N-terminal end of the calponin homology domain, it is possible that this site has a crucial role in modulating mal3p head to tail auto-inhibition. Our results indicate that $mal3p^{S4A}$ could be undergoing a conformational change since the relative amounts of mal3p isoforms are very different when comparing to wild type strain (Figure 3.3E). It is thus likely that some previously buried sites are now much more exposed and can be post-translationally modified. This does not appear to be phosphorylation since we do not find an increase in intensity the of phosphorylated spots in the phosphopeptide map of $mal3p^{S4A}$ expressing cells. Moreover, *Xenopus* $EB1^{S16A}$, the equivalent of $mal3p^{S4A}$, was shown to bind microtubules when over-expressed, although with much reduced affinity, which can be explained by the protein being in an "inactivated" state (Anamarija Kruljac-Letunic, Karsenti laboratory, personal communication). Finally, it is also possible that S4 provides critical microtubule binding function as it lies in a very conserved and crucial malp3/tubulin interface. The molecular structure of a mal3p-tubulin interaction would shed light on these different hypothesis.

5.3 Mal3p is phosphorylated in the linker region

Our phosphopeptide map analysis of mal3p suggested that phosphorylation sites are lying within the mal3p linker region that connects the calponin homology domain and the EB1 domain of mal3p. Mutating all serines (S144, S145, S147, S148 and S151) of a candidate peptide, to alanine or mutating just S144 and S145, completely abolished the phosphorylated, upper mal3p band on western blots (Figure 3.5F and G). However, simultaneously mutating S147, S148 and S151 to alanine only reduced the intensity of this mal3p band (Figure 3.5G). These experiments suggest phosphorylation of S144, S145 to be "dominant", since failure to phosphorylate these sites obviously abolishes further linker phosphorylation. This fits well with the fact that NetPhos predicts the highest phosphorylation probability for S144 (Annex II). In addition S144 is in a sequence context that contains a considerable number of predicted kinase consensus sites (Figure 3.5A). Our results agree well with recent studies that show BIM1 to be phosphorylated on six serine residues and EB3 to be phosphorylated in S176, all of which are located in the respective linker region (Ban *et al.*, 2009; Zimniak *et al.*, 2009). However, both of these studies find Aurora kinase to phosphorylate these serine residues, while we could not find any evidence for this to occur.

5.4 Are there additional mal3p phosphorylation sites?

The biochemical and bioinformatics methods used for phosphosite determination are often limited and cannot reveal all phosphorylation sites present in a protein. The most powerful method that allows overcoming this problem of phosphosite identification is mass spectrometry (MS). However, this method also has limitations. Phosphorylated species are usually of low abundance and may not be detected with conventional MS measurments. In this case, there is no possibility for phosphopeptide signal amplification as done with immunobloting or phosphoimaging techniques. In addition, full characterization of protein phosphorylation often requires complete sequence coverage for a given protein. This may not always be achieved since too big or too small peptides may be generated by protease digestion (Blackburn and Goshe, 2009). So the best method usually relies on the use of MS in combination with biochemical methods. Preliminary results of a first MS analysis, which we did in collaboration with the laboratory of Kathy Gould (Howard Hughes Medical Institute, Vanderbilt University School of Medicine, USA) revealed many, putatively phosphorylated serines in the linker region. It also revealed S286 at the mal3p carboxy-terminus, which was also predicted by NetPhos to be

phosphorylated (AnnexII). However, these hits cannot yet be considered significant since to date individual peptides were only detected a few times. In addition, an important control experiment would be to check for the presence of phosphopeptides in *mal3*^{S144,145,147,148,151A} mutant cells by phosphopeptide mapping. In this mutant we could not detect phosphorylation bands by western blotting, suggesting no more phosphorylation sites exist. However, it is still possible that in these cells other sites such as S286 are phosphorylated but not detectable by western blot. This could be explained by low phosphorylation abundance or by phosphorylation not causing a band shift in gel electrophoresis. In fact, the flexible C-terminal tail is an interesting and likely region for post-translational modifications since it is a solvent-exposed, unstructured region.

Other unexplored residues that could be phosphorylated lie in the coiled coil region. In this region, phosphorylation of three serines is predicted, with S223 having the highest score. This serine lies in the hydrophobic groove where the SxIP motif of mal3p interacting proteins binds. It was reported that this interaction is regulated by phosphorylation, and so S223 would an interesting candidate for further study (Honnappa *et al.*, 2009).

5.5 Other mal3p post-translational modifications

In a two-dimensional gel mal3p displays several isoforms from which only 3 are of high abundance. This pattern uncovers a much higher isoform complexity than seen in one-dimensional gels (Figure 3.3E). It is not clear from our experiments if all these isoforms are derived from phosphorylation. In fact we cannot exclude the existence of other post-translational modifications. Besides phosphorylation, glycosylation also often causes protein *pI* shifts and is easily detected by 2D gel electrophoresis. In fact S144,S145 and S151 are also predicted to be O-glycosylated but the "train" of spots seen for mal3p is not characteristic of glycosylation. Furthermore, we did not find evidence for mal3p O-glycosylation. This is not surprising since usually O-glycosylated proteins possess a signal peptide, which targets them to the O-glycosylation machinery present in the golgi apparatus. Mal3p does not contain such a peptide.

Mal3p sequence screening using the available post-translational modification prediction tools (http://expasy.org/tools/#proteome) predicted K71 as a putative sumoylation site. In addition, S2 was predicted to be acetylated. However, changing S2 to proline did not have an obvious effect on mal3p function or localization (Figure 3.1D). Finally other plausible post-translational modifications include ubiquitination. This will be discussed in more detail in Section 5.7.

5.6 Mal3p phosphorylation is cell cycle dependent

Cell cycle synchronization by genetic means (*cdc22-25*) or by lactose gradients, allowed for synchronous release of *S. pombe* cells into mitosis. Using both methods we were able to show that i) mal3p phosphorylation is regulated in a cell cycle dependent way; ii) mal3p phosphorylation changes at the metaphase to anaphase transition (Figure 3.7B and F) iii) mal3p dephosphorylation occurs before mitosis onset (Figure 3.7B) and iv) cell cycle dependent phosphorylation occurs in the mal3p linker region (Figure 3.9). In summary, these results demonstrate that mal3p phosphorylation levels in the linker region oscillate during the cell cycle. Phosphorylation levels decrease before mitosis onset and increase at the metaphase to anaphase transition. Mal3p continues being phosphorylated throughout most of interphase before being dephosphorylated again on the onset of the following mitosis, completing the cycle. These results agree well with previous studies on BIM1 and EB3, showing that cell cycle dependent regulation of phosphorylation levels is a conserved mechanism (Ban *et al.*, 2009; Zimniak *et al.*, 2009). In particular, our results were very similar to what was observed in *S. cerevisiae* where BIM1 is also phoshorylated at the metaphase to anaphase transition. In the mammalian EB3, phosphorylation peaks already during prometaphase and persists until mitotic exit showing a somewhat distinct behavior (Ban *et al.*, 2009).

5.7 Mal3p protein levels vary inversely to phosphorylation levels

When performing experiments with synchronized cells we observed that at the same time as phosphorylation increased, the total protein level decreased (Figure 3.7F and Figure 5.1). Quantification of these observations suggested that protein levels continuously decrease throughout mitosis, achieving a minimum at mitotic exit (Figure 3.8B). These are population studies, where we achieved a maximum of 60% cell synchronization, and so, not all cells are exactly at the same cell cycle stage. Thus, precise timing of mal3p protein level decrease or increase is not possible. It is also unclear whether these changes are abrupt or gentle. In this view, it would be interesting to quantify mal3p levels by fluorescence imaging in single cells through a complete cell cycle.

It is not known how mal3p protein levels are regulated. This may happen at the mRNA level similar to what happens with BIM1 (Tirnauer *et al.*, 1999). Alternatively, mal3p protein levels may be regulated by protein ubiquitination and subsequent protein degradation. Such regulation was shown to occur for both EB1 and EB3 (Peth *et al.*, 2007; Ban *et al.*, 2009).

Interestingly, mal3p is predicted to have three ubiquitination sites, two that lie in the linker region (K154 and K175) and one in the C-terminal tail (K277) (http://www.ubpred.org/). The localization of two of the predicted ubiquitination sites in the linker region raises the intriguing possibility that phosphorylation may regulate protein ubiquitination, similar to what happens with EB3 (Ban *et al.*, 2009). The fact that we observe mal3p protein levels decreasing concomitantly with a phosphorylation increase, leads us to speculate that phosphorylation may promote mal3p degradation by promoting its ubiquitination. Consistently, mal3p levels in all phosphomutants, except in mal3p^{S151A}, are higher than in wild type cells (Figure 3.11). Nevertheless, EB3 phosphorylation seems to have the inverse effect, as phosphorylation protects EB3 from degradation rather than promoting it (Ban *et al.*, 2009). Obviously nature has adopted different strategies to control protein concentration by phosphorylation. Whether this is protein- or organism-specific remains to be shown.

Our preliminary lactose synchronization experiments with the phosphomutans, showed that despite the higher mal3p levels seen in these strains, protein concentration still decreases during mitosis (Figure 3.10). This suggests that phosphorylation is not essential for the oscillation of mal3p levels during the cell cycle, but merely promotes mal3p degradation. Such behavior could be explained if multiple ubiquitination sites exist. In this case, it would be possible that mal3p phosphorylation in the linker region promotes mal3p linker ubiquitination, while ubiquitination of the sites in the C-terminus occurs by default. The latter sites would still be able to drive mal3p degradation during mitosis in the absence of linker phosphorylation.

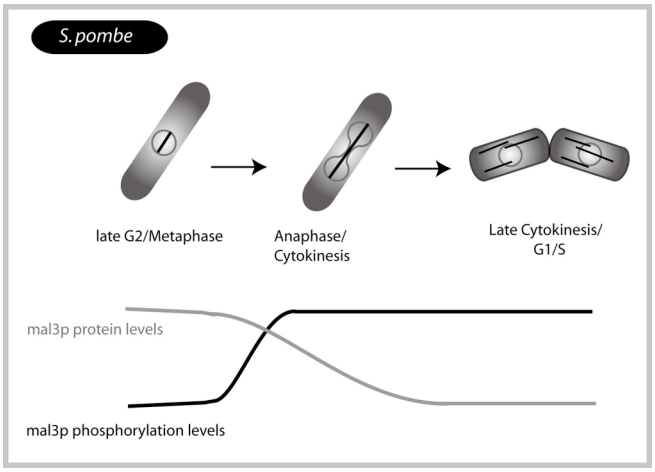

Figure 5.1: Mal3p levels vary inversely to phosphorylation levels. Before mitosis onset and in early mitotic stages, mal3p levels reach a maximum while phosphorylation levels are at a minimum. At the anaphase to metaphase transition, mal3p is phosphorylated. At the same time mal3p protein levels start decreasing, achieving a minimum in late cytokinesis. For comparision between different model organisms see Figure 1.8.

Ablation of all predicted ubiquitination sites together with mal3p level quantification throughout the cell cycle would be an informative future experiment.

Taken together, our results show that at early stages of mitosis cells contain dephosphorylated mal3p at high levels and that at the metaphase to anaphase transition mal3p is dephosphorylated and its levels decrease. What could be the biological significance of these changes? At mitotic onset a high number of dynamic microtubules have to be nucleated at both SPBs to start forming the mitotic spindle. A simple explanation is that high mal3p levels would promote the growth of these high numbers of newly nucleated microtubules. However, these microtubules have to be unstable enough to be able to search for and capture kinetochores. Phosphomutants mimic mal3p in early mitosis, since mal3p is mainly in its dephosphorylated state in this phase. Interestingly, phosphomutants have not only higher protein levels but also higher microtubule catastrophe rates during interphase. Thus, dephosphorylated mal3p may promote microtubule formation in early mitosis while still supporting microtubule instability. Previous *in vitro* studies showed that higher levels of EB protein family members promote slower microtubule catastrophe rates, which contradicts our *in vivo* observations (Vitre *et al.*, 2008; Katsuki *et al.*, 2009). However, high microtubule shrinkage rates can be achived if mal3p dephosphorylation results in mal3p binding to different partners, modifying in this way microtubule dynamics. Consistent with this idea, it was reported that in the transition interphase / mitosis EB1 and other MAPs, change its binding partners and this has an impact in microtubules dynamics (towards higher instability in mitosis) (Niethammer *et al.*, 2007).

At the metaphase to anaphase transition fast spindle elongation takes place by anti-parallel microtubule sliding at the spindle midzone. No new microtubules are nucleated and there is a drastic decrease in spindle microtubule number concomitantly with spindle elongation. The few remainig microtubules are stabilized and cannot depolymerize away from the midzone, which is achieved by frequent rescues occurring in the midzone and possibly by suppression of catastrophes (Sagolla *et al.*, 2003). In this scenario, phosphorylating mal3p may be necessary to decrease its levels, since higher amounts of mal3p are no longer necessary to stabilize newly nascent microtubules. In fact, high levels of mal3p at this stage could be harmful leading to a decrease in Anaphase B spindle organization, by helping nucleating and/or stabilizing unnecessary newly formed microtubules. Kymographs of spindles in mal3p phosphomutants show a much more disorganized mid-zone when compared with wild type (Figure 3.15C). This could be caused by newly nucleated microtubules in Anaphase B in the presence of the higher mal3p levels seen in the phosphomutants. However, if this were the case, one would expect the number of microtubules in the spindles to be higher in the phosphomutant strains. Despite the fact

we have no data concerning the number of microtubules in the spindles of both wild type and phosphomutant strains, during interphase this is not what is happening. In fact, a tendency towards lower microtubules number per bundle was observed together with higher catastrophe rates. Thus, it would be important to know in the future if the numbers of microtubules in the spindle are altered in the mutant strains, by measuring tubulin intensity in the spindles. Alternatively, the mutant kymographs can also be explained if mal3p phosphomutants show an impaired microtubule rescue at the spindle midzone. This could be due to higher microtubule catastrophe rates or by affecting interactions of mal3p with its binding partners. For example, it could be possible to imagine that mal3p may be interacting with the microtubule rescue factor cls1p (Bratman and Chang, 2007). In mammalian cells, the cls1p homologues (CLASPs) interact with EB1 and act as local rescue factors at microtubule tips during interphase (Mimori-Kiyosue *et al.*, 2000). In fission yeast such an interaction between cls1p and mal3p was not addressed, most probably because during interphase clsp1 does not localize to microtubule plus-ends like its mammalian counterparts CLASP1 and CLASP2. However, this does not exclude that during mitosis such interaction occurs at the spindle midzone during anaphase B.

In addition to the changes in microtubule dynamicity, most phosphomutants show a higher speed of spindle elongation (Table 3.1). The same was observed in *S. cerevisiae* experiments (Zimniak *et al.*, 2009). This is a puzzeling observation, since phosphomutants have a higher interphase microtubule catastrophe rate, and so we could expect the same to be true during mitosis. Since Anaphase B spindle microtubules are very stable and grow by incorporation of tubulin subunits at its ends, higher microtubule catastrophe rates would result in impaired spindle growth or premature spindle disassembly. However this is the opposite of what we observed, suggesting that during mitosis microtubules may have a distinct behavior from the one seen during interphase, or that, increased catastrophe rates do not have a significant impact in spindle elongation. This could be explained by the fact that catastrophe rates are only moderately increased in the phosphomutants (achieving a maximum of ~30% in the fully dephosphorylated mutant). The fact that the mutants have higher mal3p levels may instead promote faster spindle elongation, by promoting faster subunit incorporation at spindle microtubules plus-ends. Alternatively, dephosphorylated mal3p may somehow affect klp9p function, a plus-end directed kinesin that drives spindle elongation in *S. pombe*.

In *S. cerevisiae* it was shown that in cells expressing non-phosphorylatable BIM1, not only the spindle grows faster, but it also grows longer and has spindle disassembly difficulties (Zimniak *et al.*, 2009). While we were not able to confirm the last two results, it is possible that the reduced mal3p levels are also important in the later stages of mitosis. Lower mal3p levels

could contribute to spindle disassembly facilitating by the sequential depolymerization of individual microtubules (Sagolla *et al.*, 2003). Yet, one should keep in mind that mitotic mechanisms may differ considerably between fission and budding yeast since mal3p and BIM1 localization to anaphase B spindles are quite distinct. It would therefore be interesting to analyze spindle disassembly kinetics in the mal3p phosphomutant strains that contain increased mal3p levels.

5.8 Mal3p^{S147,S148A} generates a metaphase arrest

Analysis of the different phosphorylation mutants showed that their phenotypes can differ significantly. For example, mal3p^{S147,S148A} shows a transient metaphase arrest that was not observed in any other mutant (Figure 3.16 and Figure 3.17). Such effects suggest differential phosphorylation of the different sites, possibly by different kinases, such that different combinations of phosphorylated sites give rise to different functions. For example, S147 and S148 are putative cdc2 phosphorylation sites whereas S144, S145 and S151 are not (Figure 3.5). It is thus possible that phosphorylation of S147 and S148 has an important function and may occur specifically in metaphase. Like its mammalian homologue mal3p could be involved in kinotochore-microtubule interactions. For example, phosphorylation could be important for the previously reported role of mal3p in preventing monopolar kinetochore attachment in cooperation with bub1/bub3/mad3/mph1 dependent checkpoint (Asakawa *et al.*, 2005). Preventing phosphorylation may hyperactivate the spindle checkpoint resulting in the observed metaphase arrest, which is typical for checkpoint activation and seen in many organisms (Table 1.1). For further investigations on this point checkpoint mutants would now need to be integrated into the analysis.

5.9 Mal3p phosphorylation affects post anaphase array

Quite some evidence points towards a role of proteins of the EB protein family in mitotic exit and in midbody function. For example, in *Drosophila* and in *Xenopus* egg extracts, the lack of EB1 caused a telophase arrest (Rogers *et al.*, 2002) (Iva Kronja, Karsenti laboratory, personal communication) and in cultured *Drosophila* cells lacking EB1 the spindle midbody was absent (Rogers *et al.*, 2002). Our results with truncated versions of mal3p, show that mal3p and more specifically its C-terminal tail, is important for the stabilization of microtubules that nucleated at

the eMTOC (Figure 4.4 and Figure 4.5). Surprisingly, preventing phosphorylation of the mal3p linker region causes significant bundling of the microtubules emerging from the eMTOC (Figure 3.18). It is not clear whether unphosphorylated mal3p promotes such bundling or whether phosphorylation prevents such bundling from occurring. Notably, EB1 bundling promoting activity has already been described when over-expressing EB1 in human cultured cells (Bu and Su, 2001).

5.10 Truncations

Mal3p was shown to have several distinct and independent roles. The protein was shown to stabilize the microtubule lattice seam, serve as loading factor for plus tip proteins and to promote microtubule polymerization, probably when autonomously tracking growing microtubule plus-ends (Sandblad *et al.*, 2006; Bieling *et al.*, 2007). In order to better understand and if possible separate the distinct mal3p functions, we constructed several strains containing different C-terminally truncated mal3p (Figure 4.1A). These are discussed bellow.

5.10.1 Monomeric mal3p is able to bind microtubules, but high affinity is only achived by homodimerization.

The calponin homology domain was shown to be essential for microtubule binding of EB protein family. It was further shown that these domains act in pairs since truncated monomeric protein forms are not able to bind microtubules (Askham *et al.*, 2002; Rehberg and Gräf, 2002; Bu and Su, 2003). We confirmed that this is also the case for mal3p since mal3p^{N123}, containing only the calponing homology domain, did not bind to microtubules *in vitro* or *in vivo,* even when over-expressed (Figure 4.1C and D, Linda Sandblad, personal communication)(Des Georges *et al.*, 2008). Consistent with these results and with published *in vitro* data on similar truncations of EB1, mal3p^{N123} did not provide any microtubule polymerizing activity (Linda Sandblad, personal communication) (Des Georges *et al.*, 2008). Together this data clearly show that the presence of only one calponin homology domain region is not sufficient for EB protein family microtubule targeting. Consistently, in mammalian cells, the calponing homology domain is able to target EB3 to microtubules ends if fused to an artificial dimerization domain (Komarova *et al.*, 2009). This result suggested that the calponin homology domain (without the linker) is only able to localize EB protein family members to microtubule plus-ends if artificial dimerization is provided.

However, here we show that monomeric mal3p^{N166}, in which simply the linker region is added to the calponing homology domain, is able to bind microtubule plus-ends. This happens without artificial dimerization, although microtubule binding is of very low affinity (Figure 4.1D). This suggests, that monomeric EB protein family forms can bind microtubules and it confirms, the positive influence of the linker region in promoting mal3p microtubule binding. Consistently, *in vivo* studies performed with mammalian cells, demonstrated that the addition of the linker region improved the plus-end binding of the artificially dimerized EB1 calponin homology domain, but it was not essential for binding (Komarova *et al.*, 2009). The importance of the linker domain was further highlighted *in vitro* by Georges and co-workers. They showed that abolition of only eight amino acids from the mal3p^{N143} linker resulted in loss of microtubule binding and polymerization activity (Des Georges *et al.*, 2008). Yet, despite the favorable effects on microtubule plus-end targeting provided by the linker region, and the fact that monomeric protein forms are able to do so, efficient targeting requires protein dimerization. In agreement with this, we show efficient mal3p loading onto microtubules *in vivo* only in the presence of dimerized mal3p forms such as mal3p^{N252}.

Unfortunately, we could not clearly determine weather mal3p^{N166} is microtubule plus-end binding or if it associates evenly with the entire microtubule lattice. This is due to the high cellular background, the short microtubules and a very weak mal3p^{N166} microtubule association. It would be interesting to know more about this, since monomeric mal3p^{N166} seems to be able to bind all along the entire lattice of Taxol stabilized microtubules *in vitro* (Des Georges *et al.*, 2008) (Linda Sandblad, PhD thesis, 2007), while EB3 monomeric forms were shown to display weak binding to microtubule plus-ends *in vivo* (Komarova *et al.*, 2009).

When comparing our *in vivo* results with the *in vitro* results obtained by our laboratory or published in a number of reports, several discrepancies appear (Table 5.1): i) *In vitro*, both mal3p^{N166} and mal3p^{N203} were able to induce microtubule polymerization with near wild type activity (Linda Sandblad, personal communication). This was also seen for a mal3p^{N143} protein version, although in this case polymerization activity seemed slightly decreased when compared to full-length protein (Des Georges *et al.*, 2008). However, *in vivo*, mal3p^{N166} and mal3p^{N203} were not able to induce microtubule polymerization, showing *mal3Δ*-like short microtubules; ii) Monomeric forms of mal3p, like mal3p^{N143}, mal3p^{N166} and mal3p^{N203}, were able to bind the lattice of Taxol stabilized microtubules *in vitro* (Des Georges *et al.*, 2008) (Linda Sandblad, personal communication), even if mal3p^{N143} showed reduced microtubule affinity when compared to full-length protein (Maurer *et al., 2011*). However, this does not happen *in vivo*, since no significant binding of mal3^{N166} or mal3p^{N203} was detected at near wild type expressions levels (Figure 4.1C).

Only strong mal3p^{N166} over-expression was able to yield very weak microtubule labeling (Figure 4.1D); iii) *In vitro*, monomeric mal3p^{N143} preferentially binds the growing plus-ends of dynamic microtubules but not the microtubule lattice, as with Taxol stabilized microtubules (Maurer *et al.*). Also monomeric forms of EB1 were seen to weakly localize to growing microtubule plus-ends *in vivo* (Komarova *et al.*, 2009).

Table 5.1: **Resume of the properties of monomeric mal3p forms in the different experimental settings.** In this table we indicate if monomeric mal3p forms induce microtubule polymerization and if they bind to microtubules (either to the lattice or to microtubule plus-ends), in the presence of the different type of microtubules: *In vitro* dynamic or Taxol stabilized microtubules; or *in vivo* microtubules (both with and without mal3p monomer over-expression). See text for details.

	Taxol stablized MT	**Dynamic MT**	***In vivo* MT (Monomeric mal3p wild type levels)**	***In vivo* MT (Monomeric mal3p over-expression)**
MT polymerization	YES	YES	NO	**?**
MT binding	YES	YES	NO (Yes, in mammalian cells, very weak)[2]	YES
MT lattice binding	YES	NO	NO	**?**
MT plus-end binding	NO	YES[1]	NO (Yes, in mammalian cells, very weak)[2]	**?**

1 – (Maurer *et al., 2011*)
2 - (Komarova *et al.*, 2009)

But why is there such a difference between *in vitro* and in *vivo* situations? This is not clear, but there are several likely hypothesis. The fact that *in vitro* monomeric forms of mal3p can bind to microtubules, explain why they are also able to polymerize microtubules *in vitro*. Since the *in vivo* binding is very weak, microtubules remain short. Weak binding *in vivo* may be explained by the lower concentration levels of mal3p, when compared to the *in vitro* situation, or to different mal3p/tubulin ratios. Notably, the presence of other microtubule and/or mal3p binding proteins may be preventing monomeric mal3p from stronger microtubule binding *in vivo*. Another

possibility is that monomeric mal3p truncations may be unstable *in vivo*, since EB1^{I224A} that cannot dimerize is degraded much faster than wild type protein (Peth *et al.*, 2007). Additionally, one has to be aware that using Taxol to stabilize microtubules *in vitro* may enhance monomeric mal3p binding to the microtubule lattice by affecting the structure of the lattice towards that of a growing microtubule plus-end (Arnal and Wade, 1995). However, this doesn't explain why only the monomeric forms but not the full-length protein bind all along the microtubule lattice in the presence of Taxol. It is possible though that full-length mal3p has a stronger and more specific binding activity for the microtubule seam, which has an A-lattice conformation, while monomeric mal3p forms can instead or in addition bind the B-lattice conformation.

5.10.2 Mal3p^{N203} localizes in discrete and dynamic cytoplasmatic patches

When observing mal3p^{N203}, that lacks mal3p C-terminal tail and part of the coiled coil region, we were surprised to find that this mutant localized in discrete dispersed cytoplasmatic patches (Figure 4.1D and 4.2). Time-lapse movies showed these patches are very dynamic and seem to fuse and separate from each other. These mal3p^{N203} patches are remarkably similar to actin patches both dynamically and morphologically. However, in our preliminary observations most cells do not show a polarized distribution of mal3p^{N203} patches, as previously described for actin (Pelham and Chang, 2001). Furthermore, most of these patches seem to move in a non-directional way, while actin patches were shown to move both in a directional and non-directional way (Pelham and Chang, 2001). It is possible that single calponin homology domains can bind actin. This was shown to be the case for the single calponin homology domain of IQGAP, an actin binding protein (Mateer *et al.*, 2004). Calponin homology domains are known to bind both actin and microtubules. However, actin binding is usually associated with cis-pairs of calponin homology domains, whereas trans-pairs formed by protein dimers, are found in microtubule binding proteins, like EB1. IQGAP is an unusual actin binding protein that contains only one calponin homology domain, rather than a tandem, in its sequence. Its calponin homology domain is sufficient for IQGAP actin binding properties (Mateer *et al.*, 2004). Thus, it is tempting to speculate that a single mal3p calponin homology domain is able to bind actin patches. Moreover, the presence of one coiled coil domain seems necessary for the putative actin binding properties since mal3p^{N166} binds microtubules. Whether such actin binding occurs *in vivo* with the wild type protein is not clear. To further study this hypothesis co-localization studies between mal3p^{N203} and actin patch markers should be performed.

5.10.3 Tip1p localization in cells expressing the different mal3p truncations

Tip1p localization at the microtubule tips and cell ends requires mal3p. In the absence of mal3p, tip1p is fully delocalized and distributed throughout the cytoplasm (Busch and Brunner, 2004). Furthermore, the mal3p coiled coil region was shown to be the minimum module required for tip1p binding to mal3p *in vitro* (Busch and Brunner, 2004). This interaction is important for proper tip1p localization at microtubule plus-ends, since tip1p is loaded onto the microtubules after association with mal3p. There, tip1p detaches from mal3p and is transported to the growing microtubule ends by tea2p, where it accumulates (Bieling *et al.*, 2007). In this way tip1p reaches the cell poles together with the growing microtubule ends and it is deposited, probably during microtubule catastrophe (Brunner and Nurse, 2000).

As expected, our results confirm that efficient tip1p localization requires the mal3p coiled coil region (Figure 4.1F). However, faint staining at cell ends was still detected in mal3p^{N166}, which does not contain this region, and consequently, is not expected to bind tip1p. Also, near wild type tip1p localization at cell ends was achieved with the mal3p^{N203} truncation, which contains only the part of the coiled coil domain that was shown not to bind tip1p *in vitro* (Busch and Brunner, 2004). Thus, mal3p^{N203} is also not expected to bind tip1p. Furthermore, tip1p localization experiments with mal3p$^{163-252}$, containing only the the coiled coil region, showed that tip1p accumulation at the tip of the cell was faint, comparable to what was observed in mal3p^{N166} (Figure 4.3C). Unfortunately, it was not possible to see whether tip1p accumulated at the microtubule plus-ends in these cells, due to the high cytoplasmatic background and the presence of auto-fluorescent filamentous structures reminiscent of mitochondria. Thus, the ability of the truncated mal3p forms to load tip1p on the microtubules could not be accessed. Nevertheless, our results suggest the coiled coil region is not the only important factor determining proper tip1p localization at cell ends by mal3p. Besides, our results also suggest the existence of a microtubule independent mechanism for tip1p accumulation at cell ends, since both mal3p^{N166} and mal3^{N203} showed very short *mal3Δ*-like microtubules, but were still able to accumulate tip1p at the cell ends. This has been shown to happen with tea1p, a polarity marker with similar localization to tip1p that is also transported towards the cells ends by microtubules. In this case, even with depolymerized microtubules, tea1p could localize to at least one cell end by a microtubule independent mechanism (Snaith and Sawin, 2003).

But, how can we explain the presence of tip1p at cell ends in mal3p^{N166} and mal3p^{N203} expressing cells? We could imagine that spontaneous, mal3p independent accumulation of tip1p

at cell ends may occur. However, if this were the case, one would expect to see this effect also in mal3p^{N123} or in *mal3Δ* cells, which is not the case (Figure 4.1F)(Busch and Brunner, 2004). These results show that tip1p needs mal3p to properly localize at cell ends, but the mal3p calponin homology domain alone is not sufficient. Addition of the linker region alone, or together with part of the coiled coil, to the mal3p calponin homology domain, promotes weak tip1p localization at cell ends, similarly to the full coiled coil region. One explanation is that mal3p^{N166} and mal3p^{N203} may unexpectedly be able to bind tip1p, in this way promoting its cell end binding activity. It was shown that mal3p^{N123} does not bind tip1p *in vitro*, but unfortunately these experiments were not done with mal3p^{N166} or mal3p^{N203} (Busch and Brunner, 2004). It is possible that mal3p linker and/or calponin homology domain together with the coiled coil domain form the optimal module for tip1p interaction with mal3p. In this case, the calponin homology domain together with the linker and/or part of the coiled coil region may retain some tip1p binding activity.

In summary, our *in vivo* results suggest that: i) tip1p localization at cells ends may be microtubule independent. In this case, tip1p microtubule tip tracking may provide a mechanism that improves efficiency of tip1p delivery at cell ends. Alternatively, tip1p accumulation at microtubule plus-ends may provide a mechanism for guiding microtubule to the cell poles, while not being essential for tip1p binding at cell ends (Brunner and Nurse, 2000); ii) tip1p localization at cells ends requires mal3p; iii) the full mal3p coiled coil domain appears to be important, but not absolutely required for tip1p localization; iv) at least, the full mal3p coiled coil domain or the mal3p calponin homology domain together with the linker region must be present to localize tip1p at cell ends, v) mal3p dimerization and its ability to bind microtubules are not essential for mal3p dependent tip1p localization.

5.10.4 The mal3p coiled coil domain binds to the MTOCs

Unexpectedly, we found the truncated mal3p containing only the coiled coil domain to co-localize to MTOCs while also being enriched in the nucleus (Figure 4.3B and D). So far, mal3p localization at MTOCs was only seen in connection with newly nucleated microtubules that had not yet grown long enough to separate microtubule plus-end accumulation from MTOC binding. Our results suggest mal3p may actually be actively recruited to MTOCs via its coiled coil domain. The function(s) of EB protein family at the centrosome remains to be elucidated. It was previously proposed that EB protein family could be functional components of the centrosome,

promote microtubule anchoring, stabilize newly formed microtubules, or even, play a role in microtubule nucleation (Askham *et al.*, 2002; Tirnauer *et al.*, 2002b; Louie *et al.*, 2004; Yan *et al.*, 2006).

Besides accumulation at MTOCs, mal3p$^{163\text{-}252}$ was also accumulated in the nucleus. We hypothesized that this was not purely an artifact of the truncation but that this part of the protein may be required for nuclear mal3p recruitment during mitosis. Since *S. pombe* has a closed mitosis, in which the nuclear envelope is not eliminated, mal3p needs to be able to shuttle between cytoplasm and nucleus. Mal3p$^{163\text{-}252}$ could thus be retained in the nucleus due to deletion of a putative nuclear export signal or inversely, it could be more efficiently targeted to the nucleus due to the lack of inhibition of an import signal within the coiled coil domain. A search for nuclear import- or export signal motifs using the available standard bioinformatics programs, did not produce any hits (http://www.cbs.dtu.dk/services/NetNES/, https://www.predictprotein.org/). At this stage we cannot exclude that the observed nuclear localization is due to the fusion of GFP with mal3p$^{163\text{-}252}$, although GFP also does not contain any nuclear localization sequences.

5.10.5 Mal3p plays an important role at stabilizing nascent microtubules at eMTOC

When analyzing the localization of truncated mal3p proteins we noticed a clear difference between mal3p^{N252}, lacking the C-terminal flexible tail, and full-length mal3p localization on late anaphase spindles and on eMTOCs. Mal3p^{N252} uniformly stained the right and left thirds of the spindle but was not present in the middle (Figure 4.4A). This apparent "exclusion" from spindle midzones may be due to the fact that only few short new microtubules are growing from the eMTOC in mal3p^{N252} cells, despite the fact mal3p^{N252} is recruited to eMTOCs (Figure 4.4D and E). These results suggest that the flexible C-terminal tail of mal3p is essential for microtubule stabilization and growth from eMTOCs. Movie analyses from *mal3Δ* cells expressing GFP-tagged tubulin confirm these results and showed only very small and unstable microtubule growing from eMTOCs (Figure 4.5). These results suggest a fundamental role for mal3p, and in particular its C-terminal tail, in the stabilization of microtubules emerging from eMTOCs.

5.11 Future directions

This study on phopshorylation of mal3p raises several questions that need to be addressed in future studies. Our observations indicate that aurora kinase may not be phosphorylating mal3p or may at least not be the only kinase responsible for mal3p phosphorylation. Consequently, one of the first things that has to be elucidated is if ark1p is a mal3p kinase at all. Also, other candidate kinases need to be identified and tested. For this, a screen similar to the one performed in the beginning of this study can now be performed including the higher phosphoband separation power of Phostag gels. Production of phosphospecific antibodies to specific serines in the linker region would also provide an additional crucial tool for future analysis and would in addition allow gaining spatio-temporal information about mal3p phosphorylation states in cells. Furthermore, *in vitro* phosphorylation experiments with kinases that are likely, or predicted, to phosphorylate mal3p (for example, ark1p, PKCs, cki1p and cdc2p) could be performed, since *in vitro* phosphorylation is a good way to circumvent problems with kinase redundancy. Alternatively, double mutants for kinases can be tested with western blotting.

An aspect that should be further investigated is the potential relationship between protein degradation and mal3p phosphorylation. Here we will need to continue the work with which we evaluated mal3p protein levels throughout the cell cycle with synchronized mutant cells. In addition, experiments should be designed to evaluate the possibility that mal3p is ubiquitinated, including mutating the identified putative ubiquitination sites.

Similar to the previously published work on other EB protein family, this work cannot provide a clear answer to the biological importance of mal3p phosphorylation and/or mal3p protein level oscillations along the cell cycle. It's possible that mal3p phosphorylation plays different roles in several distinct processes, like regulation of kinetochore-microtubule attachment, spindle elongation, or eMTOC microtubule nucleation and/or growth. It is also likely that mal3p phospho-regulation is a complex process, where different phospho-isoforms play different biological roles. One problem preventing a clear understanding certainly is the fact that mal3p and its posttranslational modifications do not play an essential role under standard laboratory growth conditions. Instead they appear to provide robustness or increased efficiency to the processes we have analysed. New experiments will need to be designed that provide quantitative information and eventually will allow exploring these processes with computational models.

Finally, the importance of mal3p at the MTOCs is still far from being understood. Our results suggest mal3p is actively recruited to the MTOCs. Particularly, we show mal3p has a critical role in promoting eMTOC microtubule growth and that this is dependent on the flexible C-terminal mal3p tail. Further elucidation of this process may shed new light on the processes of localized microtubule nucleation and microtubule growth promotion.

Chapter 6

Materials and Methods

6. Materials and Methods

6.1 S. pombe cell culture techniques

Standard methods were used for growth of fission yeast strains (Moreno *et al.*, 1991). Either rich yeast extract medium (YE5S) or Edinburgh Minimal Medium 2 (EMM2) containing the appropriate amino acid supplements were used for cell growth. Briefly, fission yeast cells were awake from a medium containing 50% glycerol and 50%YE (ou EMM with apropriate supplements). A small loop of the frozen stock was spread in a YE5S or EMM2 agar plate and incubated at 25°C or 30°C, depending on the strain. After 1-3 days cells were visible. 5ml liquid pre-cultures were set for 8-16 hours and then used to inoculate larger culture volumes. These cultures were normally let grown o/night or for a minimum of two generations, until cell culture reach an optical density (OD) absorvance $(A)_{595}$ of 0.4 to 0.6 before harvesting. In this way, we ensure harvested cells were in exponential growth phase. These cells were then used for microscopy, protein extracts or strains construction. All medium and solutions used for cell culture were autoclaved or filter sterilized, and cell culture manipulation was always done using appropriate sterile techniques.

6.1.1 Strains under control of the Pnmt promoters

Strains which genes were under the control of the Pnmt1 promoter were grown and imaged in the presence of 30µM thiamine to repress over-expression from this promoter, unless over-expression was intended. Strains with genes under the Pnmt81 promoter were grown in EMM containing all necessary supplements. If down-regulation was intended, 30µM thiamine was added to the medium.

6.1.2 Strains used in this study

All strains used on the kinase screen are described elsewhere (Bimbo *et al.*, 2005). All other used strains are displayed in Table 6.1.

Table 6.1: Strains used in this study

Strain	Genotype	Source
DB 558	*h⁻*	Lab stock
DB712	*h⁺ mal3Δ::his3 his3-D1 or his3-237*	Lab stock
DB489	*h⁺ tip1Δ::kanr*	Lab stock
DB1016	*h⁻ sid2-250 ura4.d18 leu1-32 ade6M210*	Lab stock
DB597	*h⁺ orb2-34 leu1-32 ade6-M216*	(Verde *et al.*, 1995)
DB1175	*h⁺ plo1.d1 leu1-32 ura4.d18 ade6? his2*	Lab stock
DB1176	*h⁻ plo1.d1 leu1.32 ura4.d18 ade6?*	Lab stock
DB431	*h? cdc2-33 ban1 leu1-32*	Lab stock
DB593	*h- orb5-19 leu1-32 ade6-M216*	Lab stock
DB600	*h- orb6-25 leu1-32 ade6-M210*	Lab stock
DB1162	*Pnmt41-HA-pck1 pck2::LEU2 leu1-32*	(Arellano *et al.*, 1999)
DB1160	*Pnmt41-HA-pck2 pck1::ura4⁺ ura4D18*	(Arellano *et al.*, 1999)
DB1171	*h⁻ Pnmt81-HA-Pi3k::kanMX6*	This study
DB1174	*h⁺ ark1.Δ1::LEU2+LEU2+ ura4.d18 ade6⁻ + pRep82Ark1.PkC*	(Petersen, J. and Hagan, IM, 2003)
DB1641	*h⁻ cki1Δ:: ura4⁺ Pnmt81-cki2::kanMX6 ura.d18 leu1-32*	This study
DB1642	*h⁻ cki2Δ::ura4⁺ Pnmt81-cki1::kanMX6 ura.d18 leu1-32*	This study
DB1643	*h⁻ Pnmt1-cki2::kanMX6*	This study
DB1169	*h⁻ Pnmt1-HA-tor2::kanMX6*	This study
DB1167	*h⁻ Pnmt1-HA-pi3k::kanMX6*	This study
DB1240	*h⁻ Pnmt1-HA-gsk3β::kanMX6*	This study
DB1241	*h⁻ Pnmt1-HA-kin1::kanMX6*	This study
DB1531	*h+ Fab1Δ::ura4⁺ ura.d18*	This study
DB1780	*h⁻ Pnmt81-mal3(S4A)::kanMX6*	This study
DB1778	*h⁻ Pnmt81-GFP-mal3(S4A)::kanMX6*	This study
DB1675	*h⁻ Pnmt81-GFP-mal3(S4T)::kanMX6*	This study
DB1242	*h⁻ Pnmt81-GFP-mal3(S4D)::kanMX6*	This study
DB1745	*h⁻ hph::Pnmt81-mal3(S2P)-linker-GFP::kanMX6 leu1-32*	This study
DB2274	*h⁻ kanMX6::Pnmt81-GFP-mal3-C(5-308)::hphMX6*	This study
DB1190	*h⁺ Pnmt81-mal3(S4A)::kanMX6 leu1-32 + Pnmt81-GFP-α2-tubulin::LEU2*	This study
DB914	*h- ade6-M216 leu1 x pREP81GFPatb2:leu+*	Lab stock
DB1609	*h⁺ mal3(S130,S131A) ura.d18*	This study
DB1612	*h⁺ mal3(S130,S131,138A) ura.d18*	This study
DB1613	*h⁺ mal3(S138A) ura.d18*	This study
DB1712	*h⁺ mal3(S144,145A) ura.d18*	This study
DB1713	*h⁺ mal3(S147,148A) ura.d18*	This study
DB1714	*h⁺ mal3(S151A) ura.d18*	This study
DB1715	*h⁺ mal3(S144,145,147,148,151A) ura.d18*	This study
DB1716	*h⁺ mal3(S286A) ura.d18*	This study
DB554	*h⁻ cdc25-22*	Lab stock
DB1726	*h⁻ mal3 S144,145A lys1+::nmt1-GFP-α2tub ura.d18*	This study
DB1727	*h? mal3 S147,148A lys1+::nmt1-GFP-α2tub ura.d18*	This study
DB1728	*h? mal3(S151A) lys1+::nmt1-GFP-α2tub ura.d18*	This study
DB1729	*h⁻ mal3(S144,145,147,148,151A) lys1+::nmt1-GFP-α2tub ura.d18*	This study
DB1197	*h⁻ lys1+::nmt1-GFP-α2tub ura.d18*	
DB2109	*h? mal3(S144,145A)-linker-GFP::kanMX6 ura.d18*	This study[a]
DB2110	*h? mal3(S147,148A)-linker-GFP::kanMX6 ura.d18*	This study[a]
DB2111	*h? mal3(S151A)-linker-GFP::kanMX6 ura.d18*	This study[a]

DB2112	*h? mal3(S144,145,147,148,151A)-linker-GFP::kanMX6 ura.d18*	This study[a]
DB827	*h⁻ mal3-linker-GFP::kanr leu1-32*	
DB2840	*h? ase1-GFP::kanMX6 mal3(S144,145A)::hph ura.d18 ade6-M210 leu1.32*	This study[a]
DB1670	*h⁻ ase1-GFP::kanMX6 ade6-M210 leu1.32 ura.d18?*	Lab stock[b]
DB1682	*h⁺ mal3N-123::ura4⁺ ura.d18*	This study
DB1683	*h⁺ mal3N-166::ura4⁺ ura.d18*	This study
DB1684	*h⁺ mal3N-203::ura4⁺ ura.d18*	This study
DB1685	*h⁺ mal3N-252::ura4⁺ ura.d18*	
DB1746	*h⁺ kanMX6::Pnmt81-GFP-mal3N123::ura4⁺ ura.d18*	This study
DB1747	*h⁺ kanMX6::Pnmt81-GFP-mal3N166::ura4⁺ ura.d18*	This study
DB1748	*h⁺ kanMX6::Pnmt81-GFP-mal3N203::ura4⁺ ura.d18*	This study
DB1749	*h⁺ kanMX6::Pnmt81-GFP-mal3N252::ura4⁺ ura.d18*	This study
DB2121	*h? mal3N123::ura4⁺ tip1-GFP::kanMX6 ade6-M21(0 or 6) ura.d18*	This study[a]
DB2122	*h? mal3N166:: ura4⁺ tip1-GFP::kanrMX6 ade6-M21(0 or 6) ura.d18*	This study[a]
DB2123	*h? mal3N203:: ura4⁺ tip1-GFP::kanrMX6 ade6-M21(0 or 6) ura.d18*	This study[a]
DB2105	*h? mal3N252:: ura4⁺ tip1-GFP::kanrMX6 ade6-M21(0 or 6) ura.d18*	This study[a]
DB2269	*h⁺ kanMX6::Pnmt1-GFP-mal3N123:: ura4⁺ ura.d18*	This study
DB2270	*h⁺ kanMX6::Pnmt1-GFP-mal3N166:: ura4⁺ ura.d18*	This study
DB2271	*h⁺ kanMX6::Pnmt1-GFP-mal3N203:: ura4⁺ ura.d18*	This study
DB2272	*h⁺ kanMX6::Pnmt1-GFP-mal3N252:: ura4⁺ ura.d18*	This study
DB2098	*h⁺ mal3N123::ura4⁺ lys1+::nmt1-GFP-α2-tubulin ura.d18*	This study[a]
DB2096	*h⁺ mal3N166::ura4⁺ lys1+::nmt1-GFP-α2-tubulin ura.d18*	This study[a]
DB2099	*h⁺ mal3N203::ura4⁺ lys1+::nmt1-GFP-α2-tubulin ura.d18*	This study[a]
DB2097	*h⁺ mal3N252::ura4⁺ lys1+::nmt1-GFP-α2-tubulin ura.d18*	This study[a]
DB637	*h⁻ Pnmt81-GFP-mal3::kanMX6*	Lab stock
DB1198	*h⁻ mal3Δ::his3 lys1+::nmt1-GFP-α2-tubulin ura.d18 (his3-D1 or his3-237?)*	Lab stock
DB614	*h⁻ Pnmt1-GFP-mal3::kanMX6*	Lab stock
DB417	*h⁻ tip1-GFP::kanMX6 ura.d18 leu1-32 ade6-M216*	Lab stock
DB2273	*h⁺ hph::Pnmt1-GFP-mal3(163-252)::ura4⁺ ura.d18*	This study
DB2741	*h? hph::Pnmt1-GFP-mal3(163-252):: ura4⁺ sad1-dsRed::LEU2 ura.d18 leu1-32*	This study[a]
DB2579	*h? hph::Pnmt1-GFP-mal3(163-252)::ura4⁺ ura.d18 mto1Δ::kanMX6 ade6-M210? leu1-32?*	This study[a]
DB2578	*h? hph::Pnmt1-GFP-mal3(163-252)::ura4⁺ ura.d18 mto2Δ::kanMX6 ade6M212? leu1-32?*	This study[a]
DB2340	*h? hph::Pnmt1-mal3(163-252)::ura4⁺ tip1-GFP::kanMX6 ura.d18 ade6-M21 (0 or 6)*	This study
DB2341	*h? hph::Pnmt1-mal3(163-252)::ura4⁺ tea2-GFP::kanMX6 ura.d18 leu1-32*	This study
DB1750	*h⁺ kanMX6::Pnmt81-GFP-mal3(S144,145,147,148,151A)N123::ura4⁺ ura.d18*	This study
DB1751	*h⁺ kanMX6::Pnmt81-GFP-mal3(S144,145,147,148,151A)N203::ura4⁺ ura.d18*	This study
DB1752	*h⁺ kanMX6::Pnmt81-GFP-mal3(S144,145,147,148,151A)N166::ura4⁺ ura.d18*	This study
DB1753	*h⁺ kanMX6::Pnmt81-GFP-mal3(S144,145,147,148,151A)N252::ura4⁺ ura.d18*	This study

Note: a- Strain done by Imola Balogh, b- Strain done by Lindsay Murrels

6.2 Construction of strains by crossing

Strains were crossed by mixing a full loop of equal amounts of each parent strain of opposite mating type together on minimal glutamate medium (EMMG; EMM2 containing 1g/L sodium glutamate instead of Na4Cl) with 20-50 µl water. Plates were incubated at 25ºC. After 2 days the presence of spores was checked by microscopy and random spores analysis was performed. A full loop of sporulated cells was resuspended in 30% ethanol and incubated in a rotating well for 30 minutes. The spores were then diluted 1:100, 1:1000 and 1:10.000 and 100µl of each was platted onto YE5S plates. Plates were incubated at 30ºC until colonies were visible. If temperature sensitive strains were used plates were incubated at 25ºC. Colonies were replica plated onto selective medium to detect specific markers and/or checked by colony polymerase chain reaction (PCR).

6.3 Construction of strains by homologous recombination

6.3.1 Generation of PCR fragments for transformation

The homologous recombination method was used for tagging, deletion, overexpressing or down-regulation of specific genes (Bahler *et al.*, 1998). Briefly, ~100bp PCR primers (BioSpring, Frankfurt, Germany) containing 80 base pairs (bp) that are specific to the gene sequence, followed by 20 to 24 bp, specific to the plasmid template, were used to amplify a transformation cassette containing a selection marker (Uracil or Kanamycin resistance; Table 6.2) (Bahler *et al.*, 1998). The PCR reactions were all ran with the following steps: one initial step at 94ºC for 1 min, followed by 8 repeats of 30 sec at 94ºC, 1 min at 50ºC and 2-5 min at 72ºC and 25 repeats of 30 sec at 94ºC, 1 min at 55ºC and 2-5 min at 72ºC. The final step was of 10 min at 72ºC. Following this step the temperature was dropped to 4ºC until running the PCR reactions in a 1% agarose gel (Sigma-Aldrich, Hamburg, Germany) for 20 min at 120 volts. Each PCR reaction contained the final concentration of the following reagents: 1x Buffer without magnesium; 2.5 milimolar (mM) of dNTPs; 2.5 mM of magnesium sulfate; 2 units of a mixture TAQ polymerase and Vent DNA polymeraze in a 2:1 ratio (all PCR products from Sigma-Aldrich Biochemie GmbH, Hamburg, Germany).

Table 6.2: List of primers used in this study

Strain	Primer forward (5'-3')	Primer reverse (5'-3')	Plasmid
DB1170	CACAGTATTATAATTCATCATTGCTTCGTGTACTTTAGCT ACAGCCTTTCTTGTCTTACCACATTTAGTAAAGCTAGTAC GAATTCGAGCTCGTTTAAAC	GATATTCAATGAAGCAAAATTTAACCAAGAATCTGGCAGTC ACCTTGCTTGAAGGACAATATGAAAAAACAAGTCTATCCATG CACTGAGCAGCGTAATCTG	pFA6a-kanMX6-P81nmt1-3HA
DB1166	CACAGTATTATAATTCATCATTGCTTCGTGTACTTTAGCT ACAGCCTTTCTTGTCTTACCACATTTAGTAAAGCTAGTAC GAATTCGAGCTCGTTTAAAC	GATATTCAATGAAGCAAAATTTAACCAAGAATCTGGCAGTC ACCTTGCTTGAAGGACAATATGAAAAAACAAGTCTATCCATG CACTGAGCAGCGTAATCTG	pFA6a-kanMX6-P3nmt1-3HA
DB1168	CGTCATAAAAATATTACTTTTTCAATCGTGTTTCTATTGA TCTCCTCTCTGCGTATACTAAGAATTAGGTGCAAAAGTA CGAATTCGAGCTCGTTTAAAC	GCTATAACATATTCATAAAGATCATTTGCCGCTTTATTGCGA ATTTCTTCATTCCTGCTTTTCAACCCAGGAAATTCTTTCATGC ACTGAGCAGCGTAATCTG	pFA6a-kanMX6-P3nmt1-3HA
DB1240	GATTTGCTCATGTCCCGTAATGTTACCTCTTAGAAGTAC GCACTTTGTATCATGCTACTATACCCCAGAGATTATTCTA TGAATTCGAGCTCGTTTAAAC	GGGTCCACAGGAACTATTTATACGGTTAGAACAACAGCACT ATCGAAGTTAGCCAACTTACTTTTAGTACCATGATTCATGCA CTGAGCAGCGTAATCTG	pFA6a-kanMX6-P3nmt1-3HA
DB1241	GGATTTCACGCTTTTTCGTAATATTTGTCATCTTAGGTTC GCAAGGAAACTGGTGCCACGATTTACGATAACAAAGTA TTTGAATTCGAGCTCGTTTAAAC	GATATTTTAATTTTCGGCAACGCATTTAAAGCGGCAGACTTT GTCTCATTACCGACGGGTACGTTATTGGTACGGTACTCCATG CACTGAGCAGCGTAATCTG	pFA6a-kanMX6-P3nmt1-3HA
DB1531	CATGACAATTCATAGAACTTAATTAATAGAACCAATAAT TTCCGGAGATAATTTTAATCTTCGGTTTGCATTTCTGTTC AACGCCAGGGTTTTCCCAGTCACGAC	CTATCAAATACTGGGATTAAAAAGATTGTTCATATTTCTTGA CCAAACAGCGAAATATATACATTAAACTAACGTTTCTTAGCG GATAACAATTTCACACAGGA	KS-ura4
DB1641	CCTTACAACTAACGTCCACTAAAACACTCAAACCACATA ATCATTTGTTAGTCGAAAGAAAGCCTGTAACTTCTATTA AATTATAGTAATTGGGAATTCGAGCTCGTTTAAAC	CGAAAATAACACCAAACGATCCCTCACCTATTTTACGACCCA CGCGATAGTGAACCCCTACTACGCTCGTTTGGGAATTCATGA TTTAACAAAGCGACTATA	pFA6a-kanMX6-P81nmt1
DB1642	CTAACCCCTTAATCAGGCAGGAATAGAGGGAAGTGATG CACATGACACTTCCGTAACTAAAGCACCACTAAAAACAT CCGGAATTCGAGCTCGTTTAAAC	CAAAAATAACACCAAACGAGCCTTCGCCAATTCTTCTTCCAA CTTTGTAGTGGACACCGACTACATTGTTTTGTCCACTCATGAT TTAACAAAGCGACTATA	pFA6a-kanMX6-P81nmt1
DB1643	CCTTACAACTAACGTCCACTAAAACACTCAAACCACATA ATCATTTGTTAGTCGAAAGAAAGCCTGTAACTTCTATTA AATTATAGTAATTGGGAATTCGAGCTCGTTTAAAC	CGAAAATAACACCAAACGATCCCTCACCTATTTTACGACCCA CGCGATAGTGAACCCCTACTACGCTCGTTTGGGAATTCATGA TTTAACAAAGCGACTATA	pFA6a-kanMX6-P3nmt1

DB1780	CTAATTGAGAGATAGTTATTTTAATGTTTGCAACGAATA TTCCGGAATACATGTAAATTTTCAGTTATAATACCCATT AAGAATTCGAGCTCGTTTAAAC	ATAATTTTTTCAATCTAACTAAGATATTAAAGCGTACTTGGTT GATCCAAGCTAAGAGCTCTTGCCGAGCTTCAGACATCATGAT TTAACAAAGCGACTATA	pFA6a-kanMX6-P81nmt1
DB1778	CTAATTGAGAGATAGTTATTTTAATGTTTGCAACGAATA TTCCGGAATACATGTAAATTTTCAGTTATAATACCCATT AAGAATTCGAGCTCGTTTAAAC	GATAATTTTTTCAATCTAACTAAGATATTAAAGCGTACTTGG TTGATCCAAGCTAAGAGCTCTTGCCGAGCTTCAGACATTTTG TATAGTTCATCCATGC	pFA6a-kanMX6-P81nmt1-GFP
DB1675	CTAATTGAGAGATAGTTATTTTAATGTTTGCAACGAATA TTCCGGAATACATGTAAATTTTCAGTTATAATACCCATT AAGAATTCGAGCTCGTTTAAAC	GATAATTTTTTCAATCTAACTAAGATATTAAAGCGTACTTGG TTGATCCAAGCTAAGAGCTCTTGSCCGAGTTTCAGACATTTT GTATAGTTCATCCATGC	pFA6a-kanMX6-P81nmt1-GFP
DB1242	CTAATTGAGAGATAGTTATTTTAATGTTTGCAACGAATA TTCCGGAATACATGTAAATTTTCAGTTATAATACCCATT AAGAATTCGAGCTCGTTTAAAC	GATAATTTTTTCAATCTAACTAAGATATTAAAGCGTACTTGG TTGATCCAAGCTAAGAGCTCTTGCCGATCTTCAGACATTTTG TATAGTTCATCCATGC	pFA6a-kanMX6-P81nmt1-GFP
DB1745	CTAATTGAGAGATAGTTATTTTAATGTTTGCAACGAATA TTCCGGAATACATGTAAATTTTCAGTTATAATACCCATT AAGAATTCGAGCTCGTTTAAAC	GATAATTTTAATCTAACTAAGATATTAAAGCGTACTTGGTTG ATCCAAGCTAAGAGCTCTTGCCGAGATTCAGGCATGATTTAA CAAAGCGACTATA	pFA6a-hph
DB2274	CTAATTGAGAGATAGTTATTTTAATGTTTGCAACGAATA TTCCGGAATACATGTAAATTTTCAGTTATAATACCCATT AAGAATTCGAGCTCGTTTAAAC	TCGTACAACTGTGTTTCAAGACTAGTGATTTGTTGTTGTGCTT GCTTTGCCCTTAACACTGCCGCAGTATTTGCAGTCGA CATGATTTAACAAAGCGACTATA	pFA6a-hphMX6-P3nmt1
DB2109-DB2112	GTATACAGAATGCTATATGTTAAGGAAAAAGAACGAAA TTAAATGAATTTGGAGGTCATGAGGCACGCAACATTCGA TCAGAATTCGAGCTCGTTTAAAC	CGTTCCCTCTGCACCAGATTTCGTACATGCTAGGCTACAAAG TTTAGAGGTTGATGACGATGAGAATATCACGTTTATCCTTGG AGCTCCTTCAGG	pFA6a-linker-GFP-kanMX6
DB1682	CCAAACGTTTTTGGGATCAATATTATCCTGGGGGCGATT ATGATGCGCTGGCACGCCGGGGGAATAGAGGACCTGCT TAACGCCAGGGTTTTCCCAGTCACGAC	CCTATTTGGGATAATTAGACGGCTCAAACACTAAGGATTAAA GTTTATTACAATTAGCATTTGTAGTATACAGAATGC AGCGGATAACAATTTCACACAGGA	pSKura4
DB1683	GTCAGGTTTCTTCTGGTAGTTCTACACCTTCAATGACTAA GTCATCAGCAAACAACAATAACGTGTCTTCGACTGCATA ACGCCAGGGTTTTCCCAGTCACGAC	CCTATTTGGGATAATTAGACGGCTCAAACACTAAGGATTAAA GTTTATTACAATTAGCATTTGTAGTATACAGAATGC AGCGGATAACAATTTCACACAGGA	pSKura4
DB1684	CAACAACAAATCACTAGTCTTGAAACACAGTTGTACGAA GTTAATGAGACGATGTTTGGTTTGGAGAGAGAACGTGAT TAACGCCAGGGTTTTCCCAGTCACGAC	CCTATTTGGGATAATTAGACGGCTCAAACACTAAGGATTAAA GTTTATTACAATTAGCATTTGTAGTATACAGAATGCAGCGGA TAACAATTTCACACAGGA	pSKura4

DB1684	CAACAACAAATCACTAGTCTTGAAACACAGTTGTACGAA GTTAATGAGACGATGTTTGGTTTGGAGAGAGAACGTGAT TAACGCCAGGGTTTTCCCAGTCACGAC	CCTATTTGGGATAATTAGACGGCTCAAACACTAAGGATTAAA GTTTATTACAATTAGCATTTGTAGTATACAGAATGCAGCGGA TAACAATTTCACACAGGA	pSKura4
DB1685	GGAAAATATGTTGGAGCGTATTCAAGCAATACTTTATTC TACTGAGGATGGTTTTGAGTTACCACCTGATCAACCCGC ATAACGCCAGGGTTTTCCCAGTCACGAC	CCTATTTGGGATAATTAGACGGCTCAAACACTAAGGATTAAA GTTTATTACAATTAGCATTTGTAGTATACAGAATGC AGCGGATAACAATTTCACACAGGA	pSKura4
DB1746-DB1749	CTAATTGAGAGATAGTTATTTTAATGTTTGCAACGAATA TTCCGGAATACATGTAAATTTTCAGTTATAATACCCATT AAGAATTCGAGCTCGTTTAAAC	GATAATTTTTTCAATCTAACTAAGATATTAAAGCGTACTTGG TTGATCCAAGCTAAGAGCTCTTGCCGAGATTCAGACATTTTG TATAGTTCATCCATGC	pFA6a-kanMX6-P81nmt1-GFP
DB2269-DB2272	CTAATTGAGAGATAGTTATTTTAATGTTTGCAACGAATA TTCCGGAATACATGTAAATTTTCAGTTATAATACCCATT AAGAATTCGAGCTCGTTTAAAC	GATAATTTTTTCAATCTAACTAAGATATTAAAGCGTACTTGG TTGATCCAAGCTAAGAGCTCTTGCCGAGATTCAGACATTTTG TATAGTTCATCCATGC	pFA6a-kanMX6-P3nmt1-GFP
DB2273	CTAATTGAGAGATAGTTATTTTAATGTTTGCAACGAATA TTCCGGAATACATGTAAATTTTCAGTTATAATACCCATT AAGAATTCGAGCTCGTTTAAAC	TCGTACAACTGTGTTTCAAGACTAGTGATTTGTTGTTGTGCTT GCTTTGCCCTTAACACTGCCGCAGTATTTGCAGTCGATTTGTA TAGTTCATCCATGC	pFA6a-hphMX6-P3nmt1-GFP
DB1750-	CTAATTGAGAGATAGTTATTTTAATGTTTGCAACGAATA	GATAATTTTTTCAATCTAACTAAGATATTAAAGCGTACTTGG	pFA6a-kanMX6-

Two to three PCR reactions were finally pooled and the PCR fragment was purified using the phenol/chloroform purification procedure (AppliChem GmbH, Darmstadt, Germany). DNA was resuspended in 10-12µl of 10mM TE buffer (10mM Tris-HCl pH8.0 and 1mM EDTA).

6.3.2 Transformation protocol for *S. pombe* cells

Standard transformation protocols routinely performed in the lab were used to transform fission yeast cells. Briefly, 50ml exponentially growing cells (OD_{595} ~ 0.5) cultured in rich medium were washed twice with 50ml water, and the cell pellet was resuspended in 1 ml of 0.1M LiAc/TE (pH 7.5). Cells were transferred to an Eppendorf tube and centrifuged at 6000rpm for 1 min. Cell pellet was resuspended in 60ul LiAc/TE (~$2x10^9$ cells/ml). Cells were then mixed gently with 2µl salmon sperm DNA (10 mg/ml) and 10-12 µl of the transforming DNA. After 10 min incubation at room temperature, 260µl of 40% PEG4000/0.1M LiAc/TE was added. The cell suspension was mixed gently and incubated for 1 hour at 30ºC (or 25ºC for temperature sensitive strains). 43 µl of dimethylsulphoxide (DMSO) was added, and the cells were heat shocked for 5 min at 42ºC. Cells were then washed once with 1 ml of water, resuspended in 0.5 ml of water, and 250µl plated onto two rich medium non-selective plates. These plates were incubated for 1 day at 25ºC or 30ºC, resulting in a lawn of cells. The cells were then replica plated onto selective plates. Cells transformed with fragments carrying the kanMX6 marker were plated onto YE5S containing 100 mg/l Geneticin. For Pnmt1 containing strains, 200µl thyamine 30mM was spread on plates. Cells transformed with fragments carrying the ura4+ marker were plated onto EMM2 plates without uracil. The replica plates were incubated for 2–3 days at 25ºC or 30ºC, and large colonies were re-streaked onto fresh selective plates.

6.3.3 Screening transformants by colony PCR

After transformation by homologous recombination, single selected colonies were confirmed for stable integration of the DNA fragment in the desired locus. A very small loop of cells was resuspended in the 50 µl of the PCR reaction. The PCR reaction was performed such that it includes that site of integration. In this way, one primer corresponded to a sequence inside the transforming cassete, whereas its pair lies in a region outside this region. For modules containing kanMX6 we used 5'-GCTAGGATACAGTTCTCACATCACATCCG-3' and for modules containing ura4+ we used 5'-CCAAGCCGATACCAGGGGACATAG-3'. A PCR

product was obtained only for strains in which the transformation fragment was integrated on the correct locus.

6.4 Construction of point mutated strains by site directed mutagenesis

A *S. pombe* 1.9kb genomic fragment consisting of mal3 ORF with 481bp and 431bp flaking regions up- and downstream the ORF was PCR amplified. The primers used for amplification were 5'-ATCTGTCGACCTAAGATTATACCAAGTCC-3' and 5'-CTGGATCCGATATTTCAGCATCATTG-3'. The amplicon was cloned into pBluescript SK(+) as a SalI-BamHI fragment originating pBluescriptSK(+)-mal3p plasmid. Oligonucleotide directed mutagenesis was performed using the QuikChange® Site-Directed Mutagenesis Kit (Stratagene) according to the manufacture's instructions and using the primers described in the following Table 6.3. Once the mutated plasmids were obtained, the successful introduction of the point mutations was confirmed by sequencing. The selected mutated plasmids were then digested with SalI and BamHI, and ran in an agarose gel. The 1.9kb band corresponding to the mutated *mal3* fragment was excised from the gel, and the DNA recovered using GENECLEAN® Turbo Kit (Qbiogene). DNA was concentrated by precipitation with Sodium Acetate and Ethanol, in order to obtain at least 2µg of DNA fragment in 10µl TE. This DNA was then transformed into DB1530 (h+ mal3::ura4$^+$ ura4.d18) cells, using the homologous recombination based method described in (Bahler *et al.*, 1998). For efficient selection of replacement of *ura4+* by the mutated *mal3* genes, the transformants were resuspended in 1L YE5S and cells let grow o/night at 30^0C (Grimm *et al.*, 1988). From this culture, 10^7 cells were then plated in YE5S media containing 1mg/ml 5-fluoroorotic acid (5-FOA, Toronto Research Chemicals). After two days, growing colonies were visible and were re-isolated in YE5S+FOA. Fragment insertion in the correct locus was confirmed by colony PCR, and on the successful strains, point mutations were further confirmed by direct sequencing of the PCR products after Quiagen purification.

Table 6.3: Primers used for point mutations

Mutation	Primer Forward (5'-3')	Primer Reverse (5'-3')	Plasmid
S130, 131A	CACTCGTGTTATGAATGC CGCTGCAGGAGCAACTG GCCC	GGGCCAGTTGCTCCTGCA GCGGCATTCATAACACGA GTG	pBluscriptSK(+)-mal3
S138A	GGAGCAACTGGCCCTGCT CGTCGCCGTCAGG	CCTGACGGCGACGAGCA GGGCCAGTTGCTCC	pBluscriptSK(+)-mal3
S144,145A	CTCGTCGCCGTCAGGTTG CTGCTGGTAGTTCTACAC CTTC	GAAGGTGTAGAACTACC AGCAGCAACCTGACGGC GACGAG	pBluscriptSK(+)-mal3
S147,148A	CGTCAGGTTTCTTCTGGT GCTGCTACACCTTCAATG ACTAAG	CTTAGTCATTGAAGGTGT AGCAGCACCAGAAGAAA CCTGACG	pBluscriptSK(+)-mal3
S158A	CTGGTAGTTCTACACCTG CAATGACTAAGTCATCAG C	GCTGATGACTTAGTCATT GCAGGTGTAGAACTACC AG	pBluscriptSK(+)-mal3
S144,145,147,148,151A	CCTTCTCGTCGCCGTCAG GTTGCTGCTGGTGCTGCT ACACCTGCAATGACTAAG TCATCAGCAAAC	GTTTGCTGATGACTTAGT CATTGCAGGTGTAGCAGC ACCAGCAGCAACCTGAC GGCGACGAGAAGG	pBluscriptSK(+)-mal3
S286A	CTCAACGCGTTCCCGCTG CACCAGATTTCG	CGAAATCTGGTGCAGCG GGAACGCGTTGAG	pBluscriptSK(+)-mal3

6.5 Cell culture synchronization

6.5.1 Cell synchronization using *cdc25-22* strain

Synchronization of cells by transient temperature shifts in the cdc25-22 mutant expressing GFP-α2-tubulin was achieved by growing cells to mid-exponential growth at 25°C, before shifting to 36°C. Cells were then shifted back to 25°C after 4h to enter the mitotic cell cycle in synchrony. Samples were subsequently removed for protein extracts and for cell imaging.

6.5.2 Cell synchronization using lactose gradients

800ml of cells were grown in YE5S overnight to mid-late exponential phase the following day. 6 lactose gradient columns were prepared. For this, 10% lactose (lactose monohydrate, Merk) in YE5S was loaded in the gradient maker chamber away from the exit tube and 40% lactose in YE5S was loaded in the remaining chamber. A stir bar was added to the 40% lactose chamber and 5ml YE5S with 40% lactose was poured into a 50ml conical tube. Both valves of the gradient maker were open, allowing the gradient to flow down the sides of the conical tube (fill to 45ml). Cells were harvested by gently centrifugation (2500 rpm) and each 125ml of cells resuspended in 0.5ml YE5S with no lactose. These concentrated cells were then gently loaded along the inside of the conical tubes just above the gradient solution. The gradients were centrifuged in a swinging bucket centrifuge for 5 min at 1000rpm. 5ml of cells from the top of each gradient were collected in 1ml aliquots and examined using the microscope. Aliquots that showed a uniform population of small G2 cells (no septa should be visible) were pooled together, washed 1x in YE5S, resuspended in 1ml YE5S, and added to 10ml YE5S medium. The 60ml YE5S containing the synchronized cell culture were incubated at 25°C and time was started. Per time point, 5ml of cells were removed for protein extracts, 1ml of cells for calcofluor staining and septation index determination and 0.5ml cells for imaging of cut12-GFP signal to determine the exact cell cycle phase. Protein extracts were done as described in Section 6.7.2 and loaded on a Phostag or 10% acrylamide pre-cast gel (Section 6.7.4 and 6.7.6).

6.6 MBC resistancy assays

20ml of cells were grown overnight to mid exponential phase the following day at OD_{595} ~ 0.5. Cell concentration was determined using an heamocytometer and cells diluted to $2.5x10^5$ cells/ml. 1:5 serial dilutions from $2.5x10^5$ cells/ml were done and 5ul of the different cell suspensions were spotted in the several plates containing different benzimidazol-2-yl-carbamate (MBC, Merk, Darmstadt, Germany) concentrations or DMSO (Merk, Darmstadt, Germany) as a control.

6.7 Protein biochemistry methods

6.7.1 *S. pombe* protein native extracts

Protein native extracts were preformed as described (Moreno *et al.*, 1991), but using Heppes Buffer as lysis buffer in the presence of phosphatase and protease inhibitors (25mM Hepes [pH=7.2], 50mM Potassium Acetate, 1mM $MgCl_2$, 1mM EDTA, 1mM Dithiothreitol (DTT), 40µg/ml Aprotinin, 20µg/ml Leupeptin, 0.1mM Sodium Vanadate, 1mM phenylmethylsulphonyl fluoride (PMSF), 15mM *para*-Nitrophenylphosphate (pNPP), 2mM Benzamidine, 1µg/ml pepsatin A, 10mM Sodium Fluoride, Roche EDTA-free Complete Protease Inhibitor Mix). Cells were broken by using glass beads (Sigma, St. Louis, MO) in the FastPrep vortex (SAVANT, GMI, Minnesota, USA).

6.7.2 *S. pombe* fast protein extracts

Fast *S. pombe* protein extracts were preformed as described previously (Matsuo *et al.*, 2006). Briefly, cell pellet was washed with 1 ml water and cells resuspended in 150µl water and equal volume of 0.6M NaOH. Cells were incubated for 10 min at room temperature and centrifuged to remove supernatant. 60µl loading buffer (60mM Tris-HCl pH6.8, 4% β-mercaptoethanol, 4% SDS, 0.01% bromophenol blue and 5% glycerol) was added and cells resuspendend and boiled for 3 min before loading on gel.

6.7.3 Phosphatase treatment

75µl protein extracts were prepared without phosphatase inhibitors NaV and NAF and incubated for 45 min to 1hr at 30°C with or without 5µl λ-protein phosphatase (NEB, Beverly, MA). 25mM sodium fluoride and 5mM sodium ortovanadate phosphatase inhibitors were added in the controls.

6.7.4 SDS polyacrylamide gel electrophosesis (SDS-PAGE)

SDS 10% Polyacrylamide Gel electrophoreris was done as described (Laemmli *et al.*, 1970). Alternatively, either gradient (4%-12%) or 10% Acrylamide Pre-Cast gels were used (Invitrogen, CA, USA). Gels were run at 150V.

6.7.5 Anderson SDS-PAGE

Anderson gels that improve phosphorylated protein separation were also performed (Anderson *et al.*, 1973). These are very similar to normal SDS-PAGE gels described above, but have a different Acrylamide/Bisacrylamide ratio. The resolving gel consists of 15% Acrylamide (Bio-Rad), 0.086% Bisacrylamide (Bio-Rad), 375mM Tris-HCl pH=8.8, and the stacking gel contains 5% Acrylamide, 0.13% Biscarylamide, 125mM Tris-HCl pH=6.8. The gels were run at a constant voltage of 20mA until samples enter the resolving gel when the voltage was increased to 30mA.

6.7.6 Phosphate affinity SDS-PAGE

The phosphate affinity SDS-PAGE gel (Phos-tag gel) relies on the fact that the dinuclear metal complex (1,3-bis[bis(pyridin-2-ylmethyl)amino]propan-2-olato dizinc(II)) - Phos-tag, acts as a phosphate binding tag (Kinoshita *et al.*, 2004).

When the Phos-tag is co-polymerised with acrylamide in the resolving gel there's an increased mobility shift of phosphorylated proteins *vs* non-phosphorylated proteins due to the reversible phosphate trapping of phosphorylated proteins by Phos-tag molecules immobilized on the gel (Kinoshita *et al.*, 2006).

The Phos-tag gel was done as previously described in Kinoshita-Kikuta et al, 2006. The acrylamide-pendant Phos-tag^{TM} ligand was purchased from the Phos-tag consortium (http://www.phos-tag.com, Japan). All solutions and reagents were prepared following the Phos-tag supplier recommendations. Phos-tag^{TM} ligand concentrations (75-90μM) and acrylamide percentage (8%) were optimized for our particular experiments. Shortly, the Phos-tag gel consists of a stacking gel (4.5% (w/v) polyacrylamide (29:1, Fluka), 125 mM Tris-HCl (pH 6.8), and 0.10% (w/v) SDS) and an 8% acrylamide resolving gel co-polimerized with acrylamide-pendant Phos-tag^{TM} ligand (8% (w/v) polyacrylamide (29:1, Fluka), 375 mM Tris-HCl (pH 8.8), and

0.10% (w/v) SDS, 75-90μM Phos-tag^{TM} ligand concentrations). Gels were run under constant current of 30mA/gel. To remove Mn^{2+} ions, which inhibit protein electroblotting onto membrane, the gel was incubated with 1mM EDTA in Transfer Buffer for 10 minutes, and in Transfer Buffer without EDTA for additional 10 minutes, prior to protein transference. Electrobloting was performed o/night for 15h, at 250mA at 4^0C.

6.7.7 Two-dimensional gel electrophoresis

Two-dimensional gel electrophoresis (2D-gels) combines two different electrophoretic separating techniques in perpendicular directions to provide a much greater separation of complex protein mixtures than either of the individual procedures. The most common 1st dimension used is isoelectric focussing (IEF), where proteins are separated according to their pI, followed by sodium dodecyl sulphate polyacrylamide gel electrophoresis (SDS-PAGE gels) in a perpendicular direction, separating proteins according to their molecular size. This is the most powerful tool for protein separation currently available.

For the 2D-electrophoresis native *S. pombe* protein native extracts were prepared as described above, using 1%Triton in the lysis buffer. Cell extracts were cleared by centrifugation at maximal speed, for 30 min at 4^0C. Sample solubilization and alkylation was performed as described by Khoudoli (Khoudoli *et al.*, 2004) with the following modifications. 13μg of total protein extract were dissolved in 150ul Buffer 1 (7M Urea (Merk), 2M Thiourea (Fluka), 1.2% CHAPS, 0.4% ASB14 (Calbiochem), 0.25% Ampholytes (Bio-Lyte® 5 to 8 Ampholyte, 40%, Bio-Rad), 43mM Dithiothreitol (DTT), 30mM Tris-Base). Samples were run in a 7cm Narrow Range 4-7 IPG strip or Micro Range 4.7-5.9 IPG strip (Bio-Rad). The dry IPG strips were allowed to re-swell in the sample presence by active hydratation o/nigh. The isoelectric focusing was performed in two phases. The first phase was carried out to clean sample from salts prior to sample focusing. For that, IPG strips were subjected to the following programme: 1) 200V for 45 min, 2) 500V for 45 min and 3) 1000V for 1h, all fast ramping voltage gradient. The second phase, consists of a linear gradient for 2h at 3000V, to accumulate a total of 20.000 volt/h minimum. The optimal current per strip was set to 20μA and the maximal current per strip was set to 50μA. After focusing IPG strips were subjected to additional reduction and alkylation as described (Khoudoli *et al.*, 2004). Equilibrated IPG strips were finally applied to 12% Acrylamide gels. The gels were run at 100V, wet transferred for 5h at 250mA, and blotted with polyclonal anti-mal3 antibody (Busch and Brunner, 2004).

6.7.8 Quantitative western blots

Polyclonal anti-mal3 (Busch and Brunner, 2004), anti-tip (Brunner and Nurse, 2000)and monoclonal anti-tubulin (T5168, Sigma-Aldrich, Munich, Germany) primary antibodies were incubated overnight at 4°C or for 4h at room temperature in 5%milk 0.1% Tween.

Secondary antibodies anti-mouse labeled with Alexa-680 (Molecular Probes) or anti rabbit IRDye-800 (Rockland Inc., Gilbetsville, PA) were used for visualization and routinely diluted 1:2000 in 1% milk (w/v) in PBS-T (137mM NaCl, 2.7mM KCl, 10.2mM Na_2HPO_4, 1.8mM KH_2PO_4, 0.1% Tween). Detection and quantification were performed with the Odyssay Infrared Imaging System (Li-Cor). Scanning of membranes was performed at 700nm and 800nm simultaneously with a Li-Cor instrument, 169µm resolution, medium quality and intensity setting of 5 for 700nm channel and 3 for 800nm channel. Normalization of cell bands was done using α-tubulin that was used as a loading control for quantification purposes. All data analysis and image preparation was done with the Odyssay software provided with the LI-COR systems (http://www.licor.com/bio/applications/odyssey_applications/quantitative_western_blot.jsp).

6.7.9 Phosphoamino acid analysis and phosphopeptide mapping

In vivo labeling of cells was accomplished essentially as described elsewhere (Gould *et al.*, 1991). In summary, cells were grown overnight in phosphate-free minimal medium containing 50µM NaH_2PO_4 and appropriate supplements to a density of $4x10^6$ - $8x10^6$ cell/ml. Cells were collected by centrifugation and resuspended at $6x10^6$ cell/ml in phosphate free minimal medium containing 50µM NaH_2PO_4 and 2.5mCi of [^{32}P]-ortophosphate. Labelling proceeded at 32°C for 4h. *S. pombe* cells lysates were prepared as described previously (Gould *et al.*, 1991). For immunoprecipitation we used polyclonal anti-mal3 antibody (Busch and Brunner, 2004). After washing, the immunoprecipitate was resuspended in 40µl 2 x sodium dodecylsulphate (SDS) loading buffer and boiled prior loading on a 6-20% SDS polyacrylamide gradient gel. Bands were transferred to Immobilon P-membranes (Millipore) and visualized by autoradiography. [^{32}P]mal3p bands were cut from Immobilon-P membranes, and slices were hydrolyzed in 6 N HCl for 60 min at 110 °C for phosphpetide analysis (Kamps and Sefton, 1989) or subjected to trypsinization as follows: membrane slices were blocked for 30 min at 37°C with 0.1% Tween 20 in 50 mM ammonium bicarbonate. After two washes in 50 mM ammonium bicarbonate, two 10ug aliquots of trypsin were added for 2.5 h incubations each (Boyle *et al.*, 1991). Partial acid hydrolysis products were separated by electrophoresis in two dimensions on thin-layer cellulose

plates at pH 1.9 and 3.5 (Boyle *et al.*, 1991) using the Hunter thin-layer electrophoresis system (C.B.S. Scientific, Del Mar, CA). Phosphopeptides were separated on thin-layer cellulose plates by electrophoresis performed at pH 1.9 for 30 min at 1 kV (88% formic acid:acetic acid:H20; v:v:v; 1:3.12:35.88) and ascending chromatography performed in phosphopeptide chromatography buffer (N-butanol:pyridine:acetic acid:H20; v:v:v:v; 75:50:15:60) (Boyle *et al.*, 1991). Phosphoamino acids and phosphopeptides were visualized by autoradiography on Kodak XAR5 film at -70°C with intensifying screens or with Molecular Dynamics PhosphorImager screens (Sunnyvale, CA).

6.8 Live cell imaging

6.8.1 Cell preparation

20ml liquid cells cultures were grown in EMM with appropriate supplements overnight from day pre-cultures to exponential phase $O.D._{595}$ ~ 0.5. 1ml of cells were transferred to glass bottom microwell dishes (MatTek, Ashland, MA, USA) coated with 1µl 2mg/ml lectin BS-1 (Sigma-Aldrich, Hamburg, Germany) in H_2O. Dishes were spun at 300 rpm for 1 min to attach the cells to the bottom of the MatTek dish. Unattached cells were washed with three washes using 1ml medium.

6.8.2 Microscopes used for imaging

Confocal images were generated using a Carl Zeiss Axiovert 200 M microscope equipped with a PerkinElmer RS Dual spinning disc system. The Argon Krypton line laser was used at wavelength of 488 nm for GFP signal detection. Images were collected using a 100X oil immersion objective (Plan Fluor, NA1.4) in a Hamamatsu Orca ER camera (Hamamatsu, Japan) with a pixel size of 6.45 µm and analyzed with the Ultraview acquisition software (Perkin Elmer, Foster City, CA US). Z-stacks were taken with 8-13 planes per stack with a distance of 0.5 µm between planes.

Dual colour imaging was performed using a 488nm Argon Krypton dual laser line for GFP signals and dsRed signals was used. A Perkin Elmer UltraView ERS dual spinning disc system (Waltham, MA, USA) coupled to a Carl Zeiss Axiovert 200 M microscope (München, Germany) with a 100X oil immersion objective (Plan Fluor, NA1.3) was used to acquire images.

Images were acquired with a Hamamatsu C9199-02 EMCCD camera (Hamamatsu, Japan) with a pixel size of 8 μm. Z-stacks were taken with 13 planes per stack, with a distance of 0.5μm between planes.

Most of GFP imaging was done using a Perkin Elmer UltraView RS spinning disc confocal system. A 488nm Argon Krypton was used to image GFP-tagged strains. The spinning disk system was coupled to a Carl Zeiss Axiovert 200M microscope with a 100X oil immersion objective (Plan Fluor NA1.3). Images were acquired with a Hamamatsu Orca ER camera (Hamamatsu, Japan) with a pixel size of 6.45 μm. Z-stacks were taken with 13-20 planes per stack, with a distance of 0.5 μm between planes.

A Carl Zeiss Axiovert 200 M widefield system was also used in combination with a mercury lamp. Images were collected with a Coolsnap HQ camera (Roper Scientific) with a pixel size of 6.28 μm and with a 100X and 63X oil immersion objective (Plan Fluor, NA1.4). Z-stacks were collected with 13 planes per stack, with a distance of 0.5 μm between planes.

All imaging experiments were carried out at room temperature (24–26°C), except spindle growth imaging where temperature was controlled to be 25°C.

6.8.3 Image analysis

Images from the confocal spinning disc microscope systems were acquired using the Perkin Elmer software (Waltham, MA, USA). Data was analyzed using ImageJ (NIH, USA). Data acquired with the Perkin Elmer systems was imported into ImageJ using a plug in written by A. Seitz (EMBL, Heidelberg, Germany) and Z-stacks were maximum-projected using a custom routine written by T. Zimmerman (EMBL, Heidelberg, Germany). Kymograph reconstruction was done using imagej and growth and shrinkage speeds were calculated from the kymograph slopes.

Chapter 7

Annexes

7. Annexes

Annex I – Table I-1 - All kinases tested on screen

Kinase	Product	Genedb number	Similar genes[1]	Similar genes – Genedb number	WB result on screen (mal3p/tip1p)
Bub1	serine/threonine protein kinase Bub1	SPCC1322.12c	*N/F*		- / -
Ssp2 (Ucp9)	serine/threonine protein kinase Ssp2	SPCC74.03c	*Ppk9*	SPAC23H4.02	- / -
Atg1	autophagy and CVT pathway serine/threonine protein kinase Atg1	SPCC63.08c	*N/F*		- / -
Mug27 (Ppk35, Slk1)	meiosis specific protein kinase Mug27/Slk1	SPCC417.06c	*Sid2*	SPAC24B11.11c	- / -
Gad8	AGC family protein kinase Gad8	SPCC24B10.07	*N/F*		- / -
Oca2	serine/threonine protein kinase Oca2	SPCC1020.10	*Ppk8*	SPAC22G7.08	- / -
Gsk31 (Pi064)	serine/threonine protein kinase Gsk31	SPBC8D2.01	*Gsk3*	SPAC1687.15	- / -
Ppk31 (mug25)	serine/threonine protein kinase Ppk31	SPBC725.06c	*Ppk18, Cek1*	SPAPB18E9.02, SPCC1450.11c	- / -
Ppk30	Ark1/Prk1 family protein kinase Ppk30	SPBC6B1.02	*Ppk38, Ppk29*	SPCP1E11.02, SPBC557.04	- / -
Ppk29	Ark1/Prk1 family protein kinase Ppk29	SPBC557.04	*Ppk38, Ppk30*	SPCP1E11.02, SPBC6B1.02	- / -
Ppk27	serine/threonine protein kinase Ppk27 (predicted)	SPBC337.04	*N/F*		- / -
Ppk25	serine/threonine protein kinase Ppk25 (predicted)	SPBC32C12.03c	*N/I*		- / -
Ppk24	serine/threonine protein kinase Ppk24	SPBC21.07c	*SPCC70.05c*	SPCC70.05c	- / -
Ppk23	serine/threonine	SPBC18H10.15	*N/F*		- / -

Ppk22	protein kinase Ppk23 serine/threonine protein kinase Ppk22	SPBC1861.09	*Ppk14*	SPAC4G8.05	- / -
Ksp1 (Ppk20)	serine/threonine protein kinase Ksp1	SPBC16E9.13	*N/F*		- / -
Vps15 (Ppk19)	serine/threonine protein kinase Ppk19	SPBC119.07	*N/F*		- / -
Ppk16 (Mug92)	serine/threonine protein kinase Ppk16 (predicted)	SPAC890.03	*N/F*		- / -
Ppk14	serine/threonine protein kinase Ppk14 (predicted)	SPAC4G8.05	*Ppk22*	SPBC1861.09	- / -
Ppk13	erine/threonine protein kinase Ppk13 (predicted)	SPAC3H1.13	*N/F*		- / -
Lsk1	P-TEFb-associated cyclin-dependent protein kinase Lsk1	SPAC2F3.15	*Csk1*	SPAC1D4.06c	- / -
Ppk11	PAK-related kinase Ppk11	SPAC2C4.14c	*N/F*		- / -
Hal4 (Sat4, Ppk10)	halotolerence protein 4	SPAC29A4.16	*N/F*		- / -
Srb10 (Prk1, Cdk8)	cyclin-dependent protein Srb mediator subunit kinase Srb10	SPAC23H4.17c	*N/F*		- / -
Ppk9	serine/threonine protein kinase Ppk9 (predicted)	SPAC23H4.02	*Ssp2*	SPCC74.03C	- / -
Ppk8	erine/threonine protein kinase Ppk8 (predicted)	SPAC22G7.08	*Oca2*	SPCC1020.10	- / -
Sck2	serine/threonine protein kinase Sck2	SPAC22E12.14c	*Sck1*	SPAC1B9.02c	- / -
Hri2	eIF2 alpha kinase Hri2	SPAC222.07c	*Hri1*	SPAC20G4.03c	- / -
Hri1	eIF2 alpha kinase Hri1	SPAC20G4.03c	*Hri2*	SPAC222.07c	- / -
Ppk15	serine/threonine protein kinase Ppk15 (predicted)	SPAC823.03	*N/F*		- / -
Lkh1 (Kic1)	Dual specificity protein kinase Lkh1	SPAC1D4.11c	*N/F*		- / -

Ppk3	HEAT repeat protein Ppk3	SPAC15A10.13	*N/F*		- / -
Ppk2	serine/threonine protein kinase Ppk2 (predicted)	SPAC12B10.14c	*Shk1, Shk2*	SPBC1604.14c, SPAC1F5.09c	- / -
Ire1, Ppk4	serine/threonine protein kinase Ppk4/ sensor for unfolded proteins in the ER (predicted)	SPAC167.01	*N/F*		- / -
Ppk33	Serine/threonine protein kinase Ppk33 (predicted)	SPCC162.10	*N/I*		- / -
Srk1 (Mkp1)	MAPK-activated protein kinase Srk1	SPCC1322.08	*Cmk2*	SPAC23A1.06c	- / -
Wis4 (Wak1, Wik1)	MAP kinase kinase kinase Wis4	SPAC9G1.02	*Win1*	SPAC1006.09	- / -
Spo4	serine/threonine protein kinase Spo4	SPBC21C3.18	*Hsk1*	SPBC776.12c	- / -
Pak2 (Shk2)	PAK-related kinase Shk2	SPAC1F5.09c	*Shk1, Ppk2*	SPBC1604.14c, SPAC12B10.14c	- / -
Pka1 (Tpk, Git6)	cAMP-dependent protein kinase catalytic subunit Pka1	SPBC106.10	*N/F*		- / -
Mde3	serine/threonine protein kinase, meiotic Mde3	SPBC8D2.19	*Pit1*	SPAC3C7.06c	- / -
Hhp2	serine/threonine protein kinase Hhp2	SPAC23C4.12	*Hhp1*	SPBC3H7.15	- / -
Cmk2 (Mkp2)	MAPK-activated protein kinase Cmk2	SPAC23A1.06c	*Srk1*	SPCC1322.08	- / -
Chk1 (Rad27)	Chk1 protein kinase	SPCC1259.13	*N/F*		- / -
Byr2 (Ste8)	MAP kinase kinase kinase Byr2	SPBC1D7.05	*N/F*		- / -
Wis1 (Spc2, Smf2)	MAP kinase kinase Wis1	SPBC409.07c	*N/F*		- / -
Pmk1 (Spm1)	MAP kinase Pmk1	SPBC119.08	*N/F*		- / -
Pom1	DYRK family protein kinase Pom1	SPAC2F7.03c	*Ppk5*	SPAC16C9.07	d/ -
Mph1	dual specificity protein kinase Mph1	SPBC1271.16c	*N/F*		- / -

Mak3 (Phk2)	histidine kinase Mak3	SPCC74.06	*Mak1 Mak2*	SPAC1834.08 SPAC27E2.09	- / -
Hhp1	serine/threonine protein kinase Hhp1	SPBC3H7.15	*Hhp2*	SPAC23C4.12	- / -
Cmk1	calcium/calmodulin-dependent protein kinase Cmk1	SPACUNK12.02	*N/F*		- / -
Cek1	serine/threonine protein kinase Cek1	SPCC1450.11c	*Ppk18, Ppk31*	SPCC1450.11c, SPBC725.06c	- / -
Byr1 (Ste1, Ste3)	MAP kinase kinase Byr1	SPAC1D4.13	*N/I*		- / -
Wee1	M phase inhibitor protein kinase Wee1	SPCC18B5.03	*Mik1*		- / -
Spk1	MAP kinase Spk1	SPAC31G5.09c	*N/F*		- / -
Pit1	serine/threonin protein kinase, meiotic Pit1	SPAC3C7.06c	*Mde3*	SPBC8D2.19	- / -
Mkh1	MEK kinase (MEKK) Mkh1	SPAC1F3.02c	*N/F*		- / -
Mak2	histidine kinase Mak2	SPAC27E2.09	*Mak1 Mak3*	SPAC1834.08 SPCC74.06	- / -
Fin1	serine/threonine protein kinase, NIMA related Fin1	SPAC19E9.02	*N/F*		- / -
Cki3	serine/threonine protein kinase Cki3 (casein kinase I)	SPAC1805.05	*Cki1, Cki2*	SPBC1347.06c, SPBP35G2.05c	- / -
Cds1	Replication checkpoint kinase Cds1	SPCC18B5.11c	*N/F*		- / -
Sty1 (Spc1, Phh1)	MAP kinase Sty1	SPAC24B11.06	*N/F*		- / -
Gsk3 (Skp1)	serine/threonine protein kinase Gsk3	SPAC1687.15	*Gsk31*	SPBC8D2.01	- / -
Pck2 (Sts6, Pkc1)	Protein kinase C (PKC)-like Pck2	SPBC12D12.04c	*Pck1*	SPAC17G8.14c	- / -
Mik1	Mitotic inhibitor kinase Mik1	SPBC660.14	*Wee1*	SPCC18B5.03	- / -
Mak1 (Phk3)	Histidine kinase Mak1	SPAC1834.08	*Mak2, Mak3*	SPAC27E2.09, SPCC74.06	- / -
Dsk1	SR protein-specific kinase Dsk1	SPBC530.14c	*N/F*		- / -

Cki1	serine/threonine protein kinase Cki1	SPBC1347.06c	*Cki2, Cki3*	SPBP35G2.05c, SPAC1805.05	- / -
Cdr2	serine/threonine protein kinase Cdr2	SPAC57A10.02	*Cdr1 (Nim1)*	SPAC644.06c	- / -
Ssp1	serine/threonine protein kinase Ssp1	SPCC297.03	*N/F*		- / -
Pek1 (Skh1, Mkk1)	MAP kinase kinase Pek1	SPBC543.07	*N/F*		- / -
Psk1	serine/threonine protein kinase Psk1	SPCC4G3.08	*N/F*		- / -
Mek1	Cds1/Rad53/Chk2 family protein kinase Mek1	SPAC14C4.03	*N/F*		- / -
Kin1	microtubule affinity-regulating kinase Kin1	SPBC4F6.06	*N/F*		- / -
Csk1	cyclin-dependent kinase activating kinase Csk1	SPAC1D4.06c	*Lsk1*	SPAC2F3.15	- / -
Cdr1 (Nim1)	serine/threonine protein kinase Cdr1	SPAC644.06c	*Cdr2*	SPAC57A10.02	- / -
Ppk5	serine/threonine protein kinase Ppk5	SPAC16C9.07	*Pom1*	SPAC2F7.03c	- / -
Ppk21	serine/threonine protein kinase Ppk21	SPBC1778.10c	*Ksg1*	SPCC576.15c	- / -
Ppk34	serine/threonine protein kinase Ppk34	SPCC830.12	*N/I*		- / -
Ppk38	Ark1/Prk1 family protein kinase Ppk38	SPCP1E11.02	*Ppk30, Ppk29*	SPBC6B1.02, SPBC557.04	- / -
Ppk1	serine/threonine protein kinase Ppk1	SPAC140.05	*N/F*		- / -
Ppk6	serine/threonine protein kinase Ppk6	SPAPJ736.02c	*N/F*		- / -
Ckb1	CK2 (casein kinase II) family regulatory subunit Ckb1	SPAC1851.03	*SPBC2 G5.02c*	SPBC2G5.02c	- / -
Cki2	serine/threonine protein kinase Cki2, casein kinase I	SPBP35G2.05c	*Cki1, Cki3*	SPBC1347.06c, SPAC1805.05	- / -
Pef1	Pho85/PhoA-like cyclin-dependent	SPCC16C4.11	*N/F*		- / -

	kinase Pef1				
Rad3	ATR checkpoint kinase Rad3	SPBC216.05	*N/F*		d/ -
SPBC29A3.09c	AAA family ATPase Gcn20	SPBC29A3.09c	*N/F*		- / -
Ppk26	serine/threonine protein kinase, PAN complex subunit, Ppk26	SPBC336.14c	*SPAC1 B1.04c*	SPAC1B1.04c	- / -
SPCC1919.03c	AMP-activated protein kinase beta subunit	SPCC1919.03c	*N/F*		- / -
Win1	MAP kinase kinase kinase Win1	SPAC1006.09	*Wis4*	SPAC9G1.02	- / -
Ppk32	serine/threonine protein kinase Ppk32	SPBP23A10.10	*N/F*		- / -
Pck1	protein kinase C (PKC)-like Pck1	SPAC17G8.14c	*Pck2*	SPBC12D12.04c	- / -
Gen2	eIF2 alpha kinase Gcn2	SPBC36B7.09	*N/F*		- / -
Ppk18	serine/threonine protein kinase Ppk18	SPAPB18E9.02c	*Ppk31, Cek1*	SPBC725.06c, SPCC1450.11c	- / -
Fab1	1-phosphatidylinositol-3-phosphate 5-kinase Fab1	SPBC3E7.01	*N/F*		- / -

1: Information on this table was retrieved from GeneDB database (http://old.genedb.org/). The database was searched to find all the similar genes for the above kinases.

2:N/F means no similar genes were found. On geneDB database for each particular *S. pombe* gene, the *S. cerevisiae* homologue is indicated. It is also indicated weather there are more than one *S. pombe* gene similar to that *S. cerevisiae* homologue. When this was true, we considered these genes to be similar among them and so, putative paralogues. However, if only one *S. pombe* gene was found to be homologous to a particular *S. cerevisiae* gene we considered the former gene did not possess any other similar genes. We labeled these genes as Not/Found (N/F).

3:N/I (No/Information) means no information on GeneDB regarding similar genes was found. In practice this means that no information concerning *S.cerevisiae* homologues was given, for this particular gene.

4: [**-** / **-**] means it was not possible to see the absence of phosphorylation bands on the kinase deletion background specified in the first column.

5. **[d]** means it was not possible to achieve a clear conclusion regarding the presence/absence of phosphorylation bands on the kinase deletion background specified in the first column.

Annex II – Malp3 predicted phosphorylated sites with NetPhosK

```
>SPAC18G6.15    308 amino acids
#
# netphosyeast-1.0a prediction results
#
# Sequence                  # x   Context     Score   Kinase    Answer
# ------------------------------------------------------------------
# SPAC18G6.15                 2 S   ---MSESRQ   0.865   main       YES
# SPAC18G6.15                 4 S   -MSESRQEL   0.865   main       YES
# SPAC18G6.15                16 T   INQVTSLGL   0.281   main         .
# SPAC18G6.15                17 S   NQVTSLGLT   0.198   main         .
# SPAC18G6.15                21 T   SLGLTRIED   0.186   main         .
# SPAC18G6.15                38 S   QIFDSIYQD   0.423   main         .
# SPAC18G6.15                84 S   PERLSRCKM   0.490   main         .
# SPAC18G6.15               125 T   GPANTRVMN   0.194   main         .
# SPAC18G6.15               130 S   RVMNSSAGA   0.608   main       YES
# SPAC18G6.15               131 S   VMNSSAGAT   0.739   main       YES
# SPAC18G6.15               135 T   SAGATGPSR   0.557   main       YES
# SPAC18G6.15               138 S   ATGPSRRRQ   0.602   main       YES
# SPAC18G6.15               144 S   RRQVSSGSS   0.933   main       YES
# SPAC18G6.15               145 S   RQVSSGSST   0.855   main       YES
# SPAC18G6.15               147 S   VSSGSSTPS   0.856   main       YES
# SPAC18G6.15               148 S   SSGSSTPSM   0.805   main       YES
# SPAC18G6.15               149 T   SGSSTPSMT   0.838   main       YES
# SPAC18G6.15               151 S   SSTPSMTKS   0.823   main       YES
# SPAC18G6.15               153 T   TPSMTKSSA   0.433   main         .
# SPAC18G6.15               155 S   SMTKSSANN   0.664   main       YES
# SPAC18G6.15               156 S   MTKSSANNN   0.697   main       YES
# SPAC18G6.15               163 S   NNNVSSTAN   0.719   main       YES
# SPAC18G6.15               164 S   NNVSSTANT   0.506   main       YES
# SPAC18G6.15               165 T   NVSSTANTA   0.316   main         .
# SPAC18G6.15               168 T   STANTAAVL   0.569   main       YES
# SPAC18G6.15               182 T   QQQITSLET   0.444   main         .
# SPAC18G6.15               183 S   QQITSLETQ   0.686   main       YES
# SPAC18G6.15               186 T   TSLETQLYE   0.152   main         .
# SPAC18G6.15               194 T   EVNETMFGL   0.249   main         .
# SPAC18G6.15               218 T   ILVQTHLTT   0.214   main         .
# SPAC18G6.15               221 T   QTHLTTSPM   0.278   main         .
# SPAC18G6.15               222 T   THLTTSPMS   0.106   main         .
# SPAC18G6.15               223 S   HLTTSPMSM   0.930   main       YES
# SPAC18G6.15               226 S   TSPMSMENM   0.649   main       YES
# SPAC18G6.15               240 S   AILYSTEDG   0.330   main         .
# SPAC18G6.15               241 T   ILYSTEDGF   0.386   main         .
# SPAC18G6.15               256 T   PADLTTALT   0.187   main         .
# SPAC18G6.15               257 T   ADLTTALTD   0.228   main         .
# SPAC18G6.15               260 T   TTALTDHDT   0.612   main       YES
# SPAC18G6.15               264 T   TDHDTNNVA   0.436   main         .
# SPAC18G6.15               274 T   EAQMTDLKD   0.476   main         .
# SPAC18G6.15               279 S   DLKDSETQR   0.663   main       YES
# SPAC18G6.15               281 T   KDSETQRVP   0.355   main         .
# SPAC18G6.15               286 S   QRVPSAPDF   0.838   main       YES
```

Calponin Homology

Linker

Coiled Coil

C-terminal Tail

```
# SPAC18G6.15            297 S   ARLQSLEVD   0.790   main       YES
# SPAC18G6.15            307 T   DENITF---   0.548   main       YES
#
     MSESRQELLAWINQVTSLGLTRIEDCGKGYAMIQIFDSIYQDIPLKKVNF   #     50
     ECNNEYQYINNWKVLQQVFLKKGIDKVVDPERLSRCKMQDNLEFVQWAKR   #    100
     FWDQYYPGGDYDALARRGNRGPANTRVMNSSAGATGPSRRRQVSSGSSTP   #    150
     SMTKSSANNNNVSSTANTAAVLRAKQAQQQITSLETQLYEVNETMFGLER   #    200
     ERDFYFNKLREIEILVQTHLTTSPMSMENMLERIQAILYSTEDGFELPPD   #    250
     QPADLTTALTDHDTNNVAEEAQMTDLKDSETQRVPSAPDFVHARLQSLEV   #    300
     DDDENITF                                             #    350
%1   .S.S.....................................................   #     50
%1   .....................................................   #    100
%1   ............................SS...T..S.....SS.SST.   #    150
%1   S...SS......SS...T.............S.................   #    200
%1   ......................S..S.......................   #    250
%1   .........T..................S......S..........S...   #    300
%1   ......T.
```

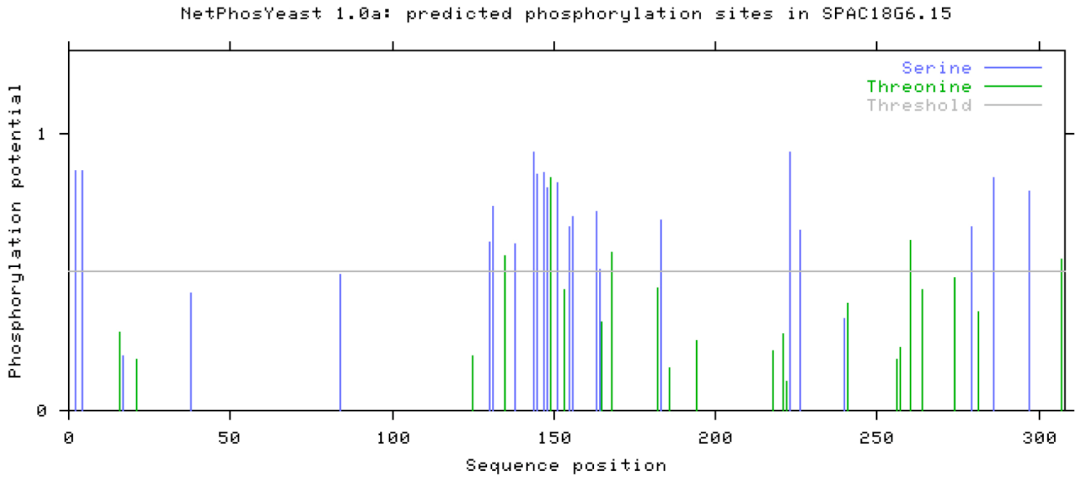

Annex III – Kinases interacting with mal3p and tip1p

Table III-1: Kinases that interact with mal3p/BIM1p

Kinase name *S. pombe*	Kinase name *S. cerevisiae*	Process involved	mal3p	BIM1p	Tested
Mph1	*MPS1*	Cell cycle – Checkpoint	✓	X	Y
Fin1	*KIN3*	Cell cycle – Mitosis onset, Citokenesis	✓	X	Y
Asp1	*VIP1*	Synthesis of 4PP-IP5 or 6PP-IP5, Regulation of the cortical actin cytoskeleton	✓	✓	N
Ppk30	*ARK1,PRK1,AKL1*	Regulation of the cortical actin cytoskeleton	✓	X	Y
Pom1	*N/F*	Cell cycle – Mitosis onset	✓	X	d
Lsk1	*CTK1*	Cell cycle – Citokinesis	✓	X	Y
Bub1	*BUB1*	Cell cycle - checkpoint	✓	✓	Y
Ark1	*IPL1*	Cell cycle - Kinetochore-microtubule attachments	X	✓	Y
Ipk1	*IPK1*	Synthesis of 1,2,3,4,5,6-hexakisphosphate (phytate or IP6)	X	✓	N
Gsk3	*MCK1*	Cell cycle - Control of chromosome segregation and in regulating entry into meiosis	X	✓	Y
Fab1	*FAB1*	Synthesis of phosphatidylinositol 3,5-bisphosphate (PtdIns(3,5)P2)	X	✓	Y
Shk2 (Pak2)	*CLA4*	Cell cycle – Cytokinesis, Cellular morphogenesis, Sterol uptake regulation.	X	✓	Y
N/F	*ELM1*	Cell cycle – Cytokinesis, Cellular morphogenesis	X	✓	N
Ppk1	*KIN4*	Cell cycle - Mitotic exit network (MEN)	X	✓	Y
SPCC162.11c	*URK1*	Uridine/cytidine kinase, component of the pyrimidine ribonucleotide salvage pathway	X	✓	N
Cds1	*RAD53*	Cell cycle – Checkpoint	X	✓	Y
Pck2	*PKC1*	Actin cytoskeleton organization, cell polarity	X	✓	Y

Data was retrieved from http://thebiogrid.org/. Kinases coloured in light grey are involved in cell cycle regulation, kinases colored in dark grey are involved in actin cytoskeleton organization and kinases coloured in intermediate grey are involved in inositol/phosphatidylinositol phosphate biosynthesis. ✓ indicates the kinase interacts with either mal3p or BIM1, while X indicates the kinase doesn't interact. Y means the kinase was tested on screen, N, means it wasn't

tested and d, means it was tested but the results were not conclusive. N/F indicated the ortologue gene for the specified kinase was not found.

TableIII-2: Kinases that interact with Tip1p/BIK1p

Kinase name *S. pombe*	Kinase name *S. cerevisiae*	Process involved	Tip1p	BIK1p	Tested
SPCC162.11C	*URK1*	Uridine/cytidine kinase, component of the pyrimidine ribonucleotide salvage pathway	✓	**X**	**N**
Tor1, Tor2	*TOR1*	Synthesis of 1-phosphatidyl-1D-myo-inositol 3-phosphate, growth control.	**X**	✓	**Y**
Bub1	*BUB1*	Cell cycle – Checkpoint	**X**	✓	**Y**
Atg1	*ATG1*	Autophagy	**X**	✓	**Y**
Wee1, Mik1	*SWE1*	Cell cycle – Mitosis onset	**X**	✓	**Y,Y**
Cki2, Cki1, Cki3	*YCK1*	Cell cycle – Citokinesis, Morphogenesis, Endocitosis	**X**	✓	**Y,Y,Y**
Ksg1, Ppk21	*PKH3*	Phosphoinositide signaling pathway	**X**	✓	**N,Y**
Cmk1	*CMK1*	Cell cycle, morphogenesis, Ca^{2+} signaling	**X**	✓	**Y**
N/F	*PTK2*	Cell cycle, cell size	**X**	✓	**N**
Sid2, Mug27	*DBF2*	Cell cycle – cytokinesis, Morphogenesis	**X**	✓	**Y,N**
Fab1	*FAB1*	Synthesis of phosphatidylinositol 3,5-bisphosphate (PtdIns(3,5)P2)	**X**	✓	**Y**

Data was retrieved from http://thebiogrid.org/. Kinases coloured in violotet are involved in cell cycle regulation and kinases coloured in yellow are involved in inositol/phosphatidylinositol phosphate biosynthesis. ✓ indicates the kinase interacts with either tip1p or BIK1, while X indicates the kinase doesn't interact. Y means the kinase was tested on screen, N, means it wasn't . N/F indicated the ortologue gene for the specified kinase was not found.

Annex IV – The EB protein family sequence alignment

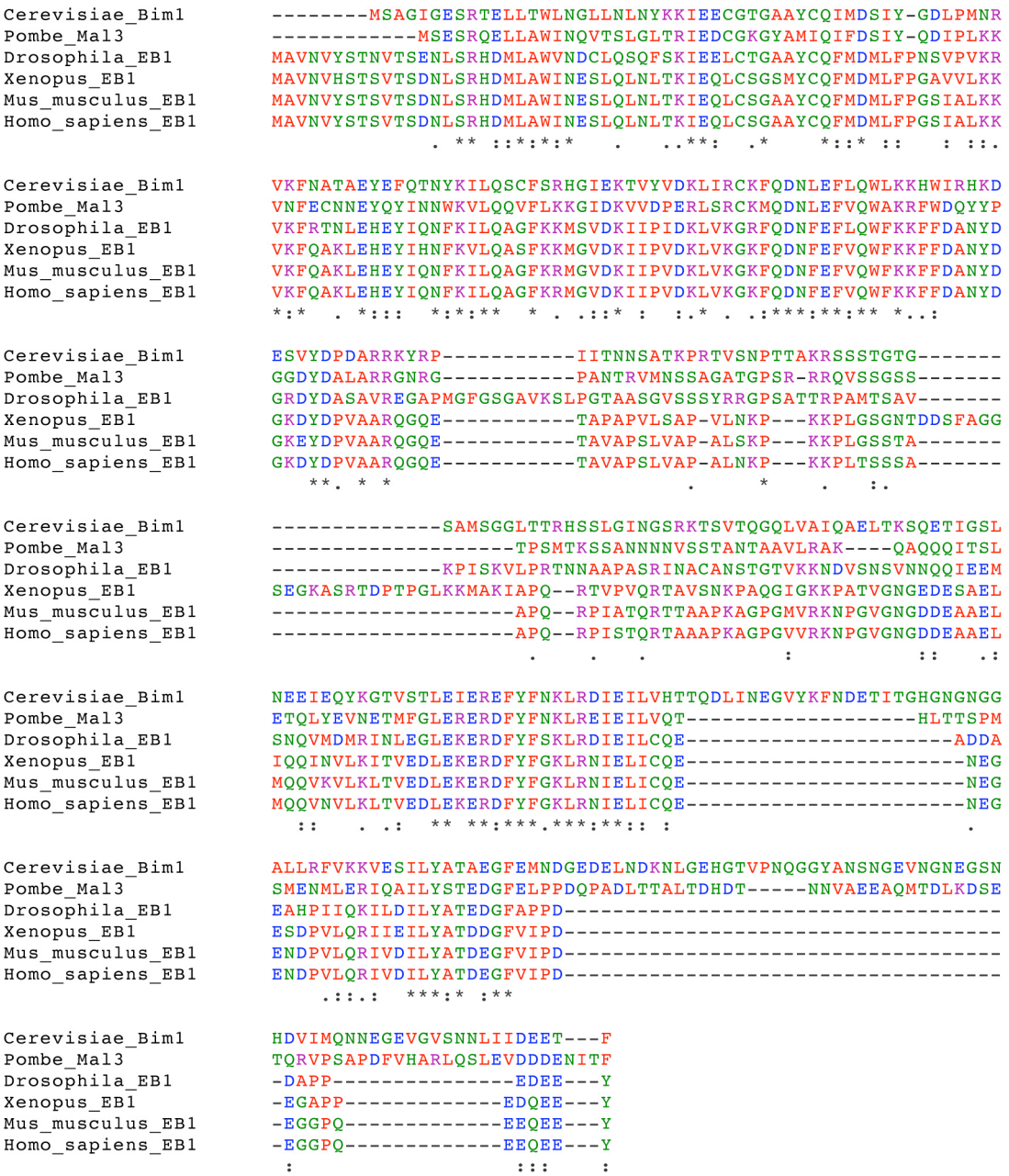

Chapter 8

References

8. References

Afzelius, B.A., Bellon, P.L., and Lanzavecchia, S. (1990). Microtubules and their protofilaments in the flagellum of an insect spermatozoon. J Cell Sci *95 (Pt 2)*, 207-217.

Akhmanova, A., and Hoogenraad, C.C. (2005). Microtubule plus-end-tracking proteins: mechanisms and functions. Current Opinion in Cell Biology *17*, 47-54.

Akhmanova, A., and Steinmetz, M.O. (2008). Tracking the ends: a dynamic protein network controls the fate of microtubule tips. Nat Rev Mol Cell Biol *9*, 309-322.

Akhmanova, A., and Steinmetz, M.O. (2010). Microtubule +TIPs at a glance. J Cell Sci *123*, 3415-3419.

Alberts, B., Johnson, A., Lewis J., Raff, M., Robersts, K., Walter, P. (2002). Molecular Biology of the Cell. Garland Science publishers, fourth edition.

Amos, L., and Klug, A. (1974). Arrangement of subunits in flagellar microtubules. J Cell Sci *14*, 523-549.

Amos, L.A., and Schlieper, D. (2005). Microtubules and maps. Adv Protein Chem *71*, 257-298.

Anderson, C.W., Baum, P.R., and Gesteland, R.F. (1973). Processing of adenovirus 2-induced proteins. J Virol *12*, 241-252.

Arellano, M., Valdivieso, M.H., Calonge, T.M., Coll, P.M., Duran, A., and Perez, P. (1999). Schizosaccharomyces pombe protein kinase C homologues, pck1p and pck2p, are targets of rho1p and rho2p and differentially regulate cell integrity. J Cell Sci *112 (Pt 20)*, 3569-3578.

Arnal, I., Heichette, C., Diamantopoulos, G.S., and Chrétien, D. (2004). CLIP-170/tubulin-curved oligomers coassemble at microtubule ends and promote rescues. Current Biology *14*, 2086-2095.

Arnal, I., Karsenti, E., and Hyman, A.A. (2000). Structural transitions at microtubule ends correlate with their dynamic properties in Xenopus egg extracts. J Cell Biol *149*, 767-774.

Arnal, I., and Wade, R.H. (1995). How does taxol stabilize microtubules? Current Biology *5*, 900-908.

Asakawa, K., Kume, K., Kanai, M., Goshima, T., Miyahara, K., Dhut, S., Tee, W.W., Hirata, D., and Toda, T. (2006). The V260I mutation in fission yeast alpha-tubulin Atb2 affects microtubule dynamics and EB1-Mal3 localization and activates the Bub1 branch of the spindle checkpoint. Mol Biol Cell *17*, 1421-1435.

Asakawa, K., Toya, M., Sato, M., Kanai, M., Kume, K., Goshima, T., Garcia, M.A., Hirata, D., and Toda, T. (2005). Mal3, the fission yeast EB1 homologue, cooperates with Bub1 spindle checkpoint to prevent monopolar attachment. EMBO Rep *6*, 1194-1200.

Askham, J.M., Vaughan, K.T., Goodson, H.V., and Morrison, E.E. (2002). Evidence that an interaction between EB1 and p150(Glued) is required for the formation and maintenance of a radial microtubule array anchored at the centrosome. Mol Biol Cell *13*, 3627-3645.

Baas, P.W., Deitch, J.S., Black, M.M., and Banker, G.A. (1988). Polarity orientation of microtubules in hippocampal neurons: uniformity in the axon and nonuniformity in the dendrite. Proc Natl Acad Sci USA *85*, 8335-8339.

Bahler, J., Wu, J.Q., Longtine, M.S., Shah, N.G., McKenzie, A., 3rd, Steever, A.B., Wach, A., Philippsen, P., and Pringle, J.R. (1998). Heterologous modules for efficient and versatile PCR-based gene targeting in Schizosaccharomyces pombe. Yeast *14*, 943-951.

Ban, R., Matsuzaki, H., Akashi, T., Sakashita, G., Taniguchi, H., Park, S.-Y., Tanaka, H., Furukawa, K., and Urano, T. (2009). Mitotic regulation of the stability of microtubule plus-end tracking protein EB3 by ubiquitin ligase SIAH-1 and Aurora mitotic kinases. Journal of Biological Chemistry *284*, 28367-28381.

Barth, A.I.M., Siemers, K.A., and Nelson, W.J. (2002). Dissecting interactions between EB1, microtubules and APC in cortical clusters at the plasma membrane. Journal of Cell Science *115*, 1583-1590.

Bartolini, F., and Gundersen, G.G. (2006). Generation of noncentrosomal microtubule arrays. J Cell Sci *119*, 4155-4163.

Beinhauer, J.D., Hagan, I.M., Hegemann, J.H., and Fleig, U. (1997). Mal3, the fission yeast homologue of the human APC-interacting protein EB-1 is required for microtubule integrity and the maintenance of cell form. The Journal of Cell Biology *139*, 717-728.

Berrueta, L., Kraeft, S.K., Tirnauer, J.S., Schuyler, S.C., Chen, L.B., Hill, D.E., Pellman, D., and Bierer, B.E. (1998). The adenomatous polyposis coli-binding protein EB1 is associated with cytoplasmic and spindle microtubules. Proc Natl Acad Sci USA *95*, 10596-10601.

Bettencourt-Dias, M., and Glover, D.M. (2007). Centrosome biogenesis and function: centrosomics brings new understanding. Nat Rev Mol Cell Biol *8*, 451-463.

Bieling, P., Kandels-Lewis, S., Telley, I.A., van Dijk, J., Janke, C., and Surrey, T. (2008). CLIP-170 tracks growing microtubule ends by dynamically recognizing composite EB1/tubulin-binding sites. The Journal of Cell Biology *183*, 1223-1233.

Bieling, P., Laan, L., Schek, H., Munteanu, E.L., Sandblad, L., Dogterom, M., Brunner, D., and Surrey, T. (2007). Reconstitution of a microtubule plus-end tracking system in vitro. Nature *450*, 1100-1105.

Bimbo, A., Jia, Y., Poh, S.L., Karuturi, R.K., den Elzen, N., Peng, X., Zheng, L., O'Connell, M., Liu, E.T., Balasubramanian, M.K., and Liu, J. (2005). Systematic deletion analysis of fission yeast protein kinases. Eukaryot Cell *4*, 799-813.

Blackburn, K., and Goshe, M.B. (2009). Challenges and strategies for targeted phosphorylation site identification and quantification using mass spectrometry analysis. Brief Funct Genomic Proteomic *8*, 90-103.

Bodenmiller, B., Wanka, S., Kraft, C., Urban, J., Campbell, D., Pedrioli, P.G., Gerrits, B., Picotti, P., Lam, H., Vitek, O., Brusniak, M.Y., Roschitzki, B., Zhang, C., Shokat, K.M., Schlapbach, R., Colman-Lerner, A., Nolan, G.P., Nesvizhskii, A.I., Peter, M., Loewith, R., von Mering, C., and Aebersold, R. Phosphoproteomic analysis reveals interconnected system-wide responses to perturbations of kinases and phosphatases in yeast. Sci Signal *3*, rs4.

Bogatcheva, N.V., and Gusev, N.B. (1995). Interaction of smooth muscle calponin with phospholipids. FEBS Lett *371*, 123-126.

Bomont, P., and Koenig, M. (2003). Intermediate filament aggregation in fibroblasts of giant axonal neuropathy patients is aggravated in non dividing cells and by microtubule destabilization. Hum Mol Genet *12*, 813-822.

Boyle, W.J., van der Geer, P., and Hunter, T. (1991). Phosphopeptide mapping and phosphoamino acid analysis by two-dimensional separation on thin-layer cellulose plates. Methods Enzymol *201*, 110-149.

Bratman, S.V., and Chang, F. (2007). Stabilization of overlapping microtubules by fission yeast CLASP. Developmental Cell *13*, 812-827.

Breitkreutz, A., Choi, H., Sharom, J.R., Boucher, L., Neduva, V., Larsen, B., Lin, Z.Y., Breitkreutz, B.J., Stark, C., Liu, G., Ahn, J., Dewar-Darch, D., Reguly, T., Tang, X., Almeida, R., Qin, Z.S., Pawson, T., Gingras, A.C., Nesvizhskii, A.I., and Tyers, M. A global protein kinase and phosphatase interaction network in yeast. Science *328*, 1043-1046.

Brenner, S.L., and Korn, E.D. (1979). Substoichiometric concentrations of cytochalasin D inhibit actin polymerization. Additional evidence for an F-actin treadmill. J Biol Chem *254*, 9982-9985.

Bretscher, A. (2005). Microtubule tips redirect actin assembly. Developmental Cell *8*, 458-459.
Browning, H., Hackney, D.D., and Nurse, P. (2003). Targeted movement of cell end factors in fission yeast. Nat Cell Biol *5*, 812-818.

Browning, H., Hayles, J., Mata, J., Aveline, L., Nurse, P., and McIntosh, J.R. (2000). Tea2p is a kinesin-like protein required to generate polarized growth in fission yeast. J Cell Biol *151*, 15-28.

Brunner, D., and Nurse, P. (2000). CLIP170-like tip1p spatially organizes microtubular dynamics in fission yeast. Cell *102*, 695-704.

Bu, W., and Su, L.-K. (2003). Characterization of functional domains of human EB1 family proteins. J Biol Chem *278*, 49721-49731.

Bu, W., and Su, L.K. (2001). Regulation of microtubule assembly by human EB1 family proteins. Oncogene *20*, 3185-3192.

Busch, K.E., and Brunner, D. (2004). The microtubule plus end-tracking proteins mal3p and tip1p cooperate for cell-end targeting of interphase microtubules. Current Biology *14*, 548-559.

Busch, K.E., Hayles, J., Nurse, P., and Brunner, D. (2004). Tea2p kinesin is involved in spatial microtubule organization by transporting tip1p on microtubules. Developmental Cell *6*, 831-843.

Busch, K.E. (2004). Coordinated activities of microtubule-associated proteins in spatial cytoskeleton organization and the mechanisms mediating their microtubule plus end-tracking. PhD Thesis, Basel University.

Buster, D.W., Zhang, D., and Sharp, D.J. (2007). Poleward tubulin flux in spindles: regulation and function in mitotic cells. Mol Biol Cell *18*, 3094-3104.

Carazo-Salas, R.E., and Nurse, P. (2006). Self-organization of interphase microtubule arrays in fission yeast. Nat Cell Biol *8*, 1102-1107.

Carvalho, P., Gupta, M.L., Hoyt, M.A., and Pellman, D. (2004). Cell cycle control of kinesin-mediated transport of Bik1 (CLIP-170) regulates microtubule stability and dynein activation. Developmental Cell *6*, 815-829.

Chan, J., Jensen, C.G., Jensen, L.C., Bush, M., and Lloyd, C.W. (1999). The 65-kDa carrot microtubule-associated protein forms regularly arranged filamentous cross-bridges between microtubules. Proc Natl Acad Sci U S A *96*, 14931-14936.

Chang, F., and Martin, S.G. (2009). Shaping fission yeast with microtubules. Cold Spring Harb Perspect Biol *1*, a001347.

Chang, L., and Goldman, R.D. (2004). Intermediate filaments mediate cytoskeletal crosstalk. Nat Rev Mol Cell Biol *5*, 601-613.

Chang, P., and Stearns, T. (2000). Delta-tubulin and epsilon-tubulin: two new human centrosomal tubulins reveal new aspects of centrosome structure and function. Nat Cell Biol *2*, 30-35.

Choi, J.H., Adames, N.R., Chan, T.F., Zeng, C., Cooper, J.A., and Zheng, X.F. (2000). TOR signaling regulates microtubule structure and function. Curr Biol *10*, 861-864.

Choi, J.H., Bertram, P.G., Drenan, R., Carvalho, J., Zhou, H.H., and Zheng, X.F.S. (2002). The FKBP12-rapamycin-associated protein (FRAP) is a CLIP-170 kinase. EMBO Rep *3*, 988-994.

Chretien, D., Fuller, S.D., and Karsenti, E. (1995). Structure of growing microtubule ends: two-dimensional sheets close into tubes at variable rates. J Cell Biol *129*, 1311-1328.

Costanzo, M., Baryshnikova, A., Bellay, J., Kim, Y., Spear, E.D., Sevier, C.S., Ding, H., Koh, J.L., Toufighi, K., Mostafavi, S., Prinz, J., St Onge, R.P., VanderSluis, B., Makhnevych, T., Vizeacoumar, F.J., Alizadeh, S., Bahr, S., Brost, R.L., Chen, Y., Cokol, M., Deshpande, R., Li, Z., Lin, Z.Y., Liang, W., Marback, M., Paw, J., San Luis, B.J., Shuteriqi, E., Tong, A.H., van Dyk, N., Wallace, I.M., Whitney, J.A., Weirauch, M.T., Zhong, G., Zhu, H., Houry, W.A., Brudno, M., Ragibizadeh, S., Papp, B., Pal, C., Roth, F.P., Giaever, G., Nislow, C., Troyanskaya, O.G., Bussey, H., Bader, G.D., Gingras, A.C., Morris, Q.D., Kim, P.M., Kaiser, C.A., Myers, C.L., Andrews, B.J., and Boone, C. The genetic landscape of a cell. Science *327*, 425-431.

Daga, R.R., Lee, K.-G., Bratman, S., Salas-Pino, S., and Chang, F. (2006). Self-organization of microtubule bundles in anucleate fission yeast cells. Nat Cell Biol *8*, 1108-1113.

Danuser, G., and Waterman-Storer, C.M. (2003). Quantitative fluorescent speckle microscopy: where it came from and where it is going. J Microsc *211*, 191-207.

Des Georges, A., Katsuki, M., Drummond, D.R., Osei, M., Cross, R.A., and Amos, L.A. (2008). Mal3, the Schizosaccharomyces pombe homolog of EB1, changes the microtubule lattice. Nat Struct Mol Biol *15*, 1102-1108.
Desai, A., and Mitchison, T.J. (1997). Microtubule polymerization dynamics. Annu Rev Cell Dev Biol *13*, 83-117.

Ding, R., McDonald, K.L., and McIntosh, J.R. (1993). Three-dimensional reconstruction and analysis of mitotic spindles from the yeast, Schizosaccharomyces pombe. The Journal of Cell Biology *120*, 141-151.

Ding, R., West, R.R., Morphew, D.M., Oakley, B.R., and McIntosh, J.R. (1997). The spindle pole body of Schizosaccharomyces pombe enters and leaves the nuclear envelope as the cell cycle proceeds. Mol Biol Cell *8*, 1461-1479.

Dixit, R., Barnett, B., Lazarus, J.E., Tokito, M., Goldman, Y.E., and Holzbaur, E.L.F. (2009). Microtubule plus-end tracking by CLIP-170 requires EB1. Proceedings of the National Academy of Sciences *106*, 492-497.

dos Remedios, C.G., Chhabra, D., Kekic, M., Dedova, I.V., Tsubakihara, M., Berry, D.A., and Nosworthy, N.J. (2003). Actin binding proteins: regulation of cytoskeletal microfilaments. Physiological Reviews *83*, 433-473.

Drummond, D.R., and Cross, R.A. (2000). Dynamics of interphase microtubules in Schizosaccharomyces pombe. Current Biology *10*, 766-775.

Dujardin, D., Wacker, U.I., Moreau, A., Schroer, T.A., Rickard, J.E., and De Mey, J.R. (1998). Evidence for a role of CLIP-170 in the establishment of metaphase chromosome alignment. The Journal of Cell Biology *141*, 849-862.

Dutcher, S.K. (2003). Long-lost relatives reappear: identification of new members of the tubulin superfamily. Curr Opin Microbiol *6*, 634-640.

Dutcher, S.K., and Trabuco, E.C. (1998). The UNI3 gene is required for assembly of basal bodies of Chlamydomonas and encodes delta-tubulin, a new member of the tubulin superfamily. Mol Biol Cell *9*, 1293-1308.

Fantes, P.A. (1977). Control of cell size and cycle time in Schizosaccharomyces pombe. J Cell Sci *24*, 51-67.

Feierbach, B., and Chang, F. (2001). Roles of the fission yeast formin for3p in cell polarity, actin cable formation and symmetric cell division. Curr Biol *11*, 1656-1665.

Fodde, R., Kuipers, J., Rosenberg, C., Smits, R., Kielman, M., Gaspar, C., van Es, J.H., Breukel, C., Wiegant, J., Giles, R.H., and Clevers, H. (2001). Mutations in the APC tumour suppressor gene cause chromosomal instability. Nat Cell Biol *3*, 433-438.

Foethke, D., Makushok, T., Brunner, D., and Nédélec, F. (2009). Force- and length-dependent catastrophe activities explain interphase microtubule organization in fission yeast. Mol Syst Biol *5*, 241.

Fu, C., Ward, J.J., Loiodice, I., Velve-Casquillas, G., Nedelec, F.J., and Tran, P.T. (2009). Phospho-regulated interaction between kinesin-6 Klp9p and microtubule bundler Ase1p promotes spindle elongation. Dev Cell *17*, 257-267.

Fujii, T., Yamana, K., Ogoma, Y., and Kondo, Y. (1995). Interaction of calponin with phospholipids. J Biochem *117*, 999-1003.

Goldman, R.D., Grin, B., Mendez, M.G., and Kuczmarski, E.R. (2008). Intermediate filaments: versatile building blocks of cell structure. Current Opinion in Cell Biology *20*, 28-34.

Goldstone, S., Reyes, C., Gay, G., Courthéoux, T., Dubarry, M., Tournier, S., and Gachet, Y. (2010). Tip1/CLIP-170 protein is required for correct chromosome poleward movement in fission yeast. PLoS ONE *5*, e10634.

Goshima, G., Nédélec, F., and Vale, R.D. (2005a). Mechanisms for focusing mitotic spindle poles by minus end-directed motor proteins. The Journal of Cell Biology *171*, 229-240.

Goshima, G., Wollman, R., Stuurman, N., Scholey, J.M., and Vale, R.D. (2005b). Length control of the metaphase spindle. Current Biology *15*, 1979-1988.

Gould, K.L., Moreno, S., Owen, D.J., Sazer, S., and Nurse, P. (1991). Phosphorylation at Thr167 is required for Schizosaccharomyces pombe p34cdc2 function. EMBO J *10*, 3297-3309.

Green, R.A., Wollman, R., and Kaplan, K.B. (2005). APC and EB1 function together in mitosis to regulate spindle dynamics and chromosome alignment. Mol Biol Cell *16*, 4609-4622.

Grimm, C., Kohli, J., Murray, J., and Maundrell, K. (1988). Genetic engineering of Schizosaccharomyces pombe: a system for gene disruption and replacement using the ura4 gene as a selectable marker. Mol Gen Genet *215*, 81-86.

Gupta, K.K., Paulson, B.A., Folker, E.S., Charlebois, B., Hunt, A.J., and Goodson, H.V. (2009). Minimal plus-end tracking unit of the cytoplasmic linker protein CLIP-170. J Biol Chem *284*, 6735-6742.

Gupton, S.L., and Gertler, F.B. (2007). Filopodia: the fingers that do the walking. Science's STKE *2007*, re5.

Hagan, I.M. (1998). The fission yeast microtubule cytoskeleton. Journal of Cell Science *111 (Pt 12)*, 1603-1612.

Hagan, I.M., and Petersen, J. (2000). The microtubule organizing centers of Schizosaccharomyces pombe. Curr Top Dev Biol *49*, 133-159.

Hammond, J.W., Cai, D., and Verhey, K.J. (2008). Tubulin modifications and their cellular functions. Current Opinion in Cell Biology *20*, 71-76.

Hayashi, I., and Ikura, M. (2003). Crystal structure of the amino-terminal microtubule-binding domain of end-binding protein 1 (EB1). J Biol Chem *278*, 36430-36434.

Hayashi, I., Wilde, A., Mal, T.K., and Ikura, M. (2005). Structural basis for the activation of microtubule assembly by the EB1 and p150Glued complex. Mol Cell *19*, 449-460.

Heitz, M.J., Petersen, J., Valovin, S., and Hagan, I.M. (2001). MTOC formation during mitotic exit in fission yeast. Journal of Cell Science *114*, 4521-4532.

Herrmann, H., and Aebi, U. (2004). Intermediate filaments: molecular structure, assembly mechanism, and integration into functionally distinct intracellular Scaffolds. Annu. Rev. Biochem. *73*, 749-789.

Herrmann, H., Bär, H., Kreplak, L., Strelkov, S.V., and Aebi, U. (2007). Intermediate filaments: from cell architecture to nanomechanics. Nat Rev Mol Cell Biol *8*, 562-573.

Herrmann, H., Strelkov, S.V., Burkhard, P., and Aebi, U. (2009). Intermediate filaments: primary determinants of cell architecture and plasticity. J Clin Invest *119*, 1772-1783.

Hill, T.L., and Kirschner, M.W. (1982). Bioenergetics and kinetics of microtubule and actin filament assembly-disassembly. Int Rev Cytol *78*, 1-125.

Hirokawa, N., Nitta, R., and Okada, Y. (2009). The mechanisms of kinesin motor motility: lessons from the monomeric motor KIF1A. Nat Rev Mol Cell Biol *10*, 877-884.

Honnappa, S., Gouveia, S.M., Weisbrich, A., Damberger, F.F., Bhavesh, N.S., Jawhari, H., Grigoriev, I., van Rijssel, F.J.A., Buey, R.M., Lawera, A., Jelesarov, I., Winkler, F.K., Wüthrich, K., Akhmanova, A., and Steinmetz, M.O. (2009). An EB1-binding motif acts as a microtubule tip localization signal. Cell *138*, 366-376.

Honnappa, S., John, C.M., Kostrewa, D., Winkler, F.K., and Steinmetz, M.O. (2005). Structural insights into the EB1-APC interaction. EMBO J *24*, 261-269.

Honnappa, S., Okhrimenko, O., Jaussi, R., Jawhari, H., Jelesarov, I., Winkler, F.K., and Steinmetz, M.O. (2006). Key interaction modes of dynamic +TIP networks. Mol Cell *23*, 663-671.

Höög, J.L., Schwartz, C., Noon, A.T., O'Toole, E.T., Mastronarde, D.N., Mcintosh, J.R., and Antony, C. (2007). Organization of interphase microtubules in fission yeast analyzed by electron tomography. Developmental Cell *12*, 349-361.

Horio, T., and Hotani, H. (1986). Visualization of the dynamic instability of individual microtubules by dark-field microscopy. Nature *321*, 605-607.

Howell, B., Deacon, H., and Cassimeris, L. (1999a). Decreasing oncoprotein 18/stathmin levels reduces microtubule catastrophes and increases microtubule polymer in vivo. J Cell Sci *112 (Pt 21)*, 3713-3722.

Howell, B., Larsson, N., Gullberg, M., and Cassimeris, L. (1999b). Dissociation of the tubulin-sequestering and microtubule catastrophe-promoting activities of oncoprotein 18/stathmin. Mol Biol Cell *10*, 105-118.

Janson, M.E., de Dood, M.E., and Dogterom, M. (2003). Dynamic instability of microtubules is regulated by force. The Journal of Cell Biology *161*, 1029-1034.

Janson, M.E., Loughlin, R., Loïodice, I., Fu, C., Brunner, D., Nédélec, F.J., and Tran, P.T. (2007). Crosslinkers and motors organize dynamic microtubules to form stable bipolar arrays in fission yeast. Cell *128*, 357-368.

Janson, M.E., Setty, T.G., Paoletti, A., and Tran, P.T. (2005). Efficient formation of bipolar microtubule bundles requires microtubule-bound gamma-tubulin complexes. The Journal of Cell Biology *169*, 297-308.

Kamps, M.P., and Sefton, B.M. (1989). Acid and base hydrolysis of phosphoproteins bound to immobilon facilitates analysis of phosphoamino acids in gel-fractionated proteins. Anal Biochem *176*, 22-27.

Katsuki, M., Drummond, D.R., Osei, M., and Cross, R.A. (2009). Mal3 masks catastrophe events in Schizosaccharomyces pombe microtubules by inhibiting shrinkage and promoting rescue. J Biol Chem *284*, 29246-29250.

Keating, T.J., and Borisy, G.G. (2000). Immunostructural evidence for the template mechanism of microtubule nucleation. Nat Cell Biol *2*, 352-357.

Khmelinskii, A., Roostalu, J., Roque, H., Antony, C., and Schiebel, E. (2009). Phosphorylation-dependent protein interactions at the spindle midzone mediate cell cycle regulation of spindle elongation. Dev Cell *17*, 244-256.

Khoudoli, G.A., Porter, I.M., Blow, J.J., and Swedlow, J.R. (2004). Optimisation of the two-dimensional gel electrophoresis protocol using the Taguchi approach. Proteome Sci *2*, 6.

Kikkawa, M., Ishikawa, T., Nakata, T., Wakabayashi, T., and Hirokawa, N. (1994). Direct visualization of the microtubule lattice seam both in vitro and in vivo. The Journal of Cell Biology *127*, 1965-1971.

Kinoshita, E., Kinoshita-Kikuta, E., Takiyama, K., and Koike, T. (2006). Phosphate-binding tag, a new tool to visualize phosphorylated proteins. Mol Cell Proteomics *5*, 749-757.

Kinoshita, E., Takahashi, M., Takeda, H., Shiro, M., and Koike, T. (2004). Recognition of phosphate monoester dianion by an alkoxide-bridged dinuclear zinc(II) complex. Dalton Trans, 1189-1193.

Kline-Smith, S.L., and Walczak, C.E. (2004). Mitotic spindle assembly and chromosome segregation: refocusing on microtubule dynamics. Mol Cell *15*, 317-327.

Komarova, Y., De Groot, C.O., Grigoriev, I., Gouveia, S.M., Munteanu, E.L., Schober, J.M., Honnappa, S., Buey, R.M., Hoogenraad, C.C., Dogterom, M., Borisy, G.G., Steinmetz, M.O., and Akhmanova, A. (2009). Mammalian end binding proteins control persistent microtubule growth. The Journal of Cell Biology *184*, 691-706.

Komarova, Y.A., Akhmanova, A.S., Kojima, S.-I., Galjart, N., and Borisy, G.G. (2002). Cytoplasmic linker proteins promote microtubule rescue in vivo. The Journal of Cell Biology *159*, 589-599.

Kozlowski, C., Srayko, M., and Nedelec, F. (2007). Cortical microtubule contacts position the spindle in C. elegans embryos. Cell *129*, 499-510.

Kronja, I., Kruljac-Letunic, A., Caudron-Herger, M., Bieling, P., and Karsenti, E. (2009). XMAP215-EB1 interaction is required for proper spindle assembly and chromosome segregation in Xenopus egg extract. Mol Biol Cell *20*, 2684-2696.

La Carbona, S., Le Goff, C., and Le Goff, X. (2006). Fission yeast cytoskeletons and cell polarity factors: connecting at the cortex. Biol Cell *98*, 619-631.

Laemmli, U.K., Molbert, E., Showe, M., and Kellenberger, E. (1970). Form-determining function of the genes required for the assembly of the head of bacteriophage T4. J Mol Biol *49*, 99-113.

Lansbergen, G., Komarova, Y., Modesti, M., Wyman, C., Hoogenraad, C.C., Goodson, H.V., Lemaitre, R.P., Drechsel, D.N., van Munster, E., Gadella, T.W.J., Grosveld, F., Galjart, N., Borisy, G.G., and Akhmanova, A. (2004). Conformational changes in CLIP-170 regulate its binding to microtubules and dynactin localization. The Journal of Cell Biology *166*, 1003-1014.

Lee, H.-S., Komarova, Y.A., Nadezhdina, E.S., Anjum, R., Peloquin, J.G., Schober, J.M., Danciu, O., van Haren, J., Galjart, N., Gygi, S.P., Akhmanova, A., and Borisy, G.G. (2010). Phosphorylation controls autoinhibition of cytoplasmic linker protein-170. Mol Biol Cell *21*, 2661-2673.

Li, H., Liu, X.S., Yang, X., Wang, Y., Wang, Y., Turner, J.R., and Liu, X. (2010). Phosphorylation of CLIP-170 by Plk1 and CK2 promotes timely formation of kinetochore-microtubule attachments. EMBO J *29*, 2953-2965.

Loïodice, I., Staub, J., Setty, T.G., Nguyen, N.-P.T., Paoletti, A., and Tran, P.T. (2005). Ase1p organizes antiparallel microtubule arrays during interphase and mitosis in fission yeast. Mol Biol Cell *16*, 1756-1768.

Louie, R.K., Bahmanyar, S., Siemers, K.A., Votin, V., Chang, P., Stearns, T., Nelson, W.J., and Barth, A.I.M. (2004). Adenomatous polyposis coli and EB1 localize in close proximity of the mother centriole and EB1 is a functional component of centrosomes. J Cell Sci *117*, 1117-1128.
Lu, B., Roegiers, F., Jan, L.Y., and Jan, Y.N. (2001). Adherens junctions inhibit asymmetric division in the Drosophila epithelium. Nature *409*, 522-525.

Lüders, J., and Stearns, T. (2007). Microtubule-organizing centres: a re-evaluation. Nat Rev Mol Cell Biol *8*, 161-167.

Maiato, H., and Lince-Faria, M. (2010). The perpetual movements of anaphase. Cell Mol Life Sci *67*, 2251-2269.

Maiato, H., Sampaio, P., and Sunkel, C.E. (2004). Microtubule-associated proteins and their essential roles during mitosis. Int Rev Cytol *241*, 53-153.

Mallavarapu, A., Sawin, K., and Mitchison, T. (1999). A switch in microtubule dynamics at the onset of anaphase B in the mitotic spindle of Schizosaccharomyces pombe. Current Biology *9*, 1423-1426.

Mandelkow, E.M., Schultheiss, R., Rapp, R., Müller, M., and Mandelkow, E. (1986). On the surface lattice of microtubules: helix starts, protofilament number, seam, and handedness. The Journal of Cell Biology *102*, 1067-1073.

Manna, T., Honnappa, S., Steinmetz, M.O., and Wilson, L. (2008). Suppression of microtubule dynamic instability by the +TIP protein EB1 and its modulation by the CAP-Gly domain of p150glued. Biochemistry *47*, 779-786.

Margolis, R.L., and Wilson, L. (1981). Microtubule treadmills--possible molecular machinery. Nature *293*, 705-711.

Margolis, R.L., and Wilson, L. (1998). Microtubule treadmilling: what goes around comes around. Bioessays *20*, 830-836.

Martin, S.G., and Berthelot-Grosjean, M. (2009). Polar gradients of the DYRK-family kinase Pom1 couple cell length with the cell cycle. Nature *459*, 852-856.

Martin, S.G., McDonald, W.H., Yates, J.R., and Chang, F. (2005). Tea4p links microtubule plus ends with the formin for3p in the establishment of cell polarity. Developmental Cell *8*, 479-491.

Martín-García, R., and Mulvihill, D.P. (2009). Myosin V spatially regulates microtubule dynamics and promotes the ubiquitin-dependent degradation of the fission yeast CLIP-170 homologue, Tip1. J Cell Sci *122*, 3862-3872.

Mastronarde, D.N., McDonald, K.L., Ding, R., and McIntosh, J.R. (1993). Interpolar spindle microtubules in PTK cells. J Cell Biol *123*, 1475-1489.

Mata, J., and Nurse, P. (1997). tea1 and the microtubular cytoskeleton are important for generating global spatial order within the fission yeast cell. Cell *89*, 939-949.

Mateer, S.C., Morris, L.E., Cromer, D.A., Bensenor, L.B., and Bloom, G.S. (2004). Actin filament binding by a monomeric IQGAP1 fragment with a single calponin homology domain. Cell Motil Cytoskeleton *58*, 231-241.

Matsuo, Y., Asakawa, K., Toda, T., and Katayama, S. (2006). A rapid method for protein extraction from fission yeast. Biosci Biotechnol Biochem *70*, 1992-1994.

Maurer, S.P., Bieling, P., Cope, J., Hoenger, A., and Surrey, T. GTPgammaS microtubules mimic the growing microtubule end structure recognized by end-binding proteins (EBs). Proc Natl Acad Sci U S A *108*, 3988-3993.

McConnell, S.J., and Yaffe, M.P. (1993). Intermediate filament formation by a yeast protein essential for organelle inheritance. Science *260*, 687-689.

Mcintosh, J.R., Morphew, M.K., Grissom, P.M., Gilbert, S.P., and Hoenger, A. (2009). Lattice structure of cytoplasmic microtubules in a cultured Mammalian cell. Journal of Molecular Biology *394*, 177-182.

McKean, P.G., Vaughan, S., and Gull, K. (2001). The extended tubulin superfamily. J Cell Sci *114*, 2723-2733.

Miller, R.K., D'Silva, S., Moore, J.K., and Goodson, H.V. (2006). The CLIP-170 orthologue Bik1p and positioning the mitotic spindle in yeast. Curr Top Dev Biol *76*, 49-87.

Mimori-Kiyosue, Y., Shiina, N., and Tsukita, S. (2000). The dynamic behavior of the APC-binding protein EB1 on the distal ends of microtubules. Current Biology *10*, 865-868.

Minin, A.A., and Moldaver, M.V. (2008). Intermediate vimentin filaments and their role in intracellular organelle distribution. Biochemistry Moscow *73*, 1453-1466.

Mitchison, T., and Kirschner, M. (1984). Dynamic instability of microtubule growth. Nature *312*, 237-242.

Mollinari, C., Kleman, J.P., Jiang, W., Schoehn, G., Hunter, T., and Margolis, R.L. (2002). PRC1 is a microtubule binding and bundling protein essential to maintain the mitotic spindle midzone. J Cell Biol *157*, 1175-1186.

Moores, C.A., Cooper, J., Wagenbach, M., Ovechkina, Y., Wordeman, L., and Milligan, R.A. (2006). The role of the kinesin-13 neck in microtubule depolymerization. Cell Cycle *5*, 1812-1815.

Moores, C.A., and Milligan, R.A. (2006). Lucky 13-microtubule depolymerisation by kinesin-13 motors. J Cell Sci *119*, 3905-3913.

Moreno, S., Klar, A., and Nurse, P. (1991). Molecular genetic analysis of fission yeast Schizosaccharomyces pombe. Methods Enzymol *194*, 795-823.

Morrison, E.E., Wardleworth, B.N., Askham, J.M., Markham, A.F., and Meredith, D.M. (1998). EB1, a protein which interacts with the APC tumour suppressor, is associated with the microtubule cytoskeleton throughout the cell cycle. Oncogene *17*, 3471-3477.

Moseley, J.B., Mayeux, A., Paoletti, A., and Nurse, P. (2009). A spatial gradient coordinates cell size and mitotic entry in fission yeast. Nature *459*, 857-860.

Motegi, F., Arai, R., and Mabuchi, I. (2001). Identification of two type V myosins in fission yeast, one of which functions in polarized cell growth and moves rapidly in the cell. Mol Biol Cell *12*, 1367-1380.

Nabeshima, K., Nakagawa, T., Straight, A.F., Murray, A., Chikashige, Y., Yamashita, Y.M., Hiraoka, Y., and Yanagida, M. (1998). Dynamics of centromeres during metaphase-anaphase transition in fission yeast: Dis1 is implicated in force balance in metaphase bipolar spindle. Mol Biol Cell *9*, 3211-3225.

Nakano, A., Kato, H., Watanabe, T., Min, K.-D., Yamazaki, S., Asano, Y., Seguchi, O., Higo, S., Shintani, Y., Asanuma, H., Asakura, M., Minamino, T., Kaibuchi, K., Mochizuki, N., Kitakaze, M., and Takashima, S. (2010). AMPK controls the speed of microtubule polymerization and directional cell migration through CLIP-170 phosphorylation. Nat Cell Biol *12*, 583-590.

Neumann, B., Held, M., Liebel, U., Erfle, H., Rogers, P., Pepperkok, R., and Ellenberg, J. (2006). High-throughput RNAi screening by time-lapse imaging of live human cells. Nat Methods *3*, 385-390.

Nicastro, D., McIntosh, J.R., and Baumeister, W. (2005). 3D structure of eukaryotic flagella in a quiescent state revealed by cryo-electron tomography. Proc Natl Acad Sci U S A *102*, 15889-15894.

Niccoli, T., and Nurse, P. (2002). Different mechanisms of cell polarisation in vegetative and shmooing growth in fission yeast. J Cell Sci *115*, 1651-1662.

Niethammer, P., Kronja, I., Kandels-Lewis, S., Rybina, S., Bastiaens, P., and Karsenti, E. (2007). Discrete states of a protein interaction network govern interphase and mitotic microtubule dynamics. Plos Biol *5*, e29.

Nigg, E.A. (1995). Cyclin-dependent protein kinases: key regulators of the eukaryotic cell cycle. Bioessays *17*, 471-480.

Nigg, E.A., Blangy, A., and Lane, H.A. (1996). Dynamic changes in nuclear architecture during mitosis: on the role of protein phosphorylation in spindle assembly and chromosome segregation. Exp Cell Res *229*, 174-180.

Nogales, E. (2000). Structural insights into microtubule function. Annu. Rev. Biochem. *69*, 277-302.

Nogales, E., and Wang, H.-W. (2006). Structural mechanisms underlying nucleotide-dependent self-assembly of tubulin and its relatives. Curr Opin Struct Biol *16*, 221-229.

Nogales, E., Whittaker, M., Milligan, R.A., and Downing, K.H. (1999). High-resolution model of the microtubule. Cell *96*, 79-88.

Nurse, P. (1990). Universal control mechanism regulating onset of M-phase. Nature *344*, 503-508.

Oakley, C.E., and Oakley, B.R. (1989). Identification of gamma-tubulin, a new member of the tubulin superfamily encoded by mipA gene of Aspergillus nidulans. Nature *338*, 662-664.

Ohi, R., and Gould, K.L. (1999). Regulating the onset of mitosis. Curr Opin Cell Biol *11*, 267-273.

Paoletti, A., and Bornens, M. (2003). Kar9 asymmetrical loading on spindle poles mediates proper spindle alignment in budding yeast. Developmental Cell *4*, 289-290.

Pardo, M., and Nurse, P. (2003). Equatorial retention of the contractile actin ring by microtubules during cytokinesis. Science *300*, 1569-1574.

Pelham, R.J., Jr., and Chang, F. (2001). Role of actin polymerization and actin cables in actin-patch movement in Schizosaccharomyces pombe. Nat Cell Biol *3*, 235-244.

Perez, F., Diamantopoulos, G.S., Stalder, R., and Kreis, T.E. (1999). CLIP-170 highlights growing microtubule ends in vivo. Cell *96*, 517-527.

Petersen, J., and Hagan, I.M. (2003). S. pombe aurora kinase/survivin is required for chromosome condensation and the spindle checkpoint attachment response. Curr Biol *13*, 590-597.

Petersen, J., Heitz, M.J., and Hagan, I.M. (1998). Conjugation in S. pombe: identification of a microtubule-organising centre, a requirement for microtubules and a role for Mad2. Current Biology *8*, 963-966.

Peth, A., Boettcher, J.P., and Dubiel, W. (2007). Ubiquitin-dependent proteolysis of the microtubule end-binding protein 1, EB1, is controlled by the COP9 signalosome: possible consequences for microtubule filament stability. Journal of Molecular Biology *368*, 550-563.

Pfister, K.K. (2005). Dynein cargo gets its groove back. Structure *13*, 172-173.

Piehl, M., and Cassimeris, L. (2003). Organization and dynamics of growing microtubule plus ends during early mitosis. Mol Biol Cell *14*, 916-925.

Piehl, M., Tulu, U.S., Wadsworth, P., and Cassimeris, L. (2004). Centrosome maturation: measurement of microtubule nucleation throughout the cell cycle by using GFP-tagged EB1. Proc Natl Acad Sci USA *101*, 1584-1588.

Pierre, P., Pepperkok, R., and Kreis, T.E. (1994). Molecular characterization of two functional domains of CLIP-170 in vivo. Journal of Cell Science *107 (Pt 7)*, 1909-1920.

Pierre, P., Scheel, J., Rickard, J.E., and Kreis, T.E. (1992). CLIP-170 links endocytic vesicles to microtubules. Cell *70*, 887-900.

Pollard, T.D., and Borisy, G.G. (2003). Cellular motility driven by assembly and disassembly of actin filaments. Cell *112*, 453-465.

Pollard, T.D., and Mooseker, M.S. (1981). Direct measurement of actin polymerization rate constants by electron microscopy of actin filaments nucleated by isolated microvillus cores. J Cell Biol *88*, 654-659.

Popov, A.V., Severin, F., and Karsenti, E. (2002). XMAP215 is required for the microtubule-nucleating activity of centrosomes. Current Biology *12*, 1326-1330.

Prince, V.E., and Pickett, F.B. (2002). Splitting pairs: the diverging fates of duplicated genes. Nat Rev Genet *3*, 827-837.

Ramírez, G., Alvarez, A., Garcia-Abreu, J., Gomes, F.C., Moura Neto, V., and Maccioni, R.B. (1999). Regulatory roles of microtubule-associated proteins in neuronal morphogenesis. Involvement of the extracellular matrix. Braz J Med Biol Res *32*, 611-618.

Rehberg, M., and Gräf, R. (2002). Dictyostelium EB1 is a genuine centrosomal component required for proper spindle formation. Mol Biol Cell *13*, 2301-2310.

Revenu, C., Athman, R., Robine, S., and Louvard, D. (2004). The co-workers of actin filaments: from cell structures to signals. Nat Rev Mol Cell Biol *5*, 635-646.

Rickard, J.E., and Kreis, T.E. (1990). Identification of a novel nucleotide-sensitive microtubule-binding protein in HeLa cells. The Journal of Cell Biology *110*, 1623-1633.

Rickard, J.E., and Kreis, T.E. (1991). Binding of pp170 to microtubules is regulated by phosphorylation. J Biol Chem *266*, 17597-17605.

Robinson, D.N., and Spudich, J.A. (2004). Mechanics and regulation of cytokinesis. Current Opinion in Cell Biology *16*, 182-188.
Rodionov, V.I., and Borisy, G.G. (1997). Microtubule treadmilling in vivo. Science *275*, 215-218.

Rogers, G.C., Rusan, N.M., Peifer, M., and Rogers, S.L. (2008). A multicomponent assembly pathway contributes to the formation of acentrosomal microtubule arrays in interphase Drosophila cells. Mol Biol Cell *19*, 3163-3178.

Rogers, S.L., Rogers, G.C., Sharp, D.J., and Vale, R.D. (2002). Drosophila EB1 is important for proper assembly, dynamics, and positioning of the mitotic spindle. The Journal of Cell Biology *158*, 873-884.

Roque, H. (2009). A closer look at *Schizosaccharomyces pombe* interphase microtubule arrays. PhD Thesis, Heidelberg University.

Roque, H., Ward, J.J., Murrells, L., Brunner, D., and Antony, C. (2010). The fission yeast XMAP215 homolog Dis1p is involved in microtubule bundle organization. PLoS ONE *5*, e14201.

Ruiz, F., Krzywicka, A., Klotz, C., Keller, A., Cohen, J., Koll, F., Balavoine, G., and Beisson, J. (2000). The SM19 gene, required for duplication of basal bodies in Paramecium, encodes a novel tubulin, eta-tubulin. Curr Biol *10*, 1451-1454.

Sagolla, M.J., Uzawa, S., and Cande, W.Z. (2003). Individual microtubule dynamics contribute to the function of mitotic and cytoplasmic arrays in fission yeast. Journal of Cell Science *116*, 4891-4903.

Samejima, I., Lourenco, P.C., Snaith, H.A., and Sawin, K.E. (2005). Fission yeast mto2p regulates microtubule nucleation by the centrosomin-related protein mto1p. Mol Biol Cell *16*, 3040-3051.

Sandblad, L., Busch, K.E., Tittmann, P., Gross, H., Brunner, D., and Hoenger, A. (2006). The Schizosaccharomyces pombe EB1 homolog Mal3p binds and stabilizes the microtubule lattice seam. Cell *127*, 1415-1424.

Sandblad, L. (2007). Seam Binding, a novel mechanism for microtubule stabilization. PhD Thesis, Heidelberg University.

Savage, C., Hamelin, M., Culotti, J.G., Coulson, A., Albertson, D.G., and Chalfie, M. (1989). mec-7 is a beta-tubulin gene required for the production of 15-protofilament microtubules in Caenorhabditis elegans. Genes Dev *3*, 870-881.

Sawin, K.E., Lourenco, P.C.C., and Snaith, H.A. (2004). Microtubule nucleation at non-spindle pole body microtubule-organizing centers requires fission yeast centrosomin-related protein mod20p. Current Biology *14*, 763-775.

Sawin, K.E., and Nurse, P. (1998). Regulation of cell polarity by microtubules in fission yeast. J Cell Biol *142*, 457-471.

Schuyler, S.C., Liu, J.Y., and Pellman, D. (2003). The molecular function of Ase1p: evidence for a MAP-dependent midzone-specific spindle matrix. Microtubule-associated proteins. J Cell Biol *160*, 517-528.

Schuyler, S.C., and Pellman, D. (2001). Microtubule "plus-end-tracking proteins": The end is just the beginning. Cell *105*, 421-424.

Schwartz, K., Richards, K., and Botstein, D. (1997). BIM1 encodes a microtubule-binding protein in yeast. Mol Biol Cell *8*, 2677-2691.

Sept, D., Baker, N.A., and McCammon, J.A. (2003). The physical basis of microtubule structure and stability. Protein Sci *12*, 2257-2261.

Slep, K.C., and Vale, R.D. (2007). Structural basis of microtubule plus end tracking by XMAP215, CLIP-170, and EB1. Mol Cell *27*, 976-991.

Snaith, H.A., and Sawin, K.E. (2003). Fission yeast mod5p regulates polarized growth through anchoring of tea1p at cell tips. Nature *423*, 647-651.

Srayko, M., Kaya, A., Stamford, J., and Hyman, A.A. (2005). Identification and characterization of factors required for microtubule growth and nucleation in the early C. elegans embryo. Developmental Cell *9*, 223-236.

Strelkov, S.V., Herrmann, H., and Aebi, U. (2003). Molecular architecture of intermediate filaments. Bioessays *25*, 243-251.

Strickland, L.I., Donnelly, E.J., and Burgess, D.R. (2005). Induction of cytokinesis is independent of precisely regulated microtubule dynamics. Mol Biol Cell *16*, 4485-4494.

Su, L.K., Burrell, M., Hill, D.E., Gyuris, J., Brent, R., Wiltshire, R., Trent, J., Vogelstein, B., and Kinzler, K.W. (1995). APC binds to the novel protein EB1. Cancer Res *55*, 2972-2977.

Sun, L., Gao, J., Dong, X., Liu, M., Li, D., Shi, X., Dong, J.-T., Lu, X., Liu, C., and Zhou, J. (2008). EB1 promotes Aurora-B kinase activity through blocking its inactivation by protein phosphatase 2A. Proceedings of the National Academy of Sciences *105*, 7153-7158.

Tanenbaum, M.E., Galjart, N., Van Vugt, M.A.T.M., and Medema, R.H. (2006). CLIP-170 facilitates the formation of kinetochore-microtubule attachments. EMBO J *25*, 45-57.

Thadani, R., Ling, Y.C., and Oliferenko, S. (2009). The fission yeast TACC protein Mia1p stabilizes microtubule arrays by length-independent crosslinking. Curr Biol *19*, 1861-1868.

Tighe, A., Johnson, V.L., and Taylor, S.S. (2004). Truncating APC mutations have dominant effects on proliferation, spindle checkpoint control, survival and chromosome stability. J Cell Sci *117*, 6339-6353.

Tilney, L.G., Bryan, J., Bush, D.J., Fujiwara, K., Mooseker, M.S., Murphy, D.B., and Snyder, D.H. (1973). Microtubules: evidence for 13 protofilaments. J Cell Biol *59*, 267-275.

Tirnauer, J.S., and Bierer, B.E. (2000). EB1 proteins regulate microtubule dynamics, cell polarity, and chromosome stability. The Journal of Cell Biology *149*, 761-766.

Tirnauer, J.S., Canman, J.C., Salmon, E.D., and Mitchison, T.J. (2002a). EB1 targets to kinetochores with attached, polymerizing microtubules. Mol Biol Cell *13*, 4308-4316.

Tirnauer, J.S., Grego, S., Salmon, E.D., and Mitchison, T.J. (2002b). EB1-microtubule interactions in Xenopus egg extracts: role of EB1 in microtubule stabilization and mechanisms of targeting to microtubules. Mol Biol Cell *13*, 3614-3626.

Tirnauer, J.S., O'Toole, E., Berrueta, L., Bierer, B.E., and Pellman, D. (1999). Yeast Bim1p promotes the G1-specific dynamics of microtubules. The Journal of Cell Biology *145*, 993-1007.

Tischer, C., Brunner, D., and Dogterom, M. (2009). Force- and kinesin-8-dependent effects in the spatial regulation of fission yeast microtubule dynamics. Mol Syst Biol *5*, 250.

Tolić-Nørrelykke, I.M., Sacconi, L., Thon, G., and Pavone, F.S. (2004). Positioning and elongation of the fission yeast spindle by microtubule-based pushing. Current Biology *14*, 1181-1186.

Tran, P.T., Marsh, L., Doye, V., Inoué, S., and Chang, F. (2001). A mechanism for nuclear positioning in fission yeast based on microtubule pushing. The Journal of Cell Biology *153*, 397-411.

Vale, R.D. (2003). The molecular motor toolbox for intracellular transport. Cell *112*, 467-480.
van den Ent, F., Amos, L.A., and Lowe, J. (2001). Prokaryotic origin of the actin cytoskeleton. Nature *413*, 39-44.

Verbrugghe, K.J., and White, J.G. (2004). SPD-1 is required for the formation of the spindle midzone but is not essential for the completion of cytokinesis in C. elegans embryos. Curr Biol *14*, 1755-1760.

Verde, F., Labbe, J.C., Doree, M., and Karsenti, E. (1990). Regulation of microtubule dynamics by cdc2 protein kinase in cell-free extracts of Xenopus eggs. Nature *343*, 233-238.

Verde, F., Mata, J., and Nurse, P. (1995). Fission yeast cell morphogenesis: identification of new genes and analysis of their role during the cell cycle. J Cell Biol *131*, 1529-1538.

Visa, N., and Percipalle, P. (2010). Nuclear functions of actin. Cold Spring Harbor Perspectives in Biology *2*, a000620.

Vitre, B., Coquelle, F.M., Heichette, C., Garnier, C., Chrétien, D., and Arnal, I. (2008). EB1 regulates microtubule dynamics and tubulin sheet closure in vitro. Nat Cell Biol *10*, 415-421.

Voter, W.A., and Erickson, H.P. (1984). The kinetics of microtubule assembly. Evidence for a two-stage nucleation mechanism. J Biol Chem *259*, 10430-10438.

Wade, R.H. (2007). Microtubules: an overview. Methods Mol Med *137*, 1-16.

Wade, R.H. (2009). On and around microtubules: an overview. Mol Biotechnol *43*, 177-191.

Wagner, O.I., Rammensee, S., Korde, N., Wen, Q., Leterrier, J.-F., and Janmey, P.A. (2007). Softness, strength and self-repair in intermediate filament networks. Experimental Cell Research *313*, 2228-2235.

Walczak, C.E., and Heald, R. (2008). Mechanisms of mitotic spindle assembly and function. Int Rev Cytol *265*, 111-158.

Waterman-Storer, C.M., and Salmon, E.D. (1997). Microtubule dynamics: treadmilling comes around again. Curr Biol *7*, R369-372.

Wegner, A. (1976). Head to tail polymerization of actin. J Mol Biol *108*, 139-150.

Wieland, G., Orthaus, S., Ohndorf, S., Diekmann, S., and Hemmerich, P. (2004). Functional complementation of human centromere protein A (CENP-A) by Cse4p from Saccharomyces cerevisiae. Mol Cell Biol *24*, 6620-6630.

Wiese, C., and Zheng, Y. (2000). A new function for the gamma-tubulin ring complex as a microtubule minus-end cap. Nat Cell Biol *2*, 358-364.

Wiese, C., and Zheng, Y. (2006). Microtubule nucleation: gamma-tubulin and beyond. J Cell Sci *119*, 4143-4153.

Wilson-Grady, J.T., Villén, J., and Gygi, S.P. (2008). Phosphoproteome analysis of fission yeast. J Proteome Res *7*, 1088-1097.

Winey, M., and O'Toole, E.T. (2001). The spindle cycle in budding yeast. Nat Cell Biol *3*, E23-27.

Wittmann, T., Hyman, A., and Desai, A. (2001). The spindle: a dynamic assembly of microtubules and motors. Nat Cell Biol *3*, E28-34.

Yan, X., Habedanck, R., and Nigg, E.A. (2006). A complex of two centrosomal proteins, CAP350 and FOP, cooperates with EB1 in microtubule anchoring. Mol Biol Cell *17*, 634-644.

Yang, X., Li, H., Liu, X.S., Deng, A., and Liu, X. (2009). Cdc2-mediated phosphorylation of CLIP-170 is essential for its inhibition of centrosome reduplication. J Biol Chem *284*, 28775-28782.

Zanic, M., Stear, J.H., Hyman, A.A., and Howard, J. (2009). EB1 recognizes the nucleotide state of tubulin in the microtubule lattice. PLoS ONE *4*, e7585.

Zigmond, S.H. (2004). Beginning and ending an actin filament: control at the barbed end. Curr Top Dev Biol *63*, 145-188.

Zimmerman, S., Tran, P.T., Daga, R.R., Niwa, O., and Chang, F. (2004). Rsp1p, a J domain protein required for disassembly and assembly of microtubule organizing centers during the fission yeast cell cycle. Developmental Cell *6*, 497-509.

Zimniak, T., Stengl, K., Mechtler, K., and Westermann, S. (2009). Phosphoregulation of the budding yeast EB1 homologue Bim1p by Aurora/Ipl1p. The Journal of Cell Biology *186*, 379-391.

Zimniak, T. (2010). Molecular insights into the function and regulation of the budding yeast EB1 homologue Bim1p. PhD Thesis, Vienna University.